

Northumbria Research Link

Citation: Gariani, Salah (2019) Development and Evaluation of a Novel Supply System to Reduce Cutting Fluid Consumption and Improve Machining Performance. Doctoral thesis, Northumbria University.

This version was downloaded from Northumbria Research Link:
<https://nrl.northumbria.ac.uk/id/eprint/39469/>

Northumbria University has developed Northumbria Research Link (NRL) to enable users to access the University's research output. Copyright © and moral rights for items on NRL are retained by the individual author(s) and/or other copyright owners. Single copies of full items can be reproduced, displayed or performed, and given to third parties in any format or medium for personal research or study, educational, or not-for-profit purposes without prior permission or charge, provided the authors, title and full bibliographic details are given, as well as a hyperlink and/or URL to the original metadata page. The content must not be changed in any way. Full items must not be sold commercially in any format or medium without formal permission of the copyright holder. The full policy is available online: <http://nrl.northumbria.ac.uk/policies.html>

Northumbria Research Link

Citation: Gariani, Salah (2019) Development and Evaluation of a Novel Supply System to Reduce Cutting Fluid Consumption and Improve Machining Performance. Doctoral thesis, Northumbria University.

This version was downloaded from Northumbria Research Link:
<http://nrl.northumbria.ac.uk/id/eprint/39469/>

Northumbria University has developed Northumbria Research Link (NRL) to enable users to access the University's research output. Copyright © and moral rights for items on NRL are retained by the individual author(s) and/or other copyright owners. Single copies of full items can be reproduced, displayed or performed, and given to third parties in any format or medium for personal research or study, educational, or not-for-profit purposes without prior permission or charge, provided the authors, title and full bibliographic details are given, as well as a hyperlink and/or URL to the original metadata page. The content must not be changed in any way. Full items must not be sold commercially in any format or medium without formal permission of the copyright holder. The full policy is available online: <http://nrl.northumbria.ac.uk/policies.html>

**Development and Evaluation of a Novel
Supply System to Reduce Cutting Fluid
Consumption and Improve Machining
Performance**

SALAH GARIANI

PhD

2019

Development and Evaluation of a Novel
Supply System to Reduce Cutting Fluid
Consumption and Improve Machining
Performance

SALAH GARIANI

A thesis submitted in partial fulfilment of
the requirements of the University of
Northumbria at Newcastle for the degree of
Doctor of Philosophy

Research undertaken in the
School of Engineering and Environment
Department of Mechanical Engineering

January 2019

Abstract

Reducing cutting fluid consumption remains a goal of the machining industry. Despite their reported advantages such as heat dissipation, friction reduction, extended tool life, and improved surface quality, cutting fluids pose several health and environmental concerns throughout their lifecycle, in particular when conventional mineral oil-based, semi-synthetic or synthetic fluids are used. Manufacturers are encouraged to reduce the use of harmful conventional fluids. However, the usage of cutting fluid is still an unavoidable industrial practice, especially when machining titanium alloys, due to the generation of large quantities of heat. High cutting temperature is one of the main reasons for rapid tool wear and hence the poor machinability of titanium alloys. Vegetable oil (VO)-based fluids have been suggested as favourable alternatives to the conventional fluids due to their superior tribological properties and high biodegradability. Several cutting fluid supply systems have been developed to reduce cutting fluid use, such as minimum quantity lubricant (MQL) and cryogenic cooling or to control the temperature in the cutting zone, for example flood, and high pressure cooling (HPC) systems, to improve productivity and increase the overall performance of machining processes. Even though process improvements are achieved by these systems, inaccuracies in estimating cutting fluid flow rates, high fluid consumption and low penetrability, as well as high set-up costs, are their technical and economic drawbacks. For these reasons, the need for an innovative supply system to deliver fluids in machining processes has become crucial.

In this PhD project, a novel controlled cutting fluid impinging supply system known as 'CUT-LIST' is developed to deliver an accurate quantity of cutting fluid into machining zones through precisely-oriented coherent nozzles. The design of CUT-LIST is supported by numerous fluid dynamic and metal cutting theories along with extensive experimentation. The performance of the new system is evaluated against a conventional flood system during the step shoulder milling of Ti-6Al-4V using a water-miscible vegetable oil-based cutting fluid. The effect of cutting conditions on the key measures of the process are investigated, including cutting force, workpiece temperature, tool flank wear, burr formation and average surface roughness (Ra). The effect of CUT-LIST on the micro-hardness and microstructure of the machined surface as well as chip formation are also evaluated. The study shows that the new system provides a dramatic decrease in cutting fluid consumption of up to 42% with noticeable reductions in cutting force, tool flank wear and burr height of 16.41%, 46.77% and 60% respectively. Relatively smaller surface roughness (Ra) values are also found with the use of the CUT-LIST supply system. In terms of the effect of the new system parameters on key process measures, feed rate has a major effect on cutting force, burr formation and surface roughness, with the highest percentage contribution ratios (PCRs) of 47.46%, 38.69% and 39.10% respectively. Meanwhile, the cutting speed has a major effect on workpiece temperature and flank wear, with the highest PCRs of 46.5% and 59.23% respectively. Nozzle position at a 15° angle in the feed direction and 45° or 60° against feed direction helped in

minimising workpiece temperature. An impinging distance of 55 or 75 mm is also necessary to control burr formation, workpiece temperature, and Ra. Metallurgical observation shows that both systems achieved acceptable micro-hardness values for aerospace components (386.3 to 419 HV₁₀₀). However, a slight reduction in micro-hardness of ~5.5% was recorded with the use of CUT-LIST. The hardness is lower at distances < 50 μm below the machined surface as a result of thermal softening, while it becomes higher at distances <100 μm from the surface due to cyclic internal work hardening. The micro-hardness then gradually decreases until it reaches the base material's nominal hardness.

Both systems also produce a thin, plastically deformed layer below the machined surface under all conditions investigated. Despite the noticeable reduction in cutting fluid consumption achieved by CUT-LIST, no significant disparity is found in the microstructural subsurface damage caused by the two systems. Microstructural alteration is strongly affected by cutting speed and fluid flow rate. At higher cutting speeds, the conventional system shows visible surface defects such as smearing, surface cavities and erosion in workpiece material. With both systems, desirable discontinued serrated chips are generated. However, the increase in fluid flow rate significantly influences chip morphology, while the average distance between chip segments is more pronounced and evident with the increase in cutting speed. Severe crack propagation (up to a depth of 200 μm) is observed in the chip end free surface, with the use of the conventional system.

In addition, CUT-LIST shows decreases of up to 12.5 % in saw-tooth height (h_{\max}) and increased segment width up to 13.63 % at higher speeds, while the transition from aperiodic to periodic serrated chip formation is closely controlled by cutting speed and feed rate. Chip segmentation frequency and shear angle are also found to be sensitive to cutting speed, whilst CUT-LIST provides a larger shear angle compared to the conventional system.

Based on the results achieved by CUT-LIST, it is apparent that the new system possess various advantages over the conventional system. Hence, CUT-LIST can be considered as a feasible, efficient, and ecologically beneficial solution, offering less fluid consumption in machining processes.

Table of Contents

Abstract.....	I
Table of Contents	III
List of Figures.....	IX
List of Tables	XVI
List of Publications	XVIII
Acknowledgment.....	XIX
Declaration.....	XX
Nomenclature and Abbreviations.....	XXI
Chapter 1 Introduction	1
1.1 Background and motivation.....	1
1.2 Aims and objectives	3
1.3 Research novelty and originality	5
1.4 Scope of the research.....	5
1.5 Importance of the project to industry.....	6
1.6 Thesis structure.....	6
Chapter 2 Literature Review.....	9
2.1 Machining technology	10
2.1.1 Cutting conditions in machining process	11
2.2 Titanium and its alloys	11
2.3 Machining of titanium alloys.....	13
2.4 Heat generation when machining titanium alloys	15
2.5 Cutting tool materials for machining titanium.....	17
2.5.1 Uncoated cemented carbide tools.....	17
2.5.2 Coated cemented carbide tools.....	18
2.6 Tool wear mechanisms in machining titanium.....	19
2.7 Surface integrity in machining of titanium.....	20
2.7.1 Surface roughness	20
2.7.2 Micro-hardness.....	22
2.7.3 Microstructural subsurface damage	22
2.8 Chip formation and morphology in machining titanium	24
2.9 Cutting fluids in the machining industry	25
2.9.1 Function and action of cutting fluid in machining processes	26
2.9.2 Types of cutting fluid and their properties	28
2.9.2.1 Neat cutting oils.....	28
2.9.2.2 Water-soluble cutting fluids	29

2.9.2.3	Gas-based fluids	31
2.9.3	Ecological effect of conventional cutting fluids.....	32
2.9.4	The need for vegetable oil-based fluids in machining	33
2.10	Cutting fluids supply systems used in the machining industry.....	36
2.10.1	Conventional flood cooling.....	37
2.10.2	High pressure cooling (HPC).....	38
2.10.3	Mist cooling	39
2.10.4	Compressed air/water vapour/gas-based cooling.....	39
2.10.5	Minimum quantity lubrication (MQL).....	40
2.10.6	Cryogenic cooling.....	41
2.10.7	Air blow cooling (dry cutting)	42
2.10.8	Critical evaluation of cutting fluid systems in machining	42
2.11	Applications of cutting fluid supply systems in machining of different materials using VO-based cutting fluids	45
2.11.1	Non-refractory materials (aluminium, copper and steel alloys)	45
2.11.2	Refractory materials (titanium and nickel-based alloys)	46
2.12	Cutting fluid nozzles.....	47
2.12.1	Conventional sloped nozzle	48
2.12.2	Coherent nozzle	48
2.12.3	Importance of nozzle positioning and angles in metal cutting.....	50
2.13	Cutting temperature and measurement techniques in machining	52
2.13.1	Thermocouples (TCs)	54
2.13.1.1	Importance of the positions of drilled holes in temperature measurement...55	
2.13.2	Infrared (IR) pyrometers.....	57
2.13.3	Thermal image cameras	57
2.13.4	Metallographic method.....	58
2.14	Design of experiments (DOE) and data analysis methods	58
2.14.1	Full factorial design	60
2.14.2	Taguchi design methodology	61
2.14.3	Analysis of means (ANOM)	61
2.14.4	Analysis of variance ANOVA	62
2.15	Summary of the literature review findings	63
Chapter 3	Design and Manufacture of the Novel Supply System.....	65
3.1	Design tools	65
3.2	Design concept and baselines	65
3.3	New system configuration.....	67

3.4	CUT-LIST component design	69
3.4.1	Overhead angled nozzle ring.....	69
3.4.2	Angled mounting wedge	70
3.4.3	Movable angled nozzle holder	70
3.4.4	Impinging coherent round nozzle.....	71
3.4.5	Workpiece fixture.....	73
3.5	Manufacturing of the new system components	74
3.6	Determination of parameters of the fluid supply system.....	76
3.6.1	Computation of MRR and cutting power	76
3.6.2	Calculations of accurate flow rate (Q_{acc}).....	77
3.6.3	Determination of nozzle aperture diameter and impinging fluid velocity	79
3.6.4	Chapter summary	82
Chapter 4	Experimental Work	83
4.1	Evaluation of different vegetable oil- and mineral oil-based cutting fluids and tool materials.....	85
4.1.1	Design of experiment (DOE)	85
4.1.2	Machine tool and workpiece material	85
4.1.3	Cutting tool materials and coatings	87
4.1.4	Cutting fluids.....	88
4.1.5	Measurement equipment	89
4.1.5.1	Refractometer	89
4.1.5.2	3D surface profiler (Alicona InfiniteFocus)	89
4.1.5.3	Leica EZ4 D microscope	91
4.1.5.4	Surface roughness testing	91
4.2	Pre-selection of cutting conditions	92
4.2.1	Experimental design.....	92
4.2.2	Workpiece material and set-up.....	93
4.2.3	Tool material and cutting fluid.....	94
4.2.4	Equipment for measuring surface roughness and tool wear.....	94
4.3	Selection of vegetable oil-based fluid and cutting tool material	94
4.3.1	Design of experiment	94
4.3.2	Workpiece material and machine tool.....	95
4.3.3	Tool materials and cutting fluids.....	95
4.3.4	Equipment	95
4.4	Assessment of cutting fluid concentration ratio	96
4.4.1	Experimental design.....	96

4.4.2	Workpiece material and sample preparation	96
4.4.3	Tool material	97
4.4.4	Cutting fluid concentration.....	97
4.4.5	Tool life analysis	98
4.4.6	Micro-hardness test	98
4.4.7	Equipment	99
4.4.7.1	Surface roughness and tool wear measurement.....	99
4.4.7.2	Materialographic sample preparation and instrumentation	99
4.4.7.3	Cutting fluids viscosity and specific heat capacity measurement.....	102
4.5	Evaluation of the CUT-LIST cutting fluid supply system.....	103
4.5.1	Design of experiments.....	103
4.5.2	Machine tool and workpiece material	105
4.5.3	Tool material and cutting fluid.....	106
4.5.4	Measurement equipment	108
4.5.4.1	Cutting force dynamometer	108
4.5.4.2	Workpiece temperature measurement with embedded thermocouples	109
4.5.4.3	Surface roughness and tool wear measurements	110
4.5.4.4	Digital depth gauge for burr height measurement	111
4.5.4.5	Surface topography analysis.....	112
4.5.4.6	Scanning electron microscopy (SEM).....	112
4.5.4.7	Materialographic sample preparation and instrumentation	113
4.5.4.8	Fluid system instrumentation	115
4.6	Chapter summary (experimental work dashboard).....	118
Chapter 5 Results and Discussion.....		119
5.1	Evaluation of different vegetable oil- and mineral oil-based cutting fluids and tool materials.....	119
5.1.1	Surface roughness analysis.....	119
5.1.2	Tool wear	123
5.1.3	Summary	124
5.2	Pre-selection of cutting conditions	125
5.2.1	Effect of machining parameters on surface roughness.....	125
5.2.2	Tool wear	127
5.2.3	Summary	129
5.3	Selection of vegetable oil-based fluid and cutting tool material	130
5.3.1	Surface roughness analysis.....	130
5.3.2	Tool wear analysis.....	133

5.3.3	Chip thickness	136
5.3.4	Summary	138
5.4	Assessment of cutting fluid concentration ratio	139
5.4.1	Analysis of average surface roughness results	139
5.4.1.1	Fluid concentration effect.....	140
5.4.1.2	Effect of machining conditions.....	141
5.4.2	Analysis of tool wear and tool life results	142
5.4.3	Analysis of micro-hardness.....	145
5.4.4	Summary	147
5.5	Evaluation of the CUT-LIST cutting fluid supply system.....	148
5.5.1	Performance comparison with a conventional flood supply system	148
5.5.1.1	Cutting force analysis.....	148
5.5.1.2	Workpiece temperature	149
5.5.1.3	Tool wear analysis.....	151
5.5.1.4	Burr formation	152
5.5.1.5	Average surface roughness and surface quality.....	153
5.5.1.6	Micro-hardness analysis	156
5.5.1.7	Analysis of microstructure	158
5.5.1.8	Chip formation analysis.....	161
5.5.2	Analysis and optimisation of the new system parameters.....	170
5.5.2.1	Cutting force.....	171
5.5.2.2	Workpiece temperature analysis.....	173
5.5.2.3	Tool wear analysis.....	175
5.5.2.4	Burr formation analysis	178
5.5.2.5	Surface roughness analysis.....	181
5.5.2.6	Effect of nozzle position.....	183
5.5.2.7	Impinging distance effect	184
5.5.3	Repeatability of trials	185
Chapter 6	Conclusions and Recommendations for Future Work	187
6.1	Conclusions	187
6.1.1	Turning-based experimental trials.....	187
6.1.2	Milling-based experimental trials using CUT-LIST	188
6.2	Recommendations for future work.....	192
References		194
Appendix A	2D CAD drawings of the CUT-LIST supply system components.....	218
Appendix B	CNC and MATLAB programmes	226

Appendix C	Design specifications of the CUT-LIST supply system.....	231
Appendix D	Technical data sheets (TDS).....	233
Appendix E	Bill of Materials (BOM).....	241
Appendix F	ISO designations for the indexable inserts and tool holders	245
Appendix G	Heat capacity measurement results for Vasco 1000 cutting fluid.....	248
Appendix H	Certificate of conformance for T-type thermocouples	250
Appendix I	Experimental results.....	251

List of Figures

Fig. 1-1 Thesis structure	8
Fig. 2-1 Literature review topics.....	9
Fig. 2-2 Schematic view of 2D machining [25].....	10
Fig. 2-3 Phase transformations diagram of titanium alloys [31]	12
Fig. 2-4 Conventional machining range of various engineering materials [3]	13
Fig. 2-5 Feed rate range used for machining of various engineering materials [39]	14
Fig. 2-6 Sources of heat in the machining zone [45]	16
Fig. 2-7 Heat distribution in machining titanium using different tool materials [42].....	16
Fig. 2-8 Typical phases of tool wear in machining [54]	19
Fig. 2-9 Various tool wear patterns caused by a machining process [61]	20
Fig. 2-10 Schematic illustration of a roughness profile of machined surface [66]	21
Fig. 2-11 Subsurface deformation regions: highly deformed grains (P3); moderately deformed grains (P2); and unaffected grains (P1) [72]	23
Fig. 2-12 SEM images showing various segmentation distance when turning Ti-6Al-4V at a cutting speed of: (a) 50 m/min; and (b) 150 m/min [79].....	25
Fig. 2-13 Distribution of manufacturing costs in the European automotive industry [9]	26
Fig. 2-14 Cutting fluid action at various phases of a chip formation cycle [9]	28
Fig. 2-15 Classification of cutting fluids [16].....	28
Fig. 2-16 Categories of water-soluble cutting fluids [6, 16].....	29
Fig. 2-17 Conventional fluids life cycle and their ecological impacts [107].....	33
Fig. 2-18 Chemical structure of various VO fatty acids [16]	34
Fig. 2-19 Shape of well-arranged polar heads of VO's molecules [115]	34
Fig. 2-20 The random alignment of MO's non-polar molecules [115].....	35
Fig. 2-21 Cutting fluid supply systems used in the machining industry [4]	37
Fig. 2-22 Image of conventional flood method [126].....	38
Fig. 2-23 Random directional effect of the fluid stream in a flood supply system [19]	38
Fig. 2-24 Cryogenic cooling in the turning process using liquid nitrogen (LN ₂) [145].....	41

Fig. 2-25 Positioning of the proposed system among other supply methods	44
Fig. 2-26 Image of Loc-Line type conventional sloped nozzle [206].....	47
Fig. 2-27 Sectional view of the conventional sloped nozzle [207].....	48
Fig. 2-28 2D sectional view of round coherent nozzle [207]	49
Fig. 2-29 Temperature versus cutting speed under various cooling conditions [219].....	52
Fig. 2-30 Influence of workpiece material type on cutting temperature [220]	53
Fig. 2-31 Temperature versus cooling condition when drilling Ti-6Al-4V [187]	53
Fig. 2-32 Embedded thermocouples used for milling temperature measurement	55
Fig. 2-33 Schematic view of temperature measurement using IR pyrometer [222]	57
Fig. 2-34 Process factors and responses in machining [240].....	59
Fig. 3-1 Basic pillars of the proposed novel supply system concept.....	66
Fig. 3-2 Design strategy adopted when developing CUT-LIST components [248]	66
Fig. 3-3 Configuration for the new CUT-LIST supply system.....	68
Fig. 3-4 Details of view (A).....	68
Fig. 3-5 Isometric 3D view of overhead angled nozzles ring	69
Fig. 3-6 3D view of the angled mounting wedge.....	70
Fig. 3-7 3D structure model of the movable angled nozzle holder/clamp.....	71
Fig. 3-8 3D sectional view of the coherent round nozzle	72
Fig. 3-9 Three-dimensional structural model of the workpiece fixture	73
Fig. 3-10 3D view of the new system assembly	74
Fig. 3-11 Prototypes of CUT-LIST components produced by the 3D printing machine.....	75
Fig. 3-12 3D view of shoulder-down milling used in the new system computations.....	77
Fig. 3-13 Calculated flow rate versus heat generated for the two supply system.....	79
Fig. 3-14 Tools utilised to determine fluid volume collected per unit time.....	81
Fig. 4-1 Process parameters affecting turning and milling processes [4, 26, 194]	84
Fig. 4-2 Image of the set-up for the external straight turning of Ti-6Al-4V.....	86
Fig. 4-3 Image of tool holder and its geometry[262].....	87

Fig. 4-4 Images of various tool materials utilised in the experiments	88
Fig. 4-5 Photograph of the portable optical refractometer used in the study.....	89
Fig. 4-6 Image of set-up for the 3D scanning of the machined Ti-6Al-4V bars.....	90
Fig. 4-7 Photograph of Leica EZ4 D optical microscope	91
Fig. 4-8 Image of Ra measurement set-up used for Ti-6Al-4V machined bars.....	92
Fig. 4-9 3D schematic view of the external straight turning of Ti-6Al-4V set-up	93
Fig. 4-10 Ti-6Al-4V bars used for turning trials	97
Fig. 4-11 Micro-hardness test: (a) cut-out sample and (b) Bakelite material type used.....	99
Fig. 4-12 Mounting press used to form the material into the Bakelite sample	100
Fig. 4-13 Grinding/polishing and ultra-fine wheels used for sample preparation	100
Fig. 4-14 Micro-hardness tester utilised for measuring Ti-6Al-4V machined samples.....	101
Fig. 4-15 Location of indentation marks used for micro-hardness test	101
Fig. 4-16 Collected fluid samples at various concentrations	102
Fig. 4-17 Viscometer used to measure the dynamic viscosity of cutting fluids	102
Fig. 4-18 Differential scanning calorimeter (DSC) [265].....	103
Fig. 4-19 Flow chart of machining experiments for the testing of CUT-LIST	104
Fig. 4-20 Shape and geometry of Ti-6Al-4V sample	105
Fig. 4-21 Image of experimental set-up using CUT-LIST	106
Fig. 4-22 Shape and geometry of R390-11 T3 08M-KM milling insert [262]	107
Fig. 4-23 Image of a typical Kistler dynamometer	108
Fig. 4-24 Thermocouple sensors and data logger used for temperature measurement.....	109
Fig. 4-25 Thermocouple configuration for workpiece temperature measurement	110
Fig. 4-26 Positions of Ra measurements	110
Fig. 4-27 Depth gauge used for top burr measurement	111
Fig. 4-28 Lieca S6D optical microscope	111
Fig. 4-29 Optical microscope used for surface topography observations.....	112
Fig. 4-30 TESCAN MIRA3 Scanning electron microscope.....	113

Fig. 4-31 Ti-6Al-4V sample for micro-hardness test.....	114
Fig. 4-32 Location of indentation marks used in micro-hardness test.....	114
Fig. 4-33 Sample prepared for subsurface microstructure test	115
Fig. 4-34 LM OG-I-PVC type digital flow meter [266]	116
Fig. 4-35 DPG 800-500 type digital fluid pressure gauge [267]	117
Fig. 4-36 Fluid system set-up	117
Fig. 5-1 Ra vs cutting fluid type (each Ra value is the average of 4 tests).....	120
Fig. 5-2 Ra vs cutting tool (each Ra value is averaged from 5 tested cutting fluids)	121
Fig. 5-3 Ra results versus cutting tools using Hocut 3450 at a 0.75 mm depth of cut.....	122
Fig. 5-4 3D scan using the Alicona G4 scanner of a cut machined surface with the CVD S05F tool and Hocut 3450 fluid at 0.75 mm depth of cut	122
Fig. 5-5 Flank wear on different cutting tools using various cutting fluids.....	123
Fig. 5-6 Tool wear of various cutting tool materials at speed of 75 min, feed rate of 0.15 mm/rev and depth of cut of 0.75 mm using the Hocut 3450 fluid	124
Fig. 5-7 Main effects plot for average surface roughness results (Ra)	126
Fig. 5-8 Interaction effects plot of process parameters on Ra	127
Fig. 5-9 Flank wear and discolouring on tool tips (H10F) used at various cutting speeds and at a feed rate of 0.2 mm/rev and depth of cut of 1 mm respectively	128
Fig. 5-10 Flank wear results at various cutting speed and depth of cut with feed rate of 0.15 mm/rev	129
Fig. 5-11 Ra results versus cutting tools at cutting speeds of 120 and 175 m/min using Vasco1000 cutting fluid.....	131
Fig. 5-12 Ra results vs cutting fluids using H13A cutting tool	132
Fig. 5-13 Interaction plot for all control factors affecting surface roughness (Ra)	133
Fig. 5-14 Flank wear results for all cutting tools using Vasco 1000 cutting fluid.....	134
Fig. 5-15 Flank wear results for different cutting fluids using the H13A cutting tool	135
Fig. 5-16 Abrasive tool wear patterns on the flank faces of different cutting tools at a cutting speed of 175 m/min using Vasco 1000 cutting fluid.....	136

Fig. 5-17 Tool wear scars on the rake faces of different cutting tools at a higher cutting speed of 175 m/min using NE250H cutting fluid.....	136
Fig. 5-18 Chip thickness versus cutting fluid at various cutting speeds using H13A tool	137
Fig. 5-19 Chip thickness ratio versus cutting fluids using H13A cutting tool.....	137
Fig. 5-20 Images of chip style formed at different cutting speeds using Vasco 1000 cutting fluid and H13A cutting tool.....	138
Fig. 5-21 Main effects plot for surface roughness results.....	140
Fig. 5-22 Surface roughness versus cutting distance	142
Fig. 5-23 Main effects plot for tool flank wear results	143
Fig. 5-24 Flank wear versus cutting distance at various cutting speeds using H13A tool.....	144
Fig. 5-25 Flank wear on H13A versus cutting distance at a cutting speed of 146 m/min	144
Fig. 5-26 Comparison of tool life recorded at cutting speeds of 58 and 146 m/min	145
Fig. 5-27 Micro-hardness results beneath the machined surface at a cutting speed of 58m/min using the H13A tool.....	146
Fig. 5-28 Micro-hardness results versus cutting distance using H13A tool	147
Fig. 5-29 Cutting force results for the two systems in various cutting conditions	149
Fig. 5-30 Average workpiece temperature results for the two systems in various cutting conditions.....	150
Fig. 5-31 Tool wear results for the two supply systems in various cutting conditions.....	151
Fig. 5-32 SEM images of the cutting tools used with CUT-LIST at a feed rate of 0.15 mm/rev and cutting speeds of 95 and 200 m/min respectively (a, b) and the conventional supply system at a feed rate of 0.15 mm/rev and cutting speeds of 95 and 200m/min respectively (c, d)	152
Fig. 5-33 Effect of cutting fluid supply system on burr height at various machining conditions	153
Fig. 5-34 Average surface roughness results versus cutting conditions for the two systems.	154
Fig. 5-35 SEM images of surface topography of Ti-6Al-4V machined parts under the conventional supply system at a cutting speed of 200 m/min and feed rates of 0.1 and 0.15 mm/rev respectively (a, b), and CUT-LIST at a cutting speed of 200 m/min and feed rates of 0.1 and 0.15 mm/rev respectively (c, d).	155

Fig. 5-36 Optical microscope image of the quality of the machined surface: (a, b) damage when using the conventional supply system; and (c) surface provided using CUT-LIST (all at cutting speed of 200 m/min and feed rate of 0.15 mm/rev)	155
Fig. 5-37 Micro-hardness results below the machined surface at a cutting speed of 95 m/min and feed rate of 0.1 mm/rev for the two systems.....	156
Fig. 5-38 Micro-hardness results beneath the machined surface at a cutting speed of 200 m/min and feed rate of 0.15 mm/rev for the two systems	157
Fig. 5-39 Maximum micro-hardness versus cutting conditions at 100 μ m beneath the machined surface for the two supply systems	158
Fig. 5-40 Typical microstructure of Ti-6Al-4V (as-received material)	159
Fig. 5-41 SEM images of surface microstructure of machined parts at 0.1 mm/rev feed rate using CUT-LIST at cutting speeds of (a, b) 95 and 200 m/min respectively and the conventional supply system at cutting speeds of (c, d) 95 and 200 m/min respectively.....	160
Fig. 5-42 SEM image of thinning and elongation of β phase (conventional system, 95 m/min cutting speed and 0.1 mm/rev feed rate).....	160
Fig. 5-43 (a) Image of the chip produced; (b) schematic view of the down-milling process	161
Fig. 5-44 Discontinuous/segmented chips formed at (a, b) 95m/min and (c, d) 200 m/min.	162
Fig. 5-45 Effect of cutting speed on chip morphology of the free surfaces for CUT-LIST at: (a) 95 m/min and (b) 200 m/min	162
Fig. 5-46 SEM photographs showing the effect of the two supply systems on the morphology of the chip back surface and end free surface at low cutting conditions (95 m/min and 0.1 mm/rev)	163
Fig. 5-47 Measured crack depth for different chips at various cutting conditions	164
Fig. 5-48 SEM images showing the effect of cutting speed on chip morphology of free surfaces for the new system at cutting speeds of: (a) 50 m/min, and (b) 200 m/min.....	164
Fig. 5-49 Measured average distance between serrated segments for the two systems at various cutting conditions.....	165
Fig. 5-50 Side view of a deformed chip showing the serration of chips produced using CUT-LIST at 200 m/min and 0.1 mm/rev	166
Fig. 5-51 Saw-tooth height at various cutting conditions for the two supply systems	167
Fig. 5-52 Saw-tooth width at various cutting conditions for the two systems.....	168

Fig. 5-53 Frequency of segmentation at various cutting conditions for the two systems.....	169
Fig. 5-54 Shear angle (ϕ) observed under both systems at feed rate of 0.15 mm/rev and cutting speeds of 95 m/min (a, b) and 200 m/min (c, d).....	170
Fig. 5-55 Main effect analysis for cutting force	171
Fig. 5-56 Interaction effects of process parameters on cutting force.....	172
Fig. 5-57 Main effects analysis for workpiece temperature	173
Fig. 5-58 Interaction effects of process parameters on workpiece temperature	174
Fig. 5-59 Main effects analysis for tool flank wear	175
Fig. 5-60 Interaction effects of process parameters on tool flank wear (VB).....	176
Fig. 5-61 SEM micrographs of worn tools used to machine Ti-6Al-4V at (a) 95 m/min, and (b) 200 m/min with feed rate of 0.1 mm/rev, nozzle positions of 15° and 45° in the feed and against feed direction respectively and an impinging distance of 75 mm.....	177
Fig. 5-62 EDX analysis performed on the rake face of the insert at cutting speed of 200 m/min and feed rate of 0.1 mm/rev	178
Fig. 5-63 Main effects analysis for average burr height	179
Fig. 5-64 Interaction effects of process parameters on burr formation.....	180
Fig. 5-65 Images of burrs formed on milled top surfaces at different cutting conditions: (a) 95 m/min x 0.1 mm/rev, (b) 95 m/min x 0.15 mm/rev, (c) 200 m/min x 0.1 mm/rev and (d) 200 m/min x 0.15 mm/rev	180
Fig. 5-66 Main effects analysis for surface roughness	181
Fig. 5-67 Interaction effects of process parameters on Ra.....	182
Fig. 5-68 Mean effects analysis of nozzle position/angle for workpiece temperature	183
Fig. 5-69 Impinging distance locations in CUT-LIST configuration	184
Fig. 5-70 Experimental error variation for all responses during the repeated tests	186

List of Tables

Table 2-1 Properties of various cutting tool materials utilised in machining [44]	18
Table 2-2 Key properties of VO and MO base stocks [124]	36
Table 2-3 Critical evaluation of cutting fluid supply systems in machining [14, 98]	43
Table 2-4 Major reports on the application of cutting fluid supply systems in machining of non-refractory materials	45
Table 2-5 Summary of research in the application of cutting fluid supply systems for machining of refractory materials	46
Table 2-6 Major studies on nozzle positions and angles in metal cutting	51
Table 2-7 Literature findings regarding the embedded thermocouple method in milling	56
Table 2-8 Evaluation of temperature measurement techniques in machining [224]	58
Table 2-9 Common DOE methods used in industrial applications [243]	60
Table 3-1 Main internal dimensions of the bespoke coherent round nozzle head	72
Table 3-2 List of main CUT-LIST components and their manufacturing techniques	75
Table 3-3 Working conditions used for MRR and cutting power computations	77
Table 3-4 Inputs and their values used for accurate flow rate computations	78
Table 3-5 Flow rate calculation results for the conventional flood supply system	78
Table 3-6 Computational outcomes for nozzle aperture diameter and fluid velocity	80
Table 3-7 Actual versus calculated accurate flow rates per nozzle and errors	81
Table 4-1 Process variables and levels	85
Table 4-2 Chemical composition of Ti-6Al-4V (ASTM B348 Grade 5) [261]	86
Table 4-3 Mechanical properties of Ti-6Al-4V (ASTM B348 Grade 5) [261]	86
Table 4-4 Properties of cutting tool materials used in the experiments [262]	87
Table 4-5 Characteristics and properties of the fluids tested	88
Table 4-6 Control factors and levels	93
Table 4-7 Operating conditions	95
Table 4-8 Process variables and levels	96

Table 4-9 Tool materials used in the experiment in section 4.4 and their properties.....	97
Table 4-10 Thermo-physical properties of the Vasco 1000 at various concentrations	98
Table 4-11 Process variables and corresponding levels.....	105
Table 4-12 Capabilities of the CNC Cincinnati Sabri-750 machine	106
Table 4-13 Chemical composition and properties of Vasco1000 at 10%	107
Table 5-1 ANOVA results for average surface roughness (Ra).....	121
Table 5-2 ANOVA results for average surface roughness (Ra).....	126
Table 5-3 ANOVA analysis results for tool flank wear	128
Table 5-4 ANOVA results for average surface roughness (Ra).....	132
Table 5-5 ANOVA results for tool flank wear (VB).....	135
Table 5-6 ANOVA results for average surface roughness (Ra).....	141
Table 5-7 ANOVA results for tool flank wear.....	143
Table 5-8 ANOVA results for cutting force.....	172
Table 5-9 ANOVA results for workpiece temperature	174
Table 5-10 ANOVA results for tool flank wear.....	176
Table 5-11 ANOVA results for burr formation.....	179
Table 5-12 ANOVA results for surface roughness (Ra)	182
Table 5-13 Responses and their measurement conditions in the repeated and original trials ...	185
Table 5-14 Experimental maximum and minimum error for all responses.....	186

List of Publications

The following publications are associated with this PhD project:

Journal Papers

1. S. Gariani, I. Shyha, Mahmoud A. El-Sayed and Dehong Huo “*Analysis of microstructure and chip formation when machining Ti-6Al-4V*”. Journal of Metals, an Open Access Journal from MDPI (Metals), vol. 8, p.185, 14th of March 2018. (Q1, Impact Factor 1.984)
2. S. Gariani, I. Shyha, F. Inam, and Dehong Huo, “*Experimental Analysis of System Parameters for Minimum Cutting Fluid Consumption when Machining Ti-6Al-4V Using a Novel Supply System*”. Journal of Advanced Manufacturing Technology, Oct. 2017.(Q1, Impact Factor 2.20)
3. S. Gariani, I. Shyha, F. Inam, and Dehong Huo, "Evaluation of a Novel Controlled Cutting Fluid Impinging Supply System When Machining Titanium Alloys". Journal of Applied Sciences, an Open Access Journal from MDPI (Applied sciences), vol. 7, p. 560, 29th of May 2017. (Impact Factor 1.679)
4. S. Gariani, I. Shyha, M. El-Sayed, and Dehong Huo, “*Investigation into the impact of cutting fluid concentration on the machinability of Ti-6Al-4V using vegetable oil-based cutting fluids*”. International Journal of Engineering Technology, vol. 6, issue II, July 2017, PP. 414-423. (Impact Factor 0.91)

Conference Proceedings

5. S. Gariani, I. Shyha, F. Inam, and D. Huo. (April 2017) “*Influence of Vegetable oil-based Controlled Cutting Fluid Impinging Supply System on Micro-hardness in machining of Ti-6Al-4V*” - proceeding of 19th International Conference on Metal Forming and Machining Processes (ICMFMP) Zurich, Switzerland.
6. S. Gariani, I. Shyha, C. Jackson, F. Inam. (July 2016) “*Tool life analysis when turning Ti-6Al-4V using vegetable oil-based cutting fluids*” - proceeding of seventh International Conference Manufacturing Science and Technology (ICMST) Sarawak, Malaysia.
7. S. Gariani, I. Shyha, F. Inam. (May 2016) “*Effect of cutting tools and working conditions on the machinability of Ti-6Al-4V using vegetable oil-based cutting fluids*” - proceeding of 2nd International Conference on Advances in Mechanical Engineering (ICAME), Istanbul, Turkey.
8. S. Gariani, I. Shyha, N. Meherun. (July 2015) “*Investigation of cutting tools and working conditions effects when cutting Ti-6Al-4V using vegetable oil-based cutting fluids*”- proceeding of the sixth Manufacturing Engineering Society International Conference (MESIC 2015), Barcelona, Spain.

Acknowledgment

First and foremost I would like to thank the Almighty *Allah* for giving me courage, determination and guidance in conducting this research work. The successful completion of this research would not have been possible without the invaluable contribution and support of many people.

I am greatly indebted to my principal supervisor *Dr Islam Shyha* for his continued support, guidance, valuable suggestions, motivation, patience, and friendship throughout the research and writing-up process of my PhD. Without his help, this dissertation would not be what it is now.

I would also like to express my deepest gratitude to my second supervisor *Dr Fawad Inam*, for his support and encouragement

Particular thanks are also reserved for the following people:

Philip Donnelly, Simon Neville, Sam and Dave, for their technical assistance during my experimental work

Colleagues and staff of the Mechanical Engineering Department at Northumbria University for their enthusiastic support and encouragement

My mother, wife, and my loved kids, for their love, prayer, perpetual encouragement and continued support throughout my research study

Also, I will not forget to dedicate this work to the soul of my dear father

Finally, recognition is highlighted to the *Ministry of Higher Education & Scientific Research and National Agency for Scientific Research (NASR)* for their funding, which made this research achievable. A token of appreciation also goes to *Cultural Affairs Department of the Libyan Embassy* in London for their administrative support during the period of my PhD study at Northumbria University, Newcastle.

Declaration

I declare that the work contained in this thesis has not been submitted for any other award and that is all my own work. I also confirm that this work fully acknowledges opinions, ideas and contributions from the work of others.

I declare that the Word Count of this thesis is **46366** Words

Name: **Salah Gariani**

Signature:

Date: **31/01/2019**

Nomenclature and Abbreviations

The following nomenclature and abbreviations are in the order of their positions in the thesis:

CUT-LIST	<u>C</u> ontrolled <u>c</u> utting <u>f</u> luid <u>i</u> mpinging <u>s</u> upply <u>s</u> ystem
V_c	Cutting speed (m/min)
f	Feed rate (mm/rev)
DoC	Depth of Cut (mm) in turning
D_{wp}	Diameter of workpiece (mm) in turning
L	Cutting length or distance (mm)
t	Cutting time (min) in turning
a_p	Axial depth of cut (mm) in milling
a_e	Radial depth of cut (mm) in milling
V_f	Table speed (mm/min) in milling
N	Spindle speed (RPM)
D_c	Cutter/cutting tool diameter (mm) in milling
K_1	Compensation factor as function of (D_c/a_e)
Z	Number of teeth
U	Specific cutting power (W.s/mm ³)
MRR	Material removal rate (mm ³ /min)
MRV	Metal removal volume (mm ³)
P_c	Cutting power (Watt)
Q_{acc}	Accurate flow rate (L/min)
C	Heat capacity of the cutting fluid (cal/g·°C)
ρ	Mass density of the cutting fluid (g/cm ³)
η_{nozzle}	Coherent round nozzle efficiency
$\Delta\theta$	Cutting fluid maximum tolerable temperature increase in (°C)
P	Cutting fluid pressure (psi)
V_j	Cutting fluid velocity (ft/min)
SG	Specific gravity of the cutting fluid (i.e. density of cutting fluid divided by the density of water)
Q_{nozzle}	Nozzle flow rate (US gallon per minute)
CD	Coherent round nozzle discharge coefficient (0.95)
A	Coherent round nozzle exit area (in ²)

D	Coherent round nozzle internal feed pipe diameter (mm)
d	Coherent round nozzle aperture diameter (mm)
D/d	Coherent nozzle contraction ratio (CR)
α	Nozzle elevation angle (degree)
VB	The width of tool flank-workpiece contact zone (mm or μm)
Ra	Average surface roughness (μm)
T_L	Tool life (min)
R_c	Chip thickness ratio
t_o	Undeformed chip thickness (mm)
t_c	chip thickness (mm)
HV_{100}	Micro-hardness in Vickers at 100gf
h_{max}	Saw-tooth height (mm)
w	Saw-tooth width (mm)
f_{chip}	Frequency of segmentation (Hz)
ϕ	Shear angle (degree)

Acronyms

VO	Vegetable Oil
MO	Mineral Oil
SEs	Synthetic Esters fluids
MQL	Minimum Quantity Lubrication
MQCL	Minimum Quantity Cooling Lubrication
CAMQL	Cryogenic air + MQL
MQF	Minimum Quantity Fluid
HQF	High Quantity Fluid
HPC	High Pressure Cooling
HPWJ	High Pressure Water Jet
CWMJ	Cold water mist jet
LN_2	Liquid Nitrogen
CO_2	Carbon Dioxide
NP	Nanoparticles
PCD	Poly Crystalline Diamond
CBN	Cubic Boron Nitride
PCBN	Poly Crystalline Cubic Boron Nitride
W/Co	Tungsten/Cobalt carbide
PVD	Physical Vapour Deposition
CVD	Chemical Vapour Deposition

TiAlNi	Titanium Aluminium Nitride
TiNi	Titanium Nitride
TiCNi	Titanium Carbide Nitride
ZrNi	Zirconium Nitride
AlCrSiNi	Aluminium Chromium Silicon Nitride
BUE	Built-up-edge
SS	Stainless Steel
TRS	Tensile rupture strength (MPa)
BOM	Bill of Materials
TCs	Thermocouples

Chapter 1 Introduction

This introductory chapter covers the background and motivation of the research via a discussion of issues relevant to cutting titanium and the use of conventional cutting fluids in machining operations, with an emphasis on problems of employing standard cutting fluid supply systems in metal cutting processes. The research aim and objectives, scope and plan, and its novelty and originality are also discussed, along with a description of the structure of this thesis.

1.1 Background and motivation

Cutting titanium is more demanding than other engineering materials such as steel and stainless steel. Titanium-based alloys offer high strength-to-weight ratios (i.e. 60 % of the density of steel alloys), high strength, high operating temperatures and exceedingly good corrosion resistance, making them highly attractive materials to use, especially in aerospace applications [1]. However, the same properties that give the alloys appropriate qualities also make them notoriously difficult to cut, owing to their low thermal conductivity, high dynamic shear strength (e.g. up to 1200 MPa for annealed Ti-6Al-4V) and high hardness (e.g. up to 360 HV for solution + aged Ti-6Al-4V), as well as high chemical reactivity at elevated temperatures (i.e. > 500 °C) [1, 2]. Low thermal conductivity (e.g. 7.3 W/m·K for annealed Ti-6Al-4V) causes the accumulation of heat at the apex of the cutting tool, resulting in poor surface quality and geometrical accuracy and high tooling costs. Without cutting fluid, titanium alloys have a great tendency to react with cutting tool materials at an elevated temperature, which can also negatively affect their mechanical properties, causing embrittlement and reduced alloy fatigue strength [3]. Thus, using cutting fluids is crucial to reduce the heat generated during titanium machining [4, 5]. Additionally, cutting fluids serve two key roles in machining: cooling (heat dissipation) and lubrication (to reduce friction) [6]. However, the misuse of harmful conventional cutting fluids such as petroleum/mineral oil-based, synthetic and semi-synthetic fluids not only has environmental and health restrictions [7, 8] but also they are costly (up to 17.9 % of the total manufacturing costs) due to strict regulations for their disposal [9]. Thus, a new avenue has opened for biodegradable lubricants or/ fluids

as superior alternatives to their conventional cutting fluid counterparts [10]. Vegetable oil (VO) base stocks are being investigated as a potential source of environmentally favourable cutting fluids due to a combination of biodegradability, good lubrication properties, low toxicity, high flash points, low volatility, high viscosity indices and good thermal conductivity [10-13]. In the same vein, a good comprehension of cutting fluid supply methods or systems in machining operations can significantly help in controlling fluid consumption as well as enhancing cooling/lubrication capacity and consequently improving product surface quality [14]. Presently, conventional flood supply systems are the dominant cutting fluid systems in machine tooling [15, 16]. These systems deliver a steady-state stream of cutting fluid to the machining zone with high flow rates (up to 225 L/min for multi cutters) [17]. A flood supply method is more favourable than dry cutting, particularly in machining of the refractory materials such as titanium where heat dissipation is a priority [18]. However, high fluid consumption, low fluid penetrability, particularly at higher cutting speed (owing to the formation of a fluid vapour blanket at high temperatures), and failure to control the cutting fluid stream (due to the use of randomly-positioned conventional nozzles) at localised heated zones are the main demerits of these systems [19]. To address the issue of low fluid penetrability, high pressure cooling (HPC) was introduced, in which high-powered controlled jets of cutting fluid are targeted into the machining zone to eliminate the fluid vapour barrier so that the heat generated is removed rapidly and effectively. In HPC, fluid jets can effectively penetrate to the tool cutting tip to provide a short shear zone which leads to the creation of thin chips that readily break into small pieces of the base material. However, HPC is the most energy-consuming method, and requires costly micro-particle filtering equipment ($<20\ \mu\text{m}$) and high pressure pumping systems (up to 200 bar) with flow rates ranging up to 75 L/min [20]. In addition, minimum quantity lubrication and cooling (MQL/MQCL) and misting cooling techniques were suggested as a bridging technology to tackle the fluid consumption issue associated with flood and HPC systems [14]. In these methods, a smaller amount of cutting fluid is atomised by misting with compressed air and is applied as an aerosol spray through well-directed special nozzles so that air and oil can be mixed together. Although technical benefits are gained from these systems, particularly in interrupted cutting such as milling owing to their ability to reduced thermal shocks because of low fluid volume, the additional costs of air compressors, including bespoke MQL nozzles, as well as dangerous fumes resulting from these systems are the

main obstacles [14]. Recently, cryogenic supply systems were developed in which liquid nitrogen (LN_2) is sprayed into the machining zone (particularly the tool-chip interface) under moderate pressure and flow rates (up to 4 L/min) and low temperature below -196°C [21]. Improved tool life, especially at low cutting speeds and eliminating the use of liquid-based fluids are its main advantages. However, dimensional inconsistencies, poor product quality due to overcooling, and high set-up costs, including of consumables such as liquid nitrogen (LN_2), are the main limitations [18, 22]. Additionally, it was revealed that the majority of the aforementioned supply systems rely on inaccurate flow rate estimation during the delivery of fluid into the machining zone. The overestimation of cutting fluid flow rates not only has a negative impact on product quality (e.g. geometrical inconsistencies in cryogenic cooling) but is also costly. Therefore, the necessity has arisen for an innovative and inexpensive supply method/ or system to deliver an accurate amount of cutting fluid into the machining zone and at the same time improve machining performance. In the same vein, increasing fluid penetrability at less cost is another goal in machining. Additionally, a new type of round coherent nozzle instead of the conventional sloped nozzle widely used in existing CNC machine tools, with the appropriate positioning of the nozzles is desired. It has been noted that there is extremely limited information available in respect of nozzle positions and angles and stand-off distances in machining processes except in MQL applications [23]. Finding the most effective nozzle positions and angles could help to vastly improve cutting performance. Thus, it is crucial to investigate ways to improve machinability. Finally, to gain more advantages for a new supply system, a vegetable oil-based cutting fluid was utilised to enhance its cooling and lubricating potency and at the same time mitigate ecological hazards of the fluids used, especially when the machine tool operator's health as well as the working environment are at risk.

1.2 Aims and objectives

The principal aim of this research is to increase the technical, ecological and economic efficacy of machining processes through the development of an efficient and inexpensive novel supply system to reduce cutting fluid consumption while improving machining performance. To serve these aims, the following specific objectives should be accomplished:

- a) To perform a comprehensive literature review, particularly on machining titanium, cutting fluids and their supply systems. This provides a basis for understanding the demand to reduce cutting fluid consumption in machining processes and to assist in the design concept of the proposed system.
- b) To design a controlled cutting fluid impinging supply system (named CUT-LIST) structure and the arrangement of its main parts (i.e. fluid pump, flow meter, pressure gauges, etc.) to fulfil the intended design requirements.
- c) To design the novel system components. This includes the design of the overhead angled nozzle ring, nozzle mounting wedges, movable nozzle holder/clamps, and impinging round coherent nozzles. In order to determine the required accurate flow rates that should be supplied to the machining zone, fluid system parameter computations are elaborated for this purpose, comprising calculations of metal removal rate (MRR) and heat generated in combination with the properties of the cutting fluid used.
- d) To manufacture the system components. This is accomplished by means of different machine tools and 3D prototyping machines.
- e) To select the process variables for the evaluating of CUT-LIST. Prior to testing CUT-LIST, crucial parameters such as vegetable oil-based cutting fluid type, concentration ratio and cutting tool material are selected. These parameters are evaluated at different levels based on criteria including surface roughness, tool wear, tool life, chip formation and micro-hardness. Only optimal levels of each parameter are chosen as a machining input for evaluating CUT-LIST.
- f) To test the novel system (CUT-LIST) by comparing its performance against a conventional flood supply system in terms of cutting fluid consumption, cutting force, workpiece temperature, tool flank wear, and burr and chip formation as well as surface integrity (i.e. surface roughness, micro-hardness, and microstructure)
- g) To investigate the effect of cutting conditions (cutting speed and feed rate) as well as the new system parameters (nozzle angle and impinging distance) on machining output such as cutting force, workpiece temperature, tool flank wear, burr formation and surface roughness (Ra).
- h) To identify the new system's optimal parameters (cutting speed, feed rate, nozzle positions/angles and impinging distance) for CUT-LIST best practice.

1.3 Research novelty and originality

The main contributions of the research are as follows:

- a) The development of an efficient (i.e. high cooling capacity with less fluid consumption) and inexpensive novel supply system that can be used to deliver an accurate amount of cutting fluid into the machining zone via accurately-positioned coherent nozzles. The design of CUT-LIST is supported by extensive experimentation along with a critical analysis of the system parameters and process optimisation.
- b) The synchronisation of the calculated heat generated in the machining zone (in combination with thermo-physical properties of cutting fluid) with the exact cutting fluid quantity required to reduce its consumption and at the same time improve the machinability of titanium alloys.

1.4 Scope of the research

The main scope of this research is to design, manufacture and test CUT-LIST and to compare its performance against that of a conventional flood system in terms of fluid consumption, cutting force, workpiece temperature, tool flank wear, burr and chip formation and surface integrity (i.e. surface roughness, micro-hardness and microstructure). Investigation of the impact of the new system parameters such as cutting condition (cutting speed and feed rate), nozzle positions and angles and impinging distances on machining performance as well as process optimisation are also other scopes of this project. This study is an intensive experimental research project; hence, various resources were allocated including workpiece materials (Ti-6Al-4V), cutting inserts, VO-based cutting fluids, and machines tools. State-of-the-art instruments for measuring cutting force, surface topography, workpiece temperature, and tool flank wear as well as fluid system monitoring devices, were also assigned. The machining strategy adopted throughout this research included external straight turning and step shoulder down-milling machining, which is largely used in industrial production. The former was chosen for all experimental work prior to testing the new system, while the latter was selected for evaluating the performance of CUT-LIST as described in detail in chapter 4.

1.5 Importance of the project to industry

This project is important to the machining industry in that it contributes to controlling and reducing the use of cutting fluids, making it immensely attractive in machining applications. In addition, the developed CUT-LIST system can be integrated into existing CNC machine tools without substantial additional costs. This can be practically performed by means of a machine tool control system to which new setting parameters are added, including cutting conditions, cutting tool geometry, workpiece material and cutting fluid properties that can be easily obtained from manufacturers or suppliers.

1.6 Thesis structure

Fig. 1-1 depicts the layout of the thesis structure. This thesis is presented in six chapters as follows:

Chapter 1: Introduction. This provides the project background, motivation, aims and objectives, research novelty and originality, research scope as well as the importance of the project to the machining industry.

Chapter 2: Literature Review. This presents a comprehensive discussion of the literature on titanium machining, cutting tool materials and coatings, and cutting fluids and their key functions and properties. In addition, a survey of the applications of cutting fluid supply systems in machining different materials using vegetable oil-based cutting fluids is presented. Cutting fluid nozzles and their application in machining processes and the temperature measurement techniques as well as design of experiments (DOE) and data analysis methods used are briefly described. A critical evaluation of the literature, including key findings and research gaps, is also provided at the end of the chapter.

Chapter 3: Design and Manufacture of the Novel Supply System. In this chapter, the overall system structure and its configuration are detailed. This includes the arrangement of the system's parts, including the fluid pump, flow meter, pressure gauge, and filters. The design of the system main components such as coherent nozzles, overhead angled nozzle ring, nozzle holders and mounting wedges as well as workpiece fixture are also presented. In addition, the manufacturing techniques utilised to produce CUT-LIST

components are described. Computations of the fluid system's main parameters of accurate flow rates, nozzles aperture diameter and cutting fluid impinging velocities are also provided at the end of the chapter.

Chapter 4: Experimental Work. This covers the design of experiments (DOE), equipment, and machines utilised in the research, including workpiece materials, cutting tools and cutting fluids. The instruments, methodology and standards employed to measure key process outputs such as cutting force, workpiece temperature, tool wear, surface roughness, and burr and chip formation are documented. Additionally, the equipment utilised for measuring the thermo-physical properties of cutting fluid, and micro-hardness and microstructure of the machined Ti-6Al-4V samples is described. This chapter is organised into five main sections. The first four sections describe turning-based experimental work prior to evaluating CUT-LIST, while the last section covers milling-based machining trials to evaluate the CUT-LIST supply system.

Chapter 5: Results and Discussion. This reports all of the experimental results and observations and presents an analysis and discussion of each experimental study. This chapter is also divided into five main sections to reflect the logical sequence of the previous chapter. The latter section (evaluating the developed supply system), in turn, is also split into subsections. The first presents a performance comparison between CUT-LIST and the conventional supply system in terms of cutting force, workpiece temperature, tool flank wear, and burr and chip formation as well as surface integrity (i.e. R_a , micro-hardness and microstructure). The second gives a critical analysis of the system parameters of cutting speed, feed rate, nozzles positions/angles and impinging distances and process optimisation. The results of repeatability trials are also provided at the end of the chapter.

Chapter 6: Conclusions and Recommendations. This lists the relevant conclusions that have arisen mainly from the evaluation of the new supply system and offers suggestions for future work that would be beneficial to improve cutting fluid application in machining using CUT-LIST.

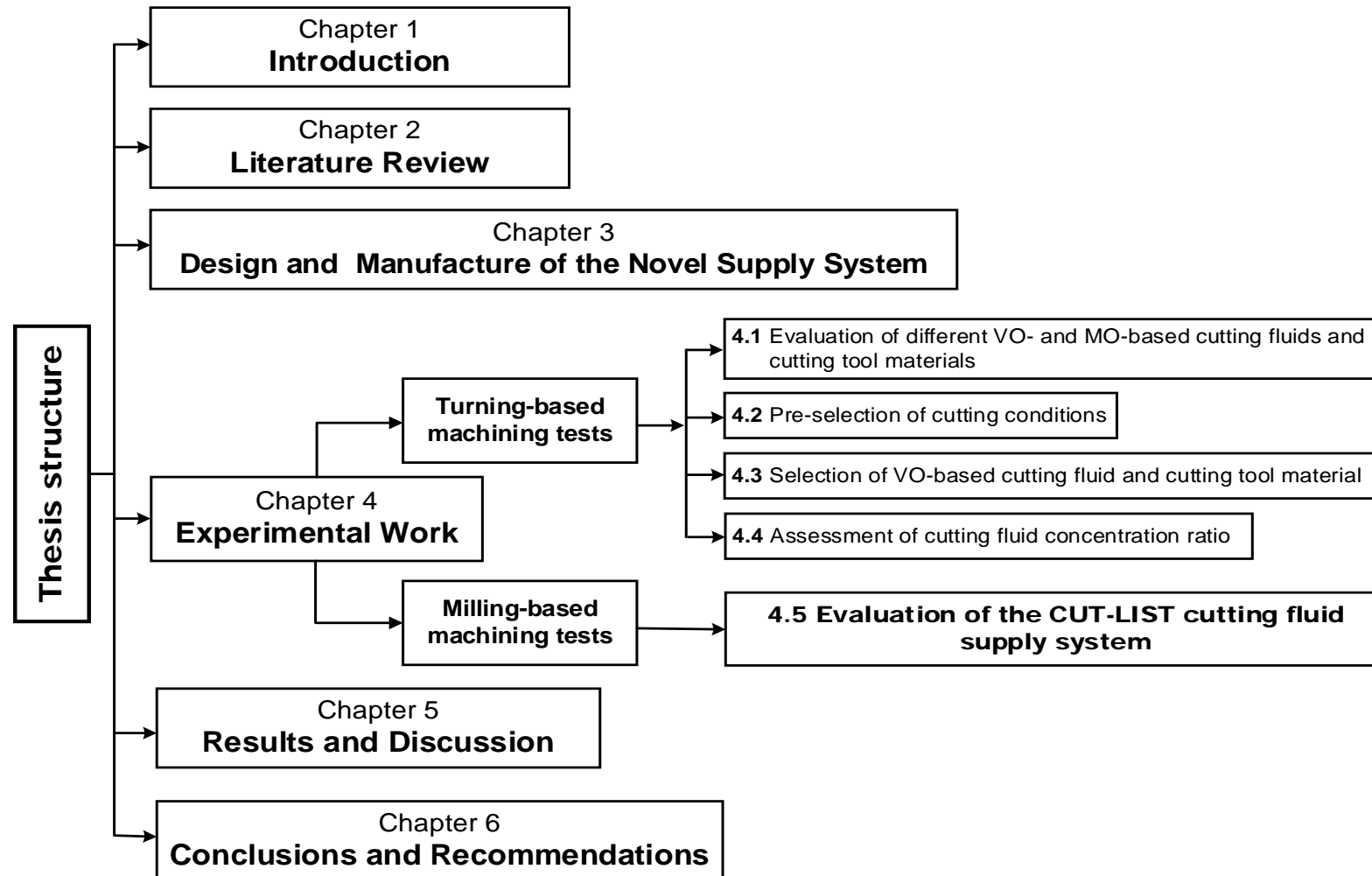


Fig. 1-1 Thesis structure

Chapter 2 Literature Review

This chapter provides an overview of the literature concerning titanium and aspects of its machining, cutting fluids and their supply systems along with the ecological effects of conventional fluids. A comprehensive literature survey on the applications of cutting fluid supply systems in the machining of different materials, including titanium, using VO-based fluid is then provided. Cutting fluid nozzles and temperature measurement methods in machining, as well as the design of experiments (DOE) and data analysis techniques used are also thoroughly illustrated. The chapter then concludes with a critical evaluation of the literature, comprising of key findings and research gaps in the subject area. Fig. 2-1 outlines the literature topics covered in this chapter.

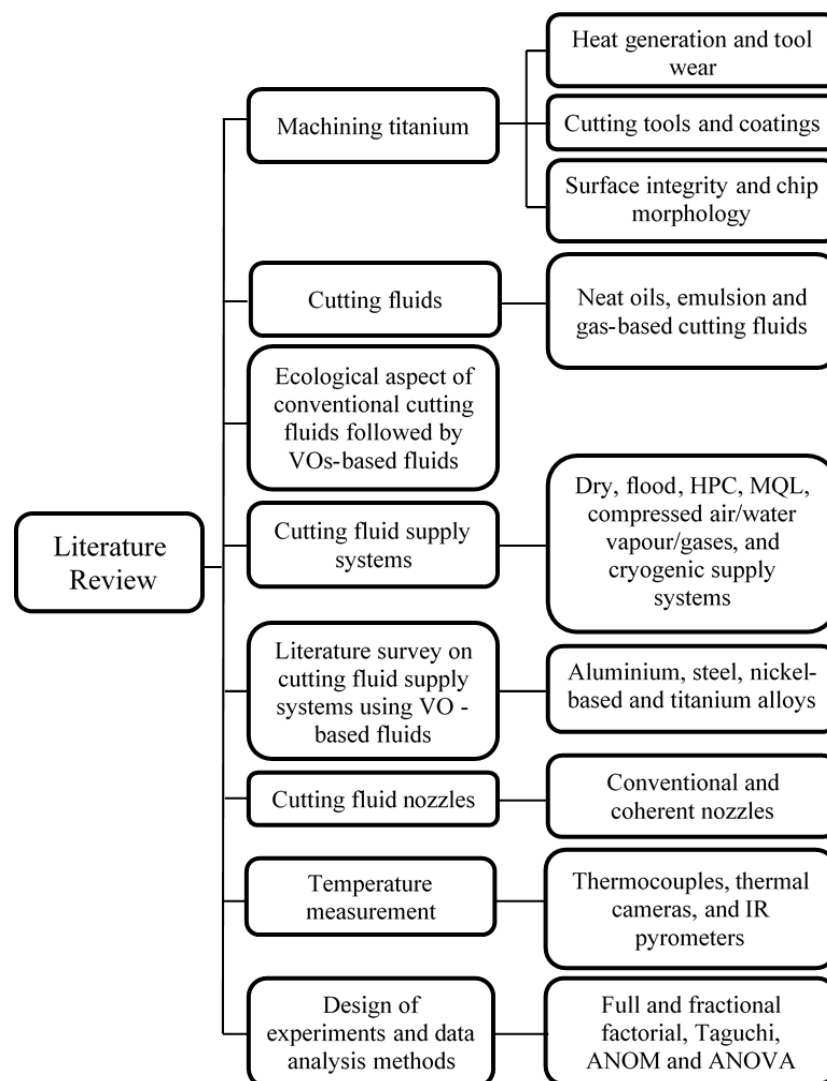


Fig. 2-1 Literature review topics

2.1 Machining technology

Historically, machining is one of the oldest industrial processes and it is the most frequently used in the manufacture of engineering parts. It is estimated that about 15% of the value of all mechanical parts manufactured globally is obtained from machining operations [24]. Machining including turning, milling, and other cutting actions, can be defined as a set of processes which employ a relatively sharp cutting tool to remove excess materials from workpiece surfaces in the form of chips to attain the required product shape. The shear deformation of a workpiece material is the principal cutting action in machining to form a chip. When the cutting tool encounters workpiece material, a chip is removed and a newly machined surface is generated. To carry out machining operations, a relative motion between the cutting tool and work material is required. Speed and feed rate are the major relative motions associated with machining (also known as cutting conditions or parameters which are described in the next section). Tool shape and geometry and its contact with the workpiece surface, combined with these motions, provides the final shape of the product. The cutting tool tip has two faces; namely the rake face and flank face. The rake face is aligned with an angle termed the rake angle with respect to the plane perpendicular to the workpiece surface. The rake angle could be positive (finishing) or negative (roughing). Additionally, chip flow direction can also be controlled by the rake face rather than the flank face. The flank face is aligned with an angle termed the clearance angle, which saves the newly generated surface from abrasion by affording a clearance between the tool and newly generated surfaces [25]. Fig. 2-2 shows a schematic view of a two-dimensional machining process.

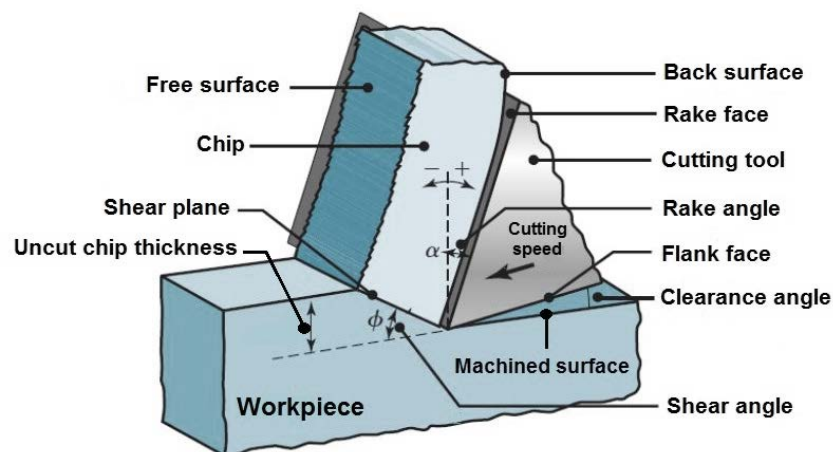


Fig. 2-2 Schematic view of 2D machining [25]

2.1.1 Cutting conditions in machining process

In conventional machining, relative motion is required between the tool and workpiece to perform the machining operation. The primary motion, which is usually the fastest, is accomplished at a certain cutting speed (V_c). For instance, in turning, this is the rotation speed of the workpiece, while in drilling and milling it is the speed of the cutting tool. Also, in turning, the tool must move laterally across the workpiece. The lateral movement is a slower motion, called feed rate (f). Depth of cut (d in turning and a_p and a_e in milling) is the distance into the workpiece that the cutting tool engages with [26]. Collectively, cutting speed, feed rate, and depth of cut are named the main cutting parameters or conditions. Cutting conditions determine the rate of material removal (MRR), power requirements, tool life and surface finish. Additionally, the magnitude of cutting conditions or parameters depend upon many factors such as workpiece and cutting tool materials used as well as the type of machining operation employed (e.g. roughing or finishing) [27].

2.2 Titanium and its alloys

To understand titanium machining, the variants of titanium alloys and their properties and applications need to be detailed. Titanium alloys are one of the families of material that are valuable, particularly in the aerospace and aircraft industry, due to their outstanding mechanical properties such as high strength-to-weight ratios, high operating temperatures and excellent corrosion resistance [28]. They are commonly employed for structural airframe parts and demanding components of aero-engines. Titanium alloys can be classified into two main groups according to their applications: corrosion resistant alloys and structural alloys [29].

- 1) Corrosion resistant alloys are also known as pure alpha alloys (α - alloys) based on their metallurgical characteristics. They contain α stabilisers, usually in combination with neutral elements such as oxygen, palladium, or aluminium. These alloys are mainly used in the chemicals, food, and energy sectors [30].
- 2) Structural alloys are, in turn, sub-divided into three main categories (near α , α - β and β alloys) and depend on the amount of β stabiliser as shown in Fig. 2-3:

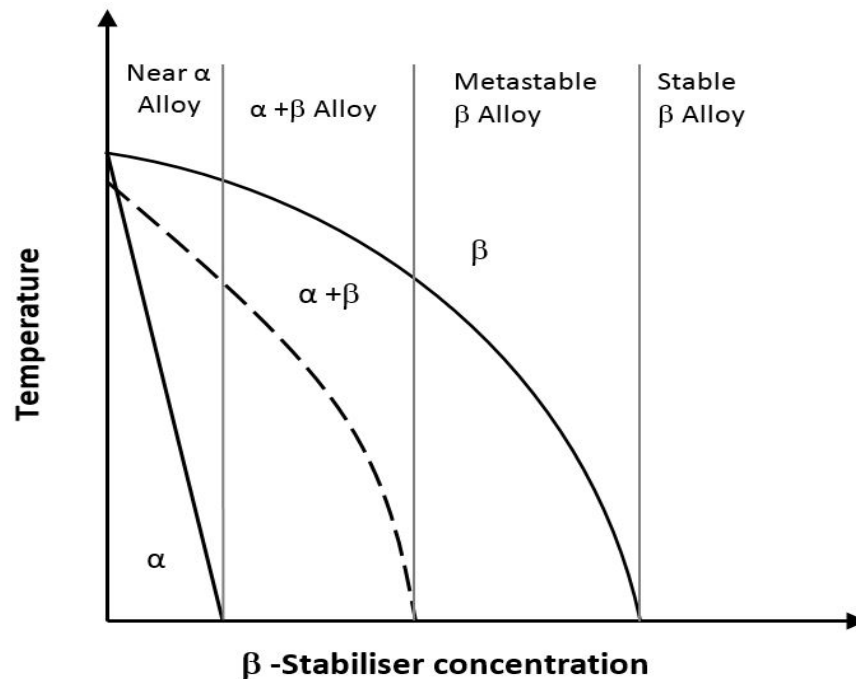


Fig. 2-3 Phase transformations diagram of titanium alloys [31]

- **Near α -Alloys:** This group of alloys contains only small amounts of β - stabilising elements with high α stabilisers, and hence are characterised by a microstructure comprising of an α -phase with only small quantities of β -phase. Owing to their resistance to fatigue, these alloys are capable of operating at elevated temperatures $> 600^{\circ}\text{C}$ and are used mainly in internal combustion turbine engines [32].
- **α - β Alloys:** These alloys contain additions of α -and β -stabilisers and thus possess microstructures comprising of blends of α - and β - phases. Alloy Ti-6Al-4V is the most common alloy in this group. This alloy has superior mechanical properties such as high strength and toughness at a temperature range of 315 to 400°C , when in an aged state condition [3].
- **β Alloys:** This group of alloys contains copious quantities of β - stabilisers and provides a good hardenability, cold formability and improved forgeability, but have inferior mechanical properties to those of $\alpha - \beta$ alloys at elevated temperatures [33].

All of the above material properties make Ti-6Al-4V an excellent alloy to use in manufacturing. This alloy accounts for more than 50% of the global production of titanium [34]. However, titanium is still not as widely used as, for example, steel or

aluminium. This is due to titanium being difficult to cut owing to its low thermal conductivity and high shear strength [28, 32]. Most of the engineering parts currently manufactured for aerospace and automotive applications are machined from solid titanium billets. These parts will, however, usually be thin-walled. It can, therefore, be deduced that most of the materials will be removed by means of machining. An effective machining method is consequently required.

2.3 Machining of titanium alloys

Titanium alloys exhibit poor machinability (in terms of the ease with which a metal can be cut) with ratings of < 0.3 compared to other engineering alloys such as steel (> 0.5), and aluminium (> 2) owing to inherent characteristics such as low thermal conductivity, high dynamic shear strength and ability to maintain high hardness at elevated temperatures [1, 28]. Traditionally, machine shops cut titanium at low cutting speeds (< 100 m/min) using W/Co carbide tools and feed rates ≤ 0.15 mm/rev. At higher cutting speed than the industry norm, cutting titanium becomes a challenge, resulting in low productivity of titanium parts and shorter tool life (< 10 min) [35-38]. Fig. 2-4 and Fig. 2-5 show the conventional machining range and feed rates used for the cutting of various engineering materials, including titanium.

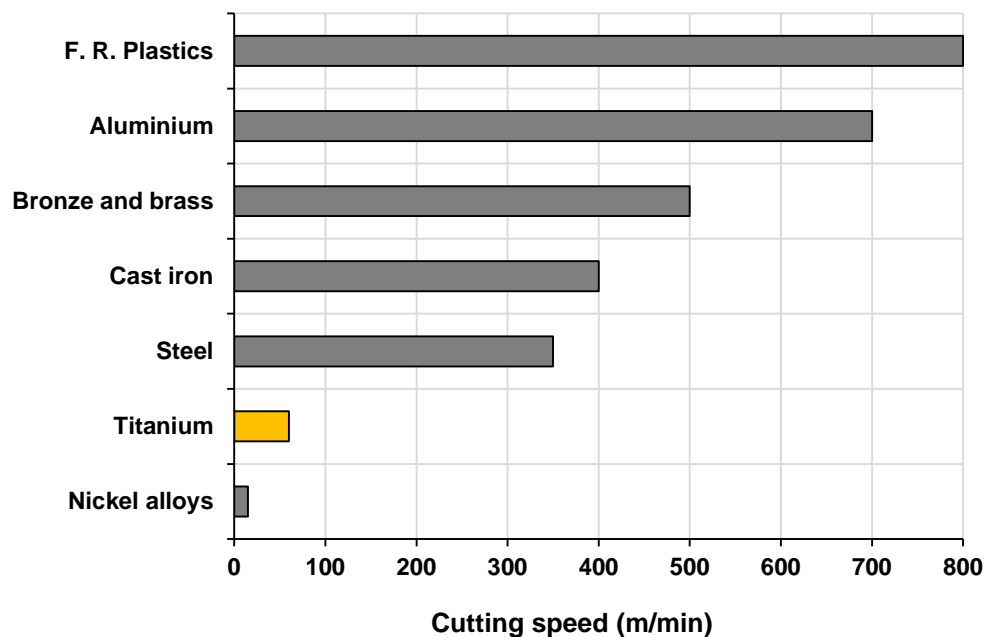


Fig. 2-4 Conventional machining range of various engineering materials [3]

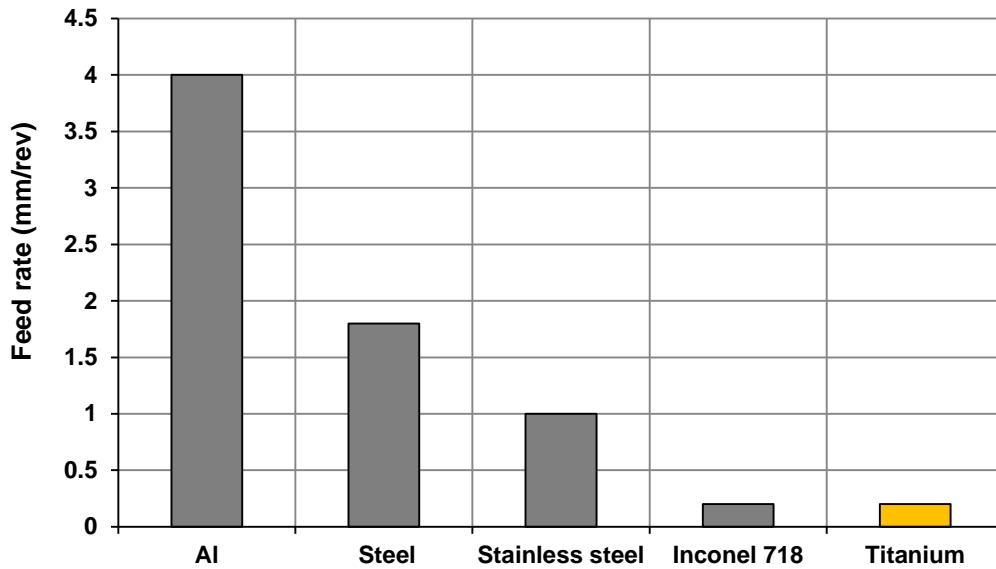


Fig. 2-5 Feed rate range used for machining of various engineering materials [39]

When classifying titanium alloys in ascending order in terms of their machinability, the alloys are beta, alpha-beta, near beta and pure alpha alloys. Titanium is chemically very reactive and, therefore, has an affinity to weld to the cutting tool material (particularly ceramics and high speed steels) during the cutting process at temperatures above 500 °C, hence leading to galling, smearing chipping, rapid tool wear and premature tool failure [1]. In fact, many of its properties work together to lead this metal to be categorised as a refractory material. These properties are:

- a) Titanium is a poor conductor of heat. Heat generated by cutting actions does not dissipate quickly due to low thermal conductivity (i.e. 7.3 W/m-K for annealed Ti-6Al-4V) compared with that of steel (60 W/m-K), which leads to the greater concentration of heat close to the cutting tool tip [40, 41], adversely influencing tool life.
- b) The peculiar work hardening of titanium alloys leads to the absence of Built-up-edge (BUE) in front of the cutting tool and an increase in the shearing angle, which in turn promotes a thin chip to contact a relatively small area in the cutting face, causing a high bearing stress per unit area. The high bearing load, combined with the friction between the chip and bearing area, promotes a significant heat rise in a narrow area of the cutting tool close to the tool tip, causing rapid tool breakdown.

- c) The low Young's modulus of titanium alloys (e.g. 110 GPa for annealed Ti-6Al-4V compared to steel (200 GPa) generates chatter, deflection and spring-back issues resulting in vibration and product geometry problems, particularly when machining small components.
- d) The high strength and hardness of titanium alloys (i.e. up to 360 HV for solution + aged Ti-6Al-4V) can also contribute to high cutting forces and temperatures that may lead to tool deformation and notching failure [42].
- e) Without cutting fluids, titanium alloys tend to react with common atmospheric gases N_2 , H_2 and O_2 , helping to form nitrides, hydrides and oxides respectively. These phases promote embrittlement and reduced alloy fatigue strength. Furthermore, reactivity with the cutting tool material induces the galling, smearing, cavities and chipping of the workpiece surface and rapid tool wear [1].

2.4 Heat generation when machining titanium alloys

Excessive heat and consequently wear formation are the key complications affecting productivity and performance when cutting titanium alloys. Heat can be generated due to contact between the tool-chip and workpiece material. During cutting operations, three main shear/deformation zones can be formed; namely, primary, secondary and tertiary deformation zones, as shown in Fig. 2-6. Heat generation particularly in primary and secondary shear zone are highly dependent on the cutting conditions. The heat generated by plastic deformation in the primary shear/deformation zone is transferred to the workpiece and chip under formation via conduction [27]. The secondary deformation zone transfers the heat to the cutting tool via the conduction of the frictional heat produced by chip-tool contact. The heat extracted by the chip can be transferred via conduction or convection, depending on the cooling method used (i.e. in dry or wet cutting). Unlike steel, titanium alloys generate excessive heat, particularly in the secondary deformation zone, due to the low thermal conductivity and specific heat capacity of titanium alloys (e.g. 522.5 J/kg·K for annealed Ti-6Al-4V) [43]. This promotes the concentration of heat generated mainly at the cutting tool tip, and a large proportion of the heat generated (i.e. 80%) is retained in the tool tip and about 20 % in the chip (see Fig. 2-7), which negatively

influencing the life of the cutting tool. Additionally, the heat in the tertiary deformation zone, which is the just-machined subsurface near the tool flank face, is transferred from the primary and secondary deformation zones. The heat in this zone implies the source of thermal residual stresses induced in the machining process [44].

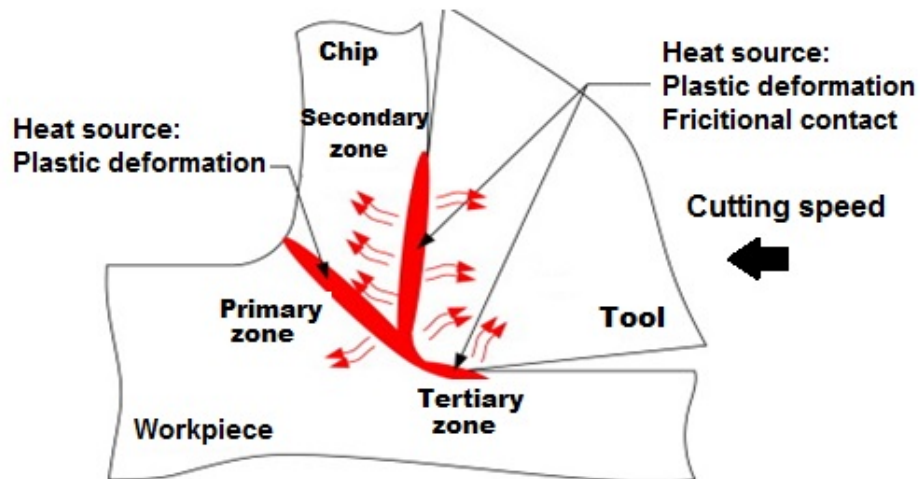


Fig. 2-6 Sources of heat in the machining zone [45]

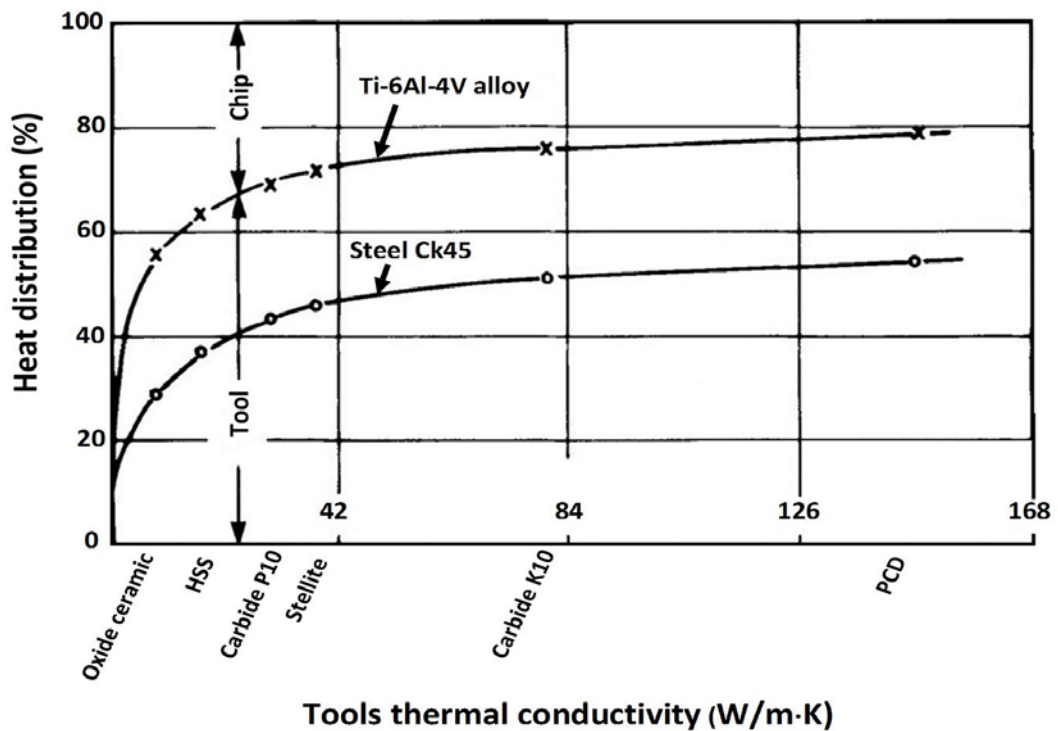


Fig. 2-7 Heat distribution in machining titanium using different tool materials [42]

2.5 Cutting tool materials for machining titanium

Presently, the machining industry mostly utilises WC/Co coated and uncoated cemented carbide tools for cutting titanium, which are thoroughly described in the next section. Other super-hard tool materials such as cubic boron nitride (CBN) and poly crystalline diamond (PCD) are also employed for cutting titanium at higher cutting speeds in excess of 300 m/min. However, they are not widely used due to their high cost [46]. Ceramic tool materials are not favourable for machining titanium in wet cutting conditions owing to their low fracture toughness and high reactivity with titanium [47]. Ezugwu et al.[48] proposed that improved tools need to demonstrate the following characteristics:

- High thermal conductivity and stability to reduce thermal shocks and thermal gradients
- High hot hardness to resist the high stresses involved
- Good fatigue and toughness resistance to withstand the chip segmentation process
- Good chemical inertness to suppress reactions with titanium
- High compressive, tensile and shear strength
- Sharp edges to resist rubbing and high stiffness for tool holder to compensate for the elasticity of workpiece material and to reduce vibrations.

2.5.1 Uncoated cemented carbide tools

Uncoated tungsten-based cemented carbide (WC/Co) is the most common cutting tool material used for machining titanium, particularly at low cutting speeds (< 100 m/min) [28]. These tools offer a combination of high hot hardness and toughness properties for limiting primary tool failure due to flank wear. Their properties are mainly based on the ratio of tungsten carbide to cobalt binder and the grain size of the compound. Commercially, uncoated carbides are available in two basic grades, straight and alloyed (mixed). Straight carbide grades are a mixture of 5 to 12 wt. % cobalt range and tungsten carbide (up to 94 wt. % WC), while the base composition of alloyed (mixed) grades may also contain tantalum carbide (TaC), titanium carbide (TiC), and other rare-earth elements. Mixed grade carbides with TaC are favoured for boring holes in titanium alloys, whereas, straight coarse grain (3.5 to 5 μm) carbide grades are preferred for heavy

interrupted cutting (e.g. milling, tapping, etc.), and the roughing of titanium alloys due to their combination of high cobalt content and improved fracture toughness [28, 49, 50].

2.5.2 Coated cemented carbide tools

Titanium alloys can be machined by coated tungsten-based carbide tools at cutting speeds up to 150 m/min [33]. The coating offers good thermal properties for the tool and a low coefficient of friction, hence minimising the cutting forces generated when cutting titanium. Additionally, coated carbides can enhance crater wear resistance because they have the ability to suppress the diffusion of tool particles into the chip at higher cutting conditions due to the formation of a protective layer saturated with tool particles [28]. Currently, most common coatings used in machining titanium are PVD (which refers to the physical vapour deposition coating technique) and CVD (chemical vapour deposition) coatings. The substrate temperature range of PVD coatings is 200-500 °C, while for CVD it is 800-1100°C. Typical coating materials used include TiAlNi, TiNi, TiC, TiCNi, ZrNi and TiB. CVD coating can be used in aggressive cutting conditions while PVD coating is used at lower cutting speeds. The average thickness of CVD coatings is much higher (5-10 µm) compared to PVD coating (2-5µm) [51, 52]. However, studies have concluded [39, 53] that these coatings are costly (15% more than uncoated tool costs) and have no merit when cutting titanium as the coatings will be removed (coating delamination) by the chemical crater wear anyway. Table 2-1 shows different tool materials and properties, including carbide tools.

Table 2-1 Properties of various cutting tool materials utilised in machining [44]

Properties	Units	W/Co Carbide	Ceramics	PCBN	PCD
Hardness Vickers	Gpa	≈ 1.8-2.1	≈ 1.9 - 2.3	≈ 2.7 - 3.8	≈ 7-8
Young's modulus	Gpa	520 - 630	300 - 380	580 - 680	766
Fracture toughness	Mpa/m ²	≈ 10 -17	3.5 - 6.5	≈ 3.7 - 7	≈ 6 -10
Transverse rupture strength	Gpa	≈ 2.0 - 2.8	≈ 0.5 - 0.8	≈ 0.8 - 1.3	≈ 1-1.5
Thermal conductivity	W/m·K	≈ 70 - 100	30 - 40	44 -100	≈ 520
Thermal expansion coefficient	10 ⁻⁶ K ⁻¹	≈ 4.5 - 5.3	7.5 - 8	4.6 - 4.9	4.2

2.6 Tool wear mechanisms in machining titanium

In the machining process, tool wear accounts for a significant proportion of the manufacturing costs of a product. Tool wear arises because of the chemical and physical interaction between tool and workpiece, resulting in a removal of small particles of the tool material from the cutting tool tip [54]. Tool wear takes place in three phases as shown in Fig. 2-8. When machining titanium; the abrasion wear mechanism is the major source of flank wear, particularly at low cutting speed, when cemented carbide tools are used, whilst adhesion, thermal diffusion, plastic deformation and oxidation wear are the most common tool damage mechanisms when cutting titanium at higher cutting conditions using uncoated and coated carbide tools. This is due to high cutting stress and the strong chemical reactivity between titanium and cutting tool materials at elevated cutting temperatures [55, 56]. It has been revealed that the maximum temperature in the tool-chip interface reaches 1400 °C when dry cutting titanium at a cutting speed of 120 m/min [30]. Rapid chipping and fracture also take place during the high-speed milling of titanium using carbide tools [57]. As for the influence of cutting fluid and its volume on tool wear behaviour, it has been found that applying cutting fluid to the cutting tool edge could significantly improve tool wear and minimise tool chipping effects [58, 59], while increases in fluid volume can profoundly enhance tool life owing to the higher cooling effect [60]. Fig. 2-9 shows images of different tool wear patterns generated by machining processes.

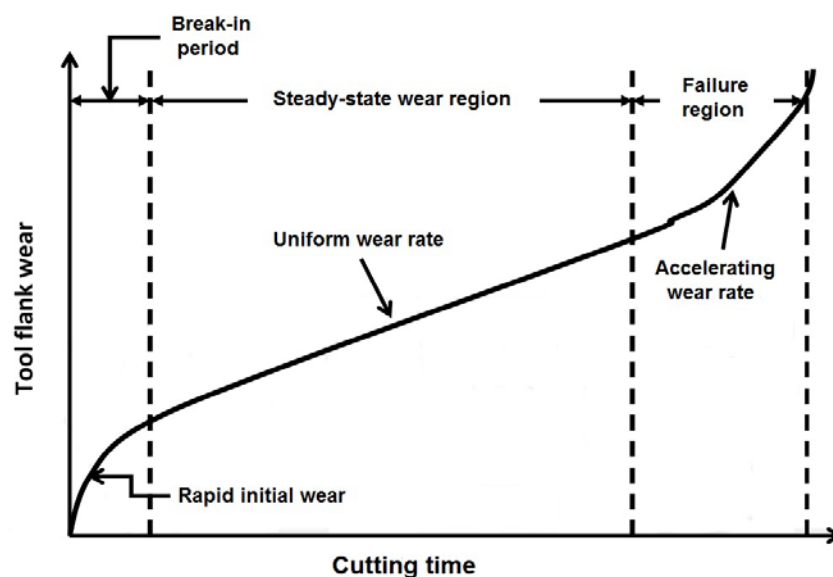


Fig. 2-8 Typical phases of tool wear in machining [54]

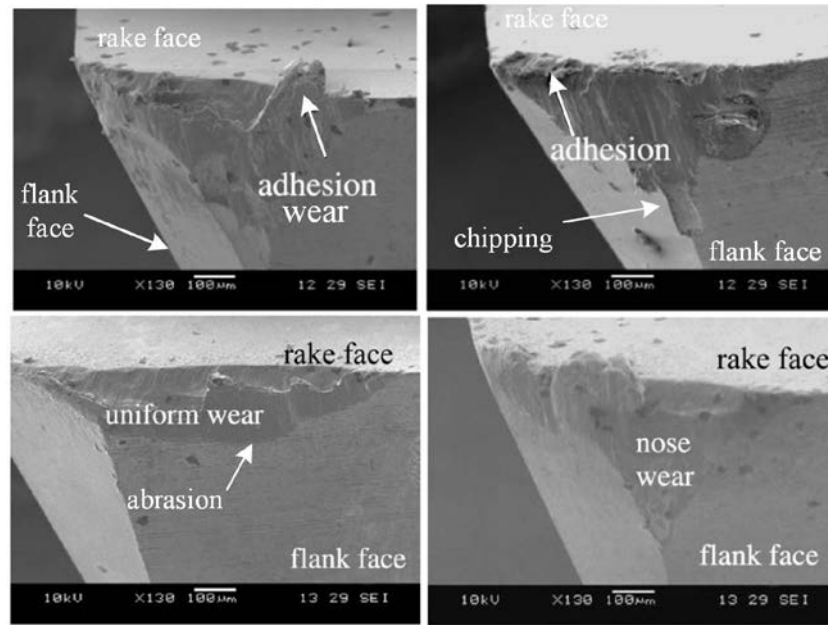


Fig. 2-9 Various tool wear patterns caused by a machining process [61]

2.7 Surface integrity in machining of titanium

Surface integrity is defined as the undamaged or enhanced surface condition of a material resulting from the effect of a controlled manufacturing process [54]. The surface integrity of titanium is of utmost priority with regard to high degrees of safety, particularly in the aerospace and aircraft industries. The investigation of failures demonstrates that the majority of failures (e.g. fatigue failures) are due to poor surface integrity of the machined parts such as high surface roughness along with high tensile stresses. Thus, surface integrity is crucial in machining operations [62]. Surface integrity induced by cutting titanium includes the anisotropic surface roughness, residual stresses, subsurface microstructure alterations, and micro-hardness. In addition, BUE, microcracks, redeposited material, plastic deformation, tearing, galling, and smearing are common types of surface damage in machining titanium [63].

2.7.1 Surface roughness

There are three key parameters in surface roughness: the arithmetical mean deviation of the profile (i.e. average surface roughness, R_a), the maximum height of the profile (R_{max}) and height of profile irregularities in ten points (R_z) as shown in Fig. 2-10. Machined

surface roughness strongly depends on factors such as cutting conditions including feed rate, cutting speed and depth of cut, tool wear, cutting fluid, cutting tool materials, and tool geometry. However, the influence on surface roughness (R_a) of feed rate is more significant when compared to other process parameters. It has been reported that surface roughness decreases with increased cutting speed, nose radius and decreased feed rate during the turning of Ti-6Al-4V using coated carbide tools [54]. Machining titanium using cutting fluid also reduces surface roughness by 44.44 % compared to dry cutting [63]. In addition, Ezugwu et al and Bakar et al. [48, 64] observed that surface finish was significantly affected by cutting fluid pressures and was below the threshold for critical applications (e.g. R_a 1.6 μm for aerospace components). Whereas Cai et al. [58] found that an increase in oil supply rate also had a positive effect on reducing surface roughness (up to 28.12%) when end milling Ti-6Al-4V under minimum quantity lubricant (MQL) cooling mode. It was also found that surface roughness increases with increased tool flank wear. However, this is not always the case, and Lopez et al. [33] pointed out that with the increase in cutting speed, surface finish first deteriorated and then improved with the tool wear progression in milling using a hard solid cutter mill. This surprising phenomenon is due to a flattening effect, which may be ascribed to the softening of the material being machined. In the same vein, it was revealed that an increase in the radial depth of the cut when milling titanium caused an increase in the value of surface roughness (up to 188.88 % at high cutting speed), while the axial depth of cut has little effect [65].

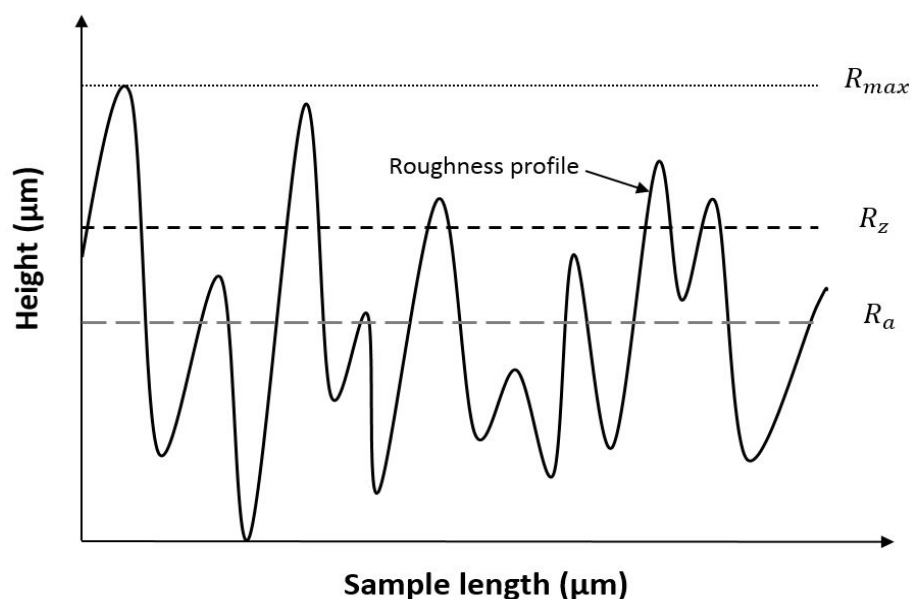


Fig. 2-10 Schematic illustration of a roughness profile of machined surface [66]

2.7.2 Micro-hardness

In machining operations, alterations in micro-hardness are often attributed to the influence of thermal, chemical and mechanical reactions. When the workpiece material is subjected to high cutting temperature and cutting pressure generated during machining, a competing process between work hardening and thermal softening takes place and affects the fundamental behaviour of the workpiece material. Moreover, the process of softening the sub-surface region can also be characterised by the effect of ageing on micro-hardness. The machined surface subjected to high cutting temperature during the machining process is similar to the ageing process. Additionally, when cutting titanium, the hardness just underneath the top layer of the machined surface was found to be lower than the base material nominal hardness owing to the thermal softening effect. However, when the depth beneath the top layer of a machined surface increases, the hardness values begin to increase before reaching their highest value and then declining gradually to the base material nominal hardness. The increase in micro-hardness is directly correlated to the effect of work hardening. This effect relies on many factors, such as temperature, the relaxation of internal stresses and cutting time [63, 67]. Hughes et al. [68] reported a reduction in micro-hardness (22%) below the machined surface (up to 60 μm) when cutting Ti-6Al-4V. In addition, Cantero et al. [69] found that the level of micro-hardness underneath the machined surface (50 μm) was 30% higher than that of the core nominal hardness when dry drilling titanium alloy. As for the impact of the cutting fluid on micro-hardness, Revankar et al. [70] discerned that wet machining under flood cooling had a positive effect when turning Ti-6Al-4V, by reducing the hardness value by 10.37%. This is attributed to a reduced friction coefficient and less heat generated in the machining zone due to the cutting fluid. Conversely, Antonialli et al. [71] found no significant disparity in micro-hardness values (always between 300 and 350 HV) during the finishing milling of Ti-6Al-4V under flood, MQL, and dry cutting conditions. This was possibly due to less shearing action generated by the tool in the finishing process.

2.7.3 Microstructural subsurface damage

Machining titanium is frequently associated with a change in grain deformation near the machined surface. The angle and depth at which the grains are deformed tend to decrease

with an increase in cutting speed [72]. Studies have shown that machining under dry conditions with a sharp tool can produce a thin distributed layer or plastically deformed layer immediately below the machined surface, while extended machining with a nearly worn tool can induce severe plastic deformation and a thicker distributed layer on the machined surface [69, 73-75]. Ginting et al. [76] attributed plastic deformation on the machined surface to the high cutting pressure at elevated temperatures in the dry cutting of titanium alloys. Conversely, Moussaoui et al. [77] concluded that no obvious defects and plastic deformation below the machined surface were observed during the dry milling of Ti-6Al-4V with coated carbide tools. With respect to the effect of cutting condition on microstructure, Hughes et al. [68] pointed out that depth of cut is the dominant factor affecting the microstructure, while others [73, 76] stress that cutting speed and feed rate are also factors which can govern microstructure. As for the influence of cutting fluid on microstructure, Ezugwu et al. and Antonialli et al. [71, 78] did not observe any subsurface microstructural alteration when machining titanium under wet cutting conditions (flood and HPC). However, these findings contradict those of a recent report by Edkins et al. [72], who observed a change in grain deformation below the machined surface (Fig. 2-11) when turning Ti-6Al-4V under flooded machining condition. It was discerned that the increased depth of cut promotes an increased deformation and larger deformation angles.

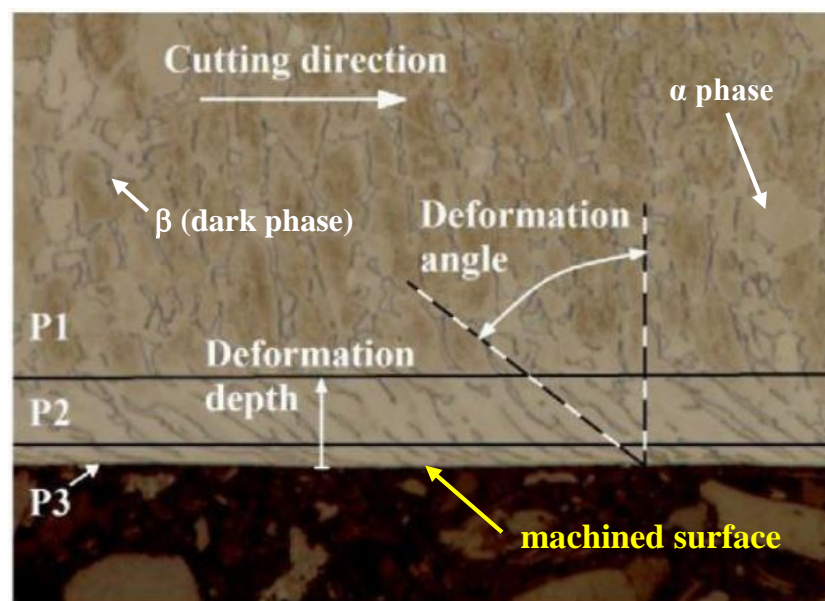


Fig. 2-11 Subsurface deformation regions: highly deformed grains (P3); moderately deformed grains (P2); and unaffected grains (P1) [72]

2.8 Chip formation and morphology in machining titanium

Chip morphology in metal cutting can be classified into continuous, lamellar, discontinuous and segmented chips. Continuous chips (known as uniform shear chips) are those which warp themselves around the workpiece, especially in the machining of ductile materials, while lamellar chips occur with highly ductile metals with increased strength, particularly at high cutting speeds [79]. Discontinuous chip formation takes place if the plastic ductility of the metal is very low, such as in the machining of cast iron with lamellar graphite. Segmented chips (also known as saw-tooth or serrated chips) result from the discontinuous formation of a chip with more or less connected elements yet with significant variations in the degree of deformation along the flow path [80]. Titanium alloys generally produce highly segmented chips at all cutting conditions owing to their thermal conductivity [48]. Three theories were proposed to explain the main reasons for chip segmentation. Firstly, segmented chip formation occurs due to a periodic (regular) crack initiation in the free surface of a workpiece because of high stress and the heat generated by friction. The cracks are then propagated inside the primary shear zone, leading to the separation of the material into two surfaces. Secondly, the formation of segmented chips takes place because of a catastrophic thermoplastic shear. This phenomenon occurs due to thermo-plastic instability owing to competition between thermal softening and work hardening in the primary shear zone, particularly at high cutting speeds. This promotes the formation of the shear bands [81]. Thirdly, the combination of the two first theories, where the cracking occurs along adiabatic shear bands at low cutting temperatures and strain rates $> 1 \text{ s}^{-1}$ [24, 82, 83]. Additionally, cutting speed is the main criterion for controlling chip segmentation, and the critical cutting speed at which a thermoplastic instability takes place has been proposed to be $\geq 9 \text{ m/min}$ [24]. Theoretically, the degree of segmentation (G_s) of titanium is also function of cutting speed (V_c), based on the equation $G_s = 1.34 \times 10^{-2} \times V_c^{0.56}$ [84]. Conversely, Sun et al. [85] underlined that segmented chip formation causes cyclic cutting forces and tool chatter. Fig. 2-12 shows segmented chips of Ti-6Al-4V at various cutting speeds. As for the effect of cutting fluid and tool geometry on chip formation, reduced chip size and improved chip breakability were observed mainly when high pressure fluid was applied [64], while cutting tool rake angle, and cutting tool radius have less impact on chip segmentation [86].

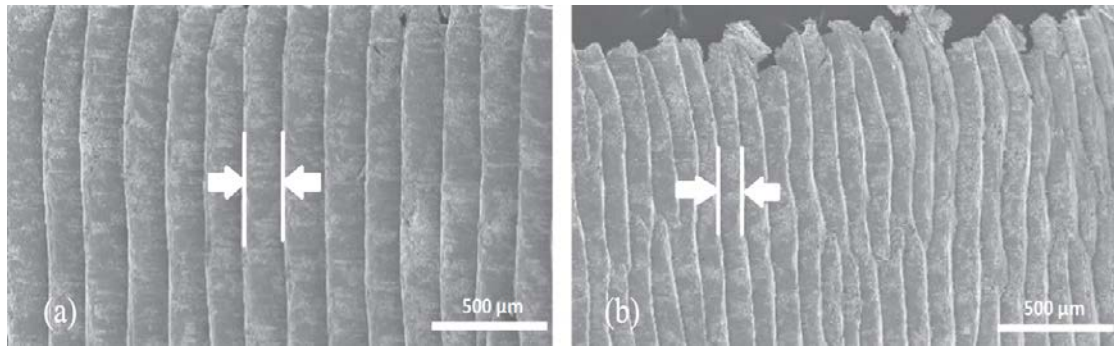


Fig. 2-12 SEM images showing various segmentation distance when turning Ti-6Al-4V at a cutting speed of: (a) 50 m/min; and (b) 150 m/min [79]

2.9 Cutting fluids in the machining industry

Manufacturing by machining has flourished due to use of cutting fluids. In 1907, F. Taylor reported that cutting speed could be increased by up to 40% without reducing tool life by delivering ample amounts of water to the machining zone [87]. Despite its high thermal capacity and availability, however, water is considered a poor lubricant leading to serious corrosion issues for machine tool components and machined parts. Since then, new formulations of cutting fluids have been developed to cover most workpiece materials and metal cutting processes [88, 89]. Petroleum/mineral oil-based, semi-syntactic (semi-chemical) and syntactic (chemical) fluids are widely used on machining shop floors in order to increase productivity and the quality of manufacturing processes by cooling and lubricating during metal cutting and other metal forming operations. Cutting fluids could effectively improve tool life, produce better dimensional accuracy and good machined surface quality. They also help to dissipate heat and transport chips away from the machining zone, minimising BUE, and protecting machined components and machine tool parts from corrosion [16, 90].

Due to their advantages, the consumption of metal cutting fluids is increasing in the machining industry. It has been estimated that the global consumption of cutting fluids is about 38 million metric tons, with an expected increase of 1.2 % over the next decade [5, 10]. Cutting fluids can also contribute significantly towards machining costs. For instance, it was estimated that the costs relevant to cutting fluids represent up to 17.9 % of total manufacturing costs in the European automotive industry, which compares to tooling costs of about 7.5%, as shown in Fig. 2-13 [9].

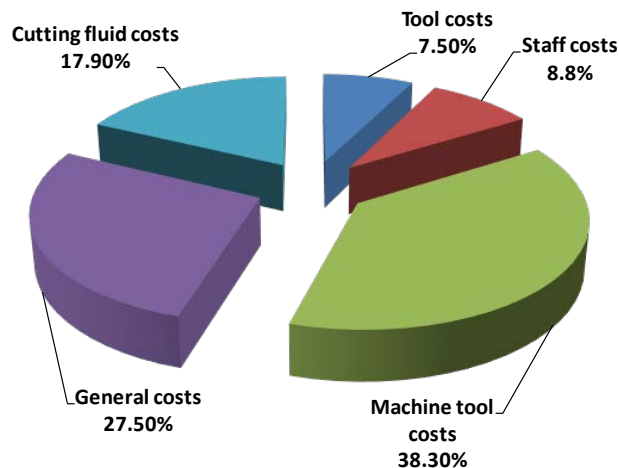


Fig. 2-13 Distribution of manufacturing costs in the European automotive industry [9]

However, the misuse of cutting fluids increases their disposal and maintenance costs (about up to 59 % of total fluid costs) [9], particularly when non-biodegradable conventional fluids are used. This is mainly due to the high content of toxic ingredients such as chemical agents (to control bacterial and fungi growth), hydrocarbons, and extreme pressure (EP) additives (to prevent seizing or to reduce it at high pressures and temperatures) [91]. Thus, extra treatment prior to disposal is required [5]. Additionally, the selection of cutting fluids depends on many factors, such as the machining process used, workpiece materials, and methods of supplying it [16].

2.9.1 Function and action of cutting fluid in machining processes

Cutting fluids perform two key functions in machining operations: lubrication at relatively low cutting speeds (to reduce the heat generated by friction) and cooling at relatively higher cutting speeds (to increase heat dissipation from the machining zone) [6]. To fulfil such functions, the fluids should demonstrate a number of tribological and thermal properties [92]. As a coolant, the cutting fluid can reduce the distortion of the workpiece material, particularly at high cutting speeds and temperatures. The ability of a cutting fluid to maintain the temperature below the thermal softening temperature of the tool material significantly extends its tool life. In addition, it reduces thermally induced tool wear; for instance by adhesion and diffusion. In high-speed machining, the cutting fluid strongly relies on its thermal properties and appropriate wettability, such as having a high specific heat coefficient and low surface tension to ensure its capacity to transfer a

large amount of heat from the machining zone and to maintain a high degree of fluid contact with the tool/chip and workpiece material [93]. As a lubricant, it minimises friction and wear in the machining zone, and thus the heat generated by frictional force and wear is also reduced. In low-speed machining with sliding friction, the lubricity (lubricant viscosity) of the cutting fluid helps to reduce the rake-face frictional force and thus increases the shear angles. Consequently, thinner and tightly curled chips are produced, decreasing the temperature in the shear zone as well as minimising power consumption in the machining operation. It is recognised that low-speed machining can benefit more from lubricity than cooling. The lubricating action of a cutting fluid, as described in the next section, in low-speed machining can prevent the formation of BUE and improve the surface integrity of machined parts [23, 94]. However, lubricant-based fluids are not effective at high cutting speeds due to their vaporisation at high temperatures before they can reach the machining zone [95]. To understand the action of cutting fluids, Astakhov [9] et al. suggested a model with 3 phases of the chip formation cycle, as shown in Fig. 2-14. The action of the cutting fluid can be summarised as follows. Firstly, lubrication is provided between the chip and the rake face at point A in all phases. Secondly, lubrication is afforded between the two chip elements sliding over each other at B in Phase 1, while offering to cool the free surface of the partially formed chip at the same zone (B) in phases 2 and 3, and at the same time reducing its plastic deformation and thus the chip compression/thickness ratio (t_0/t_c) in phase 3. Thirdly, the zone of plastic deformation at C is cooled and thus the flow shear stress in this zone in phase 1 is limited. Meanwhile cooling the zone of plastic deformation at C and E increases the flow of shear stress of the workpiece material (phase 2) and propagation of cracks promoted in phase 3. When the cutting fluid penetrates into the crack formed in the chip's free surface, it suppresses the above-discussed healing of these cracks. Finally, the lubrication and cooling of the flank-workpiece interface is achieved at D in all phases [96]. Additionally, when the cutting fluid is applied by the conventional flooding of the machining zone, its weakest action is observed at A and D. The relative effect of the cutting fluid action here significantly depends on the frequency of chip formation and thus on cutting speed. The higher the cutting speed, the lower the viscosity of the cutting fluid should be in order to penetrate into the aforementioned cracks formed on the chip's free surface [97]. This clarifies why emulsions of soluble oils with low viscosity are more efficient at high cutting speeds compared to straight oils.

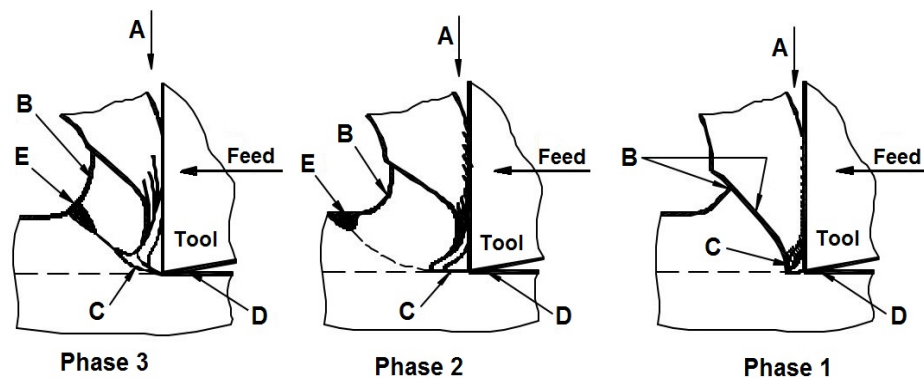


Fig. 2-14 Cutting fluid action at various phases of a chip formation cycle [9]

2.9.2 Types of cutting fluid and their properties

Previously, cutting fluids were considered as simple oils applied with brushes to cool and lubricate machined parts and machine tools. As cutting processes became more rigorous, the formulation of cutting fluids also became more complicated. Different approaches can be adopted to classify cutting fluids based on their properties and applications. El Baradei [6] and Debnath et al. [16] classified cutting fluids into three major categories, as shown in Fig. 2-15. All have different advantages and drawbacks, and the following sections present brief overviews of these types of fluid.

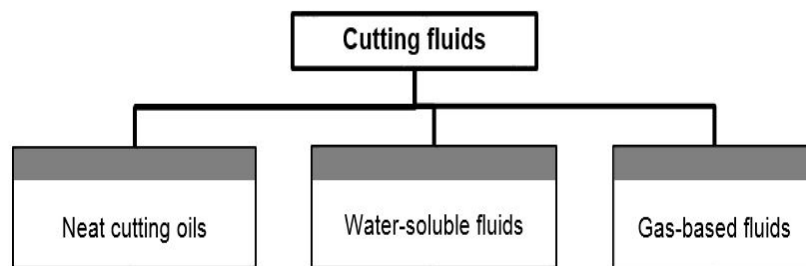


Fig. 2-15 Classification of cutting fluids [16]

2.9.2.1 Neat cutting oils

Neat cutting oils (straight oils) are often used as pure oils; mainly they are derived from minerals (petroleum-based), or vegetable or animal base oils. Conventional mineral oils are the most common neat oils employed on machine shop floors. Usually, these fluids contain particular additives to improve their lubricity. The characteristics of paraffinic

and naphthenic mineral oils can be enhanced through the addition of extreme pressure (EP) additives, fatty lubricants, odorants, thickness modifiers, and polar additives. High lubricity, anti-seizure properties and rust and corrosion control are the main advantages of neat oils. However, they offer poor cooling ability due to their low specific heat capacity of $\sim 2.10 \text{ J/g}\cdot\text{K}$ and a thermal conductivity approximately one-third that of the water [98]. High flammability and mist and smoke formation at high cutting speeds are also among the principal limitations. Hence, neat oil lubricants are more preferred in low-speed machining operations such as threading, tapping, broaching, gear hobbing and deep hole drilling where the main consideration is lubrication [6, 16, 91, 95].

2.9.2.2 Water-soluble cutting fluids

Water-soluble (water-miscible) fluids are a kind of cutting fluids containing an emulsifier to mix oil in water. Usually, these fluids are formulated from two substances (i.e. water and oil) that have a combination of good cooling and lubrication properties which makes them preferable to neat oils at high cutting speeds and low cutting pressure [6]. In addition, water-soluble fluids can be classified into three main categories, namely emulsifiable oils, and synthetic (pure chemicals) and semi-synthetic (blended chemicals and oils) fluids as shown in Fig. 2-16.

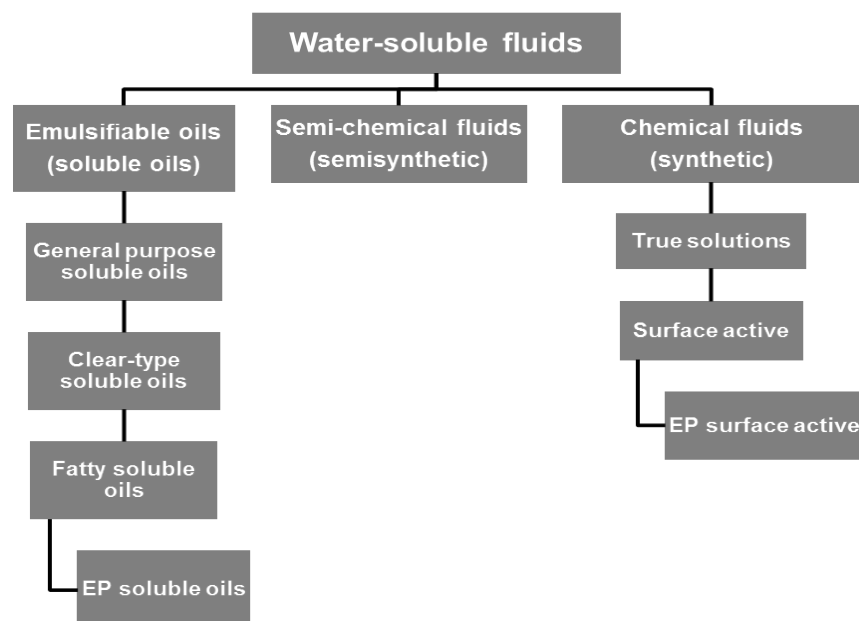


Fig. 2-16 Categories of water-soluble cutting fluids [6, 16]

Emulsifiable oils (soluble oils)

These kind of cutting fluids are oil-based concentrates, which consist of emulsifiers such as soap, wetting agents and couplers. The foremost function of emulsifiers is to disperse oil in water in order to form a stable milky-white emulsion. The stability of the emulsion is the key property of soluble oils [99]. Emulsifiable oils combine the lubrication and rust control characteristics of oil with water's outstanding cooling properties [6]. Soluble oils also contain additives similar to those found in neat oils to enhance their lubricating characteristics, particularly at severe working conditions. Emulsifiable oils are often employed at high cutting speeds with low cutting pressures where the heat rise is significant [17]. Water-soluble/miscible cutting fluids have a combination of good lubricity and cooling ability, low to moderate viscosity and thus adequate wettability, and lower flammability. However, rancidity, misting, growth of bacteria and low stability are the major drawbacks of this kind of cutting fluid [91]. Additionally, water-soluble cutting fluids require frequent checking if their performance is to be preserved. The concentration of the emulsion is unstable over time, and needs regular monitoring and replacement as water evaporates. Portable refractometers are often used for this purpose. Soluble oils are, in turn, sub-divided into four main categories as follows:

- Emulsions (i.e. milky fluids) with oil droplets of diameter $< 200 \mu\text{m}$. They are usually blended at a concentration up to 1 litre of base fluid to 40 litres of distilled water for general purpose machining
- Clear-type fluids with less oil use a higher proportion of rust inhibitors and substantially more emulsifier compared to the milky emulsions. These oils are commonly employed for grinding and light-duty machining.
- Fatty oils blend animal or vegetable fats/oils or other esters with mineral oils to provide a wide range of fluids with superior lubricating properties.
- Extreme pressure (EP) oils are fluids intended to prevent or reduce seizing at high cutting conditions of pressure and temperature, and are commonly known as extreme pressures (EP) additives. They usually contain chlorine, sulphur or phosphorous additives to withstand working conditions with high load. EP soluble oils are often employed for heavy-duty machining operations [6].

Semisynthetic fluids

Semisynthetic or semichemical cutting fluids are a mixture of chemical fluids and emulsifiable oils in water with concentration ratios up to 30% of the base fluid. Thus, they can combine some of the best qualities of chemical fluids and emulsifiable oils, with superior lubricating characteristics compared to synthetic fluids [6, 95].

Synthetic fluids

Synthetic fluids are completely chemical fluids consisting of inorganic and/or other materials dissolved in water with free mineral oils. Chemical agents can also be added to synthetic oils, for instance, amines and nitrites for rust control, phosphates and borates for water softening, nitrates for nitrite stabilization, and soap and wetting agents for lubrication and to reduce surface tension. Synthetic cutting fluids have high cooling ability. However, they are considered to be poor lubricants due to a lack of oiliness. Consequently, they are restricted to grinding operations where cooling is a priority. Synthetic fluids are in turn sub-divided into three main groups [6, 16] as follows:

- True solutions are chemical solutions without wetting agents containing highly-developed corrosion inhibitors. True solutions are used at dilutions in the range 1:50 to 1:100 for grinding operations for ferrous metals.
- Surface active fluids contain mainly water-soluble rust inhibitors and surface active load-carrying additives. They are employed at concentrations of 1:10 to 1:40 in grinding and cutting operations for both ferrous and nonferrous metals.
- EP surface active fluids have similar surface active solution properties as extreme pressure additives (EP). They are employed at concentrations of 1:5 to 1:30 for heavy machining operations.

2.9.2.3 Gas-based fluids

Air, liquid nitrogen (LN₂), carbon dioxide, argon and helium are generally considered as attractive biodegradable gas-based lubricants or cutting fluids. They can be either in gaseous form or in cooled–pressured fluids in cutting operations. They have high rust resistance and oxidation control at high cutting temperatures. In addition, gas–based

fluids can be employed in combination with conventional cutting fluids in the form of mists or minimum quantity lubrication (MQL) to enhance their lubrication performance. Gas-based fluids are superior for heavy machining conditions where conventional cutting fluid supply techniques fail to penetrate the chip-tool interface. For instance, LN₂ at -196 °C is used as a cutting fluid for refractory materials where chip formation and chip breaking is a substantial issue. However, some of these gas-based fluids, such as LN₂, helium, argon, are costly as cutting fluids and have limited application in the machining industry [91, 100].

Now that all major types of cutting fluids have been discussed, attention turns to the ecological effects of conventional cutting fluids in the next section.

2.9.3 Ecological effect of conventional cutting fluids

The use of conventional cutting fluids is potentially hazardous. Around 85% of the fluids used globally are petroleum/MO-based fluids [101]. These fluids are involved in ecological cycles with air, soil and water and their toxicity effect may damage ecosystems (see Fig. 2-17). Approximately 32% and 13% of all fluids used in the US and EU respectively are disposed to the environment [102]. Thus, most of these fluids require additional treatment before disposal [103]. It was estimated that most large manufacturing plants usually spend €1.5 million/year on replacing cutting fluids [104]. In addition, when these fluids evaporate and disperse as vapour and microparticles, they may cause serious health issues such as respiratory diseases and breathing disorders [8, 16]. It was reported that about 80% of all occupational diseases of machine tool operators were due to direct skin contact with conventional fluids [105].

Additionally, as cutting fluids are complex in their composition, they may be irritants or allergenic and suspected carcinogens. Microbial toxins can also be produced by aerobic or anaerobic bacteria and fungi present particularly in emulsion fluids, which can pose another threat to worker's health [5, 106]. For these reasons, more attention has been paid to VO-based fluids as favourable alternatives to their MO-based fluid counterparts, due to their high biodegradability offering a healthier working atmosphere and less environmental impact. It was estimated that the anticipated global demand for VO-based fluids will increase by 58% in 2018 compared to 2011 [16].

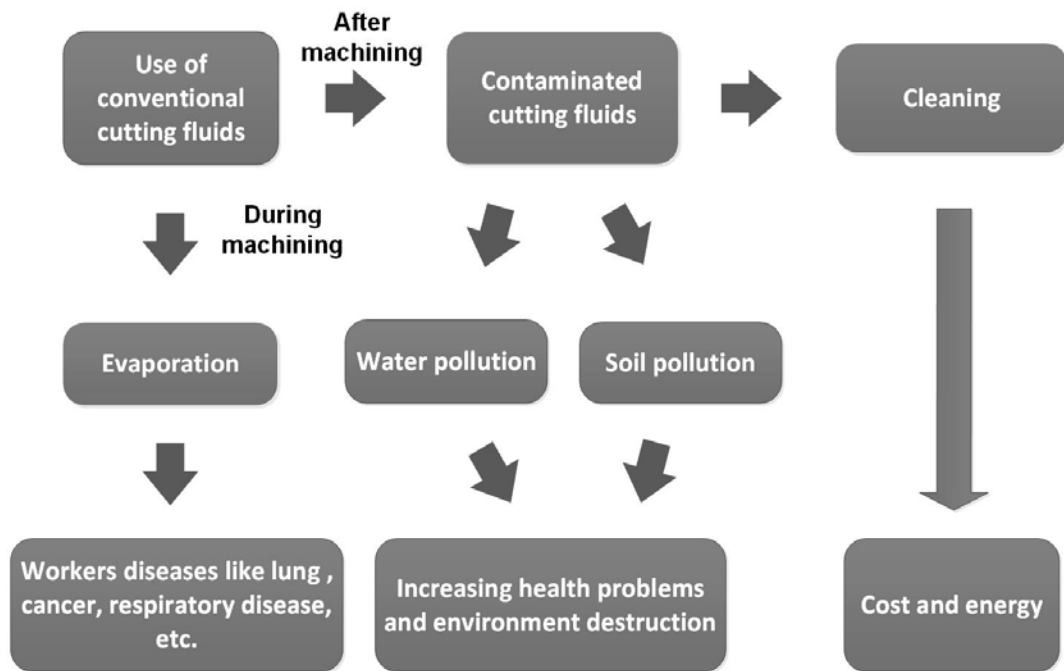


Fig. 2-17 Conventional fluids life cycle and their ecological impacts [107]

2.9.4 The need for vegetable oil-based fluids in machining

Cutting fluids made of biodegradable VO are appropriate alternatives to conventional fluids. The outstanding features of VO base stocks rely on their unique chemical structures. The majority of VO base stocks primarily consist of triglycerides, which are glycerol molecules with three long-chain fatty acids affixed to the hydroxyl groups through ester bonds [10, 108, 109]. The fatty acids in natural vegetable oils have varying chain lengths and numbers of double bonds. The composition of a fatty acid can be defined by the ratio and position of carbon-carbon double linkages. The long carbon chain is generally held together with one, two, or three double linkages in oleic, linoleic, and linolenic fatty acid components respectively [16, 101, 110].

Fig. 2-18 shows the different types of vegetable oil fatty acids. It has been recognised that the triglyceride structure provides desirable qualities for boundary lubrication. This is attributed to their long and polar fatty acid chains, which afford good tribological properties [111, 112]. In the same vein, the polarity of fatty acids generates oriented molecular films which provide oiliness and impart anti-wear properties. Thus, it is believed that the fatty acids are the key elements with regard to lubricity [113, 114].

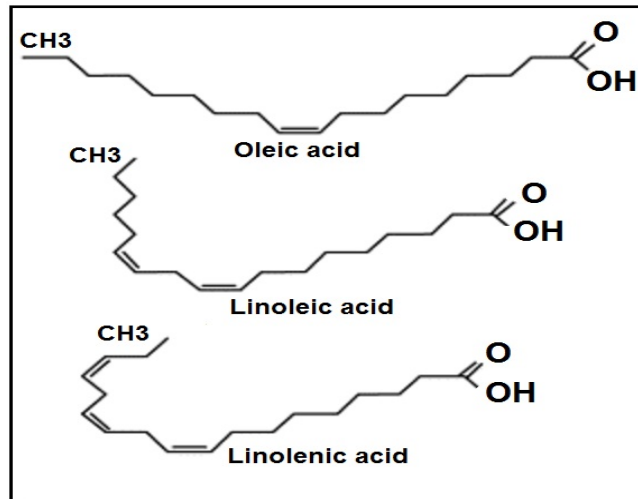


Fig. 2-18 Chemical structure of various VO fatty acids [16]

Additionally, there are other distinctive physical and chemical properties of VO which allows it to demonstrate sufficient lubricating and cooling capacity in machining operations. These properties are as follows:

- The polar heads of VO molecules have a great chemical affinity to metal surfaces and adhere themselves tightly as little magnets (see Fig. 2-19) compared to the non-polar molecules of mineral oils as shown in Fig. 2-20. Thus, VOs have more molecular dipolar attractions at the surfaces than MOs to reduce friction and heat. The natural homogeneous orientation of VO molecules affords a dense, durable and vigorous film layer of lubricant, which provides a greater load carrying capacity [115].

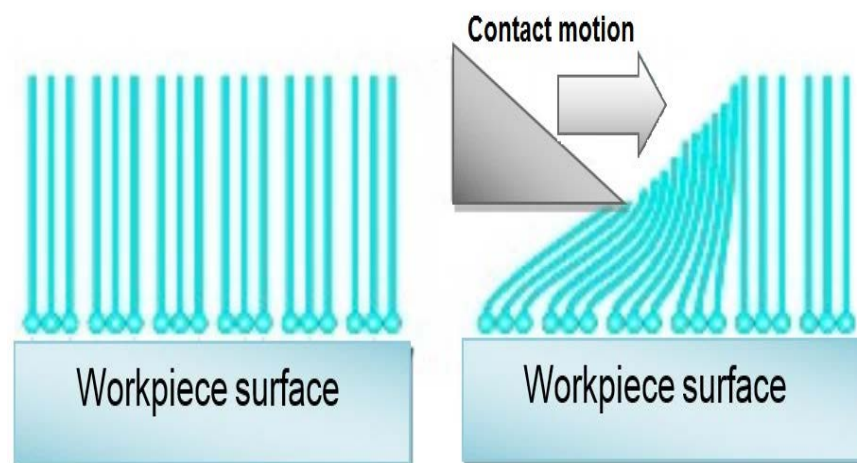


Fig. 2-19 Shape of well-arranged polar heads of VO's molecules [115]

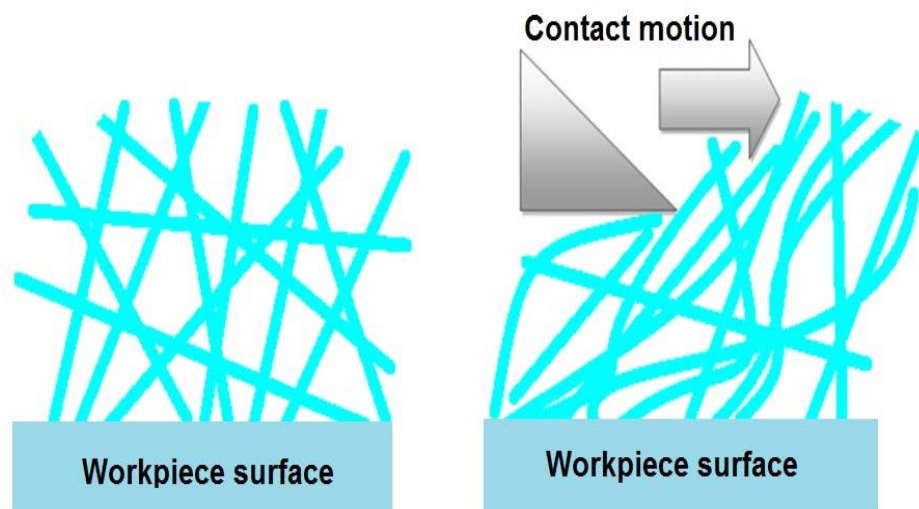


Fig. 2-20 The random alignment of MO's non-polar molecules [115]

- VO base stocks have a high natural kinematic viscosity and viscosity index (e.g. 40.05 cSt for sunflower at 40°C and 206) compared to mineral oils (20.06 cSt at 40°C and 103) respectively. Meanwhile with increases in cutting temperature, the viscosity of VOs drops more gradually than for MOs. As temperature decreases, VOs remain more fluid than MOs, enabling faster drainage from the machining zone. The higher viscosity index (i.e. change of viscosity with variations in temperature) of VOs ensures that they will provide more stable lubricity across the operating temperature range [116-118].
- Vegetable oil fatty acids such as stearic acid have a significant influence in reducing friction. A lubricating sliding friction test was carried out on a VO-based fluid (Soybean oil) and an MO using a load of 4 N for 400 min. The results revealed that the VO-based fluid generated a lower coefficient of friction (0.03) compared to 0.07 for the MO-based fluid [116].
- VOs have a higher flashpoint (e.g. 252°C for sunflower oil) than MO-based fluid counterparts (e.g. 189 °C for paraffinic oils), which minimises smoke formation and the fire risk. Thus, they offer a safer work environment with less lubricant wastage [119].
- Vegetable oils have a high rate of degradation with less toxicity. A biodegradation test (measuring the transformation of organic carbon in CO₂ under aerobic and composting conditions) has been performed without light at 25°C for four weeks. The results showed that pure rapeseed and synthetic ester oils exhibited 100 %

biodegradability, whereas for MO-based oils it was up to only 40 % biodegradability [120, 121].

- Vegetable oil base stocks have superior cooling ability owing to their high heat conductivities (up to 0.172 W/m·K) [122] compared to a value of 0.125 W/m·K for an MO [20]. This is crucial for dissipating heat from the machining zone.
- VO fatty acids such as oleic fatty acid have the ability to penetrate surface interstitial cracks and fissures to a certain depth and help to reduce the strength of the workpiece material [123]. Table 2-2 summarises the key properties of both MO and VO base stocks.

Table 2-2 Key properties of VO and MO base stocks [124]

Properties	VO base stocks	MO base stocks
Biodegradability	High	Low
Lubricity	High	Medium
Viscosity index (VI)	200	100
Hydraulic stability	High	High
Thermal conductivity	High	Relatively low
Toxicity	Low	High
Oxidative stability	Low	High
Corrosion protection	Poor	Good
Polarity	High Polar	Low Polar
Flashpoint (°F)	450	200
Pour point (°F)	-35	-35

2.10 Cutting fluids supply systems used in the machining industry

An adequate understanding of cutting fluid supply methods and techniques in machining operations is needed if friction and heat generation are to be controlled. Presently, several cooling techniques have been developed and introduced to control the temperature in the machining zone in order to improve productivity and to increase the overall performance of cutting processes. Sharma et al. [4] has categorised cutting fluid supply systems or techniques into seven major groups, as shown in Fig. 2-21.

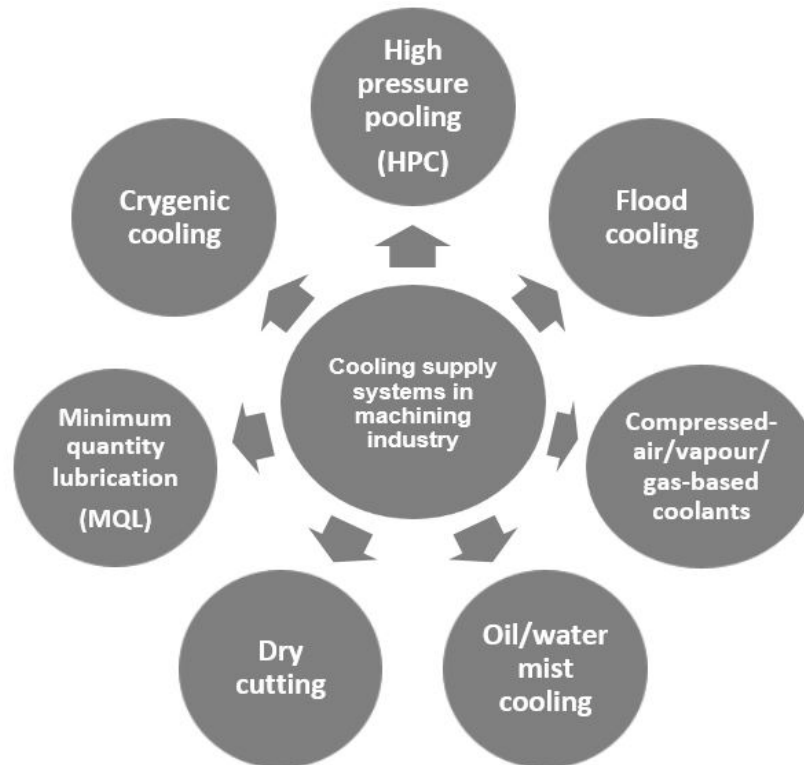


Fig. 2-21 Cutting fluid supply systems used in the machining industry [4]

2.10.1 Conventional flood cooling

Conventional flood cooling systems are the most widely used cutting fluid supply systems in standard machining operations. Flood systems introduce copious amounts of cutting fluid into the machining zone via traditional randomly positioned sloped nozzles (see Fig. 2-22). Cutting fluids are delivered under low pressure of <10 bar with flow rates up to 225 L/min (for multiple cutters) [17]. The main merits are that this helps to reduce the heat transferred to the workpiece material during cutting and also reduces part distortion as well as controlling chip flow. However, high fluid consumption, and low penetrability particularly at high cutting speeds (due to forming a high temperature vapour blanket that renders the coolant ineffective) and a failure to control the fluid stream at localised heated zones (see Fig. 2-23) are the main disadvantages of this type of supply system [14]. Additionally, according to Diniz et al. [125] good cooling performance can be achieved when the cutting fluid stream is applied to the rake and flank faces simultaneously, such as in turning processes, and this requirement cannot be properly achieved by flood cooling where the fluid is often flooded from the chip side (i.e. the rake face). The cutting tip,

therefore, experiences a great thermal load, resulting in rapid tool wear and shorter tool life [19].



Fig. 2-22 Image of conventional flood method [126]

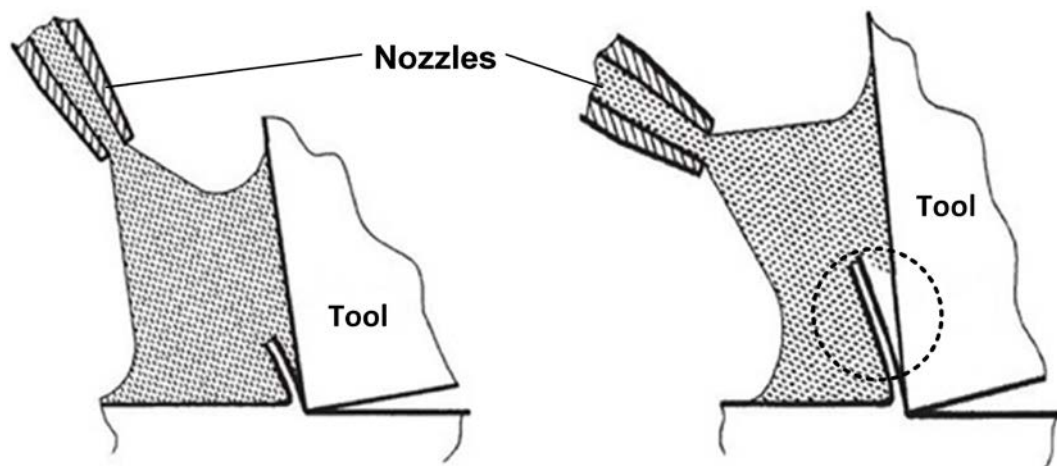


Fig. 2-23 Random directional effect of the fluid stream in a flood supply system [19]

2.10.2 High pressure cooling (HPC)

The main function of high-pressure cooling (HPC) is to increase the heat dissipation rate from the machining zone, where high temperatures become a significant factor in the increase in cutting speed and power. In this method, the cutting fluids are applied under

high pressure up to 200 bar through customised nozzles to provide a powerful jet of fluid into the machining zone [20]. The fluid pressure force in the HPC system offers superior penetration ability of the cutting fluid into the tool-workpiece and tool-chip contact regions, thus increasing tool life and reducing tool wear. In addition, HPC generates discontinuous chips which are small and easy to remove, where they are hydraulically lifted up from the tool rake face and transported away from the machining zone. However, high fluid consumption (up to 75 L/min) and the high costs of the pumping system as well as the filtering equipment for microparticles $< 20\mu\text{m}$ associated with this supply system are the main limitations [4, 127].

2.10.3 Mist cooling

Cutting fluids with the base fluid often being oils used in this technique are supplied at 0°C by a pressurised air stream up to 6 bar. The fluid droplets of about $20\mu\text{m}$ in size then evaporate and are distributed as a mist and microparticles which provide effective cooling. Fluid is supplied to unreachable zones with good visibility during the machining operation if compared to flood cooling [128]. However, one study [129] has reported that neat mineral oil mists help fluid ignition better than water-miscible fluids, particularly in grinding operations. In addition, mist cooling requires proper ventilation systems to avoid the inhalation of toxic airborne fluid particles. High-speed machining with oil mist is very dangerous compared to in low-speed machining processes due to the copious amounts of mist produced, and it thus poses a serious health hazard [130, 131].

2.10.4 Compressed air/water vapour/gas-based cooling

In this technique, water vapour or compressed cold air or gases such as N_2 , O_2 and CO_2 are delivered under pressure up to 5 bar and directed into the machining zone via a customised nozzle located on the tool holder. These gases provide cleaner working environment with less waste to assist in metal cutting operations. The application of these gases can show reductions in cutting force and average surface roughness by 33.33% and 15% respectively compared to dry and wet cutting. In addition, gas-based fluids create the highest shear angles, and this could be a reason for the lower cutting forces [132]. Furthermore, water vapour cooling shows superior cutting performance compared to

other gases due to its ability to form a boundary-lubricating layer generated by the high velocity jet flow. It has been reported that the water vapour supply method produces lower cutting force by 20-40% and 10-15% compared to dry cutting and flood cooling respectively during the turning of AISI 1045 steel [4]. However, gas-based fluids have inferior lubrication effects due to the absence of oiliness, and they also promoted more rapid tool wear at higher cutting speeds since the generated heat surpasses the cooling effect of the gases [133]. Additionally, the high cost of consumables and equipment associated with these systems, including LN₂, water vapour generators, heaters, and tubing, restricts their application in machining operations [134].

2.10.5 Minimum quantity lubrication (MQL)

This method is often referred to as near-dry lubrication or micro-lubrication. MQL was introduced as a feasible alternative to conventional flooding cooling [135]. The main concept of MQL is that it applies a fine mist of air-fluid mixture containing a small quantity of cutting fluid to the machining zone via a targeted specially designed nozzle, unlike in traditional nozzles where air and oil are mixed inside the nozzle. The pressure used in this application is up to 6 bar and the nozzle exit diameter is approximately 1mm with flow rates ranging from 10 to 500 mL/h. MQL systems offer low oil consumption (in mL/h instead of L/min) compared to flood supply systems and they commonly use biodegradable lubricants such as VO-based fluids. [130]. Neat vegetable oils and synthetic ester oils are preferable cutting fluids in MQL machining techniques due to their biodegradability and superior lubricating properties [4, 16]. It was reported that MQL could significantly reduce the frictional cutting force by 24.4 % and 32.2% at low cutting speeds compared to dry and flood cutting conditions respectively. MQL also showed significant wear reduction when the mixture was applied to the tool flank face rather than the rake face. However, most studies [136-141] consider MQL as a lubricating system rather than a cooling system, which limits its application in the machining of common hard and refractory materials such as nickel-based and titanium alloys where heat dissipation is a priority. Additionally, MQL machining often generates harmful fluid aerosols due to the spraying mechanism associated with mist application [5]. The machining of highly ignitable materials such as magnesium alloys is also extremely dangerous using MQL [130].

2.10.6 Cryogenic cooling

Cryogenic cooling systems often supply liquid nitrogen (LN_2) at -196°C to the cutting tool tip to reduce the temperature and thus maintain its level below the softening temperature of the tool material. The supercooled liquid nitrogen absorbs the heat generated during cutting and evaporates rapidly, producing a form of fluid-gas film between the chip and the tool face that acts as a lubricant [21]. Improved surface finishes with this method are attributed to decreased diffusion wear and less degraded tool hardness at lower temperatures [142]. In addition, this method uses safe, non-combustible, and non-corrosive gas (i.e. nitrogen is lighter than air and has a share of 78 % in the atmosphere) and affords clean chips that can be recycled easily as metallic scrap. However, applications of cryogenic cooling are very critical in terms of flow rate and the pressure supplied. The over-cooling of machined parts may lead to poor part accuracy and additional cutting force, resulting in embrittlement of the workpiece material [4]. Cryogenic cooling is beneficial in low-speed machining rather than at high speed because at lower speeds the tool-chip contact has a tendency to become fully elastic, which in turn allows greater penetration of the cryogenic stream into the hottest spot at the chip-tool interface. On the other hand, the high set-up costs and equipment (e.g. cryogenic nozzles, control valves, and cryogenic Dewar) of these systems make them uneconomical for standard machining processes [143, 144]. Fig. 2-24 shows the typical cryogenic cooling used in turning processes.

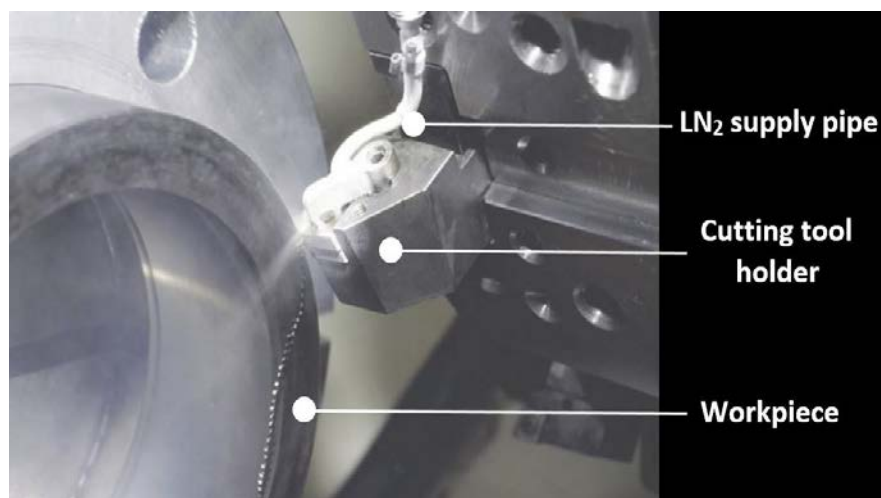


Fig. 2-24 Cryogenic cooling in the turning process using liquid nitrogen (LN_2) [145]

2.10.7 Air blow cooling (dry cutting)

In dry machining, the cutting process can be performed without the use of any cutting fluid or lubricant while atmospheric air is the main coolant utilised. Dry machining is classified as an environmentally friendly cutting technique, and it has been successfully applied particularly in the machining of aluminium, copper and steel alloys [49]. However, in some operations such as grinding processes and the machining of hard metals and refractory materials such as titanium, nickel-based, and heat resistant alloys, cutting fluid is necessary in order to obtain good results due to the large amounts of heat generated during cutting [16]. High friction and high temperatures associated with dry cutting can reduce tool life, cause the surface quality to deteriorate and may introduce thermally induced geometrical deviations to the machined components. Another important issue associated with dry cutting is the production of metallic dust, particularly when machining graphite-based material [14]. In addition, the machining of highly ignitable materials such as magnesium alloys cannot be performed in dry conditions. Although many super-hard tool materials such as CBN, PCBN and PCD have been developed to compensate for the effects of the elimination of fluids in dry machining; however, as earlier mentioned, the high costs of these tool materials are the main obstacle [5, 146].

2.10.8 Critical evaluation of cutting fluid systems in machining

Having reviewed all cutting fluid supply techniques currently utilised in machining operations, and apart from the aforementioned process improvements achieved by these supply systems, it has become clear that randomisation in the estimation of fluid flow rates in all systems, and high fluid consumption and low penetrability in the case of flood cooling, as well as the high set-up costs of HPC, cryogenic cooling, gas-based, mist cooling and MQL, are the predominant technical and economic deficiencies of these supply systems. However, in order to evaluate the existing cutting fluid supply systems and at the same time combine the findings concerning these systems, a rating scheme of very low, low, medium, high and very high is implemented for each system criterion. The evaluation criteria includes fluid consumption, flow rate estimation, penetrability, nozzle positioning, machining consistency, and the cost of the fluid. The evaluation is detailed in Table 2-3.

Table 2-3 Critical evaluation of cutting fluid supply systems in machining [14, 98]

Supply system	Key function	Fluid consumption	Fluid flow rate estimation	Nozzle position/ penetrability	Machining consistency	Cost of fluid used	Set-up cost	Tooling cost
Conventional flood	Cooling and lubrication	Very high	Roughly	Random/low at high speed	Low at high cutting speed	Medium/high	Low	Low
HPC	Cooling & lubrication	High	Roughly	Random/very high	Very high	Medium/high	Very high	Medium
Mist cooling	Cooling and/or lubrication	Low	Roughly	Targeted/high	Medium	Low/medium	Medium	Low
Compressed air/water vapour/ gas-based cooling	Cooling	Low/medium	Roughly	Targeted/high	Medium	Low/medium	Medium	Medium/high
MQL/MQC	Lubrication/ Cooling	Low	Roughly	Targeted/high	Medium	Low/medium	Medium	Low
Cryogenic cooling	Cooling	Medium	Roughly	Targeted/high	Medium	High	High	Medium
Dry cutting (air cooling)	Cooling (atmospheric air)	Very low	----	-----	Very low at high cutting speed	Very low	Very low	Very high

From Table 2-3, it can be seen that dry cutting offers minimum fluid consumption at lower cost and with less environmental impact. However, dry cutting fails to dissipate heat, particularly when cutting titanium. In wet cutting process, high fluid consumption, low penetrability and randomisation in the estimation of cutting fluid flow rate, as well as high set-up costs, are experienced. However, liquid-based supply systems such as flooding, HPC, MQL methods outperform gas-based systems due to the two key functions of cooling and lubrication instead of only cooling, which have significant effects on the output of the machining process. The main specifications for any cutting fluid supply system are the pressure and the cutting fluid quantity. Pressure helps the fluid to penetrate into the machining zone, while the amount of fluid introduced assists to dissipate heat. Although conventional systems have very high fluid flow rate, penetrability is low owing to low pressure as shown in Fig. 2-25. Whereas HPC has high fluid penetration due to high pressure, and relatively moderate flow rate capacity. However, it has high set-up costs due to the required pumping and filtration equipment. In turn, MQL and oil-mist supply systems have very low flow rate capacity, with less environmental impact, but they have also low fluid penetrability. Therefore, Fig. 2-25 suggests a gap which the proposed supply system in this research aims to fill, particularly among liquid-based systems. Reducing the quantity of cutting fluid while keeping high fluid pressure is the main concept behind the development of the proposed system, which is thoroughly described in the next chapter. Tables 2-4 and 2-5 show the application of various supply systems when machining different materials using VO-based cutting fluids.

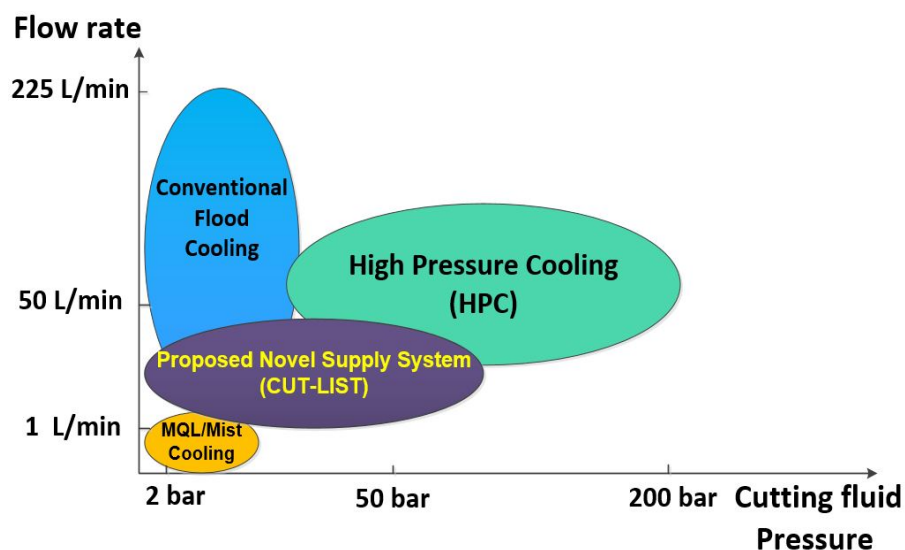


Fig. 2-25 Positioning of the proposed system among other supply methods

2.11 Applications of cutting fluid supply systems in machining of different materials using VO-based cutting fluids

2.11.1 Non-refractory materials (aluminium, copper and steel alloys)

Table 2-4 Major reports on the application of cutting fluid supply systems in machining of non-refractory materials

Authors	Material used	Supply systems and cutting fluids used	Major findings
Zhang et al. Alves et al. [147-162]	Aluminium, copper and steel alloys	Flood (VO) and flood (MO). Supply flow rates ranging from 2.5 to 6 L/min	Flood (VO) achieved longest T_L (60 min) while it reduced coefficient of friction, chip thickness, cutting force, cutting temperature (39%), cutting power (25%), Ra (36%), VB (37.5 %), and cycle time (43%).
Kelly et al. Rahman et al. Itoigawa et al. Safian et al. [163-172]	Aluminium and steel alloys	MQL (VO) and flood (MO). Supply flow rates of MQL ranging from 30 to 3000 mL/h, while in flood from 4.61 to 10 L/min	MQL (VO) offered longer T_L , lower Ra, cutting force, VB (34.21%) and cutting temperature (10%), while both systems showed similar performance in terms of cutting force and flank wear. However, flood (MO) outperformed others in terms of MRV (31%), Ra and cutting temperature (47.14%) during grinding machining trials.
Davoodi et al. [173-179]	Aluminium and steel alloys	Flood (VO), MQL (VO) and dry cutting	Flood (VO) reduced cutting force (20%), VB (60%), Ra and cutting temperature (27 %) and increased T_L (177%)
Nguyen et al. [180]	Steel alloy	MQL (VO), MQL (MO) and dry cutting	MQL(VO) provided lower Ra (1.25 μm) and longer T_L (50 min)
Karmer et al. [181]	Steel alloy	HPC (VO), flood (VO) and dry cutting. Supply flow rates ranging from 3 to 31 L/min	HPC reduced cutting force (10%) and increased T_L (5 times) compared to dry cutting

2.11.2 Refractory materials (titanium and nickel-based alloys)

Table 2-5 Summary of research in the application of cutting fluid supply systems for machining of refractory materials

Authors	Material used	Supply systems and cutting fluids used	Major findings
Tazehkandi et al. [182-184]	Titanium and nickel-based alloys	Flood (VO), dry cutting. Supply flow rate up to 45 L/min	Flood (VO) reduced cutting force (59%), Ra (18%) and provided lower VB (0.2 mm) and longer T _L (15 min)
Cai et al. Priarone et al. Revankar et al. Rahim et al. Vazquez et al. [58, 70, 185-191]	Titanium and nickel-based alloys	Flood (VO), flood (MO/ synthetic), MQL (synthetic) and MQL (VO). Supply flow rate of MQL ranging from 4.6 to 130 mL/h, while flood supply is up to 20 L/min	Flood (VO) reduced cutting force (13.5 %) and workpiece temperature (10.37%) during drilling trials. However, MQL (VO) increased MRR (40%) and reduced cutting temperature (26.6%), cutting force (45.7%) and micro-hardness (14.5%) during turning trials. Lowered VB, Ra and longest T _L (50 min) are also provided by MQL (VO) supply system
Pervaiz et al. Rosli et al. Okada et al. [59, 192-197]	Nickel-based alloys	MQL/MQCL (VO), MQL/MQCL (VO + cooled air) and dry cutting. Supply flow rate ranging from 10.3 to 37 mL/h	MQCL (VO + cooled air) increased T _L (1.6 times) and reduced cutting force (50%), cutting temperature (16.8%), tool wear (43%) and Ra (12.8%) with less BUE formation.
Shabgard et al. Sales et al. Kaynak et al. [198-202]	Titanium alloys	Flood (VO), flood (SEs), flood (MO), cryogenic cooling (LN ₂), CAMQL (VO), MQL/MQCL (VO), and MQL (VO) + LN ₂ . Supply flow rate of flood cooling ranged from 9 to 40 L/m while in MQL supply flow rate fluctuated between 30 and 400 mL/h	MQL (VO) + LN ₂ and CAMQL (VO) reduced cutting force (26% and 11.3%), cutting temperature (52% and 33.4 %), Ra (34% and 21%) and VB (18% and 8.4 %) respectively. However, MQL (VO) consumed less cutting power (7.5 W/h)

2.12 Cutting fluid nozzles

The superior application of cutting fluid in machining operations is one of the most effective ways to improve machinability and maintain high productivity. For this reason, pumping performance is critical. However, the cutting fluid supply is not only influenced by the pumps but also by the nozzle type and design, which significantly affect the cutting fluid speed and positioning as well as power consumption [203]. The conventional nozzle is the predominant nozzle type, particularly in standard machining such as turning, milling, and drilling. However, other nozzle types such as coherent, tapered, slot, spot jet, and shoe-type nozzles are often utilised during various grinding operations such as cylindrical and surface grinding [204]. It has been found that there is extremely limited information in respect of nozzle types in machining processes except in grinding machining operations, as pointed out previously. This is probably because the grinding process can generate a huge amount of heat compared to other machining operations owing to the large contact area between the grinding wheel and the workpiece surface. In practice, the majority of existing CNC machine tools in lathes and milling machines are accommodated with two or more conventional nozzles which are commercially known as the Loc-line nozzle (see Fig. 2-26). These are used particularly where flood cooling is required. These nozzles are often made of plastic with spherical or conical connectors that can be directed at the required positions manually during cutting operations [205].



Fig. 2-26 Image of Loc-Line type conventional sloped nozzle [206]

2.12.1 Conventional sloped nozzle

Fig. 2-27 shows a sectional view of the conventional sloped nozzle used in most standard machining operations. These nozzles were designed to supply cutting fluid at flow rates higher than 4400 L/h with a large nozzle aperture diameter up to 10 mm [206]. Despite their capacity to deliver a huge amount of cutting fluid at higher flow rates, *eddy formation* and *vena contracta* phenomena are the predominant issues affecting the efficiency of these nozzles. Eddy formation occurs due to sudden change in the fluid flow direction from a large zone into a smaller zone causing fluid dispersion particularly at higher fluid velocities. *Vena contracta* (a point in a fluid stream where the diameter of the stream is the lowest, and fluid velocity is at its maximum) can also reduce the physical size of the opening by up to 80% due to the adhesion of fluid on the inner edges of the nozzle [207].

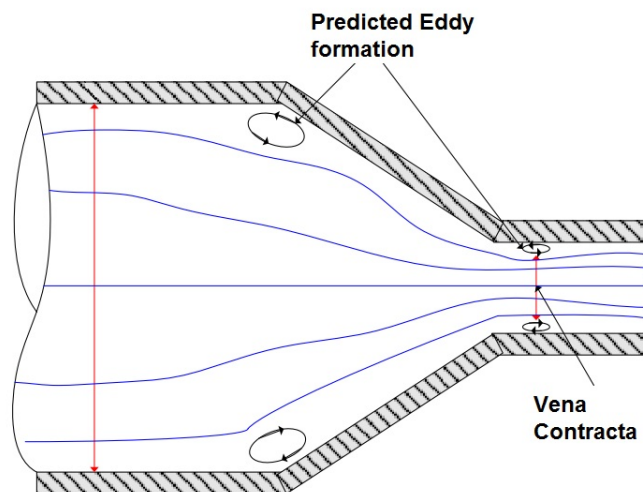


Fig. 2-27 Sectional view of the conventional sloped nozzle [207]

2.12.2 Coherent nozzle

Historically, the concept of employing a coherent fluid jet to machining was initiated in the 1950s by H. Rouse, who had observed the jets created by fire hose nozzles. The design was later transferred and developed by Webster [205] for use in cutting fluid grinding applications. The unique internal geometry of the coherent nozzle (see Fig. 2-28) prevents boundary layer growth, improves flow coherency and affords high jet stream quality with low dispersion and minimum entrained air within the jet. Coherency is the key feature of

the coherent nozzle, which is defined as “a dimensionless unit defined by the ratio of jet width at some distance downstream over the jet width at the aperture” [208].

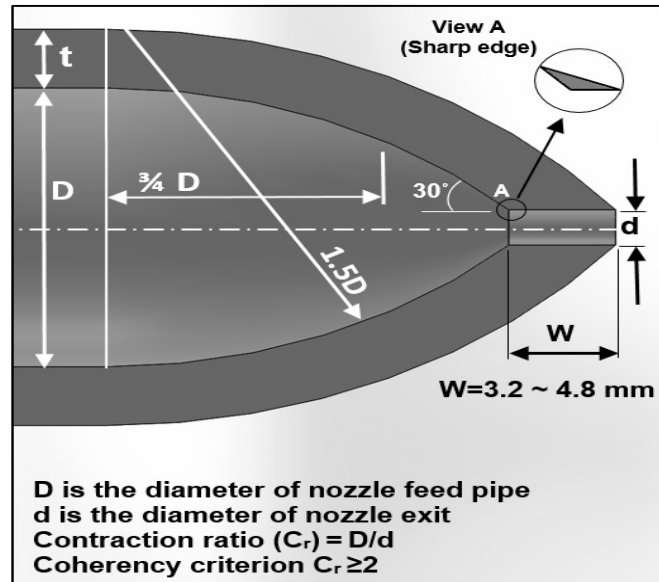


Fig. 2-28 2D sectional view of round coherent nozzle [207]

Additionally, the design needs a contraction ratio of inlet to exit diameter of $\geq 2:1$ in order to fulfil the criterion of coherency. According to the continuity (2.1) and Bernoulli's equations (2.2), the coherent nozzle can increase dynamic pressure more than fourfold as kinetic energy in the form of a homogenous jet up to 300 mm long [209].

$$A_1 \times V_1 = A_2 \times V_2 \quad [209] \quad (2.1)$$

$$\Delta P_{nozzle\ exit} = \frac{1}{2} \rho (V_2^2) \quad [209] \quad (2.2)$$

where ΔP is the fluid dynamic pressure, ρ is the fluid density, A_1 , V_1 and A_2 , V_2 are the cross sectional area and fluid velocity at the entrance and exit of the nozzle respectively in the case of a coherent nozzle where $A_1 \geq 2A_2$ and consequently $V_2 \geq 2V_1$. It has been recognised that the effective use of a coherent nozzle involves many factors. Pressure, flow rate and direction of the fluid jet all effect the fluid's cooling and lubrication efficiency. Flow rate controls the rate of heat transfer into the fluid, while pressure

governs fluid velocity [210]. It was noted that in grinding operations a coherent jet of fluid directly impinging on the machining zone can significantly reduce temperature and assist in enhancing heat and mass transfer performance between the fluid and the exposed workpiece and grinding wheel surfaces [211]. Experimentally, the performance of coherent nozzle was compared with the conventional sloped nozzle during the plunge cylindrical grinding of AISI 1045 under flood cooling with an emulsion fluid using a CBN grinding wheel. The coherent nozzle showed superior performance in terms of reducing the cutting force by 25 % and the specific grinding energy by 19.6 % [211]. The potency of round coherent nozzles was also compared with other types of cutting fluid nozzles, including slot, step, taper and traditional sloped nozzles, in grinding operations. Overall, round coherent nozzles showed superior coherency and fluid penetrability into the machining zone [204, 208].

2.12.3 Importance of nozzle positioning and angles in metal cutting

The location of the nozzle from which the fluid is directed is a critical issue in optimising cutting fluid use. Tool life and machining performance can also be considerably affected by nozzle positions and angles. Some studies have been conducted in the field of cutting fluid nozzle positions and stand-off distances, particularly for MQL machining processes. This research is summarised briefly in Table 2-6. As described in Table 2-6, it is clear that locating the nozzle in the feed direction helps immensely in increasing tool life, particularly in milling operations. This is probably because targeting the nozzle in the feed direction assists to access the fluid into machining zone at the tool-entry point (tool-workpiece engagement point). Tool life was increased by 50% when the nozzle was located in the feed direction at an angle of 12.5° compared to 9.25% for an angle of 45°. This could be attributed to the formation of fluid trapping at the acute angle (12.5°) between cutting tool and workpiece surface. This helped to increase the amount of cutting fluid reaching the machining zone [23]. In addition, placing the nozzle at an angle > 90° in the feed direction also led to a slight reduction in tool wear (by 7.40 %). Whereas placing the nozzle against the feed direction at the tool-exit point (tool-workpiece disengagement point) aided the evacuation of chips [194]. In the same vein, a stand-off distance of 25 mm caused a reduction in cutting temperature up to 8.65% compared to 45 mm stand-off distance. This could be attributed to the improved penetrability of the

cutting fluid owing to its high velocity, which is highly correlated to stand-off distance according to fluid dynamics theories [212].

Table 2-6 Major studies on nozzle positions and angles in metal cutting

Author	Operation	Supply system	Nozzle position/stand-off distance	Major findings
Lopez et al. [213]	Milling	MQL	45° and 135° in feed direction	135° helped to reduce tool wear by 7.40 %
Pereira et al. [214]	Milling	MQL/CO ₂	45° and 90°	45° assisted to increase tool life by 9.25%
I. Mulyadi [23]	Milling	MQL	12.5° and 45° in feed direction	12.5° increased tool life by 50%
Liu et al. [212]	Milling	MQL	135° and 90° at 25 and 45 mm stand-off distance	135° and 25 mm distance reduced cutting temperature by 8.65 %
Yassin et al. [179]	Turning	MQL	20° and 50°	20° produced the lower tool wear and Ra
Wang et al. [194]	Up and down face milling	MQL	45° in feed and against feed direction at tool-entry and exit point	45° in feed direction at tool entry and exit point showed better lubrication action and aided to evacuate chips
Tawakoli et al. [215]	Grinding	MQL	Horizontally toward the workpiece, wheel, contact zone and angularly at 10°/20° toward the wheel	10°/20° toward the wheel position showed better cutting fluid penetrability
Diniz et al. [125]	Turning	HPC	Rake face, flank face and rake + flank face simultaneously	Rake + flank face position induced the lower tool wear
Vazquez et al. [191]	Micro-milling	MQL	In feed and against feed direction	Fluid in feed direction reduced tool wear by 1.6%

2.13 Cutting temperature and measurement techniques in machining

Cutting temperature has been recognized as one of the major factors that affect tool performance and product quality in machining operations. It can influence dimensional accuracy by producing subsurface impairments and promoting residual stresses. However, if properly controlled, process heat can actually be employed to provide desirable workpiece surface hardening. Besides this, many factors can affect cutting temperature such as machining regime (e.g. turning/milling, drilling, grinding, etc.), cutting condition (particularly cutting speed, see Fig. 2-29), tool geometry, cutting tool and workpiece material (Fig. 2-30) as well as the cooling media used in dry or wet cutting [216]. Kikuchi et al. [217] found that dry turning Ti-6Al-7Nb provided an increase in cutting temperature values by 16.66 % and 93% compared to Ti-6Al-4V and brass respectively. For each metal, the temperature became higher when the depth of cut or the cutting speed and feed increased, whereas the increase in the cutting speed and feed was more influential on the value than the increase in the depth of cut. Rahim et al. [187] concluded that wet machining using different cooling supply systems (Flood and MQL) could reduce temperature by up to 33.96 % (particularly in flood system owing to its high cooling capacity) compared to dry cutting when high speed drilling Ti-6Al-4V, as shown in Fig. 2-31. Le Coz et al. [218] found that tool coating material and geometry can reduce cutting temperature by 10% and 6.25% respectively when dry milling Ti-6Al-4V.

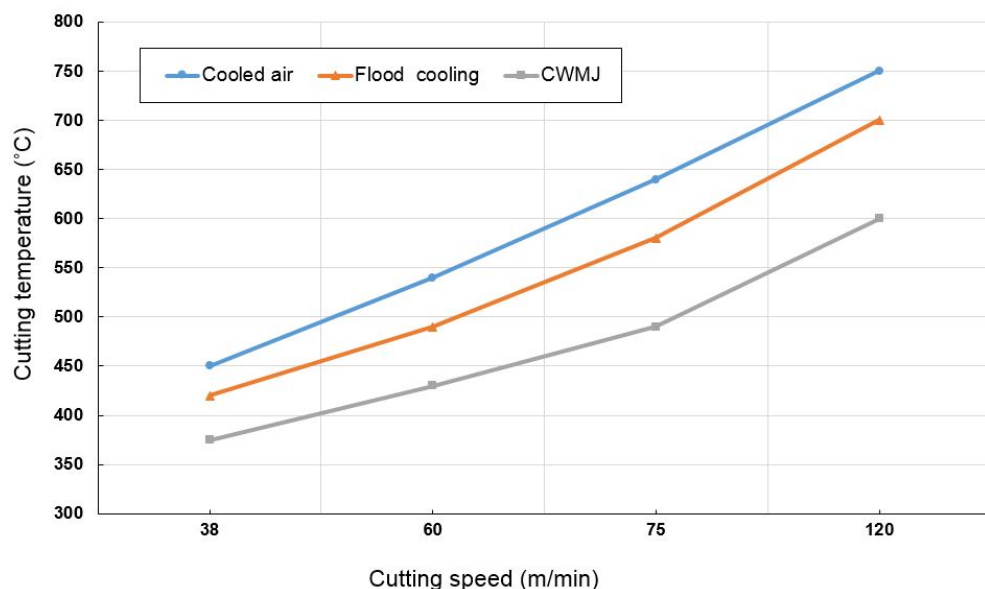


Fig. 2-29 Temperature versus cutting speed under various cooling conditions [219]

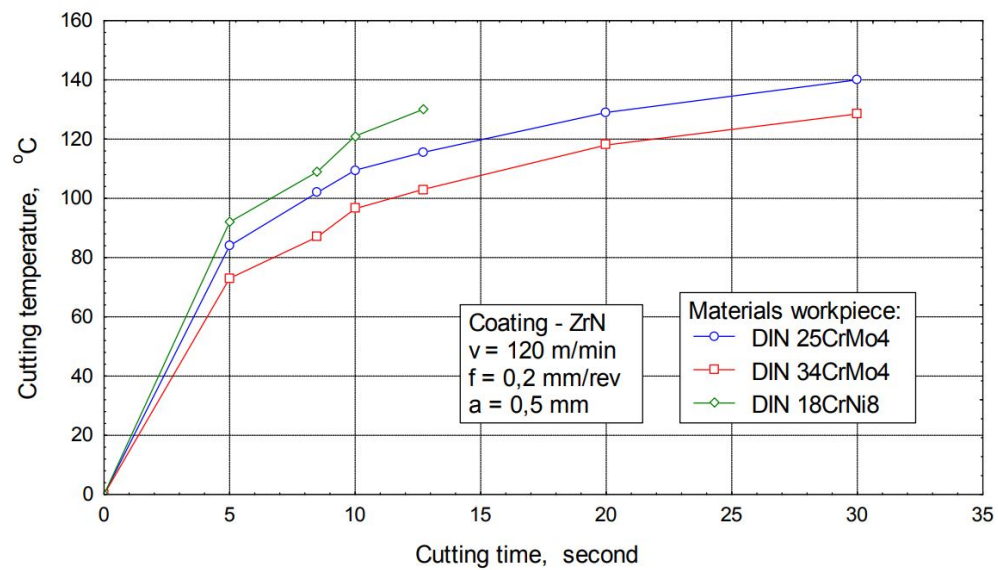


Fig. 2-30 Influence of workpiece material type on cutting temperature [220]

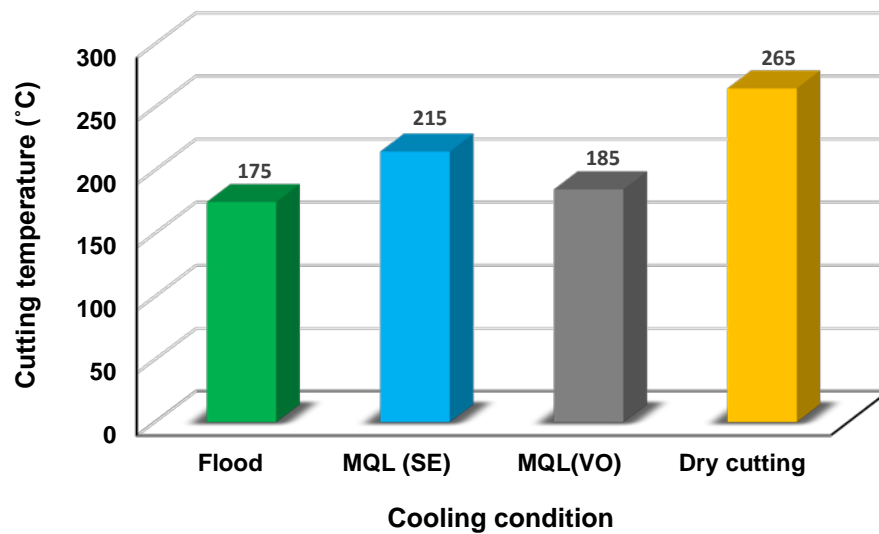


Fig. 2-31 Temperature versus cooling condition when drilling Ti-6Al-4V [187]

Unlike the measurement of cutting force, surface roughness and tool wear, temperature is the most problematic variable to measure, particularly with the use of cutting fluids, which explains the high numbers of different methods used over the years [221]. The difficulty of temperature measurement can arise from the type of machining process used. For example, collecting temperature signals during continuous cutting processes such as turning is still easier than that in intermittent processes like milling where the cutting tool repeatedly cuts the material, and in air cutting where the temperature of the cutting tool

repeatedly heats up and cools down accordingly [222]. In the same vein, there are important factors that should be considered when selecting a temperature measurement technique for a particular machining application, such as temperature range, robustness of the sensor probe, signal type and sensitivity to noise, and response time. However, these aspects should be balanced against certain other criteria such as availability, simplicity of calibration, size and cost. Relevant temperature measurement methods can be classified into four major categories as follows.

2.13.1 Thermocouples (TCs)

Thermocouples are one of the most predominant experimental techniques for investigating cutting temperature due to their simplicity, ease of calibration, and relatively low cost. This technique mainly relies on the Seebeck effect. According to this phenomenon, temperature disparities between the hot and cold junctions of two distinct electrical conductors or materials affords a voltage difference between the junctions. This voltage difference can be calibrated to measure the temperature rise in the machining zone. Thermocouple use, in turn, is sub-divided into three main groups: tool-workpiece, transverse, and embedded techniques. The tool-workpiece thermocouple technique is employed to measure the average temperature at the tool-workpiece interface; however, disparities in temperature at different places and faces on the tool are difficult to measure with this method. The transverse thermocouple technique was introduced to overcome this issue by adding another moving sensor probe fixed in the cutting tool. Both techniques are widely adopted in continuous single point cutting strategies such as turning processes, where the sensor probe can easily be mounted on the tool tip [223]. In operations like milling, drilling and grinding where tool-workpiece and transverse thermocouple methods do not work, the embedded thermocouple can be suitable, as thermocouple sensors are inserted into an appropriately sized hole in the workpiece material. In this technique, the thermocouples can be placed perpendicularly and rather close to the machined surface where the temperature needs to be measured, as shown in Fig. 2-32. In addition, hole position and geometry are crucial in embedded thermocouples and they can affect the temperature measurement process as detailed in the next section. Despite high signal accuracy provided by embedded thermocouples in both dry and wet conditions, there are some limitations associated with this method. The temperature of

the surface cannot be measured because the sensing points are below the machined surface; thus, a workpiece bulk temperature close to the machined surface is measured instead. Also in some cases the drilling of a large number of holes increases costs and can affect temperature measurements due to an irregular temperature distribution [224].

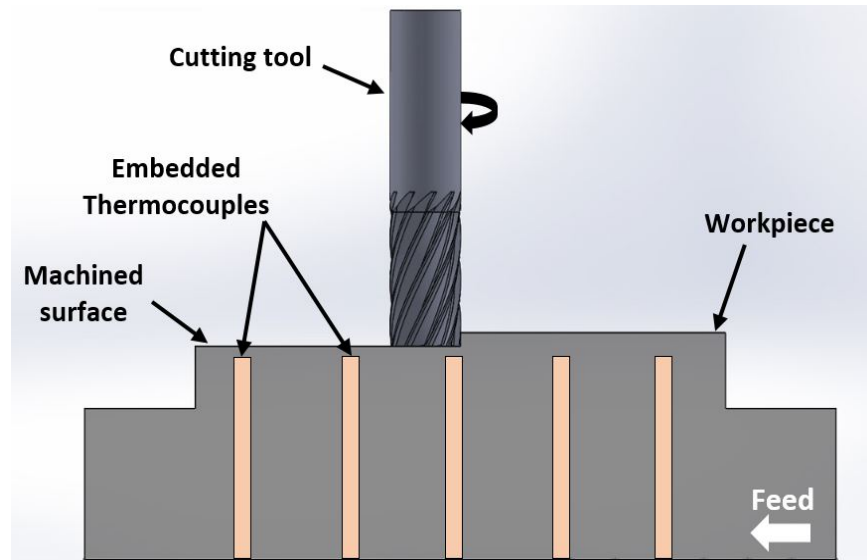


Fig. 2-32 Embedded thermocouples used for milling temperature measurement

2.13.1.1 Importance of the positions of drilled holes in temperature measurement

In the embedded thermocouple technique, the size and position of drilled holes and thermocouple diameter play crucial roles in the temperature measurement process. For instance, drilling a large number of holes in a workpiece material can affect the distribution of temperature and alter heat conduction, while inserting a thick sensing probe can influence the homogeneity and isotropy of the workpiece material blocks. Embedding thermocouple sensors close to the cutting surface can improve measurement accuracy, whereas the size of a hole cavity can affect the error resulting from the deformation of the original temperature field [225]. In the ideal case, the rounded or flat upper shape of the sensing probe tip should be similar to the shape of the hole bottom in order to secure sufficient surface contact between the workpiece material and the sensing probe. Additionally, measuring the temperature at the centre of the cutting surface is preferable to ensure a thermally stable steady state condition. Findings in the literature regarding the embedded thermocouple technique specifically in milling operations are summarised briefly in Table 2-7.

Table 2-7 Literature findings regarding the embedded thermocouple method in milling

Author	Number of holes	Distance between holes (mm)	Hole diameter (mm)	TCs diameter (mm)	Distance below the machined surface (mm)
Birmingham et al. [57]	4	10	0.9	0.81	Up to 4
Acero et al. [226]	5	22.5	1.2	1	2
Rahman et al. [227]	5	20	1	0.9	1
Brandao et al. [228]	6	15	1	0.9	0.5
Yashiro et al. [229]	2	20	0.5	0.32	0.75
Pittala et al. [230]	2	20	2	1.5	1
Lin et al. [231]	4	20	2	1.5	0.5
Aoyama et al. [232]	1	-	2.5	2.5	0.5
Park et al. [233]	1	-	2	1.5	1
Mamedov et al. [234]	2	Perpendicular of each other	150 μm	130 μm	25 μm
Lee et al. [235]	3	15	0.5	0.4	0.1
Hood et al. [236]	8	20	0.6	0.5	1

As seen in Table 2-7, although the number of drilled holes should theoretically be kept to a minimum, the numbers of drilled holes in all studies ranged between 1-8, whereas the distance between holes varied between 10-22.5mm. Also, the maximum hole diameter was 2.5mm, while the tolerance left between the holes and thermocouple was always between 0.09-0.2mm. In terms of the location of the thermocouple, thermocouple sensors were located between 25 μm -2mm below the machined surface. However, in some researches [57] sensors were placed at a distance of up to 4mm below the machined surface and this may have affect measurement accuracy.

2.13.2 Infrared (IR) pyrometers

This technique is widely used to either measure the heat radiating directly from the machining zone or through a fibre-optic cable fitted close to, or through, the tool and workpiece (see Fig. 2-33). Major advantages of the technique are that the pyrometers are contactless and excellent for surface measurement and with moving parts, and they have high responses to rapid changes in temperature and a less disturbing effect on heat distribution. However, high cost, the complexity of their calibration and the need for a dry and clean working environment without cutting fluids, dust or humidity are the main problems [216].

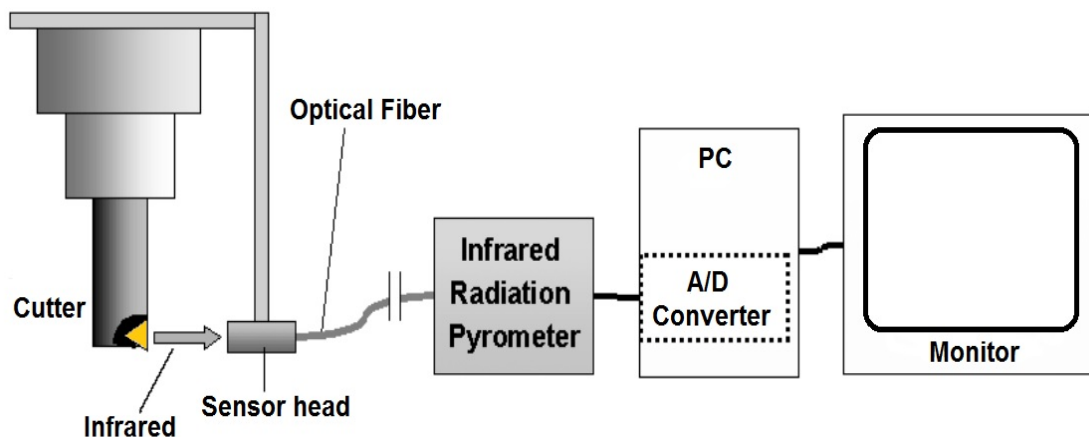


Fig. 2-33 Schematic view of temperature measurement using IR pyrometer [222]

2.13.3 Thermal image cameras

The thermal or infrared camera is a non-contact device that can produce a temperature map of the area investigated, such as tool tip, tool-workpiece interface, thus displaying areas of similar temperature. Objects can be shown in different colours to demonstrate the regions of different temperature. Thermal cameras operate in wavelengths as long as $14\mu\text{m}$. The advantages recorded in the use of this method are that heat sensed can be very precisely quantified, measurements can be taken in a precarious environment with high response time and the temperature distribution can be analysed over a wider area owing to the formation of a visual image. However, the major problems encountered in this method are that it requires a dry cutting environment and high exposure time to record

data (10-15 sec), preheating of the workpiece is needed, variations in workpiece emissivity can affect picture quality, and the cameras are very expensive [237].

2.13.4 Metallographic method

This method relies on measuring alterations in the microstructure or hardness of the cutting tool after the cutting process. The major advantages of this technique are its low cost, and a high range of temperatures (650–900°C) can be recorded. However, this method has limited applications and can only be used for tools made of high-speed steel (HSS) rather than powder-based tools such as W/Co carbide, ceramic and CBN inserts to avoid tool breakage. In addition, this method is not valid in wet cutting conditions as the microstructural change of a cutting tool is strongly affected by cooling [223, 238]. Table 2-8 summarises a critical evaluation of the common temperature measurement methods used in metal cutting processes.

Table 2-8 Evaluation of temperature measurement techniques in machining [224]

Technique	Cost	Accuracy	Compatibility with cutting fluid	Transient response	Ease of calibration
Thermocouple	Very low	High	Very high	Low	High
IR pyrometer	High	High	Very low	High	Very low
Thermal camera	High	High	Very low	High	Very low
Metallurgical method	Low	High	High	N/A	Very low

2.14 Design of experiments (DOE) and data analysis methods

Over time, the complexity of metal cutting process dynamics has increased. Consequently, solving issues related to the determination of optimal cutting conditions using a suitable optimisation method has become a critical and difficult task for researchers. In terms of the theory of optimisation, an experiment represents a series of tests in which input variables are changed according to given rules in order to identify the reasons for changes in the output response. The design of experiments (DOE) can be

defined as “a systematic method to determine the relationship between factors affecting a process and the output of that process” [239]. The objective of the DOE is to select input variables for which the response should be evaluated. The most commonly used terms in DOE methodology are controllable, uncontrollable input factors and responses, as shown in Fig. 2-34. Controllable input factors are those input parameters that can be accurately set in an experiment or process such as cutting speed, feed rate and depth of cut. Uncontrollable input factors are those parameters that cannot be changed and examples include vibration and room temperature. These factors need to be recognised in order to understand how they may affect response. Responses, or output measures for example, cutting force, cutting temperature, tool wear and surface integrity as well as burr and chip formation, are the elements of the process outcome that represent measures of the desired effect [240].

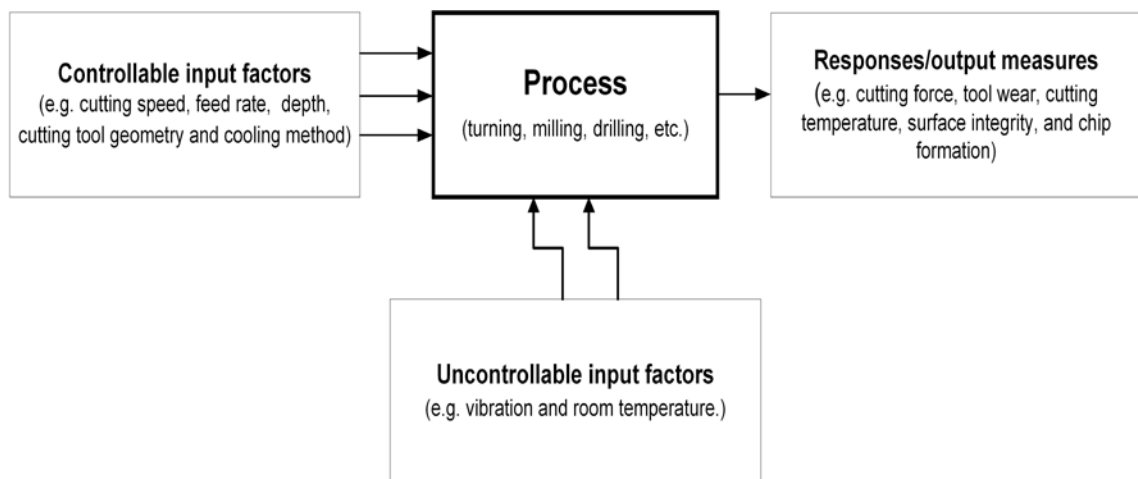


Fig. 2-34 Process factors and responses in machining [240]

Additionally, several statistical DOE techniques have been introduced to perform experiments efficiently. These include full and fractional factorial, Taguchi robust design, Box Behnken, Plackett-Burman, central composite and D-optimal designs. The choice of suitable DOE technique depends on the aim of the experimentation. For instance, if a rough estimate of the main effects is sufficient, a Plackett-Burman design would be preferable. If a more precise computation of the main and interaction effects must be accounted for, a full factorial method should be used. For response surface methodology (RSM), Box-Behnken, central composite, or D-optimal designs could be chosen [241]. However, among these techniques, the Taguchi robust design along with an ANOVA

statistical approach are now prevalent in optimisation tools in industrial practice in order to achieve the maximum level of profit and the best quality of manufactured products [178, 242]. Table 2-9 shows common statistical experimental design methods used in industrial applications and their main features.

Table 2-9 Common DOE methods used in industrial applications [243]

DOE technique	Main features/Suitability
Taguchi robust design	Addresses the influence of discrete noise variables
Full factorial	Computes the main and interaction effects, and builds response surface
Fractional factorial	Requires less effort and fewer tests
Randomised complete block design (RCBD)	Focuses on a primary factor using blocking techniques
Box Behnken design (BBD)	Builds quadratic response surfaces
Random	Builds response surfaces
Latin squares	Focuses principally on a primary factor
Plackett-Burman design (PBD)	Estimates the main effects
Central Composite design	Builds response surfaces
Halton, Faure, Sobol	Builds response surfaces
D-optimal design	Builds response surfaces

In this study, full factorial and Taguchi designs were used. Therefore, they are discussed in details in the next section.

2.14.1 Full factorial design

This design includes all possible combinations of factors (variables) at all levels. There can be two or more levels, but the number of levels has an influence on the number of experiments needed. For k factors at L levels, L^k experiments are needed for a full factorial design. In this method, each treatment combination of factors is studied in order to complete a full study of interactions between all factors. However, when factors or factor levels or both are increased, the number of treatment combinations increases. This will require a larger number of experiments, which tends to increase the running time and

costs. The statistical analysis and interpretation of results may also become more onerous [244]. In this research, the numbers of factors and factor levels were manageable (e.g. up to 108 tests).

2.14.2 Taguchi design methodology

The Taguchi method was developed by Genichi Taguchi [245] in Japan to improve the implementation of total quality control for industrial applications. The method is used to find the best values of controllable factors so as to make a process less sensitive to variations in uncontrollable factors. Taguchi designs are based on mixed levels, highly fractional factorial methods, and other orthogonal (balanced) designs. These design methods are very attractive to practitioners because they greatly reduce the costs and time needed for a set of experiments [241]. They distinguish between control variables, and discrete noise variables, which are the factors that cannot be controlled except during experiments in the laboratory. Taguchi's technique offers a more efficient design of experiments than many other statistical experimental methods by determining the minimum number of experimental runs that needs to be conducted, according to Eq. 2.3 [240].

$$N_{Taguchi} = 1 + \sum_{i=1}^{NV} (L_i - 1) \quad [240] \quad (2.3)$$

where NV is the number of independent variables and L_i is the number of levels of each of the independent variables.

2.14.3 Analysis of means (ANOM)

The analysis of means (ANOM) is a common statistical technique in quality management for presenting multiple group comparisons with an overall mean ("grand mean") in a variety of experimental designs and investigation conditions. It is basically a graphical approach, generating control charts that allow conclusions to be managed and results to interpreted easily with respect to both statistical and practical significance [246].

2.14.4 Analysis of variance ANOVA

Each of the experimental runs in this study represents a combination of different levels of the independent factors. For this reason, it is necessary to separate the individual effect of each factor, which can be achieved by the widely used statistical technique ANOVA. ANOVA is used to test a hypothesis, comparing the means of more than two factors. The null hypothesis, H_0 , is assumed which is that the difference between specified factors is insignificant and that any observed difference is due to experimental or sampling error. F-tests are used to inspect a pre-specified set of standard effects such as main effects and interactions. In other words, statistical significance in the ANOVA is tested by comparing the F value, which is defined as:

$$F \text{ value} = \frac{\text{Variance between groups}}{\text{Variance within groups}} \quad [247] \quad (2.4)$$

The F value can be further used to calculate the so-called probability value (P value), which confirms or rejects the null hypothesis. At the 95% confidence level, if the P-value is < 0.05 , the null hypothesis can be rejected and the results said to be statistically significant. Generally, the ANOVA table collectively involves F, P, S, R^2 , and Adjusted R^2 values [247]. In a similar vein, the percentage contribution ratio (PCR) of each independent factor in optimising performance characteristics can be calculated as follows:

$$PCR = \frac{SS_{\text{independent factor}}}{SS_{\text{total}}} \times 100 \quad [247] \quad (2.5)$$

where SS is the sum of squares for an independent factor and SS_{total} is the sum of squares of all of the independent factors including an error contribution.

2.15 Summary of the literature review findings

- Despite technical and environmental benefits gained from dry machining when cutting non-refractory materials such as copper and aluminium alloys, omitting a cutting fluid is untenable especially in the machining of highly ignitable magnesium alloys, graphite-based materials, and hard metals as well as refractory materials such as titanium alloys where excessive heat is generated.
- The machining process can be served by several cutting fluid supply systems. Although process improvements have been achieved by these systems, randomisation in estimating fluid flow rates in all systems, high fluid consumption, low penetrability in particular for conventional flood supply, the high set-up costs of HPC, MQL, mist cooling, gas-based and cryogenic cooling are the main economic and technological deficiencies.
- Understanding the mechanism of MQL triggered the importance of nozzle positions, angles and stand-off distances in machining processes, while they are ignored for all other supply systems. Consequently, the demand to include these parameters in a further investigation in machining operations is increasing. This is an important gap in the literature.
- Conventional sloped nozzles are the mainstay of the CNC machine tools industry, particularly in lathes and machining centres. Despite their capacity to supply a huge amount of cutting fluid at high flow rates, fluid dispersion at high fluid velocity and the reduced size of nozzle apertures owing to the *vena contracta* phenomenon are the main issues affecting their efficiency. Thus, there is a paramount need for a bridging technology to solve these issues. This is another gap in the literature.
- Neat oils offer good lubricity, anti-seizure, rust and corrosion control, particularly in low-speed machining. However, water-miscible fluid emulsions are the best choice when machining hard metals and refractory materials such as titanium and nickel-based alloys where heat dissipation is the priority.
- Flood and MQL supply systems are widely used in machining operations compared to other supply systems. Seemingly, using ample amounts of fluid is immensely useful in continuous cutting such as turning, drilling, reaming and grinding while reducing the quantity of fluid used plays a major role in minimising

the thermal shock resulting from interrupted cutting such as milling. Thus, a further study on the effect of cutting fluid quantity on machining performance is required.

- The majority of studies on the application of cutting fluid supply systems in machining using VO-based fluids have focused on non-refractory materials, particularly steel and aluminium alloys. So further investigation is required to fill the gap in knowledge and solve the outstanding issues in the machining of titanium alloys using VO-based fluids.
- Titanium has a low machinability rating and consumes a large quantity of cutting fluid due to the excessive heat generated owing to its low thermal conductivity and high dynamic shear strength. Increasing machining speed while reducing fluid consumption when cutting titanium is one of the main aims of the machining industry.
- The surface quality of machined titanium parts is crucial. Amongst other aspects of surface integrity such as surface roughness and micro-hardness, the effect of cutting fluid on microstructural change when machining titanium is still unclear. Thus, further investigation is needed to clarify such ambiguity.
- Despite all of the progress achieved by coated tungsten (W/Co) carbide tools in machining processes, there is a clear conflict regarding the feasibility of using these tools in machining titanium. Therefore, the feasibility of these tools in cutting titanium should also be re-examined.
- The measurement of cutting temperature can be performed using many techniques. However, not all techniques are valid in wet machining environments except for the embedded thermocouple method. Accuracy, low cost, and ease of calibration are its main advantages.

Chapter 3 Design and Manufacture of the Novel Supply System

The objective of this chapter is to implement phases 2 and 3 of the research project, which focus respectively on the design and manufacturing of the new system components. The chapter is organised into six main sections. Sections 3.1 and 3.2 outline the design tools and concepts and the baselines adopted in this research, while section 3.3 illustrates the new system configuration. Sections 3.4 and 3.5 describe the designs developed and then manufacturing methods utilised to produce CUT-LIST main parts. Section 3.6 presents the computation of fluid system parameters, including the calculations of MRR, cutting power, and accurate flow rate as well as the determination of diameter of the coherent nozzle apertures and fluid velocities. A summary is provided at the end of the chapter.

3.1 Design tools

The new system's 2D technical drawings were mainly performed on a computer-aided design platform. Other powerful CAD environments like SolidWorks have also been utilised, particularly in the 3D design of the new system components. The conversion of data from 2D to 3D has become easier nowadays owing to Import/Export (I/E) wizards, which allow DWG/DXF files to be imported directly into the 3D sketcher. The STL (stereolithography) file type format is also another feature of I/E wizards. This format is commonly used in computer-aided manufacturing (CAM) platforms and 3D printing or prototyping machines. All 2D technical CAD drawings of the new system components are presented in Appendix A.

3.2 Design concept and baselines

The design concept of the new system relies on four main pillars as shown in Fig. 3-1. The first is to avoid randomisation in flow rate estimation by delivering an accurate amount of cutting fluid based on a calculated amount of heat generated in the machining zone. The second is to improve fluid penetrability by means of employing coherent round nozzles using the cutting fluid pump in existing CNC machine tool. The third is the use

of precisely-oriented nozzles directing the fluid stream accurately into targeted heat-affected zones. The final pillar is the use of biodegradable VO-based cutting fluid, thus improving cooling potency and at the same time mitigating environmental and health risks during machining operations. Collectively, these pillars are the basis of the new system's novelty.

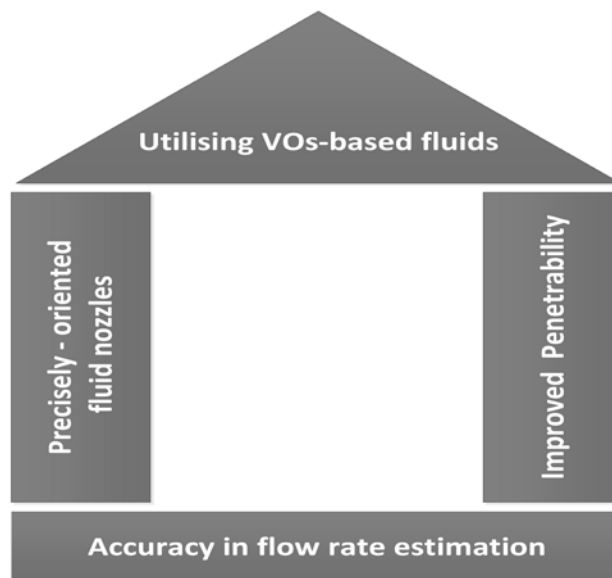


Fig. 3-1 Basic pillars of the proposed novel supply system concept

Additionally, in order to comply with current economic and environmental standards, the design baselines described below was followed when developing the new supply system and its components:

- Having a closed-loop cooling-based configuration to minimise cutting fluid waste
- Ease of integration with existing CNC machine tool configurations
- Using the least resources at lower manufacturing time and costs, which can be accomplished by implementing the design strategy shown in Fig. 3-2:



Fig. 3-2 Design strategy adopted when developing CUT-LIST components [248]

3.3 New system configuration

Fig. 3-3 presents the configuration of the new CUT-LIST supply system. As shown, the cutting fluid is conveyed by means of a centrifugal vertical immersion-type closed-loop coolant pump positioned close to the fluid tank to minimise the fluid pressure drop. A practical advantage of this type of pump is that it requires minimum tank size whilst its submerged pumping element is always primed. The level of cutting fluid can be observed using a tank level gauge. The output cutting fluid flow rate and pressure were controlled using a bypass manual control valve to provide the required flow rate at any given pressure. A safety manual valve was also allocated immediately after the pump to use in emergency cases such as pipes leakage. During fluid circulation, the flow was monitored by a digital flow meter/regulator installed at a distance of more than 300 mm from the cutting fluid pump to ensure steady state flow conditions. Additionally, a digital liquid pressure gauge was installed directly after the in-line-type filter (where the cutting fluid is cleaning fine debris $< 50 \mu\text{m}$ using an effective magnetic element) to measure the total pressure of cutting fluid delivered. Two dual scale-type pressure gauges were also mounted before the fluid entered the nozzles to observe any pressure drops in the fluid pipe at these positions. To maintain a uniform-velocity flow condition and to minimise back-pressure, elbows, bends, and changes in plumbing diameters were avoided in the CUT-LIST configuration. At the end of the cooling cycle, cutting fluid is returned back to the fluid sump where it can be filtered via a micro-mesh strainer ($< 100 \mu\text{m}$) before being re-pumped again by the pump. The present CUT-LIST configuration does not have an oil concentration sensor or level, and water is added manually only when the oil concentration is increased. This was regularly detected using a handheld refractometer. The CUT-LIST has the ability to target fluid in the feed and against the feed directions simultaneously, as shown in Fig. 3-4. The angled overhead nozzle ring was placed on a vertical spindle head holding two nozzles for the supply of fluid at different positions in the feed and similarly against the feed direction. The new system was also designed to align the nozzles in the tool-workpiece engagement point at any given elevation angle relative to the spindle axis using movable nozzle holders/clamps and angled mounting wedges. In addition, the design of the movable nozzle clamps allows the nozzle discharge tips to be relocated away from the machining zone at any given impinging distances. The next section describes the designs of the new CUT-LIST components in detail.

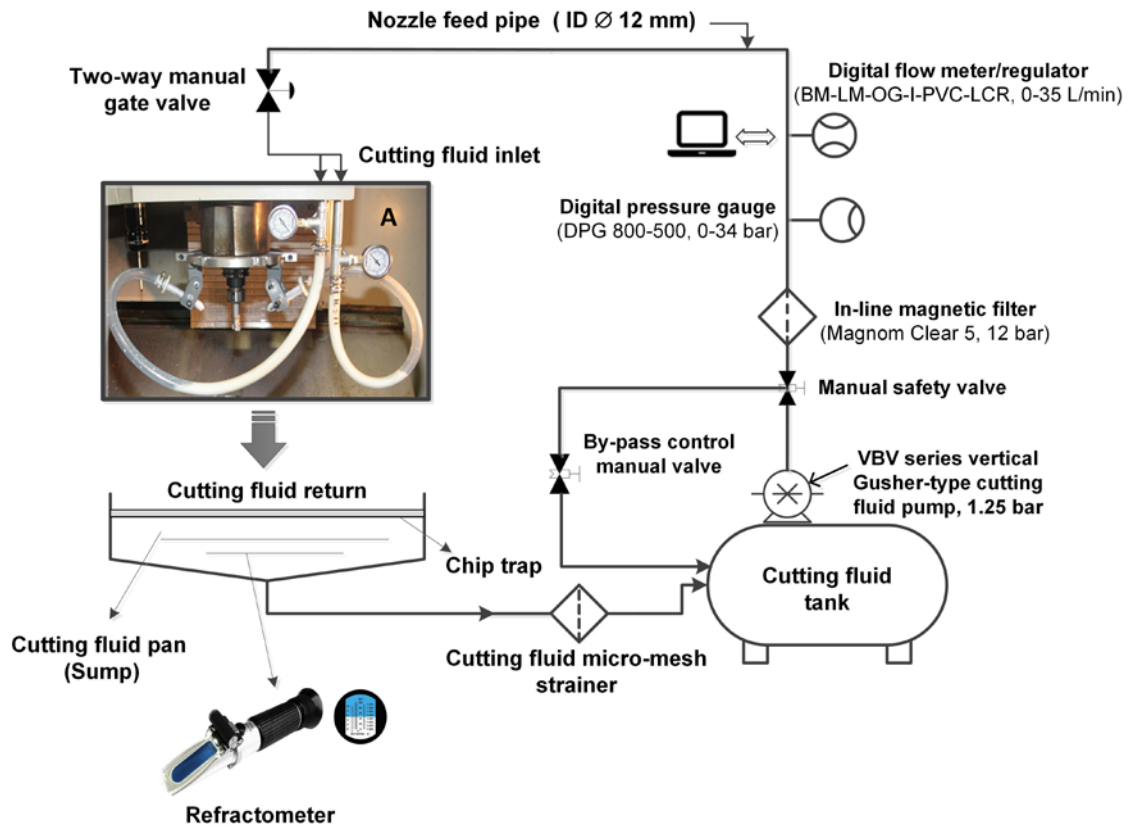


Fig. 3-3 Configuration for the new CUT-LIST supply system

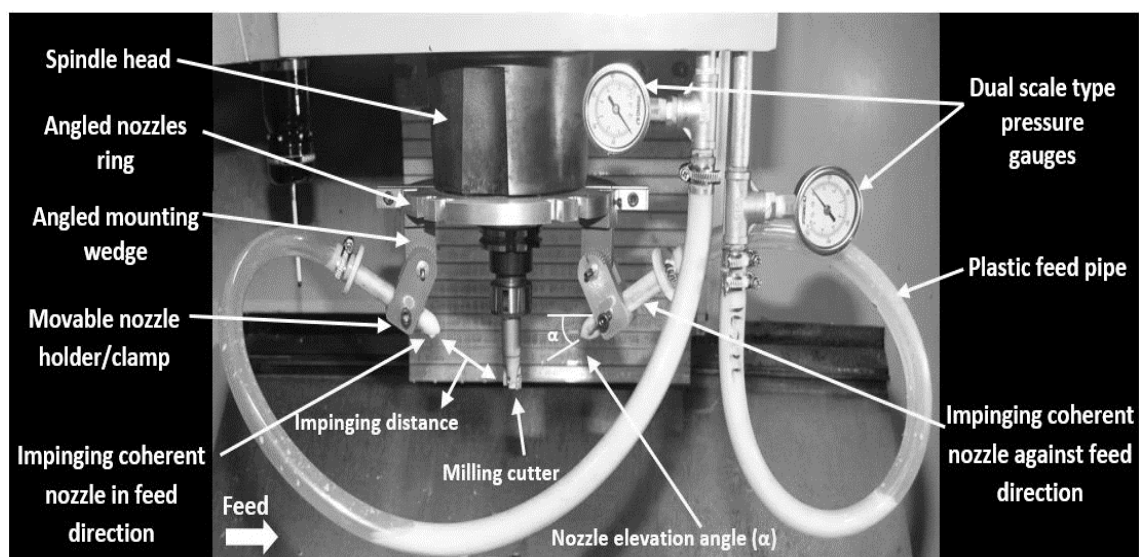


Fig. 3-4 Details of view (A)

3.4 CUT-LIST component design

3.4.1 Overhead angled nozzle ring

Fig. 3-5 presents an isometric view of the overhead angled nozzle ring. The ring consists of two major parts: the rear and front parts. The external surface of the front part was designed to be grooved symmetrically from the right and left sides at three different impinging angles of 15°, 45° and 60° for the holding and targeting of the nozzle in the feed and against the feed directions. These nozzle angles and directions were chosen as preferred nozzle placements in machining processes based on information in literature. The ring parts were built to be joined easily to the spindle head via M8 x 30 mm full thread screws. The design of the developed nozzle ring can speed up installation and the experimental set-up, thus saving time. Additionally, \varnothing 6 mm diameter holes were allocated at the middle of each grooved face of the front part to ensure the quick and reliable fitting of the mounting wedge, as thoroughly described in the next section, on the overhead nozzle ring. All edges were chamfered for safety and to prevent part damage.

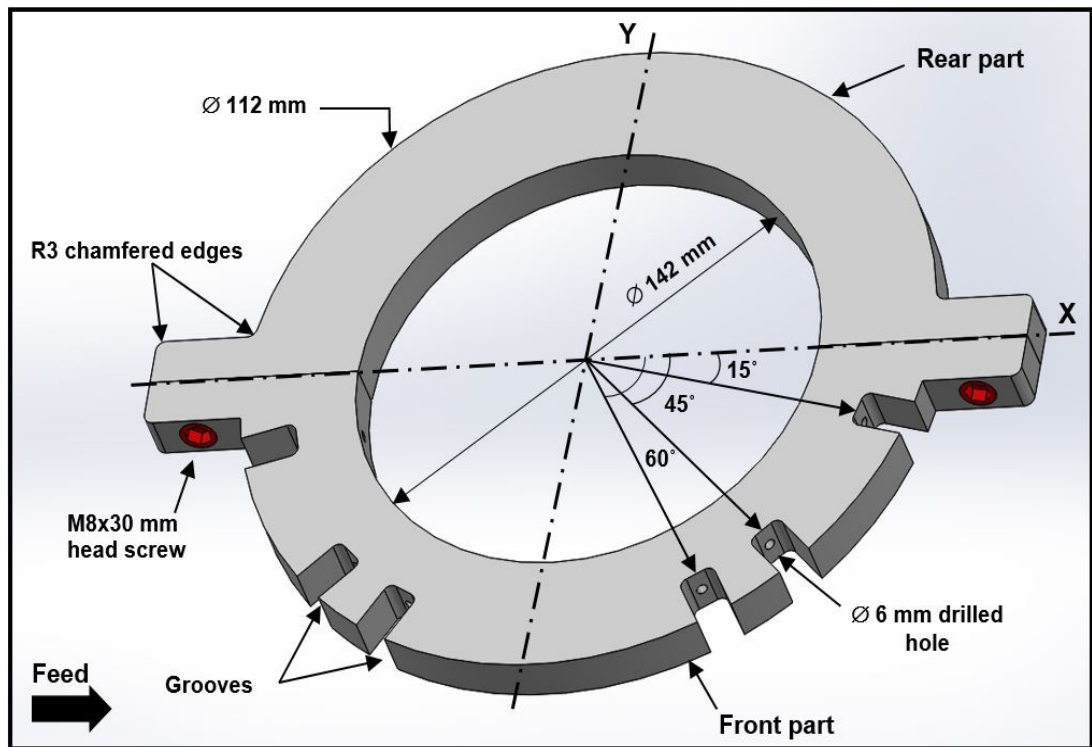


Fig. 3-5 Isometric 3D view of overhead angled nozzles ring

3.4.2 Angled mounting wedge

The angled mounting wedge comprises three main parts: the latch, top plate, and wedge shank. The latch has a unique rectangular shape that can be easily installed in the overhead angled nozzle ring's grooves using M5 x 30 mm screws, whereas the top plate was built to give more stiffness to the structure. A $\varnothing 6$ mm diameter hole was allocated at the rounded end of the part shank for the mounting of the nozzle holder/clamp. In addition, the shank of the mounting wedge was marked with small grooves at different angles (from 0 to 90 degree) on the left and right sides of both faces, as shown in Fig. 3-6. The angles were arranged to match with the angled nozzle holder so as to relocate the nozzle precisely at any given (x, z) positions in the feed and against the feed directions.

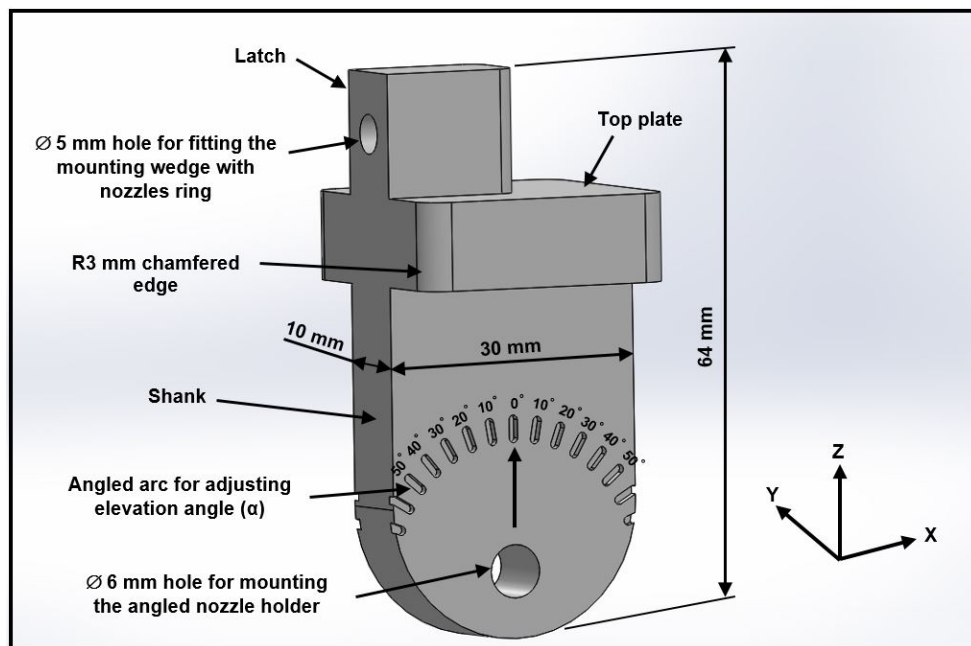


Fig. 3-6 3D view of the angled mounting wedge

3.4.3 Movable angled nozzle holder

The main function of the movable nozzle holder is to clamp the nozzle and relocate its discharge tip at any given elevation angle (α) and impinging/stand-off distance. The nozzle holder's ribs and base block are the main elements of the nozzle holder. A large $\varnothing 18$ mm diameter hole was allocated in the base block to hold and secure the main nozzle body using two M5x20 mm full thread screws. In addition, the rounded edges of the part's

ribs were designed to match the installed mounting wedges having similar graded patterns as shown in Fig. 3-7. This design allows the easy connection of the nozzle holder/clamp to the mounting wedge, offering smaller component size and higher degrees of freedom of movement in the (x, z) directions.

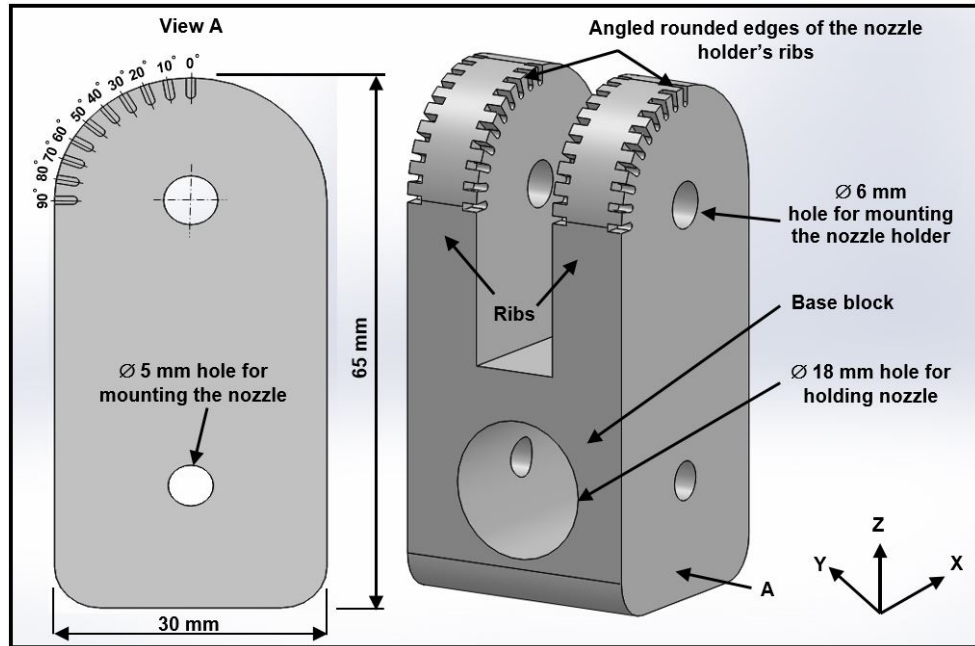


Fig. 3-7 3D structure model of the movable angled nozzle holder/clamp

3.4.4 Impinging coherent round nozzle

Contrary to the conventional sloped nozzle, CUT-LIST nozzles were designed based on the Webster jet nozzle model. The nozzle consists of a nozzle head, nozzle tube, support pad and nozzle tail. The nozzle head is an important element where the fluid jet stream can be formed, particularly at the end of the nozzle discharge tip. An enlarged view of the nozzle head cross-section is presented in Fig. 3-8. As shown, the nozzle head has a total length (L) of 16 mm and an actual inner diameter (D) of 12 mm with the radiused midsection having a radius of $1.5D$ (18 mm) and an axial length of $0.75D$ (9 mm) followed by a 30° converging passage. This passage, which is the nozzle aperture, has an exit width (w) of 3.4 mm and an outlet diameter (d) of 1.75 mm. It is worth mentioning that the nozzle aperture diameter (d) was determined based on fluid dynamics computations, as thoroughly described in the next section. The contraction ratio (D/d) was set at more than 2:1 (i.e. 6.85:1) to achieve high jet stream quality. The exit edges of the nozzle aperture

were kept very sharp to minimise jet dispersion and maintain high coherency. In addition, the design of the nozzle tube allows the nozzle tip to be located at any given impinging distance up to a maximum of 100 mm. A support pad was developed to be located at the end of the nozzle tube to reinforce the nozzle structure as well as to prevent the nozzle going further than the limits of stand-off distances during the cutting process. In order to increase nozzle stiffness to withstand high fluid pressures, nozzle thickness was set at 2.5 mm. The nozzle tail was also developed to be connected with a clear braided-type plastic feed pipe using Jubilee-type super clamps hose clip. A length of 20 mm was allocated for the nozzle tail to give adequate contact surface area between the nozzle and the plastic hose in order to prevent fluid leakage. Table 3-1 summarises the main internal dimensions of the bespoke coherent nozzle used throughout the study.

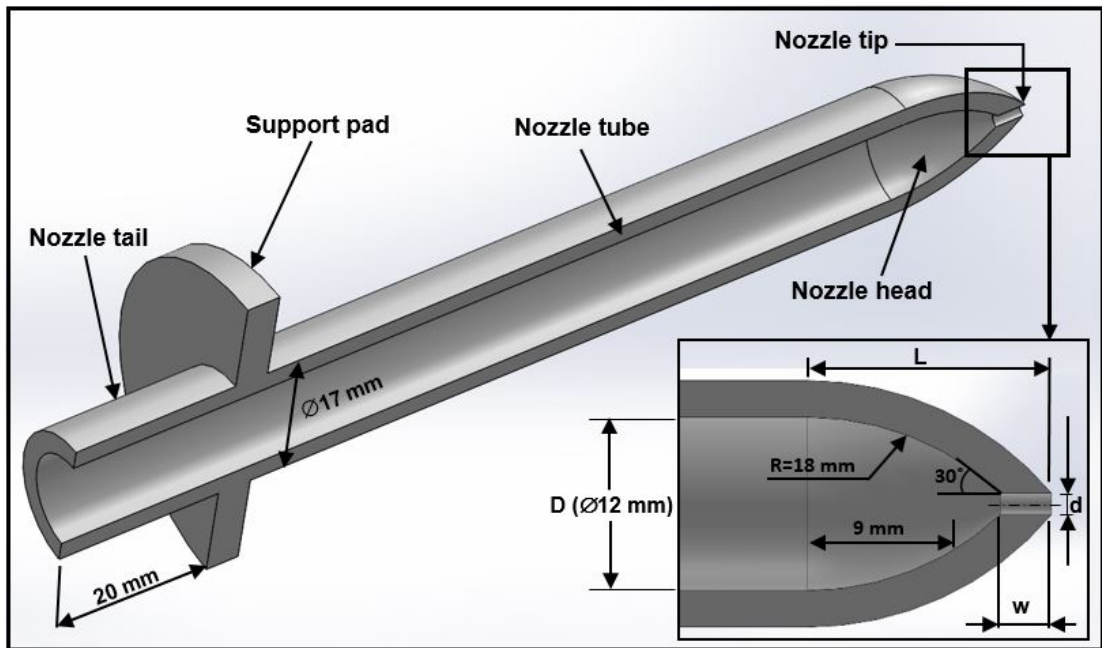


Fig. 3-8 3D sectional view of the coherent round nozzle

Table 3-1 Main internal dimensions of the bespoke coherent round nozzle head

Dimension	Value
Nozzle internal diameter (D)	12 mm
Nozzle aperture diameter (d)	1.75 mm
Contraction ratio (D/d)	6.85:1
Nozzle head length (L)	16 mm
Nozzle mid-section radius (1.5D)	18 mm
Nozzle mid-section axial length (0.75D)	9 mm
Nozzle aperture cross-sectional width (w)	3.4 mm

3.4.5 Workpiece fixture

The main purpose of the workpiece fixture is to hold it rigidly to a machine during the cutting process, and at the same time locating the part in an accurate position relative to the cutting tool. Workpiece fixture is a prerequisite for reducing the setup-time between each experimental run. It can be subjected to hundreds of repetitive loading and unloading cycles. Therefore, the durability and flexibility of this component are of critical importance. The workpiece fixture consists of rear and front parts, as shown in Fig. 3-9. Both parts were designed to be thick enough to withstand high force pressure resulting from the cutting process. The rear part was developed to hold the workpiece tightly from three different sides. To secure the front side of the workpiece during cutting, a rigid rectangular plate (front part) was designed for this purpose. In addition, the fixture was developed to relocate the workpiece about 8 mm above the fixture's upper surface to allow enough space for the tool path during the cutting process.

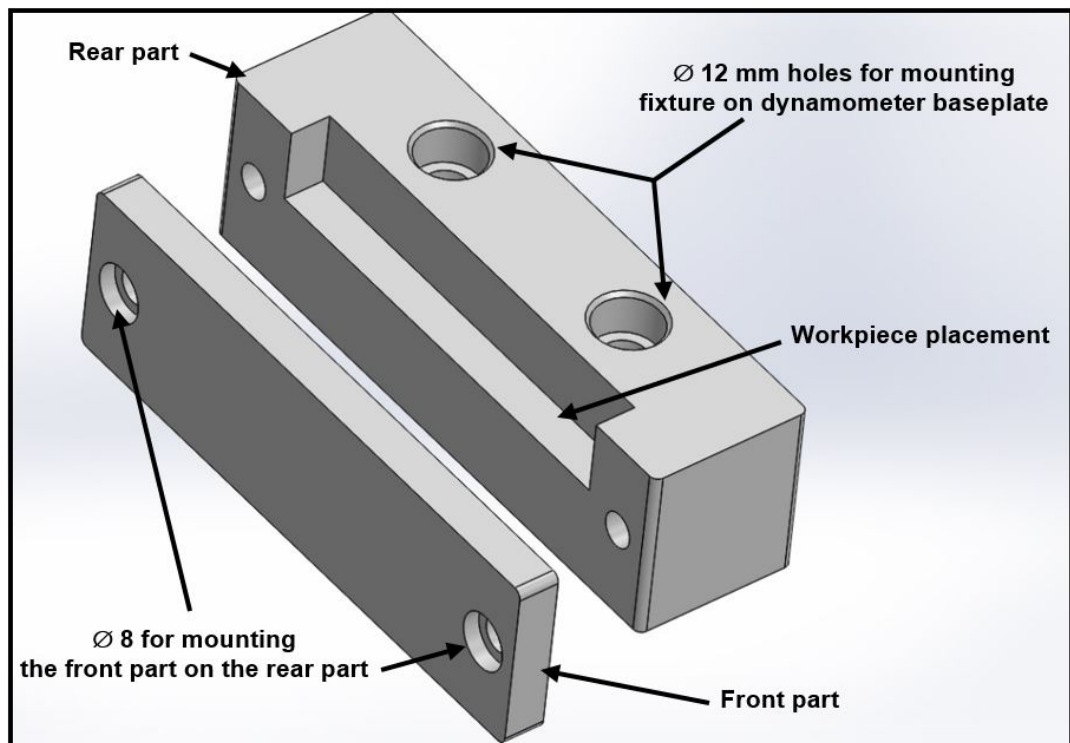


Fig. 3-9 Three-dimensional structural model of the workpiece fixture

Fig. 3-10 shows a 3D view of the new system assembly, including angled nozzle ring, nozzle holders, mounting wedges, and coherent round nozzles as well as the workpiece fixture.

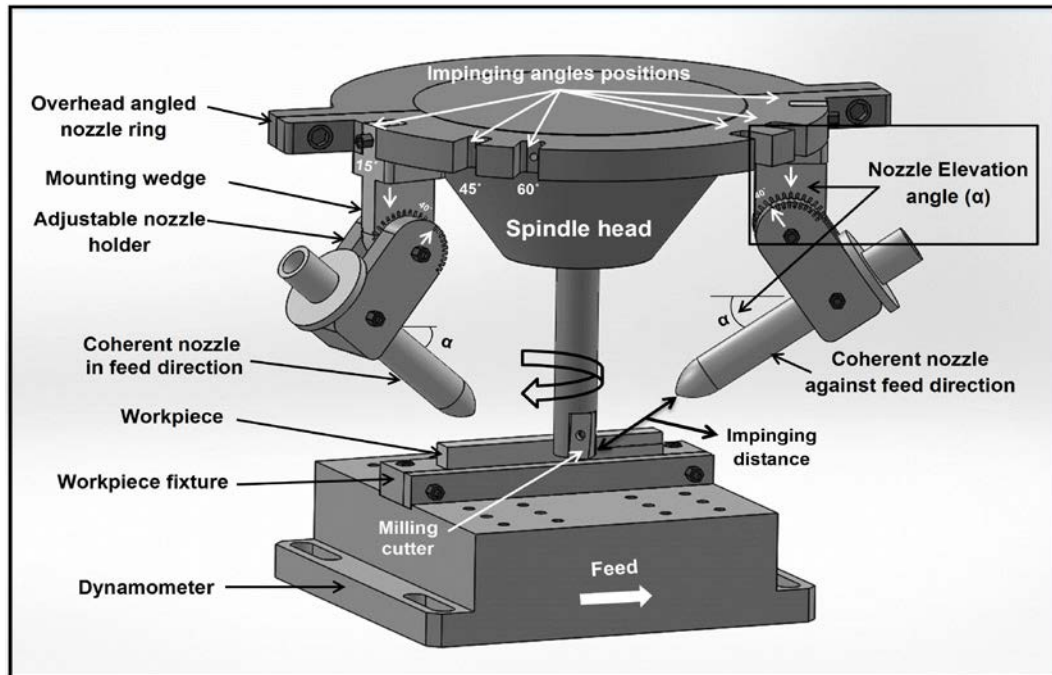


Fig. 3-10 3D view of the new system assembly

3.5 Manufacturing of the new system components

In order for the new system components to function efficiently, greater manufacturing precision and tight tolerances are required. This can be achieved by utilising the most advanced manufacturing technology and tools such as CNC machine tools and 3D printing machines. 3D printing is a rapid manufacturing method whereby physical objects are built by depositing material layer by layer under computer control. 3D printing imports virtual designs from any CAD or other animation modelling software (often in STL format files) transforming them into cross-sections, which are still virtual, and then creating each cross-section in physical space one after the next until the model is finished. Intuitively, this technology provides accurate dimensional products in a short time with less cost. In this project, a method to manufacture the new system components quickly and inexpensively was the top priority. Thus, 3D printing facilities available in the laboratory of the Faculty of Engineering and Environment, Northumbria University (see Fig. 3-11), were utilised for this purpose. Table 3-2 lists the main CUT-LIST components and their materials, including the manufacturing methods employed. The CNC programmes used for manufacturing the parts of the angled overhead nozzle ring are documented in Appendix B (B1 and B2).

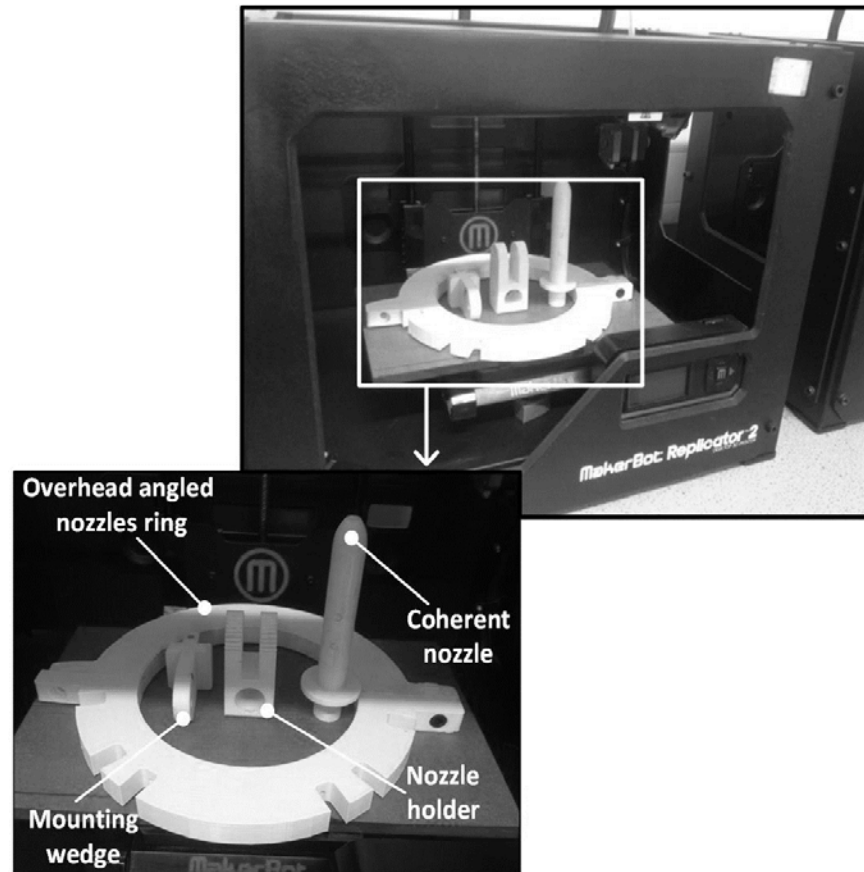


Fig. 3-11 Prototypes of CUT-LIST components produced by the 3D printing machine

Table 3-2 List of main CUT-LIST components and their manufacturing techniques

Component	Material used for prototyping	Material used for final product	Manufacturing method used for prototyping and the final product respectively
Overhead angled nozzle ring	Polylactic acid (PLA plastic)	Aluminium alloy (6082-T651)	MakerBot 3D printing machine and CNC milling machine centre
Mounting wedge	Polylactic acid (PLA plastic)	Polylactic acid (PLA plastic)	MakerBot 3D printing machine
Movable nozzle holder	Polylactic acid (PLA plastic)	Polylactic acid (PLA plastic)	MakerBot 3D printing machine
Coherent round nozzle	Polylactic acid (PLA plastic)	Rigid opaque photopolymer	MakerBot 3D and Object 30 3D printing machine
Workpiece fixture	Polylactic acid (PLA plastic)	Mild steel	MakerBot 3D printing and conventional milling machine

3.6 Determination of parameters of the fluid supply system

In this section, metal removal rate (MRR) and cutting power computations are conducted to determine the accurate flow rates required for different cutting conditions, followed by a fluid dynamics computation to determine the nozzle aperture diameter and fluid velocities. MATLAB 2015a software was utilised for this purpose. This work was carried out in three consecutive stages as follows:

3.6.1 Computation of MRR and cutting power

The step shoulder or side milling process is one of the most common metal removal operations in the machining industry because of its versatility and efficiency. It is widely used in the manufacturing of various critical and large components for aerospace and aircraft applications. Thus, step shoulder-down milling was chosen as a cutting strategy in testing the new system, as shown in Fig. 3-12. Equations 3.1-3.4 were utilised to calculate spindle speed (N), MRR , table speed, (V_f) and total cutting power (P_c) respectively [27, 50]. In step shoulder or side milling, where the cutter diameter (D_c) is larger than the radial depth of cut (a_e), the table speed (V_f) should be adjusted to avoid chip thinning effects. Hence, a compensation factor (K_1) was added and the final equation of table speed was then expressed as in Equation 3.2. The total cutting power was accordingly determined as per Equation 3.4. Table 3-3 details the input parameters selected to calculate spindle and table speeds as well as MRR and cutting power. These outcomes will be used in the next stage to determine the accurate flow rate required in each set of working conditions, which are detailed in the next section.

$$N = \frac{1000 \cdot V_c}{\pi \cdot D_c} \quad [249] \quad (3.1)$$

$$V_f = f \cdot Z \cdot N \cdot K_1 \quad [250] \quad (3.2)$$

$$MRR = V_f \cdot a_p \cdot a_e \quad [27] \quad (3.3)$$

$$P_c = \frac{U \cdot MRR}{60} \quad [26] \quad (3.4)$$

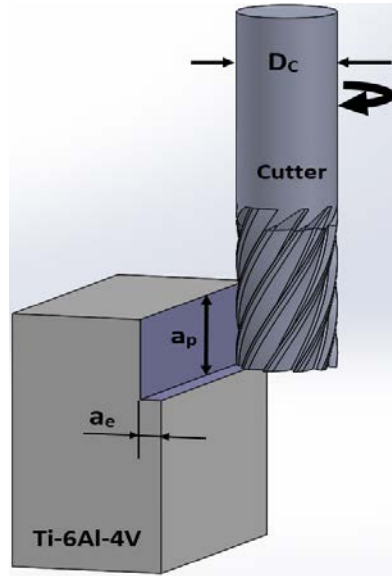


Fig. 3-12 3D view of shoulder-down milling used in the new system computations

Table 3-3 Working conditions used for MRR and cutting power computations

Input	Value
Cutting speed (m/min)	95, 200
Feed rate (mm/rev)	0.1, 0.15
Axial (a_p) and radial (a_e) depth of cut (mm) respectively	5, 1.3
Cutter diameter (mm) and number of interests (Z)	18.5, 1
Specific cutting power of titanium ($W.s/mm^3$)	4 [251]
Compensation factor (K_I)	1.96 [252]

3.6.2 Calculations of accurate flow rate (Q_{acc})

During metal cutting, cutting power is used to deform the chip and to surmount friction in the tool and workpiece and tool-chip interfaces. A great proportion of this power of 90-98% is typically converted into heat, whereas the remaining power is retained as elastic energy in the chip [253-257]. In this study, 90% of the total cutting power is assumed to be converted into the total heat generated in the primary, secondary and tertiary deformation zones. The accurate flow rate of the cutting fluid (Q_{acc}) required to cool the machining zone was then computed according to Equation 3.5 [258].

$$Q_{acc} = \frac{60 \cdot P_c}{4.148 \cdot C \cdot \rho \cdot \eta_{nozzle} \cdot \Delta\theta} \quad [258] \quad (3.5)$$

The inputs to calculate an accurate flow rate at different working conditions are presented in Table 3-4. It is worth mentioning that all computations were established for the mechanical properties of titanium alloy (Ti-6Al-4V), while the type of cutting fluid and cutting tool was chosen based on extensive experimental work. The sample material, geometry, and specifications as well as fluid physical and thermal properties along with other resources used are thoroughly described in the next chapter.

Table 3-4 Inputs and their values used for accurate flow rate computations

Input	Value
η_{nozzle}	0.95 [210]
$\Delta\theta$ (°C)	2 [259]
ρ Cutting fluid mass density at 10% concentration ratio (g/m ³)	0.988
C Cutting fluid specific heat at 10% concentration ratio (cal/g. °C)	0.948

Additionally, although there are no specific references, regarding the delivery of an exact amount of cutting fluid to the machining zone using conventional flood supply systems in the literature, Kennametal Ltd. suggest that an amount of cutting fluid not less than 13 L/min per (kW) could be supplied particularly when cutting titanium in flood cooling conditions [260]. Table 3-5 presents the calculation results obtained for the conventional flood supply system.

Table 3-5 Flow rate calculation results for the conventional flood supply system

Heat generated (kW)	Minimum flow rate per kW when cutting titanium	Flow rate (L/min)
0.124	13 L/min	13× 0.124 = 1.6
0.187	13 L/min	13× 0.187 = 2.4
0.262	13 L/min	13× 0.262 = 3.4
0.393	13 L/min	13× 0.393 = 5.1

Fig. 3-13 shows the computation outcomes obtained for the two systems. As shown, the cutting fluid can be supplied at a flow rate of 8 L/min per (kW) using the CUT-LIST supply system with a reduction in cutting fluid consumption by up to 42% compared to the conventional flood system.

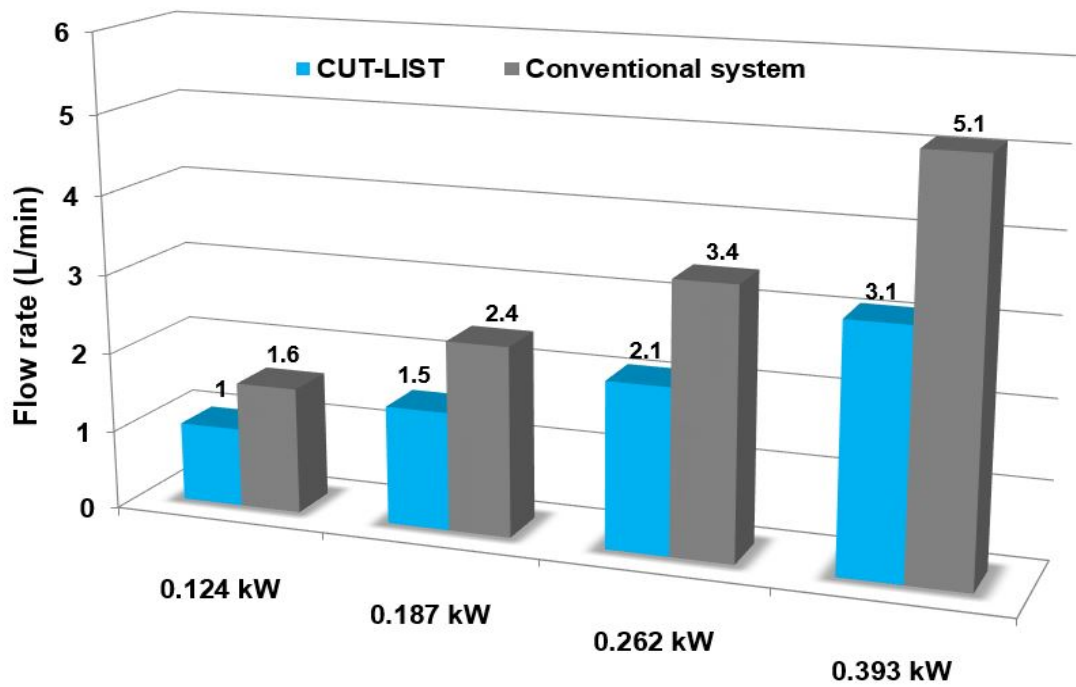


Fig. 3-13 Calculated flow rate versus heat generated for the two supply system

3.6.3 Determination of nozzle aperture diameter and impinging fluid velocity

Once accurate cutting fluid flow rates have been determined, the simplified version of Bernoulli's equation can be utilised to establish the relationship between cutting fluid pressure and fluid velocity, taking into consideration the cutting fluid's specific gravity as shown in Equation 3.6 [205, 210]. Also, at a given flow rate (Q_{nozzle}) and impinging fluid velocity (V_j), the minimal aperture diameter of the coherent round nozzle (d_{nozzle}) can be computed using the continuity Equation 3.7 [210].

$$V_j = \sqrt{\frac{P * 535824}{SG}} \quad [205] \quad (3.6)$$

$$d_{nozzle} = \sqrt{\frac{4 * 19.25 * Q_{nozzle}}{\pi * CD * V_j}} \quad [210] \quad (3.7)$$

To fulfil the above-mentioned equations, the value of actual total fluid pressure (P) is required. To find this, a digital flow meter and digital pressure gauge were utilised to

measure the actual total pressure at a given flow rate (in this case $Q_{nozzle} = Q_{acc}$) per each cutting condition as shown in Fig. 3-13. The fluid measurements were conducted using the machine tool feed pipe exit instead of the nozzle exit to minimise backpressure, as this would affect the measurements. Because the new system has two main nozzles in the feed and against the feed directions, thus they should have equal values of flow rate and fluid pressure. The actual fluid pressure and accurate flow rate per nozzle can be then computed according to Equations 3.8 and 3.9 respectively. Computational outcomes for minimal nozzle aperture diameters and impinging fluid velocities are presented in Table 3-6. All relevant MATLAB work is detailed in Appendix B (B3 and B4).

$$P_{per\ nozzle} = \frac{P_{total}}{2} \quad (3.8)$$

$$Q_{acc\ per\ nozzle} = \frac{Q_{acc\ total}}{2} \quad (3.9)$$

Table 3-6 Computational outcomes for nozzle aperture diameter and fluid velocity

Total actual fluid pressure (bar)	Impinging fluid velocity per nozzle (m/s)	Fluid specific gravity	Minimal nozzle aperture diameter - d_{min} (mm)	Total accurate flow rate (L/min)
0.34	5.86	0.988	1.42	1
0.55	7.46	0.988	1.50	1.5
0.78	8.88	0.988	1.62	2.1
1.16	10.83	0.988	1.75	3.1

To comply with the criteria of fluid dynamics and flow coherence, the contraction ratio (D/d) should be at least $\geq 2:1$ and the actual nozzle aperture diameter (d) must be \geq the theoretical minimal coherent nozzle aperture diameter (d_{min}) in order to ensure the delivery of the required amount of cutting fluid [210]. To achieve the highest jet stream quality, the actual nozzle aperture diameter (d) was tuned at 1.75 mm throughout the study, whereas the contraction ratio (D/d) was set at about 6.85:1 as previously

mentioned, which satisfies the flow coherency criterion. In order to validate these outputs prior to testing the new system, two prototypes of coherent nozzles were built according to the dimensional geometry depicted in Table 3-1. A rigid opaque photopolymer was utilised for this purpose. This material offers smooth internal surfaces that help to minimise the friction losses inside nozzles. The fluid was then circulated using the cutting fluid pump at the actual pressures shown in Table 3-6. All fluids were collected in plastic flasks and then weighed using a precision scale as shown in Fig. 3-14. Similar fluid volumes were delivered per unit time to each of the nozzles with minor errors as shown in Table 3-7.

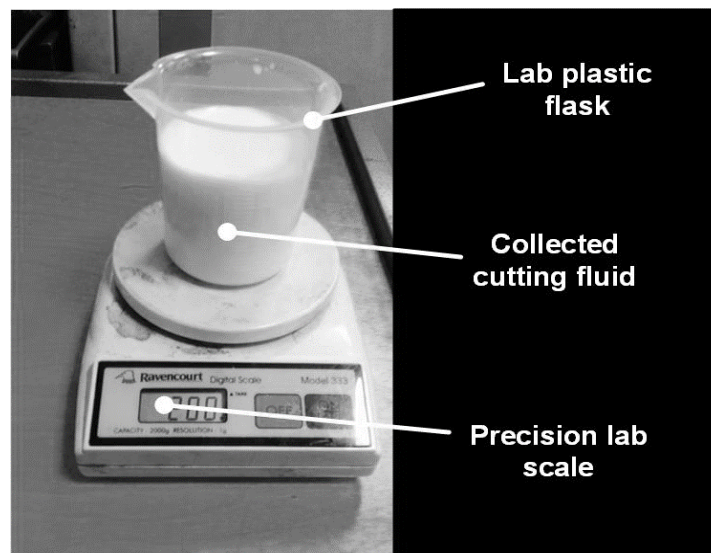


Fig. 3-14 Tools utilised to determine fluid volume collected per unit time

Table 3-7 Actual versus calculated accurate flow rates per nozzle and errors

Flow rate (L/min)	0.34 bar	0.55 bar	0.78 bar	1.16 bar
Nozzle 1	0.50	0.75	1.049	1.549
Nozzle 2	0.498	0.748	1.048	1.546
Total actual flow rate	0.998	1.498	2.097	3.095
Total calculated flow rate	1	1.5	2.1	3.1
Error (%)	0.11 %	0.133 %	0.143 %	0.161 %

3.6.4 Chapter summary

In this chapter, CUT-LIST has been designed based on a closed-loop cooling system configuration. Lower fluid consumption and high fluid penetrability are the main characteristics adopted in this inexpensive and environmentally friendly CUT-LIST supply system. Fluid flow monitoring was performed utilising high-precision flow control equipment such as a digital flowmeter and digital pressure gauges. This equipment was located apart from the cutting fluid pump by > 300 mm to ensure high measurement accuracy and steady state flow conditions. In order to provide high filtering efficiency and to protect the fluid system instruments a durable magnetic-based in-line-type filter was allocated immediately after the cutting fluid pump and just before the fluid entered the system feed pipes. Additionally, the designs for the new system parts, including overhead nozzle ring, nozzles holders and mounting wedges were developed using 2D and 3D CAD environments. All system parts were designed for ease of assembly and manufacturing to reduce costs and minimise the complexity of their fabrication processes. Different metallic and non-metallic materials were assigned for the manufacture of the new system components. The coherent nozzles were designed and manufactured based on a Webster jet nozzle model to provide high fluid jet coherency and velocity. The computation of fluid system parameters was conducted to determine accurate flow rates and nozzle aperture diameters as well as fluid velocities. Heat generation in the machining zone along with fluid properties such as fluid density and heat capacity were included in the calculations for the new system. The outcomes showed that the cutting fluid could be supplied at 8 L/min using CUT-LIST compared with ~ 13 L/min for the conventional flood system, thus offering fluid consumption saving up to 42%. In order to comply with fluid dynamics and flow coherence criteria ($d \geq d_{\min}$ and $D/d \geq 2:1$), the diameter of the nozzle aperture and inner diameter were fixed at 1.75 and 12 mm respectively, giving a contraction ratio of $\sim 6.85:1$ which fulfils the requirements of high flow jet quality and coherency. Finally, theoretical fluid system outputs of calculated accurate flow rates were validated using two coherent round nozzle prototypes. Both nozzles delivered similar volumes of fluid per unit time with a limited amount of error up to 0.16 % compared to the calculated accurate flow rates. Design specifications and aspects details of the CUT-LIST supply system are presented in Appendix C. The outcomes of phases 2 and 3 are then used in the next phase 4 to test the new system as described in chapter 4.

Chapter 4 Experimental Work

This chapter describes all of the experimental activities conducted in phase 4, including testing the new system. Specifically, it details the design of experiments (DOE), and the workpiece materials, cutting tools, and cutting fluids as well as the machine tools and measuring equipment utilised in each experimental stage. The methods and ISO standards used for measuring key process outputs (e.g. Ra, tool wear, etc.) are also presented. As pointed out earlier, in order to test the new CUT-LIST system, crucial machining inputs such as type of VO-based fluid, concentration ratio, and cutting tool material should be identified and optimised. To fulfil these requirements, the experimental work was carried out with the two cutting processes of turning and milling. The turning-based machining trials are presented in four main sections: the evaluation of different vegetable oil- and mineral oil-based cutting fluids (4.1); the pre-selection of cutting conditions (4.2); selection of vegetable oil-based cutting fluid and cutting tool material (4.3); and the assessment of cutting fluid concentration ratio (4.4). Milling-based machining trials are then detailed in section 4.5, which represent the evaluation of the CUT-LIST cutting fluid supply system. The reasons for choosing turning and milling are as follows:

- a) Turning is the most common operation utilising a single point tool where only one cutting edge is continuously engaged in the action of material removal. Thus, it offers low tooling costs and makes the measurement of tool performance easier.
- b) Integrating CUT-LIST into a CNC milling machine is more beneficial due to its variety of cutting processes compared to turning lathes and other chip removal-based machines.
- c) The requirements for the investigation of process parameters affecting machining performance prior to assessing CUT-LIST can be fulfilled using relatively simple turning. Meanwhile, cutting by milling complies with the requirements for testing the new system, where an investigation of the effect of factors such as nozzle positions and impinging distances on machining outputs are paramount. Fig. 4-1 shows the various parameters influencing turning and milling processes.
- d) Process utilisation is maximised, given the diversity in the cutting strategies adopted such as continuous cutting (turning) and interrupted machining (milling).

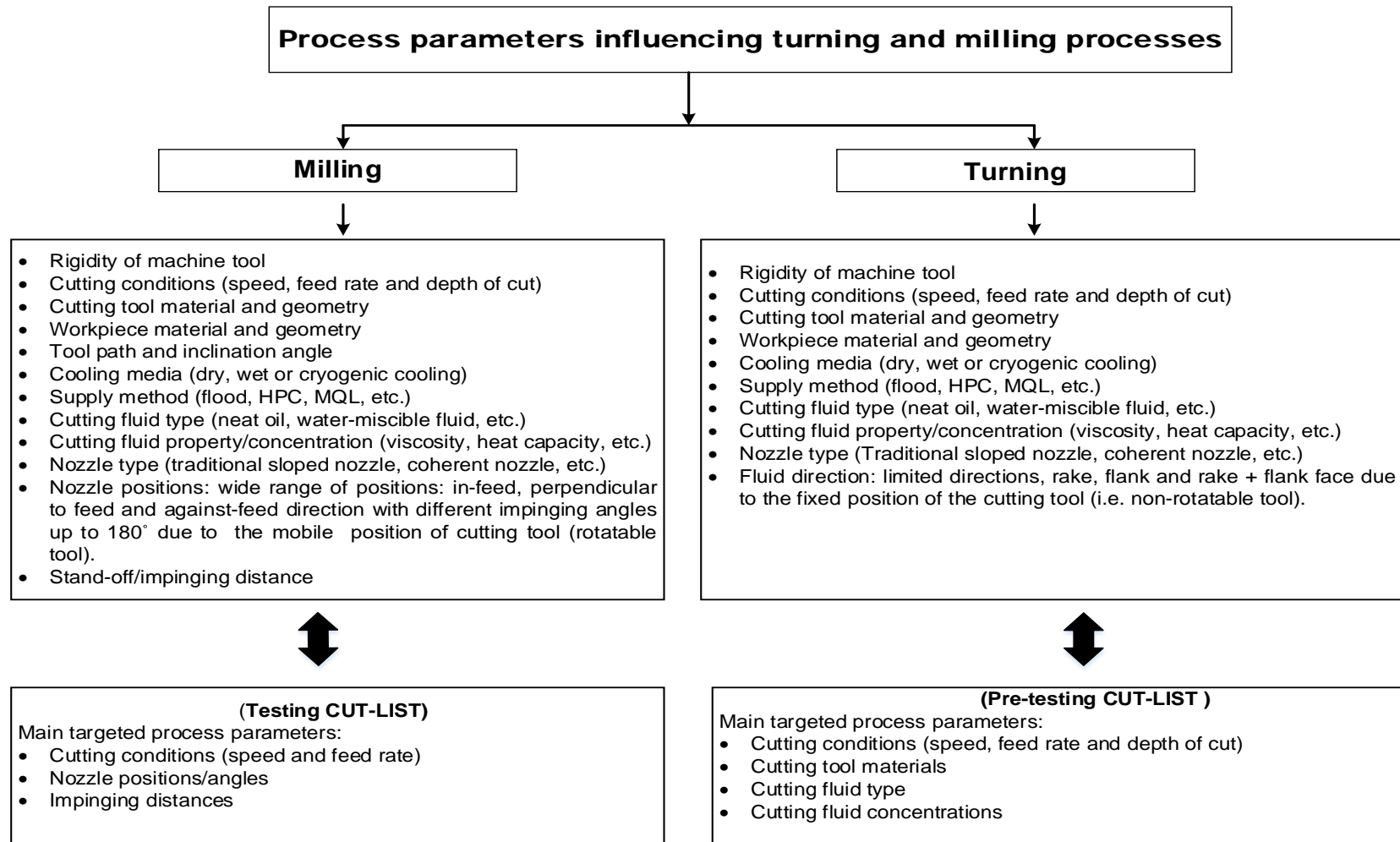


Fig. 4-1 Process parameters affecting turning and milling processes [4, 26, 194]

4.1 Evaluation of different vegetable oil- and mineral oil-based cutting fluids and tool materials

It was revealed in the literature review that a few works have been carried out, particularly on the machining of titanium alloys, using different VO-based cutting fluids and cutting tool materials and coatings. Thus, this experimental stage aims to compare the performance of four soluble types of VO-based fluid against the reference mineral oil-based cutting fluid when employing different cutting tool materials. The evaluation included the measurement of surface roughness (Ra) and tool flank wear (VB).

4.1.1 Design of experiment (DOE)

The investigation involved 20 tests using a full factorial design of experiment (5x4). Two factors were evaluated, namely cutting fluid type and cutting tool materials and coatings, each at 5 and 4 levels respectively. Cutting speed, feed rate and depth of cut were constant at 75 m/min, 0.15 mm/rev and 0.75 mm respectively. Table 4-1 shows details of the cutting tools and fluids used throughout the work.

Table 4-1 Process variables and levels

Factor	Level 1	Level 2	Level 3	Level 4	Level 5
Cutting fluid	Hocut 3450	Vasco 1000	Coolant NE250 H	Solutech	MO-based (Cooledge)
Cutting tool	Uncoated carbide, (H13A)	PVD (TiAlN coated carbide), (GC1105)	Uncoated fine grain carbide, (H10F)	CVD coated carbide, (S05F)	

4.1.2 Machine tool and workpiece material

All experiments were performed on a Graziano Tortona Centre lathe (SAG 12). Titanium Ti-6Al-4V ASTM B348 grade 5 samples of \varnothing 30 mm in diameter, and 330 mm long are used as workpieces and were mounted between the spindle chuck and centre. The chemical composition and mechanical properties of Ti-6Al-4V ASTM B348 grade 5 are detailed in Table 4-2 and Table 4-3 respectively. Each trial involved a cutting length of

100 mm. For each test, a new cutting edge was used. Fig. 4-2 shows the experimental set-up. The technical data sheets (TDS) and the bill of materials (BOM) for all consumables such as workpiece materials, cutting fluids and equipment used in this section till section 4.4 are provided in Appendices D and E (E1) respectively.

Table 4-2 Chemical composition of Ti-6Al-4V (ASTM B348 Grade 5) [261]

Weight (%)	Al	Fe	N	H	O	C	V	Ti
Min	5						3	
Max	6	0.4	0.05	0.015	0.2	0.08	4	Balance

Table 4-3 Mechanical properties of Ti-6Al-4V (ASTM B348 Grade 5) [261]

Elongation (%)	Hardness (HRC)	Tensile strength (MPa)	Elastic modulus (GPa)	Yield strength (MPa)	Fracture toughness (MPa m ^{1/2})
18	36	1000	114	910	33 - 110

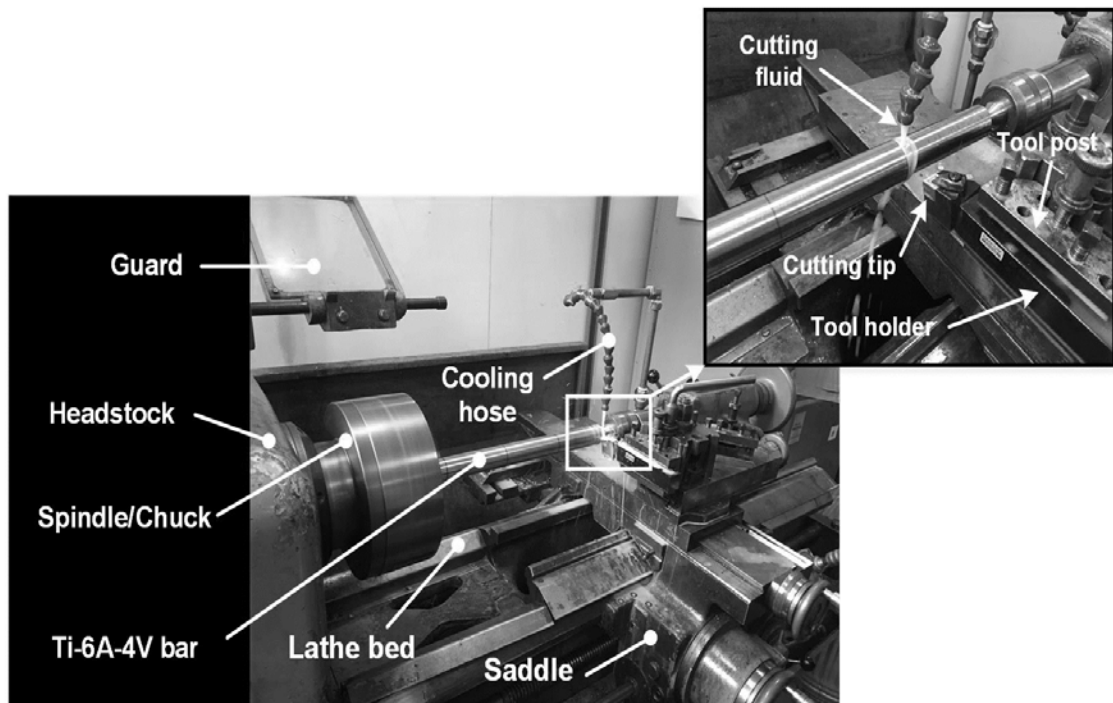


Fig. 4-2 Image of the set-up for the external straight turning of Ti-6Al-4V

4.1.3 Cutting tool materials and coatings

Four different turning indexable inserts supplied by Sandvik were tested. All inserts have a similar rhombic shape, ISO designation (CNMG120408), and chip breaker geometry (SM). All tools had the following cutting tip geometries; cutting edge angle of 95°, nose radius of 0.8 mm, clearance and tool entering angles of 0° and 80° respectively. The inserts were mounted on a Sandvik tool holder with the ISO designation (DCLNR 2525M 12). Table 4-4 shows the properties of the cutting tool materials, and Fig. 4-3 illustrates the tool holder used and its geometry, and Fig. 4-4 provides images of the cutting inserts. Descriptions of the ISO designations for the indexable inserts and tool holder are presented in Appendix F.

Table 4-4 Properties of cutting tool materials used in the experiments [262]

Tool	Elements	Density (kg/m ³)	TRS (MPa)	Grain size (µm)	Hardness (HRA)
H13A	W/Co	15000	2690	3.5	93
GC 1105	Hard metals/PVD	14750	2550	2.5	93
S05F	Hard metals/CVD	14950	2350	2.5	92
H10F	W/Co	15100	2695	1	94

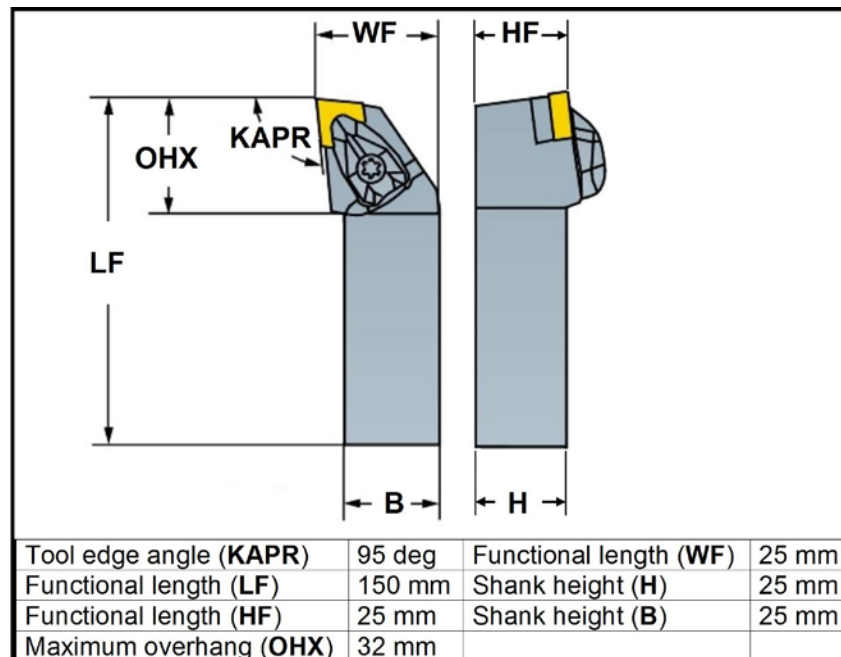


Fig. 4-3 Image of tool holder and its geometry[262]

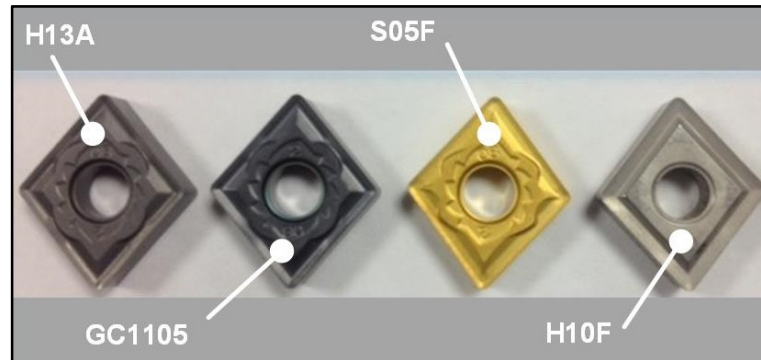


Fig. 4-4 Images of various tool materials utilised in the experiments

4.1.4 Cutting fluids

Four soluble commercial types of VO-based cutting fluid were evaluated and compared with a standard water-miscible MO-based fluid (Castrol Cooledge BI). The fluid selection was based on the different properties and characteristics inherent in each of the oils provided by the suppliers, as shown in Table 4-5. Additionally, fresh cutting fluids were blended at 5 % concentration. Cutting fluids were supplied to the machining zone via a commercial type (Loc-Line) coolant hose. Cutting fluid was flooded at a flow rate of about 10 L/min during all tests.

Table 4-5 Characteristics and properties of the fluids tested

Cutting fluid	Hocut 3450	Vasco 1000	SOLUTEC	NE250H	Cooledge BI
Base oil content	43%	45%	35%	28%	60%
Specific gravity @ 20 °C	0.97	0.95	0.97	0.98	0.93
Viscosity @ 40 °C (mm ² /s)	55	56	38	30	58
Unique tribological characteristics	High lubricity/ anti-wear property	High lubricity/ inhibition against corrosion	Good lubricity/ low foaming anti-wear property	Good inhibition against corrosion	High lubricity/ low foaming anti-wear property
Supplier (UK)	J. Clayden Lubricant	Jemtech Ltd.	John Neale Ltd.	Solutec Ltd.	Castrol Limited

4.1.5 Measurement equipment

4.1.5.1 Refractometer

Control of fluid concentration is important during the cutting process. Low concentrations can lead to rust, mixture instability and microbial growth, while foaming, heavy residues and skin irritation are common issues with high concentration fluids. A refractometer is a hand-held optical instrument that is used to measure the refractive index of a fluid. The refractive index is the degree that light is bent when passing through a fluid [90]. In this investigation, the cutting fluid mixture concentrations were kept constant at 5 % and were regularly checked using an Oxford portable optical refractometer. The technical specifications of the refractometer were: Brix scale range (up to 30 %), 11x eyepiece magnification, 4x telescopic lens magnification, and accuracy and lattice values of ± 0.0003 %, and 0.0005 % respectively. Fig. 4-5 shows the portable refractometer used in all experimental activities.

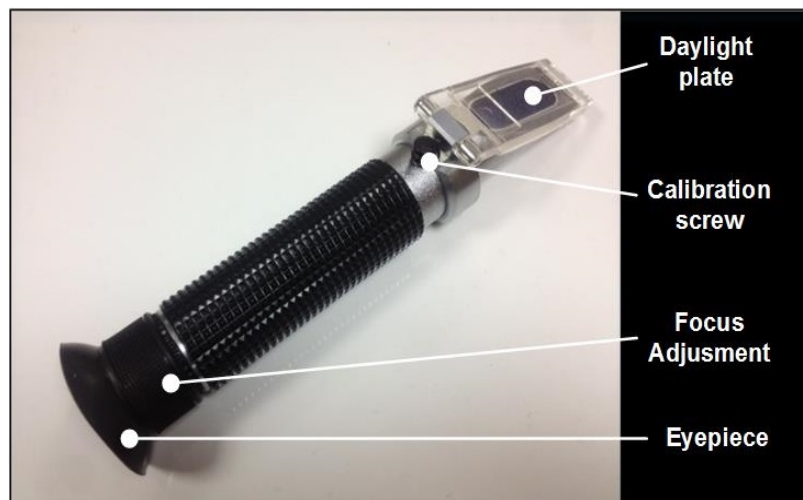


Fig. 4-5 Photograph of the portable optical refractometer used in the study

4.1.5.2 3D surface profiler (Alicona InfiniteFocus)

The Alicona InfiniteFocus is an optical scanning microscope used for 3D surface measurements. Topographic and colour data about the surface is produced through variations in focus in combination with vertical scanning. Small regions of the object are sharply imaged due to the small depth of field of the optics. The full depth of field and

complete detection of the surface are obtained when the precision optics move vertically along the optical axis, continually capturing information from the surface [263]. The Alicona InfiniteFocus G4 type optical scanner was used to assess the 3D surface topography of the machined Ti-6Al-4V bars, having a resolution down to 10 nm. The scanning area was 13mm x 4mm in the axial and circumferential directions respectively. Scans were obtained using 200 nm and 7 μm vertical (Z direction) and lateral (X and Y) resolutions respectively. Fig. 4-6 shows the set-up for the scanning of 3D surfaces of the machined Ti-6Al-4V bars. In addition, the Alicona was utilised for tool wear measurement. Average tool flank wear (VB) was measured following each trial and after cutting a 100 mm length of the titanium sample. All tool wear measurements were conducted in accordance with the ANSI/ASME B94.55M-1985. Alicona scan settings used during the tool wear measurements were: exposure time 512 μs , contrast 0.81, x10 magnification factor, and vertical and lateral resolution of 514.4 nm and 10.24 μm respectively.

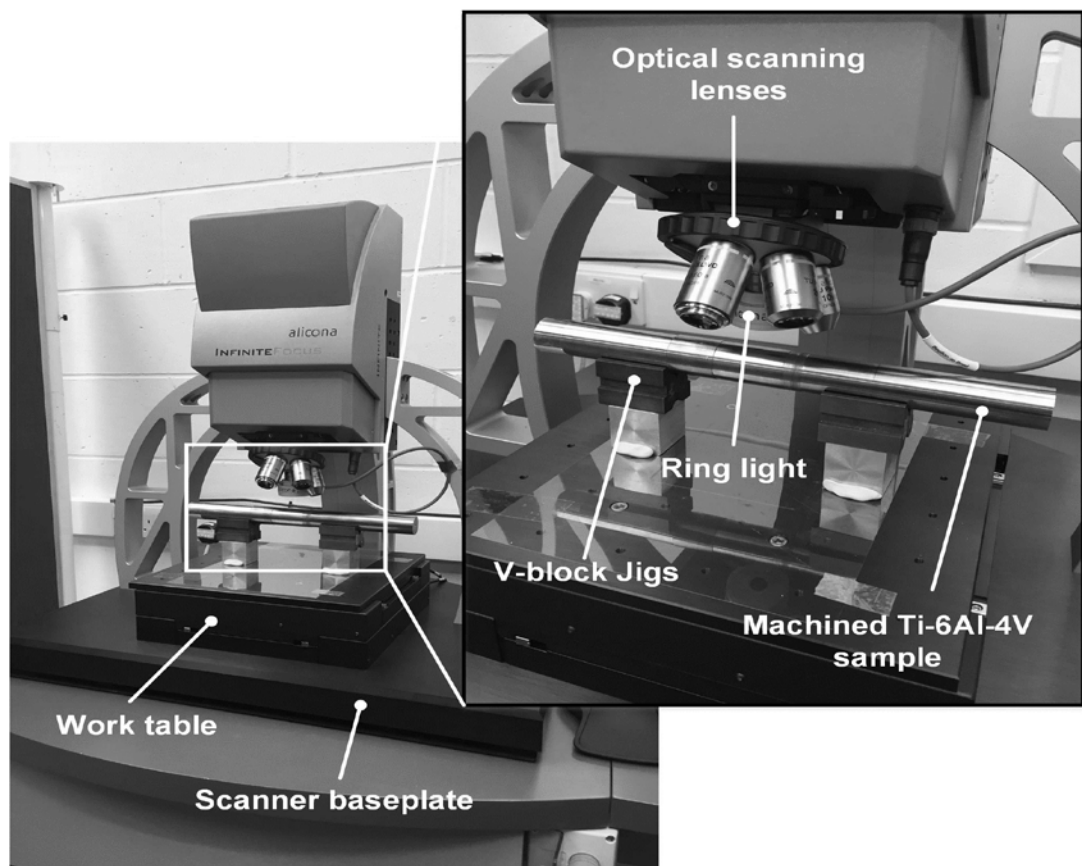


Fig. 4-6 Image of set-up for the 3D scanning of the machined Ti-6A-4V bars

4.1.5.3 *Leica EZ4 D microscope*

The Leica EZ4 D stereoscope is an optical device, as shown in Fig. 4-7, with a magnification range from x8 to x35, zoom ratio of 4.4:1, and an optimised viewing angle of 60°. In conjunction with Leica LASEZ software, the microscope was used to observe wear on the cutting tool edges, including the definition of tool discolouring, catastrophic chipping or fractures, using a magnification factor of x35.

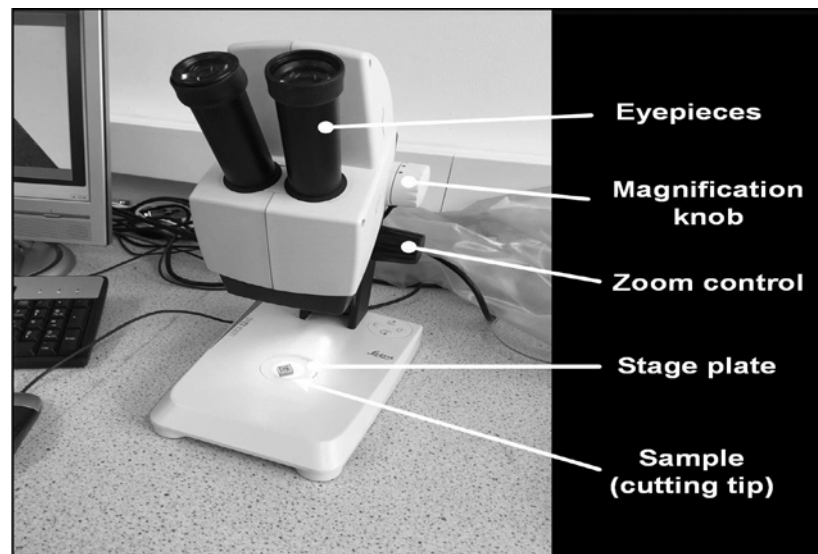


Fig. 4-7 Photograph of Leica EZ4 D optical microscope

4.1.5.4 *Surface roughness testing*

The Taylor Hobson surface tester is a stylus-type instrument which provides a numerical assessment of average surface roughness parameters. A stylus tip makes direct contact with the surface of a sample. The detector tip is accommodated within a stylus tip, which traces the surface of the sample and electrically detects the vertical motion of the stylus. The signals collected go through amplification and digital conversion processes in order to be recorded. The stylus tip radius is 10 μm . Average surface roughness (R_a) was measured using the Taylor Hobson Surtroni 3+ type instrument, which has a resolution of 0.01 μm . All measurements conformed to ISO 4287 and ISO 4288 standards using a 0.8 mm cut-off and an evaluation length of 4 mm. Three R_a readings at the beginning, middle and end of the cut were recorded and an average was then computed. Fig. 4-8 shows the set-up for the R_a measurements for the machined Ti-6Al-4V samples.

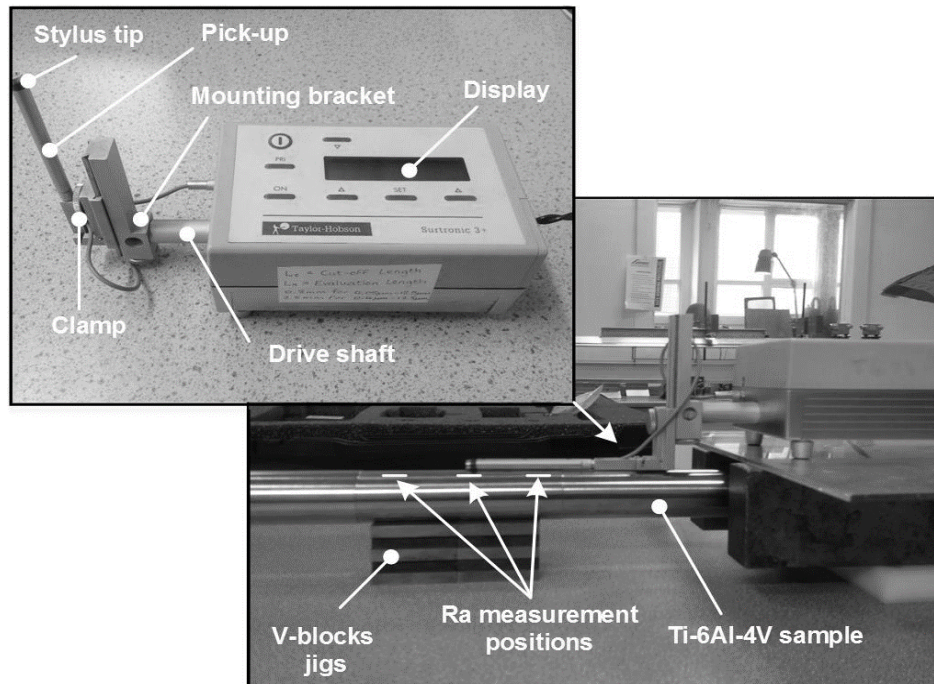


Fig. 4-8 Image of Ra measurement set-up used for Ti-6Al-4V machined bars

4.2 Pre-selection of cutting conditions

This section aims to evaluate the limits for machining titanium at different cutting conditions (cutting speed, feed rate and depth of cut) under wet cutting environments (flood cooling). The other intention is to investigate the impact of the cutting conditions of cutting speed, feed rate and depth of cut on the machining of Ti-6Al-4V alloy using a VO-based cutting fluid. The outcome of this investigation will lay the basis for the selection of cutting conditions in the next experimental section.

4.2.1 Experimental design

The experiments involved 27 trials utilising Taguchi orthogonal array of L27 (3^3). The machining parameters (control factors) considered in the experiments were: cutting speed, feed rate, and depth of cut. Each parameter has three levels, denoted 1, 2, and 3. Table 4-6 indicates the factors and their levels. In these trials, the maximum selected cutting speed was doubled up to 120 m/sec compared with titanium conventional machining speed. Statistical analysis of variance (ANOVA) was also utilised to assess the influence of process variables on the key process measures of Ra and tool wear.

Table 4-6 Control factors and levels

Factors	Level 1	Level 2	Level 3
Cutting speed (m/min)	28	75	120
Feed rate (mm/rev)	0.1	0.15	0.2
Depth of cut (mm)	0.5	0.75	1

4.2.2 Workpiece material and set-up

Straight external turning tests were conducted on Ti-6Al-4V ASTM B348 Grade 5 having a diameter of \varnothing 30 mm, and 330 mm long. All machining trials were carried out using the SAG 12 centre lathe machine. Each test comprised a cutting length of 100 mm and a new tool tip was used. The as-received bars were initially cleaned (turning at 0.5 mm depth) to ensure the consistency of the workpiece material. The experimental set-up is illustrated schematically in Fig. 4-9.

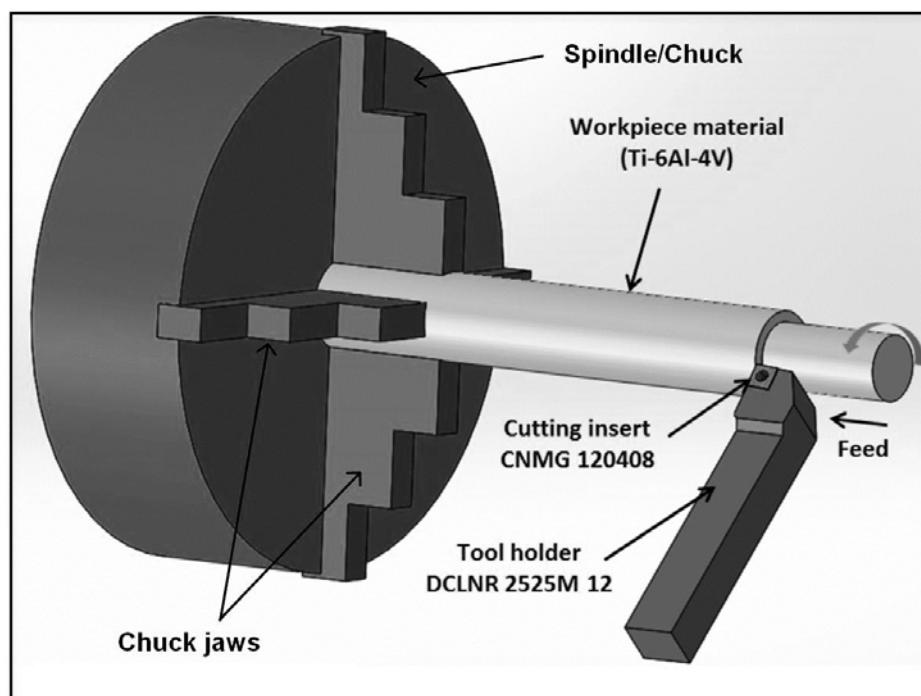


Fig. 4-9 3D schematic view of the external straight turning of Ti-6Al-4V set-up

4.2.3 Tool material and cutting fluid

Sandvik (H10F) uncoated fine-grained tungsten carbide tools were used in all trials. Hocut 3450 vegetableoil-based cutting fluid was selected for this investigation. The fresh cutting fluid was blended at 5 % concentration whilst the fluid was applied to the machining zone through a traditional flexible PVC coolant hose. The fluid was flooded at 10 L/min flow rate during all trials. The dilution was regularly checked using the portable refractometer.

4.2.4 Equipment for measuring surface roughness and tool wear

Ra was measured using a Taylor Hobson Surtroni 3+ type tester while the Alicona scanner was utilised for tool wear measurement. All measurement procedures of Ra and tool wear are similar to those described in section 4.1. Tool wear measurements were conducted using an exposure time of 241 μ s, contrast 0.67, x10 magnification, and vertical and lateral resolutions of 542 nm and 10.33 μ m respectively.

4.3 Selection of vegetable oil-based fluid and cutting tool material

This investigation aims to identify the best VO-based cutting fluid and cutting tool material for the testing of the developed system. Thus, four soluble commercial types of vegetable oil-based fluid were assessed in terms of surface roughness (Ra), tool flank wear (VB) and chip thickness at different cutting conditions and cutting tool material/coatings. The range of cutting speeds was also extended. The aim here was to improve the productivity of the cutting of titanium.

4.3.1 Design of experiment

The straight external turning experiments involved 24 trials employing a full factorial design of experiment (4x3x2). Three factors were evaluated, namely type of cutting fluid, cutting tool material and cutting speed, at four, three and two levels respectively. A feed rate of 0.1 mm/rev and depth of cut of 0.75 mm were maintained in all trials. Table 4-7 shows the operating conditions.

Table 4-7 Operating conditions

Parameters	Level 1	Level 2	Level 3	Level 4
Cutting fluid	Hocut 3450	Vasco 1000	NE250H	Solutech
Cutting tool	Uncoated carbide, (H13A)	PVD (TiAlN coated carbide), (GC1105)	CVD coated carbide, (S05F)	
Cutting speed (m/min)	120	175		

4.3.2 Workpiece material and machine tool

All turning tests were conducted on a SAG 12 centre lathe machine. The commercial Ti-6Al-4V ASTM B348 grade 5 workpiece samples used were 28 mm in diameter and 330 mm long and were mounted between the spindle chuck and the tailstock. Each test involved a cutting length of 100 mm. To avoid the influence of tool wear, all trials were performed using new cutting tips.

4.3.3 Tool materials and cutting fluids

Three different Sandvik tool materials were selected for the investigation, including uncoated W/Co carbide (H13A), PVD coated (GC1105), and CVD coated carbide (S05F). In addition, the reference MO-based fluid was excluded and only four water-miscible type VO-based fluids (Hocut 3450, Vasco 1000, NE250H and Solutech) were used. All raw fluids were blended at 5 % concentrations whilst the fluid was supplied to the machining zone via a conventional \varnothing 10 mm flexible rigid plastic coolant hose. The cutting fluid was flooded at a flow rate of approximately 10 L/min.

4.3.4 Equipment

Surface roughness (Ra) was measured using a Taylor Hobson Surtroni 3+ surface roughness tester, whereas the Alicona machine was employed for tool wear measurements. All Ra and tool wear measurements conformed to ISO 4287, ISO 4288 and ANSI/ASME B94.55M-1985 standards respectively. The Alicona scans settings were: exposure time 181 μ s, contrast 0.56, magnification factor x10, and vertical and

lateral resolutions of 497 nm and 10.75 μm respectively. Chip thickness was measured using the Mitutoyo digital micrometer.

4.4 Assessment of cutting fluid concentration ratio

This experimentation aims to identify the preferred concentration ratio of the VO-based fluid that was chosen in the previous investigation (section 4.3). Other aims are to investigate the influence of VO-based fluid concentration when machining titanium using different tool materials, and to evaluate the effect of cutting conditions of cutting speed and feed rate on the key process measures such as Ra, tool life, and micro-hardness.

4.4.1 Experimental design

The evaluation involved 27 tests using Taguchi orthogonal array of L27 (3^4). The four factors which were evaluated were cutting fluid concentration, tool material, cutting speed and feed rate, each at 3 levels as shown in Table 4-8. A constant depth of cut of 0.75mm was used. Analysis of variance (ANOVA) was also employed to evaluate the impact of process variables on the key measures.

Table 4-8 Process variables and levels

Factor	Level 1	Level 2	Level 3
Cutting fluid concentration (%)	5%	10%	15%
Cutting tool material	H10A	GC1115	H13A
Cutting speed (m/min)	58	91	146
Feed rate (mm/rev)	0.1	0.15	0.2

4.4.2 Workpiece material and sample preparation

Round bars of 24 mm in diameter and 160 mm length were used as workpiece materials as shown in Fig. 4-10. The bars were made of Ti-6Al-4V grade 5 alloy. All turning trials were performed on a Graziano SAG12 lathe machine. Each test involved a cutting length of 120 mm and a new insert was used.

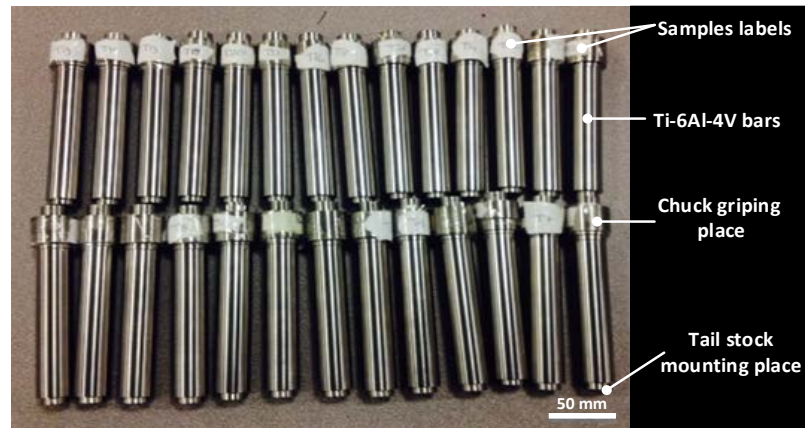


Fig. 4-10 Ti-6Al-4V bars used for turning trials

4.4.3 Tool material

Three different cutting tool materials were used, including uncoated coarse-grained carbide (H13A), fine-grained PVD coated (GC1115) and uncoated W/Co carbide tools (H10A). Tool properties and characteristics are depicted in Table 4-9.

Table 4-9 Tool materials used in the experiment in section 4.4 and their properties

Tool	Elements	Grain size	Properties
H13A	W/Co - uncoated	Coarse-grained carbide ($\geq 3\mu\text{m}$)	Combines good abrasive wear resistance and toughness for medium to a rough cutting of heat-resistant and titanium alloys.
GC 1115	Hard metals - PVD coated carbide (TiAlNi)	Fine-grained coated carbide ($<1\mu\text{m}$)	Combines hot hardness and good resistance to plastic deformation. Offers excellent resistance to smearing of material and good adhesion on tool sharp edges.
H10A	W/Co- uncoated	Fine-grained uncoated carbide ($<1\mu\text{m}$)	Good wear resistance for finishing to medium roughing of heat-resistant and titanium alloys

4.4.4 Cutting fluid concentration

A water-miscible VO-based cutting fluid (Vasco 1000) was used. Three concentration ratios of 5%, 10% and 15% were evaluated with a constant flow rate of 10 L/min. A conventional flood supply method was used to deliver the cutting fluid into the machining

zone through a conventional sloped coolant nozzle (PVC Loc-line type). Concentration was checked using the portable refractometer. The fluid's thermal and physical properties were measured at different concentrations and the results are presented in Table 4-10.

Table 4-10 Thermo-physical properties of the Vasco 1000 at various concentrations

Concentration ratio (%)	5%	10%	15%
Mass density (Kg/m ³)	996	988	976
Dynamic viscosity @ at 25°C (cP)*	1.4	1.8	2.2
Average heat capacity @ at 25°C (J/g/°C)*	4.12	3.97	3.88

*The higher is better [108, 264]

4.4.5 Tool life analysis

Following the 27 trials, tool life tests were carried out at the lower and higher speeds of 58 and 146 m/min respectively. Tool rejection criteria were determined in accordance with the ISO 3685 (1993) standard for tool life testing. A cutting insert was rejected and the machining test ceased if one or a combination of the following took place: if the maximum flank wear (VB_{max}) reached 0.3 mm, and if excessive chipping or a severe fracture of the edge occurred. After each test, tool wear and surface roughness were measured and the tool tip was reused with another sample (Ti-6Al-4V \varnothing 22.5 mm x 120 mm) until the above limits were reached. The machining conditions selected in performing the tool life test were a feed rate of 0.1 mm/rev, depth of cut of 0.75 mm, and the fluid concentration of 10 %, and uncoated tungsten carbide (H13A) tool material was used. Equation 4.1 was utilised to compute the actual cutting time.

$$t = \frac{\pi \cdot D_{wp} \cdot L}{1000 \cdot f \cdot V_C} \quad [50] \quad (4.1)$$

4.4.6 Micro-hardness test

Micro-hardness tests were performed on the Ti-6Al-4V samples, which were also examined in terms of tool life. Five samples cut at the lower cutting speed of 58 m/min and three cut at the higher cutting speed of 146 m/min were examined.

4.4.7 Equipment

4.4.7.1 Surface roughness and tool wear measurement

All Ra and tool wear measurements were carried out using the Taylor Hobson Surtroni 3+ tester and the Alicona G4 microscope respectively. Alicona scan settings used for tool wear measurements were an exposure time of 182 μ s, contrast 0.51, magnification factor x10, and vertical and lateral resolutions of 550.44 nm and 10.42 μ m respectively.

4.4.7.2 Materialographic sample preparation and instrumentation

A total of 8 machined samples were cut and prepared for the micro-hardness test. Each bar was securely held, and a power hacksaw machine was used to remove a small slice from the end of the bar (\varnothing 22.5 x 4mm), as shown in Fig. 4-11a. The sample was then mounted in Buehler red phenolic bakelite (Fig. 4-11b) utilising a mounting press (Fig. 4-12). In order to remove the surface damage caused by the cutting of the bar with the hacksaw machine, the samples were ground and polished by 1mm. This was done on the METASERV 2000 type grinding and polishing machine and different grades of \varnothing 200 mm SiC papers were used, starting with rough grades and gradually getting finer (P60, P240, P600, P1200 and P2500). In order to obtain high polished surface quality, an ultra-fine (Struers DP 9) polishing machine together with Hyprez diamond lapping fluid was utilised for this purpose. Fig. 4-13 shows the grinding and polishing and ultra-fine polishing set-up.

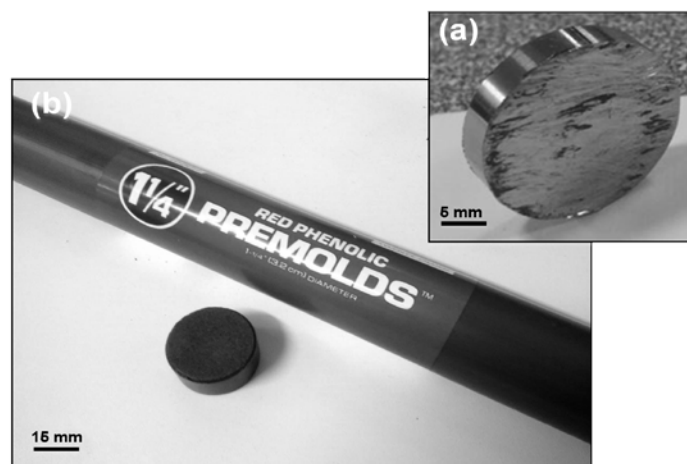


Fig. 4-11 Micro-hardness test: (a) cut-out sample and (b) Bakelite material type used



Fig. 4-12 Mounting press used to form the material into the Bakelite sample

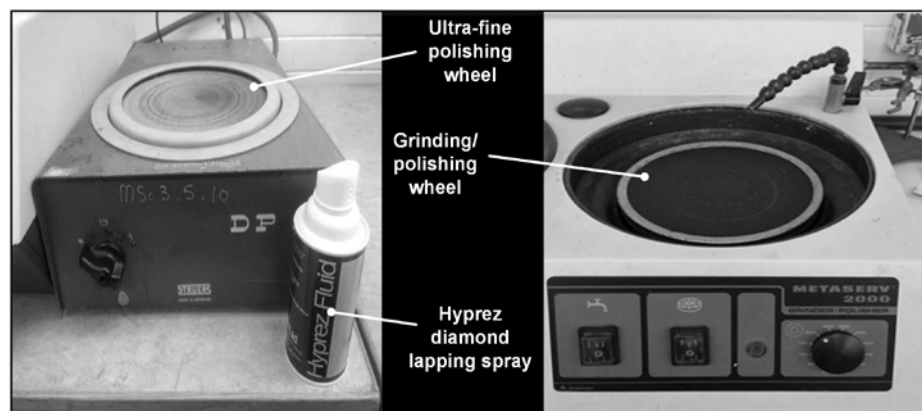


Fig. 4-13 Grinding/polishing and ultra-fine wheels used for sample preparation

Micro-hardness tester

Hardness is the resistance of a material to permanent deformation. During the loading of the tester, the indenter is positioned so as to make contact with the test material at an angle of 120 degrees. The contact period (dwell time) is usually several seconds. The degree of indentation can be measured using the Vickers/or Knoop hardness scale systems. In this experiment, a Buehler Micromet II micro-hardness tester (see Fig. 4-14) was utilised to measure the micro-hardness of the Ti-6Al-4V machined bars. All micro-hardness trials were conducted using an indentation load of 100g, a magnification of x40, and a dwell time of 12s, with the assistance of a Vickers indenter. A total of 15 indentations were made vertically in the middle of the polished surface of each at an intervals of 30 μ m

between consecutive measurements. All measurements were taken according to the ISO 6507-1 standard where the length of diagonal of each indentation $\geq 20 \mu\text{m}$. Fig. 4-15 shows the positions of indentation marks used for the micro-hardness test.

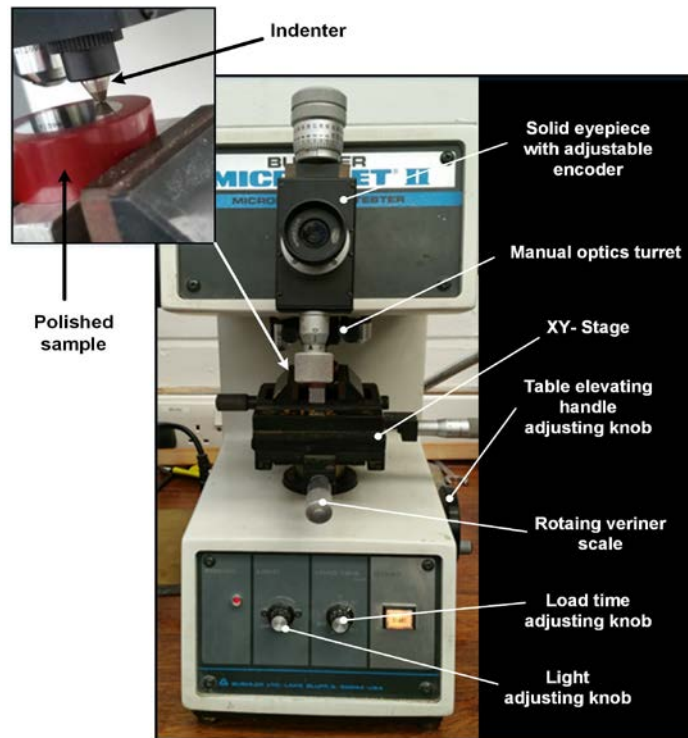


Fig. 4-14 Micro-hardness tester utilised for measuring Ti-6Al-4V machined samples

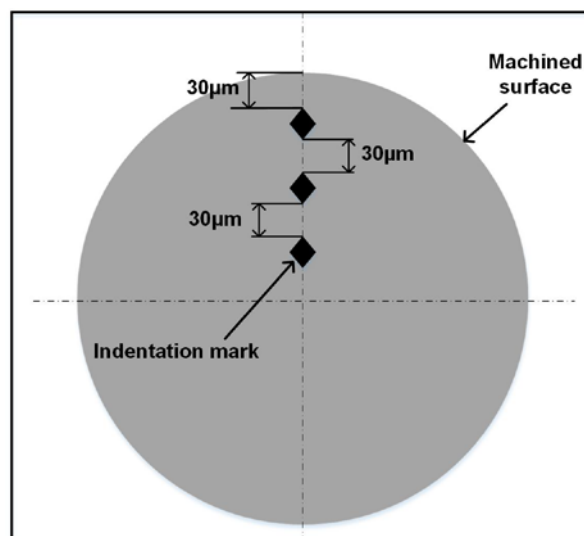


Fig. 4-15 Location of indentation marks used for micro-hardness test

4.4.7.3 Cutting fluids viscosity and specific heat capacity measurement

Viscometer

In order to test the dynamic viscosity of the Vasco1000 cutting fluid, three samples of cutting fluid at different concentrations of 5%, 10% and 15% were collected as shown in Fig. 4-16, and a portable Viscolite 700 type viscometer was utilised (see Fig. 4-17). Its specifications were; range 0 to 10,000 cP, repeatability > 1%, temperature standard -40 to + 150 °C, minimum sample 50ml, sensor weight 700g, and overall length of display unit 305 mm, and the solid sensor material was 316 stainless steel.



Fig. 4-16 Collected fluid samples at various concentrations

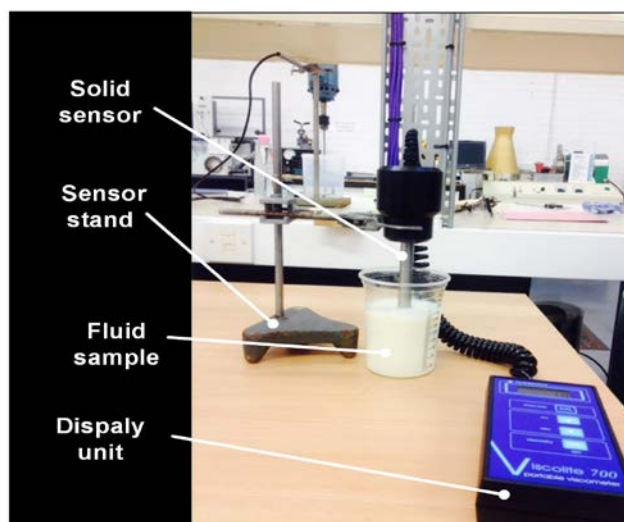


Fig. 4-17 Viscometer used to measure the dynamic viscosity of cutting fluids

Differential scanning calorimeter (DSC)

In order to measure the specific heat capacity of the collected samples of Vasco 1000 fluid at concentrations of 5%, 10% and 15% a PerkinElmer DSC 7 type differential scanning calorimeter, as shown in Fig. 4-18, was used with Pyris software v7. All samples were tested at 25 °C. The DSC analyser measured heat flow energy versus time or temperature within a controlled environment. Additionally, fluid samples were analysed in sealed aluminium sample pans, which requires three different pans to perform the complete heat capacity measurements: an empty pan, a sealed sapphire reference sample, and finally a sealed pan containing the fluid sample weighing 15 mg. Each sample bottle was well-shaken before a 15 μ L aliquot was taken using an auto pipette with a disposable tip. The fluid was then carefully transferred into the sample pan, and the sample pan was then hermetically sealed in preparation for measurement in the DSC. A new tip was used for each fluid concentration. The test results are presented in Appendix G.

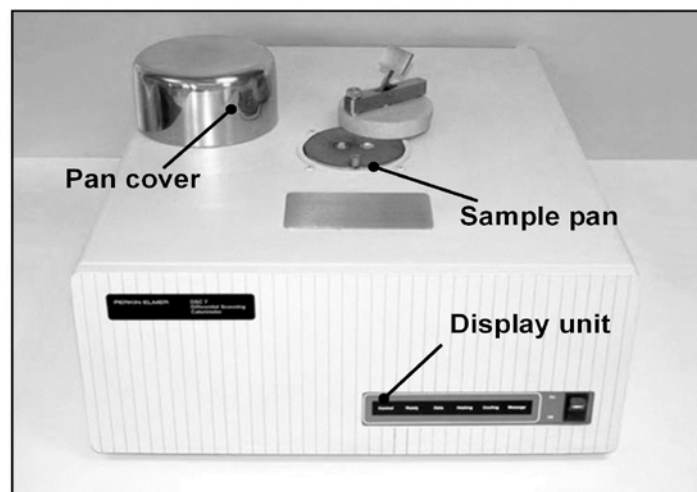


Fig. 4-18 Differential scanning calorimeter (DSC) [265]

4.5 Evaluation of the CUT-LIST cutting fluid supply system

4.5.1 Design of experiments

This phase was divided into two main parts. Part I focused on a performance comparison between the new and conventional supply systems, whereas Part II evaluated the settings of the new system. Because CUT-LIST has the capability various different settings such

as nozzle angle positions and impinging distance, compared to the existing conventional flood supply system, CUT-LIST was initially evaluated with 3 impinging angles in the feed direction, 3 impinging angles against the feed direction and 3 impinging distances, giving 27 tests at each setting of cutting speed and feed rate (i.e. 2 levels each). This gave a total of 108 experiments conducted using the new system. Only the best trial with settings of nozzle angle positions in the feed and against feed directions and impinging distance that gave the best responses in terms of lowest cutting force, workpiece temperature, tool wear, burr height and Ra of each of the 27 tests was used for the comparison with the conventional system. On the other hand, the conventional system was only assessed in four different tests, where cutting speed and feed rate were investigated at two levels each at 95 and 200 m/min and 0.1 and 0.15 mm/rev respectively. Fig. 4-19 shows a detailed experimental flowchart. Axial (a_p) and radial (a_e) depths of cut and nozzle elevation angle (α) of 5 mm, 1.3 mm and 40° respectively were maintained in all trials. Table 4-11 shows the evaluated control factors with their corresponding levels. Analysis of variance (ANOVA) was also utilised to assess the effect of process variables on machining outputs.

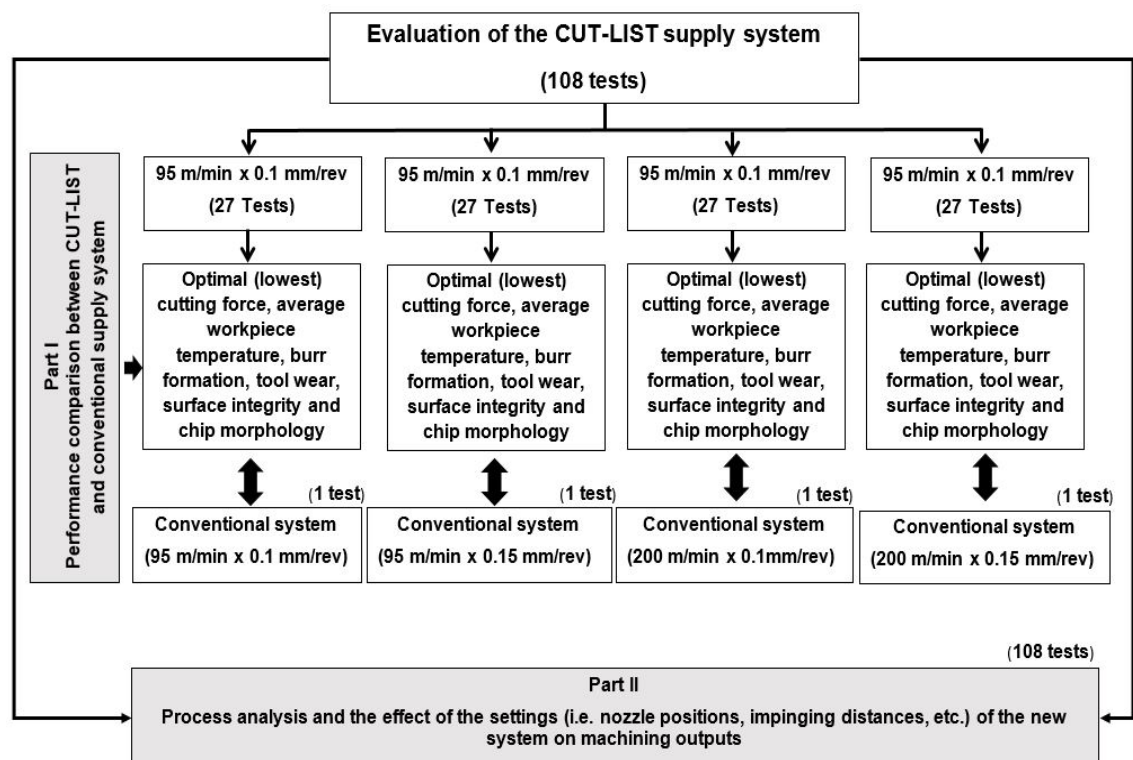


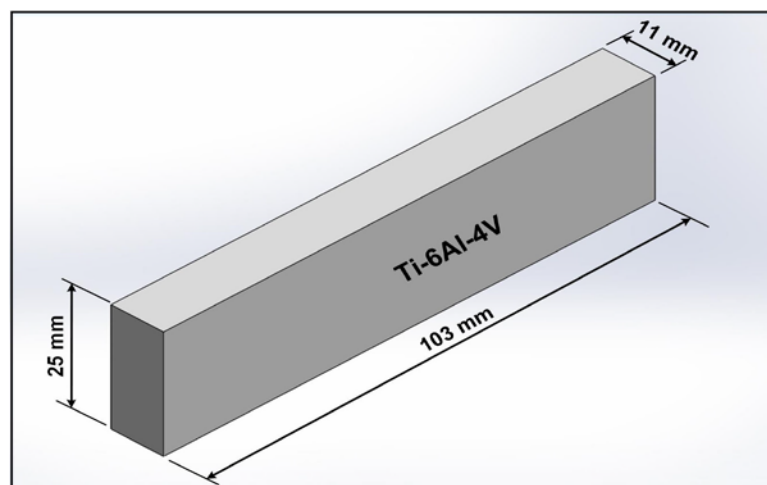
Fig. 4-19 Flow chart of machining experiments for the testing of CUT-LIST

Table 4-11 Process variables and corresponding levels

Factor	Level1	Level 2	Level3
Nozzle angle positions in feed direction	15°	45°	60°
Nozzle angle positions against feed direction	15°	45°	60°
Nozzle impinging distance (mm)	35	55	75
Cutting speed (m/min)	95	200	
Feed rate (mm/rev)	0.1	0.15	

4.5.2 Machine tool and workpiece material

Milling experiments were performed on a CNC Cincinnati Milacron 750-Sabri vertical machining centre (Cincinnati Machine UK Ltd., Birmingham, UK). Step shoulder down-milling (see Fig. 3-12) experiments were carried out on Ti-6Al-4V ASTM B348 grade 5 samples. Rectangular workpieces of dimension $103 \times 25 \times 11$ mm were used, as shown in Fig. 4-20. The chemical and mechanical properties of Ti-6Al-4V samples have been detailed earlier in Table 4-2 and Table 4-3 respectively. Each trial involved a cutting length of 103 mm and a new milling insert was used. Fig. 4-21 shows the experimental set-up while Table 4-12 presents the capabilities of the CNC Cincinnati 750-Sabri machining centre. The bill of materials (BOM) for all consumables such as workpiece materials, cutting tools, equipment and pipefittings used in this phase can be found in Appendix E (E2).

**Fig. 4-20** Shape and geometry of Ti-6Al-4V sample

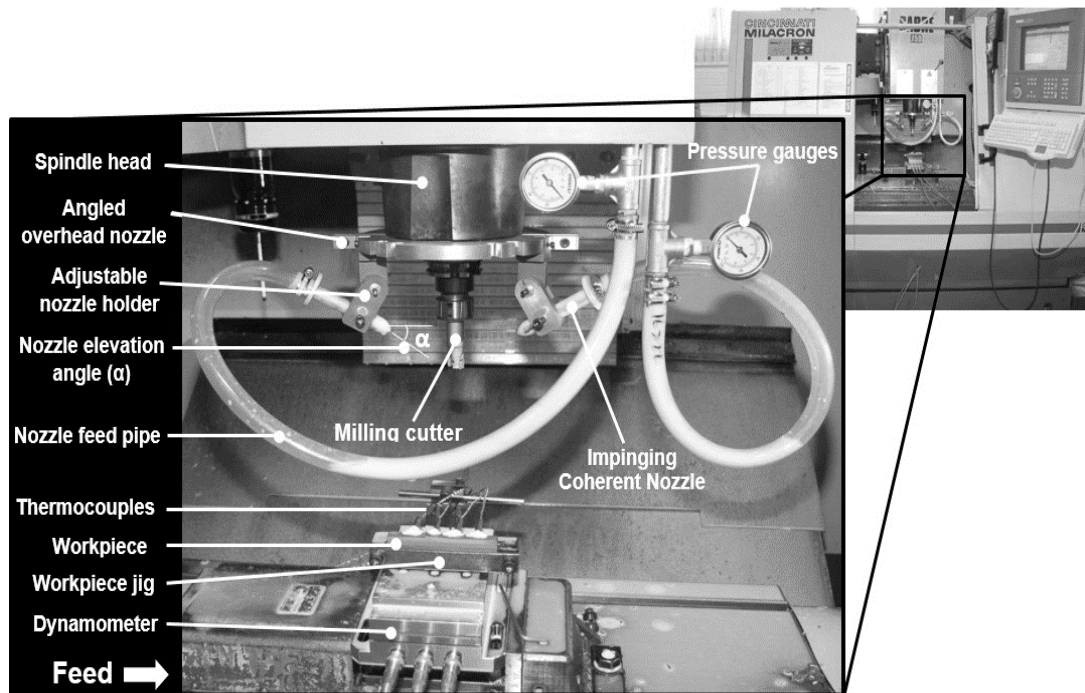


Fig. 4-21 Image of experimental set-up using CUT-LIST

Table 4-12 Capabilities of the CNC Cincinnati Sabri-750 machine

Specification	Details
Longitudinal (table, X-axis)	762 mm
Cross (saddle, Y-axis)	381 mm
Vertical (spindle, Z-axis)	508 mm
Feed rates X-Y-Z	0.1- 480 ipm (inch/minute)
Rapid traverse (X-Y-Z)	480 ipm (inch/minute)
Spindle speed range	60 - 8000 RPM
Work surface (X-Y)	863.6- 431.8 mm
Spindle length and diameter	101.6 mm , 152.4 mm
Tool storage capacity	21 tools
Control system	ACRAMATIC 850MC
AC drive motor and load capacity	11 kW, 454 Kg

4.5.3 Tool material and cutting fluid

H13A uncoated coarse-grained tungsten carbide milling inserts with a positive rake angle were used. The shape and geometry of the insert are depicted in Fig. 4-22. These inserts (R390-11 T3 08M-KM) were mounted on an $\varnothing 18.5$ mm (i.e. D_c) x 110 mm long square shoulder milling tool holder, implying a major cutting edge angle $\kappa = 90^\circ$ with an overhang distance of 60 mm to eliminate chatter.

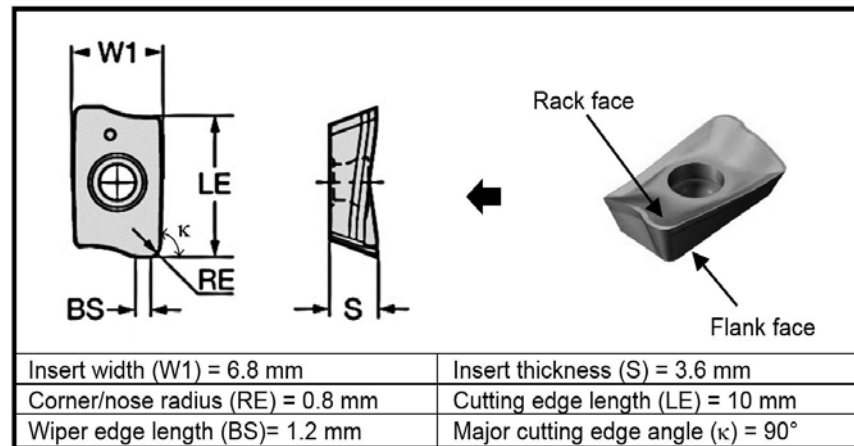


Fig. 4-22 Shape and geometry of R390-11 T3 08M-KM milling insert [262]

Water-soluble vegetable oil-based cutting fluid (Vasco1000) was used. The fluid was blended at a concentration of 10 % and this was regularly checked using the portable refractometer. The selection of fluid and its concentration level was based on the outcomes of the previous sections 4.3 and 4.4 (as described in details in the next chapter). Table 4-13 details the chemical composition and thermo-physical properties of the cutting fluid at the 10% concentration level. Cutting fluid was supplied using the new system at accurate flow rates, which were calculated based on the heat generated in the machine zone, whilst in the case of the conventional system, the cutting fluid was delivered at 13 L/min per kW heat (see Fig. 3-13).

Table 4-13 Chemical composition and properties of Vasco1000 at 10%

Composition/property	Corresponding Value
Mineral oil content	0%
VO base content	45%
Base oil colour	Yellow
Solubility in water	Emulsifiable
Methylenebismorpholine (additives)	1.0-4.9%
Zinc alkyl dithiophosphate (additives)	1.0-4.9%
Flash point	180 °C
Boiling point	>300 °C
Pour point	-15 °C
pH value	8.5-9.2
Mass density (Kg/m ³)	988
Dynamic viscosity @ at 25°C (cP)	1.8
Average heat capacity @ at 25°C (J/g°C)	3.97

4.5.4 Measurement equipment

4.5.4.1 Cutting force dynamometer

A Kistler three-component piezoelectric dynamometer is the most widely used equipment for the measurement of cutting force in machining trials. This dynamometer uses four three-component transducers fitted under high pre-loading between a base plate and a top plate (Fig. 4-23). The transducers consist of three pairs of quartz plates. Quartz is a piezoelectric material that produces an electrical charge under mechanical load. In this phase of the experimentation, cutting force signals in the axial direction (F_z), X direction (F_x) and Y direction (F_y) were collected using the three-component Kistler 9257A piezoelectric dynamometer via a multichannel laboratory charge amplifier. The dynamometer was installed on the vice of the machine tool while the workpiece was clamped using a special fixture mounted on the dynamometer's top plate. A sample frequency of 2000 Hz and high-pass filter type with (n^{64}) filter order were used to record the cutting force signals. All signals were then analysed using Kistler Dynaware software. The maximum resulting cutting force was then computed using Equation 4.2:

$$F = \sqrt{F_x^2 + F_y^2 + F_z^2} \quad [212] \quad (4.2)$$

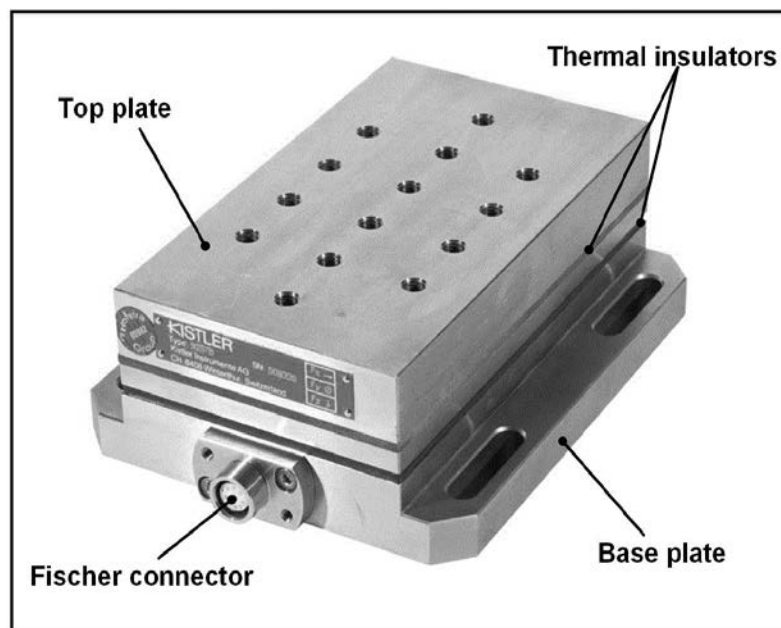


Fig. 4-23 Image of a typical Kistler dynamometer

4.5.4.2 Workpiece temperature measurement with embedded thermocouples

Workpiece temperature was measured using mineral-insulated thermocouple sensors. A digital four-channel data logger (Onset - HOBO UX120-014M) having a sampling rate of 2000 sample/s was utilised for temperature logging as shown in Fig. 4-24. Four T-type (temperature range -200 to 350 °C) thin sensing probes \varnothing 1.0 mm in diameter x 10 mm probe length x 2 m extension cable length were inserted into \varnothing 1.0 mm drilled holes in each sample 0.5 mm from the machined surface and 20 mm apart. To ensure a good contact surface between the sensor tip and workpiece material. The bottom of the drilled holes was flattened using a Sodi-Tech EDM spark erosion machine. A distance of 20 mm was also allocated before passing over the first thermocouple in order to ensure steady-state thermal conditions, as shown in Fig. 4-25. The MX-3 thermal compound supplied by Arctic Ltd., Switzerland, with a high thermal conductivity of 8.2 W/m·K and a low thermal resistance was used to minimise heat loss between the sensor probe and workpiece material. To prevent the movement of thermocouples during the cutting process, all probes were secured using an especially strong thermal adhesive (Lyreco 50g). Prior to each test, the workpiece material was left for a few seconds (\sim 30 sec) to reach ambient temperature (\sim 19 °C). The thermocouple sensors and data logger were calibrated by the supplier and the certificate is presented in Appendix H.

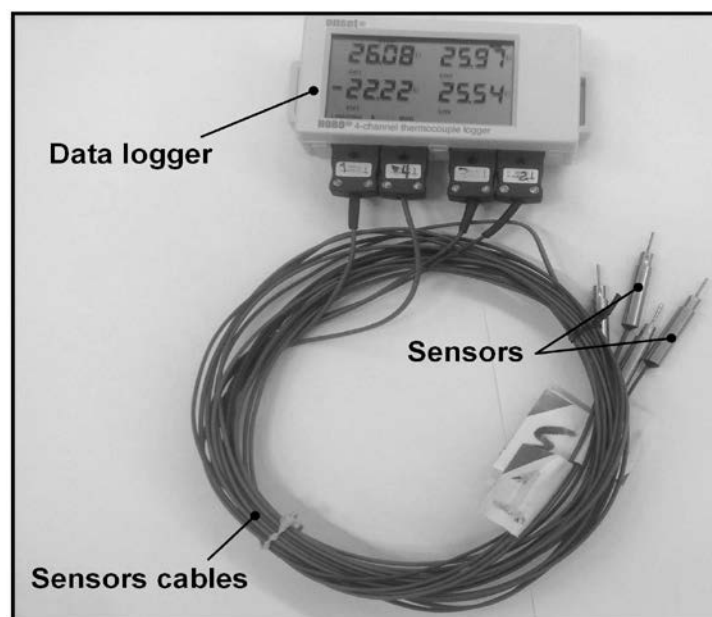


Fig. 4-24 Thermocouple sensors and data logger used for temperature measurement

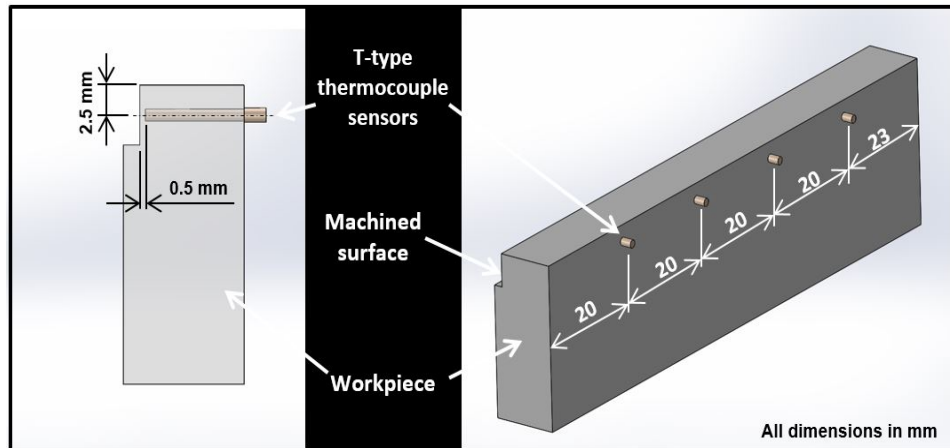


Fig. 4-25 Thermocouple configuration for workpiece temperature measurement

4.5.4.3 Surface roughness and tool wear measurements

The average surface roughness (R_a) was also measured using a Taylor Hobson Surtroni 3+ surface roughness tester. Values of R_a were measured in accordance with the ISO 4287 and ISO 4288 standards using a 0.8 mm cut-off and an evaluation length of 4 mm. R_a values were measured parallel to the machined surface at three different locations, at the beginning, middle and end, as shown in Fig. 4-26, and the average value was computed for each trial.

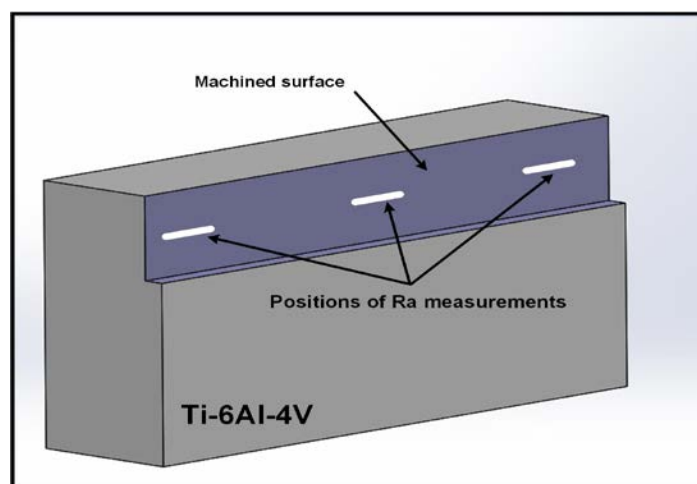


Fig. 4-26 Positions of R_a measurements

Additionally, the Alicona InfiniteFocus G4 optical microscope was utilised to assess tool flank wear (VB). Average flank wear (VB) was measured following each trial in accordance with the ANSI/ASME B94.55M-1985 standard. The main settings used for

scanning cutting tool samples were a magnification factor of $\times 10$, exposure time $173 \mu\text{s}$, contrast 0.78, and vertical and lateral resolutions of 510 nm and $10.55 \mu\text{m}$ respectively.

4.5.4.4 Digital depth gauge for burr height measurement

The burr height was measured using a precision Sealey type (Model VS0560) digital depth gauge. All burr measurements were taken at the top of each machined sample as shown in Fig. 4-27. Additionally, images of all burrs were captured using a Lieca S6D type optical microscope (Fig. 4-28).

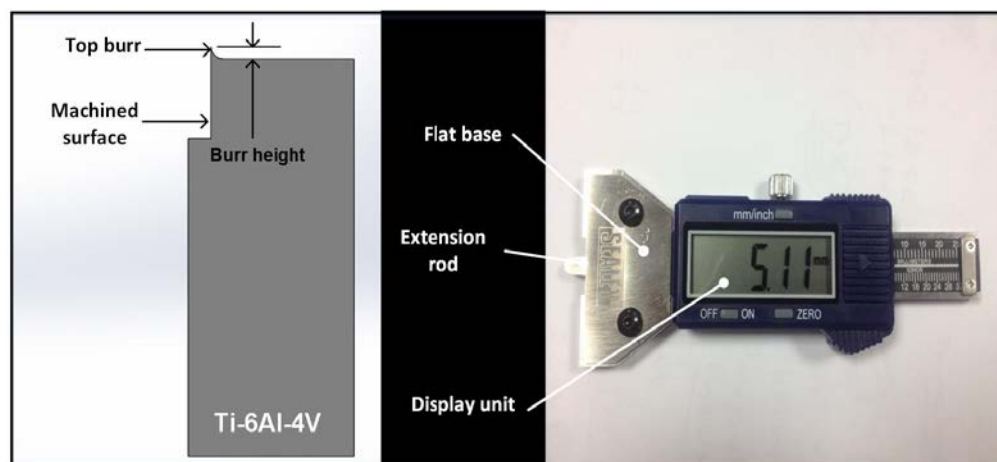


Fig. 4-27 Depth gauge used for top burr measurement



Fig. 4-28 Lieca S6D optical microscope

4.5.4.5 *Surface topography analysis*

In order to observe any signs of defects such as surface cavities or material erosion on the surfaces of the machined samples, an optical microscope (Nikon eclipse LV150) was utilised (see Fig. 4-29). All images of the machined surface topography were captured at a magnification factor of x20. To obtain clear surface topography images, all samples were vibratory-cleaned using Turbex 2 Litre Benchtop 37 kHz ultrasonic cleaner before imaging.

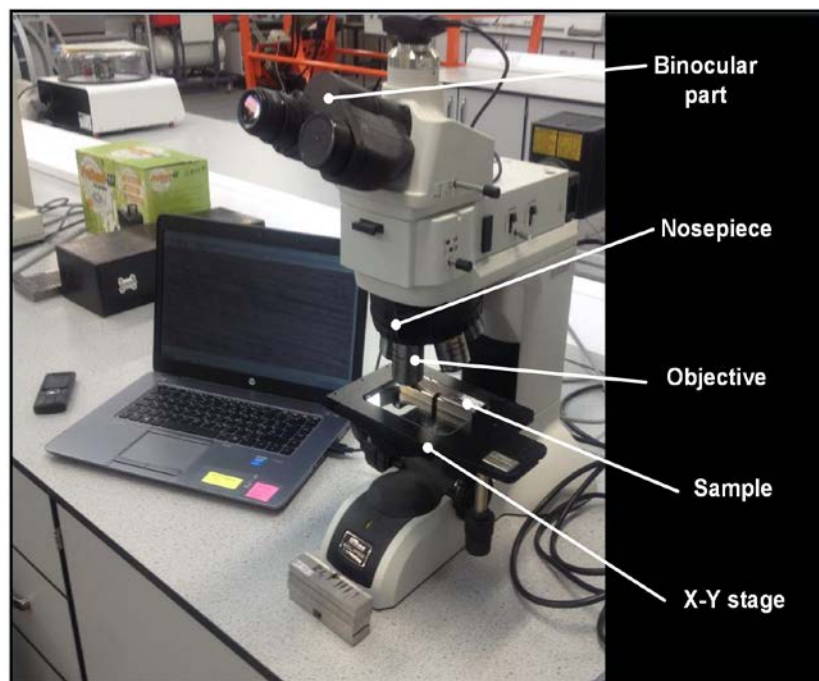


Fig. 4-29 Optical microscope used for surface topography observations

4.5.4.6 *Scanning electron microscopy (SEM)*

The TESCAN MIRA 3 type (Fig. 4-30) SEM was used mainly to investigate the chip morphology, surface topography and microstructure of the machined parts. The chips produced during the machining trials were collected, cleaned using $(\text{CH}_3)_2\text{CO}$ solution and examined using the SEM. Five chips were chosen from each supply system for each cutting condition for the measurement and analysis of saw-tooth height and width and crack depth as well as the average distance between serrated segments. In addition, the SEM in combination with EDX/EDS using Aztec software were utilised for in-depth observations of any signs of wear on the cutting edges and analysis of adhered materials.



Fig. 4-30 TESCAN MIRA3 Scanning electron microscope

4.5.4.7 *Materialographic sample preparation and instrumentation*

Micro-hardness test

Initially, five samples were chosen using CUT-LIST, which represent the preferred working conditions as found from 108 tests in terms of lowest cutting force, workpiece temperature, tool wear, burr height and Ra. Another 8 optimal samples were also added which were obtained from every 27 tests at each setting of cutting speed and feed rate in terms of lowest cutting force and workpiece temperature. The reason for this is that sub-surface quality is strongly affected by cutting pressure and temperature compared to other factors [76]. In addition, four different samples were chosen using the conventional supply system. This gave a total of 17 samples to test for micro-hardness. Only the optimal (lowest) values obtained using CUT-LIST were compared with the conventional supply system. The workpiece samples were cut-out from the middle, having dimensions of 6 mm x 10 mm, using a Sodick EDM wire machine ($<0.5\varnothing$ mm copper wire) as shown in Fig. 4-31. Samples were consequently hot-mounted in Buehler Red Phenolic Bakelite and subsequently ground and polished using different SiC paper grades and an ultra-fine Struers polishing machine together with Hyprez diamond lapping spray fluid. Micro-hardness measurements were performed on a Micromet II micro-hardness tester using an indentation load of 100g and a dwell time of 12s, with the aid of a Vickers tool indenter.

All measurements were taken according to the ISO 5607 and 2639 standards. Three main locations were selected for indents across the polished surface at 50 μ m intervals between consecutive measurements, as shown in Fig. 4-32.

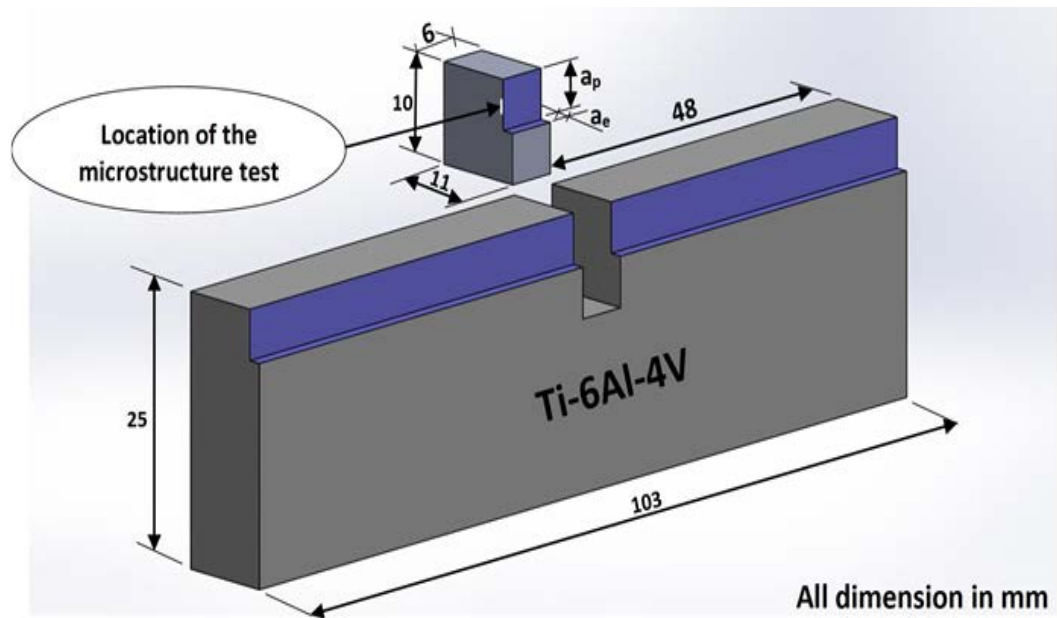


Fig. 4-31 Ti-6Al-4V sample for micro-hardness test

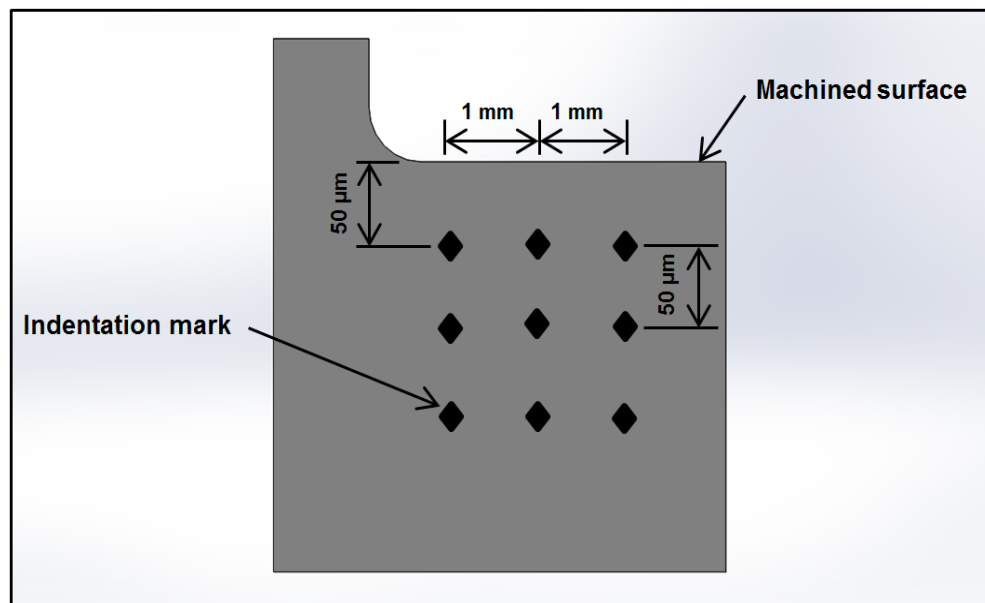


Fig. 4-32 Location of indentation marks used in micro-hardness test

Subsurface microstructure analysis

The 17 samples examined for micro-hardness were remounted in a Sturrs LaboPress-3 mounting press. Wet grinding was completed on a SAPHIR350 machine, and they were then wet polished using 300 \varnothing mm abrasive silicon carbide papers. Fine polishing was accomplished on a Sturrs LabPress-2 polishing machine using 200 \varnothing mm 6 μ m and 1 μ m polishing cloths. The prepared sections were vibratory-polished for a duration of 6 hours on a BUEHLER VIRBROMET-I fine polishing machine using a Sturrs OP-S Non Dry suspension (see, Fig. 4-33). The sections were swabbed-etched with Kroll's reagent for 10 seconds. The nominal composition of the etchant consisted of 6ml HNO₃ (Nitric acid), 800 ml H₂O (distilled water), and 3 ml HF (Hydrofluoric acid). The sections were then gold-sputtered (as they were not mounted in conducting Bakelite) and examined in a Zeiss Sigma Field Emission Scanning Electron Microscope (SEM). The images of subsurface microstructure were captured for the undeformed (as-received Ti-6Al-4V) and deformed zones underneath the machined surfaces at magnifications of x2500 and x5000.

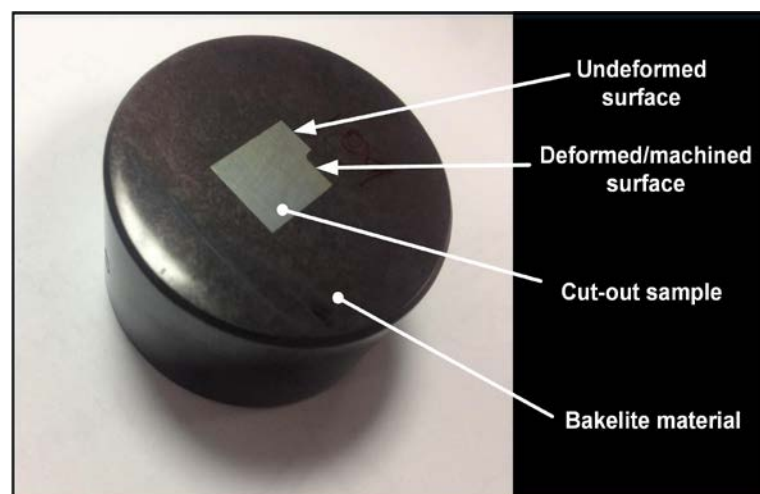


Fig. 4-33 Sample prepared for subsurface microstructure test

4.5.4.8 Fluid system instrumentation

Mass flow meter

A flow meter is a device that measures the mass flow rate of a fluid travelling through a pipe. The flow rate is the mass of the fluid travelling past a fixed point per unit time. In these experimentations, an LM OG-I-PVC digital type flow meter was used (see Fig.

4-34). As the fluid passes through the metering chamber by entering the inlet port, it forces the internal gears to rotate and then exits through the outlet port. Each rotation of the gears displaces a given volume of fluid. A controlled clearance between the gears and chamber can ensure minimum leakage. As they rotate, a magnet on each end of the gears activates the microprocessor in the register [266]. In addition, to fulfil the fluid dynamics criterion, the meter should be installed at a distance $> 10d$, where d is the feed pipe internal diameter, from the fluid pump in order to ensure steady-state flow condition. The flow meter was placed at a distance of 300 mm from the pump, which satisfies the fluid dynamics criterion.



Fig. 4-34 LM OG-I-PVC type digital flow meter [266]

Digital pressure gauge

Digital pressure gauges use advanced sensors and microprocessors to display highly accurate pressure readings on a digital indicator. A DPG 800-500 type digital pressure gauge (see Fig. 4-35) was placed after the cutting fluid filter. This type of pressure testing is based on strain gauge measurement technology. Usually this technology consists of a diaphragm with a patterned metallic strain gauge embedded in it. Increasing pressure causes the diaphragm, and subsequently the gauge, to deform which effects its resistivity. That change is measured and converted into an electrical signal proportional to the pressure. Generally, strain gauges are connected to form a Wheatstone bridge circuit to maximize the output of the sensor and to reduce sensitivity to errors [267]. The calibration of the digital pressure gauge and flow meter was undertaken by the suppliers.



Fig. 4-35 DPG 800-500 type digital fluid pressure gauge [267]

Cutting fluid filters

In order to obtain high fluid monitoring accuracy and to avoid malfunction in the flow meter and pressure gauges, the fluid should be completely filtered. Two types of filters were used, including a micro-mesh strainer ($<100\ \mu\text{m}$) which was fitted at the bottom of the fluid tank and before the suction port of the cutting fluid pump, and in-line Clear 5 type cutting fluid filter placed directly after the fluid pump. The Clear 5 model filter is a heavy duty magnet-based filter with a maximum fluid pressure of 12 bar. This filter has a high-intensity magnet field that can generate a magnetic trap to arrest fine ferrous particles up to $1\ \mu\text{m}$ in diameter. Fig. 4-36 shows the fluid system set-up including the in-line Clear 5 type filter used throughout the experimental work. Next section presents equipment, workpiece materials, cutting tools and cutting fluids as well as the design of experiments (DOE) used in the experimental work.

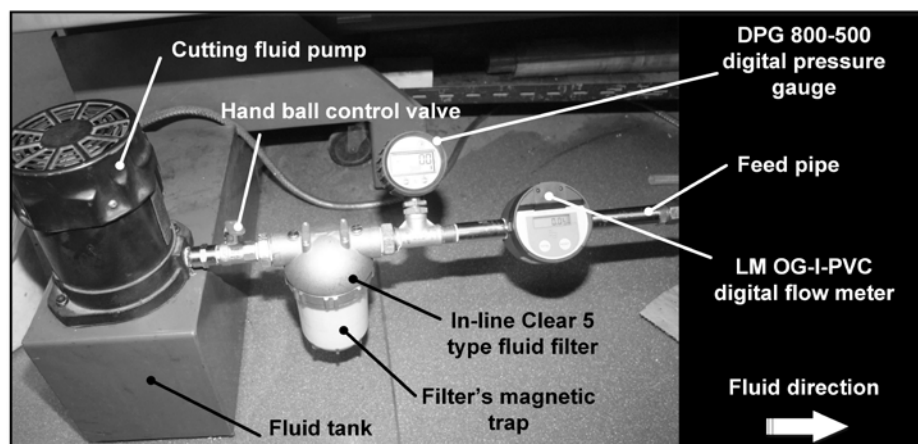


Fig. 4-36 Fluid system set-up

4.6 Chapter summary (experimental work dashboard)

Exp. seq.	Design of experiments (DOE)	Cutting strategy/Machine tools used	Workpiece material and shape	Cutting tool	Cutting fluids and their concentration (%)	Measurement equipment used*	Key machining outputs
4.1	Full factorial (5x4=20 tests)	Turning-based machining trials/ Graziano Tortona Centre lathe (SAG 12)	Ti-6Al-4V ASTM B348 grade 5 (round bars)	H13A S05F H10F GC1105	Hocut 3450 Vasco 1000 NE250H Solutec Cooledge (all at 5% concentration)	<ul style="list-style-type: none"> • Alicona InfiniteFocus • Talyor Hobson Surtroni 3+ surface tester • Refractometer • Leica EZ4D optical microscope 	<ul style="list-style-type: none"> • Surface roughness • Tool flank wear
4.2	Taguchi orthogonal array of L27 (3 ³) (27 tests)			H10F	Hocut 3450 at 5%	<ul style="list-style-type: none"> • Talyor Hobson Surtroni 3+ surface tester • Alicona InfiniteFocus • Refractometer • Leica EZ4D microscope 	<ul style="list-style-type: none"> • Surface roughness • Tool flank wear
4.3	Full factorial (4x3x2=24 tests)			GC1105 H13A S05F	Hocut 3450 Vasco 1000 NE250H Solutec (all at 5% concentration)	<ul style="list-style-type: none"> • Talyor Hobson Surtroni 3+ surface tester • Alicona InfiniteFocus • Refractometer • Digital micrometer 	<ul style="list-style-type: none"> • Surface roughness • Tool flank wear • Chip thickness & style
4.4	Taguchi orthogonal array of L27 (3 ⁴) (27 tests)			H13A H10A GC1115	Vasco 1000 at 5%, 10% and 15%	<ul style="list-style-type: none"> • Talyor Hobson Surtroni 3+ surface tester • Alicona InfiniteFocus • Refractometer • Viscometer • Micromet II • Differential scanning calorimeter (DSC) 	<ul style="list-style-type: none"> • Surface roughness • Tool flank wear • Tool life • Micro-hardness
4.5	Full factorial (3x3x3x2x2=108 tests) for CUT-LIST + 4 tests for flood system = 112 tests + 11 tests (repeatability tests)	Milling-based machining trials/CNC Cincinnati Sabri-750 Milling machine	Ti-6Al-4V ASTM B348 grade 5 (rectangular blocks)	H13A	Vasco 1000 at 10%	<ul style="list-style-type: none"> • Kistler dynamometer (Kistler 9257A) • Embedded thermocouples & Data logger (TEMPCON) • TESCAN SEM • Zeiss Sigma SEM • Nikon eclipse LV150 microscope • VS0560 digital depth gauge • Lieca S6D microscope • Talyor Hobson Surtroni 3+ surface tester • Alicona InfiniteFocus • Metaserv 2000 and Struers DP9 • Micromet II • Sodik EDM wircut • Refractometer (Oxford portable optical type) • Digital flowmeter/regulator (LM OG-I-PVC) • Digital pressure gauge (DPG 800-500) 	<ul style="list-style-type: none"> • Cutting force • Workpiece temperature • Tool flank wear • Burr height • Surface integrity: <ul style="list-style-type: none"> • Surface roughness • Surface defects/quality • Micro-hardness • Microstructure • Chip formation <ul style="list-style-type: none"> • Chip style/shape • Chip geometry • Chip segmentation • Segmintaion frequency • Shear angle (φ)

* All measurement equipment are calibrated by the suppliers.

Chapter 5 Results and Discussion

This chapter presents all of the results and observations, analysis and discussion of each experimental study. The chapter is divided into two main parts; the first part exhibits the results and discussion of the pre-evaluation phase of the new supply system (i.e. turning-based trials), which are in turn, presented in four main sections as follows:

- Evaluation of different vegetable oil- and mineral oil-based cutting fluids and tool materials (5.1)
- Pre-selection of cutting conditions (5.2)
- Selection of vegetable oil-based fluid and cutting tool material (5.3)
- Assessment of cutting fluid concentration ratio (5.4)

The second part (section 5.5) presents the results and discussion for all milling-based trials using the new supply system. It compares the performance of CUT-LIST and a conventional supply system and then provides a critical analysis of the new system parameters and process optimisation. The results of repeatability trials are also provided at the end of the chapter. All detailed experimental results can be found in Appendix I.

5.1 Evaluation of different vegetable oil- and mineral oil-based cutting fluids and tool materials

5.1.1 Surface roughness analysis

Fig. 5-1 shows the effect of cutting fluid type on the average surface roughness (R_a) of the machined surfaces. Despite the high content of base oil (>60%) in the reference MO-based fluid (Castrol Cooledge BI), relatively marginal variations in average roughness values were observed between the fluids evaluated (with maximum of 0.15 μm). This could be attributed to the superior lubricity of the VO-based fluids. The similarity in the performance of MO- and VO-based fluids was anticipated, since VO-based fluids give inherently higher lubrication and higher cooling effects in the cutting zone compared with MO-based fluids. VOs typically possess higher heat conductivity, therefore dissipating the heat generated away from the tool/workpiece interface. Their higher lubrication capability also decreases the frictional forces contributing to this heat, and thus less deformation and fewer surface defects will result. Overall, NE250H provided the highest

average Ra of 0.93 μm owing to its lower base oil content (<28 %) compared with the reference MO-based fluid which gave the lowest value of Ra (0.78 μm). The Hocut 3450 and Vasco 1000 fluids achieved similar cooling potency owing to their comparable lubricating properties, with VO content always between 43-45%. In addition, values of Ra for all fluids tested were within the acceptable range of less than <1.6 μm for critical aerospace applications [78]. This supports the findings in the literature that VO-based fluids can be favourable alternatives to their MO-based fluid counterparts.

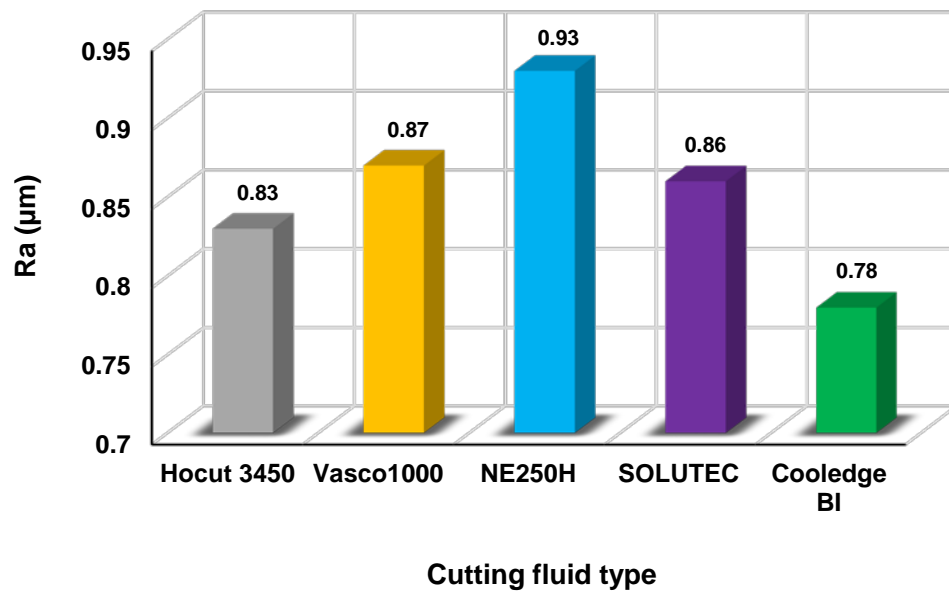


Fig. 5-1 Ra vs cutting fluid type (each Ra value is the average of 4 tests)

Fig. 5-2 shows the results of average surface roughness (Ra) for different cutting tool materials. In general, Ra values for all cutting tools materials were also in the acceptable range for aerospace machined components at below 1.6 μm . The PVD-coated carbide tool (GC1105) produced the lowest average Ra of 0.72 μm owing to its superior mechanical properties such as thermal stability, a low friction coefficient of 0.5 and high hardness of 2300 HV [33]. Its thermal stability may have resulted in precision being maintained during cutting. This result is in agreement with previous research [183] which found that coated carbide outperformed uncoated carbide tools in relation to Ra. Surprisingly, the highest Ra of 0.97 μm was achieved by the coarse-grain W/Co carbide tool H13A. This could be attributed to the variation seen in the fluid flow rate during the experiments. ANOVA results are shown in Table 5-1, and the effect of cutting tool material on Ra was found to be statistically significant, having the highest PCR of 44.5% compared to cutting

coated S05F tools showed relatively similar machining performance in terms of Ra. It seems that the influence on surface finish of a high cobalt content in the uncoated fine-grained H10F tool is similar to the effect of CVD coating materials on Ra. Error bars added to the figure were relatively small, suggesting that the measurements were accurately performed. Noticeable feed marks and slight furrows (Fig. 5-4) were also seen on the samples machined using Hocut 3450 with the CVD S05F tool, which might be due to the plastic flow of the material during the cutting process.

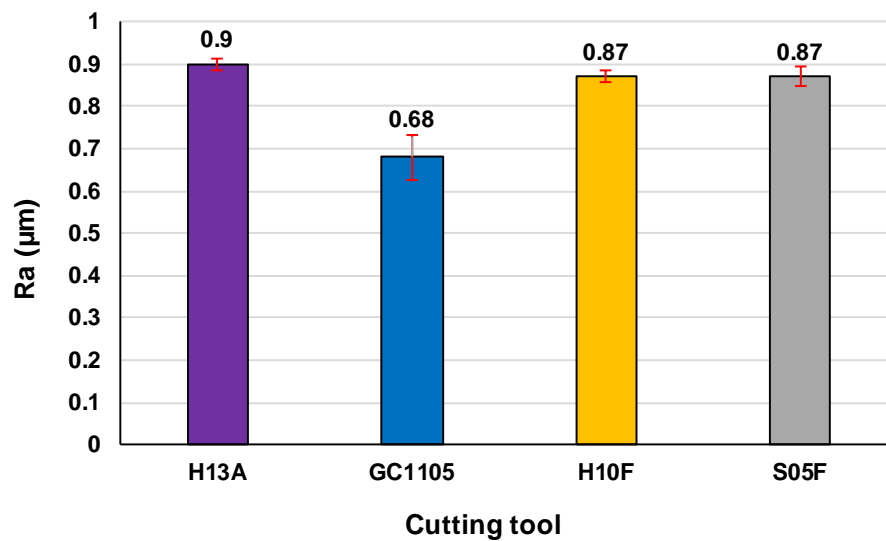


Fig. 5-3 Ra results versus cutting tools using Hocut 3450 at a 0.75 mm depth of cut

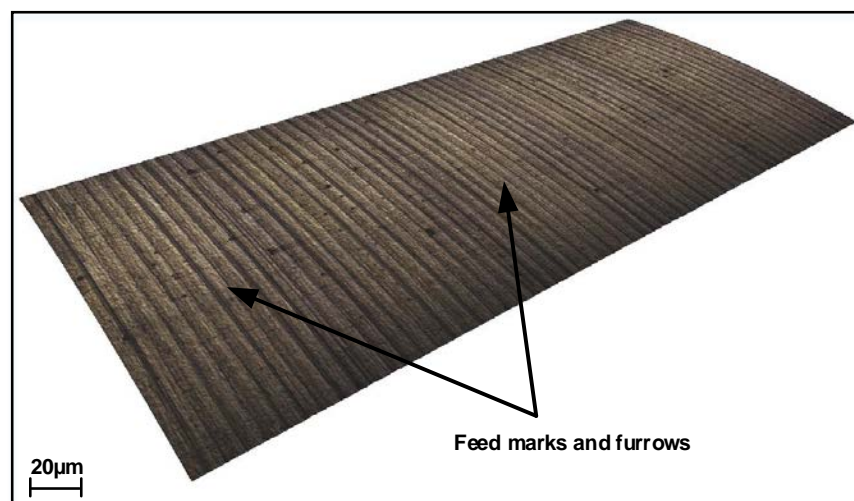


Fig. 5-4 3D scan using the Alicona G4 scanner of a cut machined surface with the CVD S05F tool and Hocut 3450 fluid at 0.75 mm depth of cut

5.1.2 Tool wear

Fig. 5-5 shows the results for flank wear (VB) versus cutting fluid type using different cutting tools. In general, uncoated (H10F) and PVD TiAlNi-coated (GC1105) tools produced very similar low tool flank wear, owing to their inherently superior mechanical properties such as wear resistance and high hot hardness (always in the range between 90-94 HRA). On the other hand, the H13A tool exhibited the highest flank wear value of 59.4 μm particularly when the highly viscous MO-based fluid with a base oil content greater than 60% was used. As mentioned previously, this is likely to be due to the variation witnessed in the fluid flow rate during the experiments. It can be deduced that CVD multilayer coating materials (TiNi, Al_2O_3 and TiCNi) failed to suppress the progress of tool wear compared to the PVD monolayer coating (TiAlNi). In addition, the NE250H fluid gave relatively lower tool flank wear values owing to its low oil content (< 28%) compared to the Mo-based fluid (>60%). Less viscous fluids are apparently more efficient in heat dissipation than highly viscous fluids. Hocut 3450 and Vasco 1000 exhibited similar performance owing to their comparable base oil contents. Fig. 5-6 shows tool wear progress on various cutting tools using the Hocut 3450 fluid.

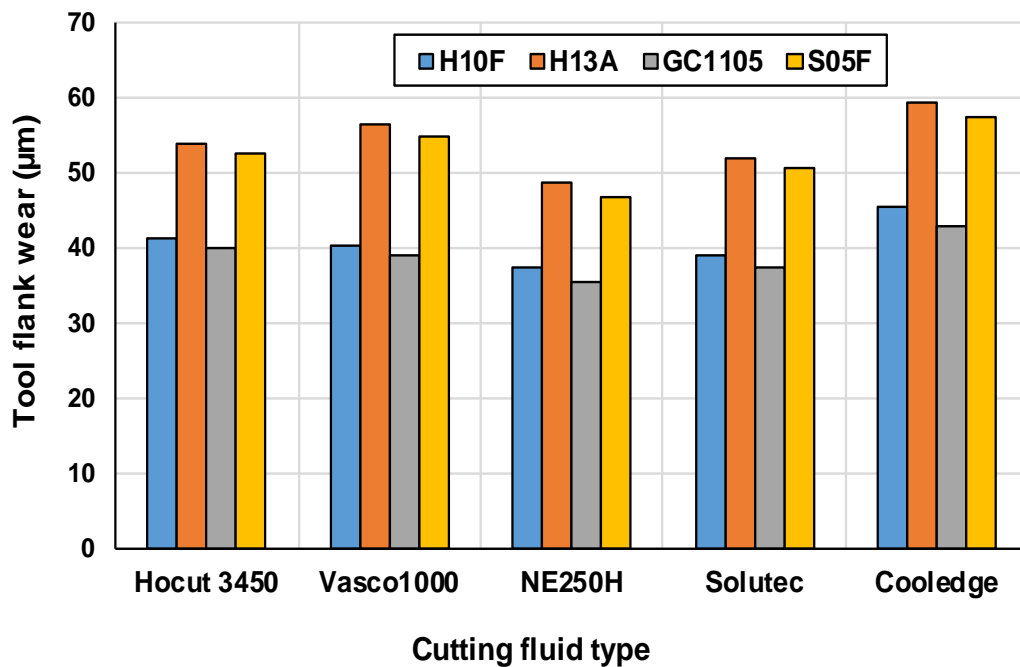


Fig. 5-5 Flank wear on different cutting tools using various cutting fluids

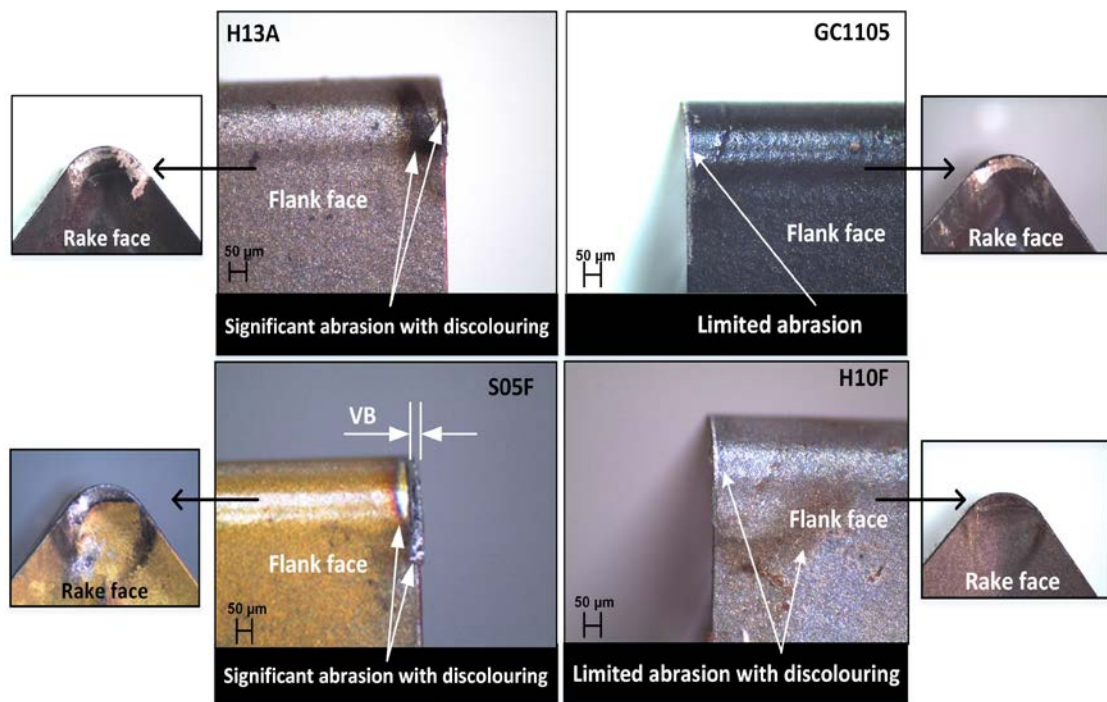


Fig. 5-6 Tool wear of various cutting tool materials at speed of 75 min, feed rate of 0.15 mm/rev and depth of cut of 0.75 mm using the Hocut 3450 fluid

5.1.3 Summary

Despite the high content of the base oil ($> 60\%$) in the reference MO-based fluid, all fluids tested showed relatively marginal variations (by a maximum of $0.15\ \mu\text{m}$) in average surface roughness values. This supports the view that VO-based fluids can be suitable alternatives to MO-based fluids when cutting titanium. Thus, the Cooledege BI fluid is excluded from the next experimental phase. The use of the GC 1105 tool resulted in relatively lower Ra values, while GC1105 and H10F showed similar performance in terms of tool wear. The multilayer CVD coatings (TiNi, Al_2O_3 and TiCNi) showed inferior machining performance, particularly in relation to tool flank wear, compared to the PVD monolayer coating (TiAlNi) under all cutting conditions. The performance of the H13A tool lagged behind that of other tools tested due to the variation observed in the fluid flow rate during the machining experiments. Thus, further investigation with this tool is needed. Cutting tool material had a statistically significant effect on average surface roughness, with a PCR of 44.5% compared to cutting fluid type (11.44%). The Hocut 3450 fluid and H10F tool showed superior cutting performance in terms of Ra and tool

wear respectively, and therefore they were chosen for the next experimental phase. H10F was selected rather than GC1105 due to its availability during the experimentation, as both exhibit similar performance in terms of tool wear.

5.2 Pre-selection of cutting conditions

5.2.1 Effect of machining parameters on surface roughness

Fig. 5-7 shows the main effects plot for the surface roughness (Ra) results. Values of Ra ranged between 0.56 μm and 1.81 μm . The best combination of the control factors to reduce Ra when turning Ti-6Al-4V is a cutting speed of 120 m/min, 0.1 mm/rev feed rate and 0.75 mm depth of cut. Additionally, from the ANOVA analysis shown in Table 5-2, it can be seen that feed rate has the major contribution (94.4%) in minimising Ra. The ANOVA results also showed that the recorded error was relatively small (4.9%), indicating that all important parameters had been considered and that the measurements were accurately carried out. Ra varied almost linearly with feed rate, which is in line with the classical theory of metal machining [26]. As the feed rate increased, Ra also increased. This can be attributed to the lack of sufficient time to carry the heat away from the machining zone, high rates of material removal and an accumulation of chips in the tool-workpiece regions [70]. Additionally, Ra values declined slightly with increasing cutting speed. This is likely to be due to the reduced effect of built-up edge (BUE) at high cutting speeds. At low cutting speed, the temperature at the machining interfaces is more than enough to promote the unstable larger BUE and the chips fracture readily, providing a rough surface. As the cutting speed increases, the machining time is reduced and the BUE eliminated, and chip fracture decreases, hence leading to a better surface finish [268, 269]. These results conform to observations in a previous study [73] during the turning of Ti-6Al-4V where a low Ra was obtained with higher cutting speed. However, it is also clear that cutting speed should be controlled at an optimum value, as increases may lead to changes in frictional conditions owing to the higher cutting temperature and failure of the tool nose due to increased tool wear, thus significantly affecting product surface quality [154]. Furthermore, it is quite evident from Fig. 5-7 that there is no considerable change in surface roughness with alterations in the depth of cut as Ra values remain almost constant in all conditions investigated. A Similar trend has been reported elsewhere [183]

interaction between cutting speed and feed rate. On the other hand, the effect of the change in depth of cut on surface roughness at any feed rate is negligible, whereas surface roughness (Ra) is strongly sensitive to feed rate variations irrespective of the depth of cut. It can be concluded that depth of cut has no significant impact on surface roughness, thus indicating that maximum material removal rates can be obtained by increasing the depth of cut without a substantial change in the values of Ra when operating at the optimal cutting conditions as stated above.

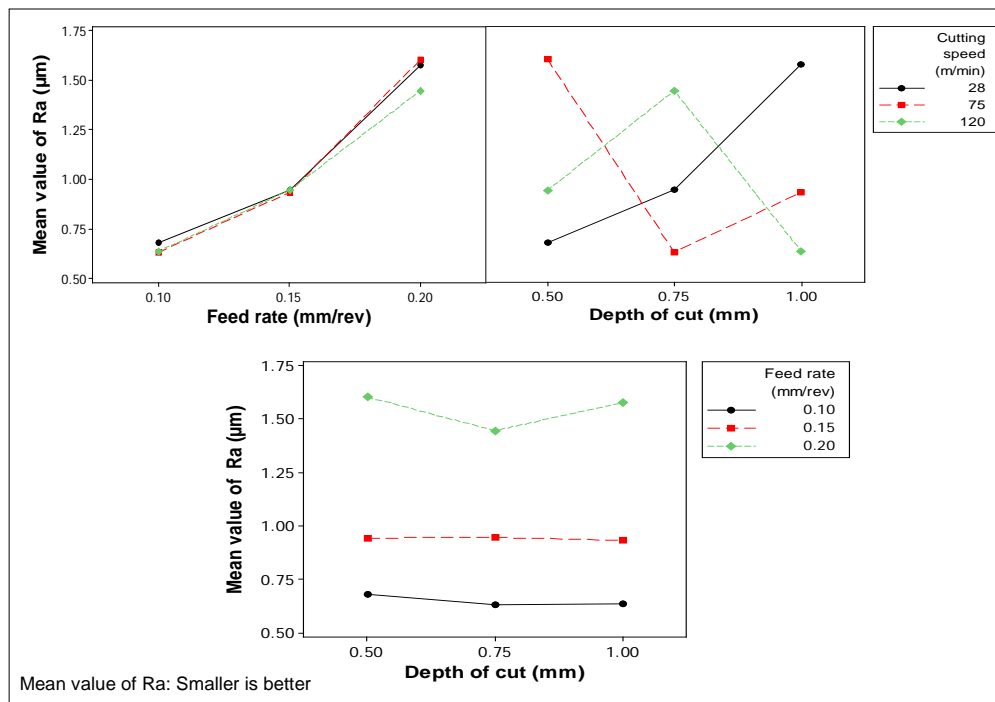


Fig. 5-8 Interaction effects plot of process parameters on Ra

5.2.2 Tool wear

Table 5-3 shows the results of the ANOVA analysis for tool flank wear. Cutting speed has the major contribution with a PCR of 65.85%. At higher cutting speed the heat in the cutting zone increases, causing the tools to lose their strength and plastic deformation occurs. Thus, the extent of flank wear and cutting edge deformation increased with cutting speed. Depth of cut also has a considerable effect on tool wear, with a PCR of 20.86% compared to only 5.84 % for feed rate. The recorded error is relatively small (7.44%), suggesting that all important factors had been considered and the measurements were accurately performed.

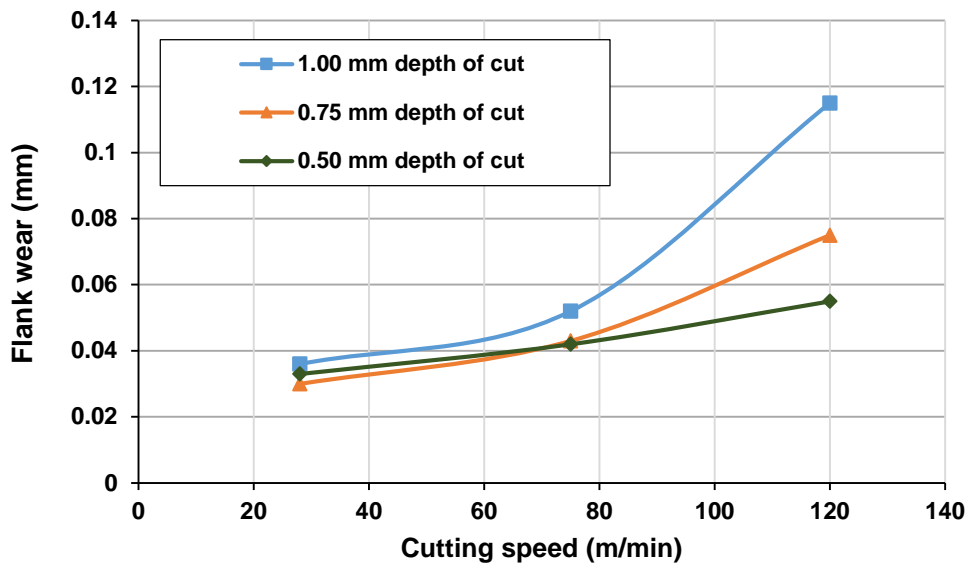


Fig. 5-10 Flank wear results at various cutting speed and depth of cut with feed rate of 0.15 mm/rev

5.2.3 Summary

Values of average surface roughness R_a ranged from $0.56 \mu\text{m}$ to $1.81 \mu\text{m}$ and the ANOVA analysis showed that the main contributory factor was feed rate with a high PCR of 94.4%. Lower R_a values can be obtained using the feed rate at 0.1 mm/rev, depth of cut of 0.75 mm and cutting speed of 120 m/min. Thus, these optimal values of feed rate and depth of cut will be retained in the next experimental study while the cutting speed limit is extended in a further investigation. Additionally, a considerable mutual interaction effect was observed, particularly between cutting speed and depth of cut, while the impact of changing in depth of cut on R_a at any feed rate is insignificant. The surface roughness is highly sensitive to feed rate variations regardless of the depth of cut used. It was revealed that the material removal rate can be maximised by increasing the depth of cut without a significant change in the value of R_a when turning Ti-6Al-4V at the stated optimal cutting conditions. In the same vein, it was found that cutting speed was the most influential factor (PCR of 65.85%) affecting tool flank wear, while depth of cut showed a significant contribution to tool wear (PCR of 20.86%) compared to a PCR of only 5.84% for feed rate. Flank wear increased with higher cutting speeds particularly at high levels of depth of cut owing to the increase in thermal and mechanical loading during the cutting of Ti-6Al-4V alloy.

5.3 Selection of vegetable oil-based fluid and cutting tool material

5.3.1 Surface roughness analysis

Fig. 5-11 presents the values of Ra versus cutting tools at cutting speeds of 120 and 175 m/min using the Vasco1000 cutting fluid. Generally, Ra values for all tested tools were below 1.6 μm . The uncoated coarse-grain W/Co carbide tool H13A produced the smallest average values of Ra of 0.55 μm and 0.51 μm at 120 and 175 m/min respectively. This could be attributed to its superior mechanical properties such as high toughness and high tensile rupture strength, which offer good cutting edge stability during cutting [49]. The CVD-coated S05F tool demonstrated the poorest performance in relation to Ra. A noticeable variation in Ra values at higher speed was observed between the S05F tool (0.031 μm) compared with only 0.008 μm for H13A as shown in the error bars in Fig. 5-11. It seems that the impact of the high content of cobalt (12%) in the H13A tool outweighed the effect of CVD coating (TiNi, Al₂O₃ and TiCNi) in minimising Ra. The PVD TiAlNi-coated tool GC1105 outperformed the CVD tool by achieving an overall average Ra of 0.55 μm compared to 0.6 μm for the CVD tool. Apparently, the monolayer TiAlNi coating material is more effective than multi-layer coatings when cutting titanium. A similar observation has been reported [187] that PVD TiAlNi coating outperforms CVD in suppressing the diffusion of tool particles into the chip at high speeds by the formation of a protective layer saturated with tool particles during the drilling of Ti-6Al-4V. In addition, the increase in coating thickness leads to an increase in the cutting edge radius. Since a sharp cutting edge is of particular importance in the machining of hard metals, a thin layer is often favoured in titanium machining [49]. Additionally, it can be seen that the values of Ra decrease with increased cutting speed. This is due to the reduced probability of BUE formation at higher cutting speeds, which results in a better surface finish. These findings are consistent with those of a recent report on the turning of Ti-6Al-4V [271]. Overall, all tools tested showed almost similar trends of a reduction in Ra values at higher cutting speeds. Although both PVD- and CVD- coated tools showed relatively similar Ra values at low cutting speed, the results showed a notable reduction in Ra values by up to ~ 10 % at the higher cutting speed when the PVD cutting tool was used. It can be noted that the disparity between PVD and CVD coating materials is more obvious at higher cutting conditions. This is probably because the TiAlNi coating

maintains its properties at elevated temperatures, which helps in transferring heat away from the tool and into the part or chip leading to less tool damage and lower Ra. This result supports findings in the literature that TiAlNi coatings are more effective than CVD coatings in applications where excessive heat is generated [187].

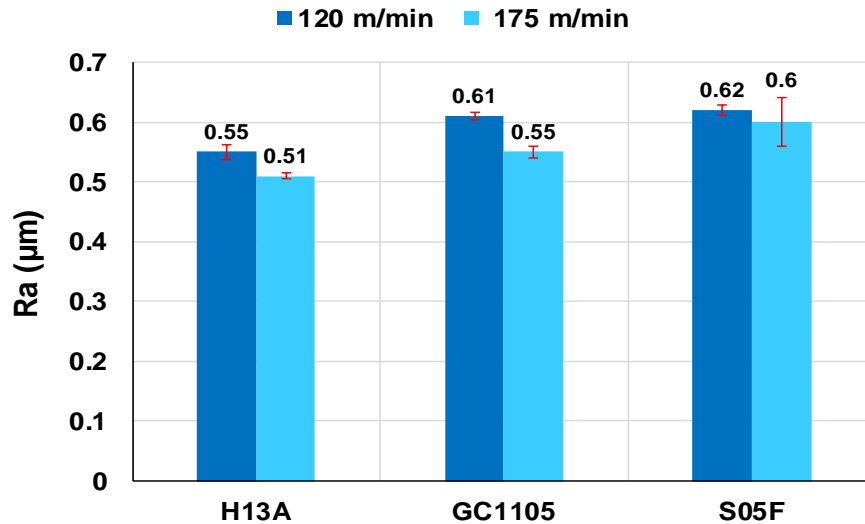


Fig. 5-11 Ra results versus cutting tools at cutting speeds of 120 and 175 m/min using Vasco1000 cutting fluid

Fig. 5-12 shows values of Ra recorded for all fluids using the H13A tool. Although a marginal variation was observed among the VO-based fluids tested (by a maximum of 0.16 μm), lower Ra values were obtained at all cutting conditions using the Vasco1000 fluid. This shows that Vasco1000, which has relatively higher VO content ($\sim 45\%$) possesses better lubrication and cooling properties, resulting in reducing heat and friction between the cutting tool and workpiece material and hence minimising Ra. On the other hand, the NE250H fluid demonstrated inferior machining performance in terms of Ra followed by the SOLUTEC cutting fluid. This is likely due to less VO content in the NE250H ($< 28\%$) compared to SOLUTEC fluid ($< 35\%$). This result is consistent with previous work [89] which concluded that the fluids with high oil content (viscosity $> 85 \text{ mm}^2/\text{s}$) achieved the lowest Ra value of $\sim 2.1 \mu\text{m}$ compared to $2.4 \mu\text{m}$ for those with low oil content fluid (viscosity $< 71 \text{ mm}^2/\text{s}$) when cutting ductile AISI 314 stainless steel. The high content of base oil in a cutting fluid can apparently create an adequate layer of oil film between the workpiece and cutter surface, resulting in minimised friction and contact pressure and producing a better surface finish. At the same time, only a marginal variation

in Ra values (0.03 μm) was recorded between the Hocut 3450 and Vasco1000 fluids, because of their similarity in tribological properties (with VO content always between 43 - 45 %).

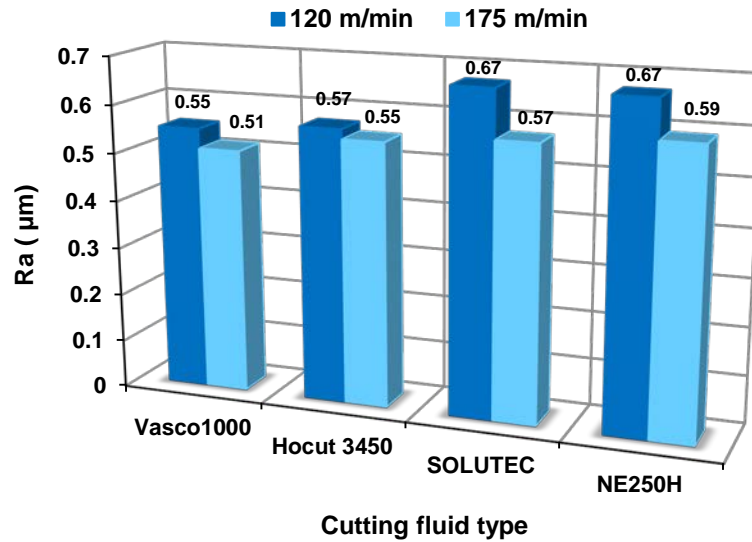


Fig. 5-12 Ra results vs cutting fluids using H13A cutting tool

Besides, it was noted that there was a notable drop of up to 14.92 % in Ra values at the higher cutting speed when the SOLUTEC and NE250H fluids were employed, whereas a slight drop of 7.27 % in Ra was recorded when the Vasco1000 and Hocut 3450 fluids were used at higher cutting speed. This is likely to be due to the disparities in their physical and chemical stability at different cutting temperatures. In addition, the ANOVA results shown in Table 5-4 reveal that all of the factors studied have significant effects on Ra where all P values <0.05 with the highest PCR (34.61%) for cutting tool material.

Table 5-4 ANOVA results for average surface roughness (Ra)

Source	DF	SS	MSS	F	P	PCR
Cutting tools	2	0.087	0.03465	11.5	0.001*	34.61%
Cutting fluids	3	0.082	0.02733	7.23	0.002*	31.16%
Cutting speeds (m/min)	1	0.026	0.02666	7.05	0.017*	10.23%
Error	17	0.064	0.00378			24. %
Total	23	0.260				
S= 0.0614849 R-Sq = 75.31% R-Sq (adj) =						
DF = Degree of freedom			* Significant at the 5 % level and confidence level of 95%			
SS = Sum of squares			P = Probability			
F= F- test value						

Fig. 5-13 shows the interaction plot between all factors affecting surface roughness (Ra). A lower degree of interaction can only be observed between cutting speed and cutting fluid type at the higher cutting speed, while a slight or trivial interaction was seen between cutting tool and cutting fluid type. On the other hand, the parallel trends of the lines shown at the top right of the figure clearly show no interaction between cutting speed and cutting tool. In general, this implies that the effect of interactions among the factors studied is insignificant except between cutting speed and cutting fluid type, particularly at the higher cutting speed, while confirming that all process parameters influence Ra almost independently.

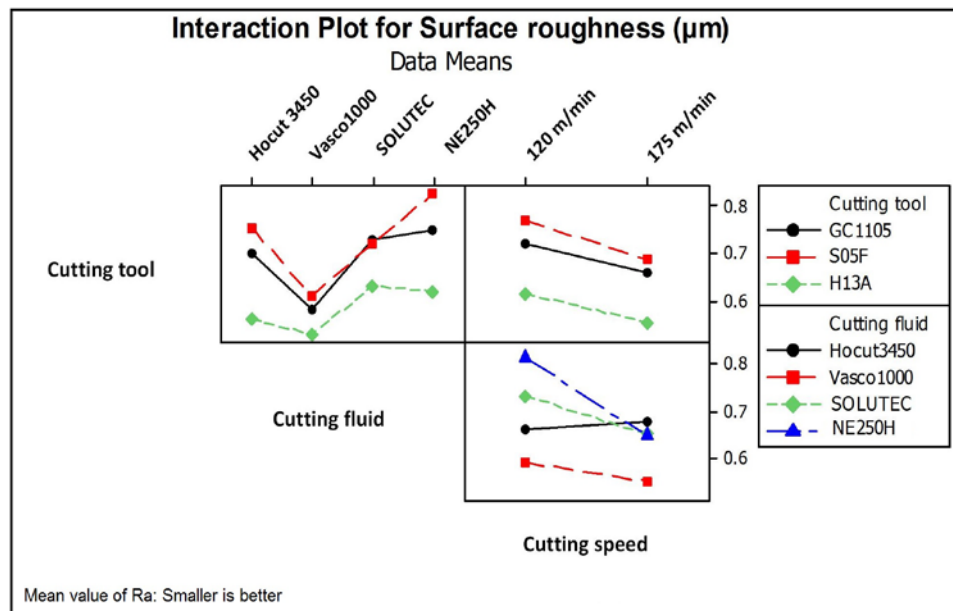


Fig. 5-13 Interaction plot for all control factors affecting surface roughness (Ra)

5.3.2 Tool wear analysis

Fig. 5-14 shows the results for flank wear at different cutting speeds using the Vasco 1000 cutting fluid. It is clear that, as cutting speed increased, flank wear also increased. This is mainly due to the heat generated in the machining zone, confirming that cutting speed has the largest influence on tool wear. A typical rise in flank wear with increasing cutting speed can also be seen with all cutting tools tested. In general, the coarse uncoated W/Co carbide tool H13A produced lower flank wear (50.34 and 97.18 μm respectively) compared to other cutting tools tested. This could be attributed to its peculiar mechanical

properties and thermal stability, especially high toughness and tensile rupture strength (TRS ~2690 MPa), and hot hardness (>91 HRA) [262]. On the other hand, the CVD-coated tool (S05F) exhibited the highest flank wear values of 118.19 and 141.83 μm at cutting speeds of 120 and 175 m/min respectively. The PVD TiAlNi carbide tool outperformed the CVD tool in terms of flank wear under all cutting conditions. This supports findings in the literature [187, 262] that titanium aluminium nitride (TiAlNi) coatings have high hardness compared to CVD in combination with resistance to oxidation, which improves wear resistance.

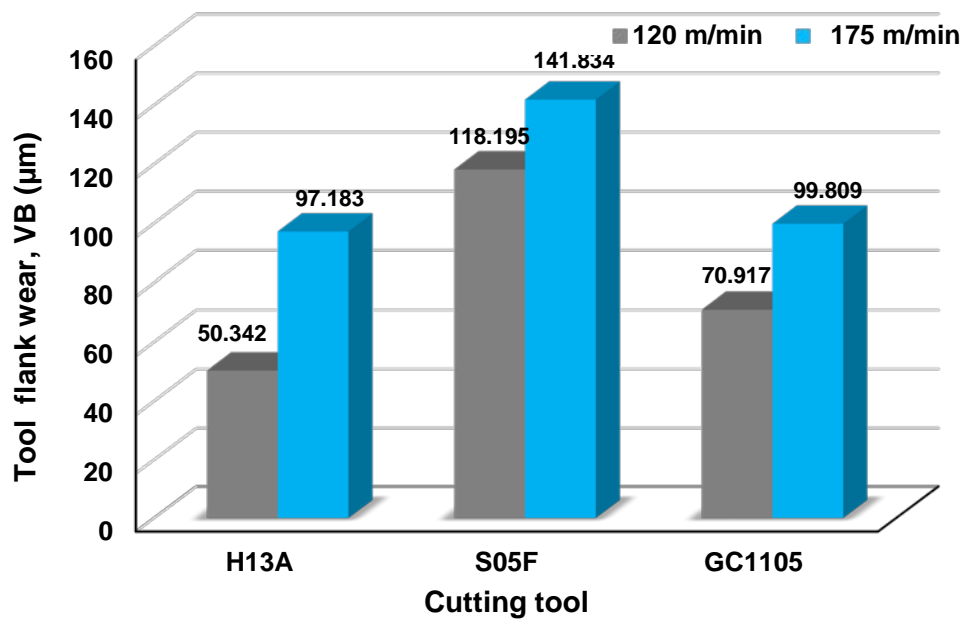


Fig. 5-14 Flank wear results for all cutting tools using Vasco 1000 cutting fluid

Fig. 5-15 shows the flank wear results for different types of cutting fluid at cutting speeds of 120 and 175 m/min. In general tool flank wear ranged between 50 and 105 μm . No major variations were observed when changing cutting fluid type except Hocut 3450 at the lower cutting speed of 120 m/min. Conversely, cutting speed caused the largest variation. All fluids produced relatively similar values of tool flank wear (with VB always between 95-105 μm) at the higher cutting speed of 175 m/min. Additionally, a typical rise in flank wear values from lower to higher cutting speeds was observed using all fluids. Table 5-5 shows the ANOVA results, where cutting speed and cutting tools were found to have statistically significant effects. Cutting speed has the highest PCR of 57.75% followed by cutting tool at 31.68%, while the type of cutting fluid has little impact on minimising tool flank wear.

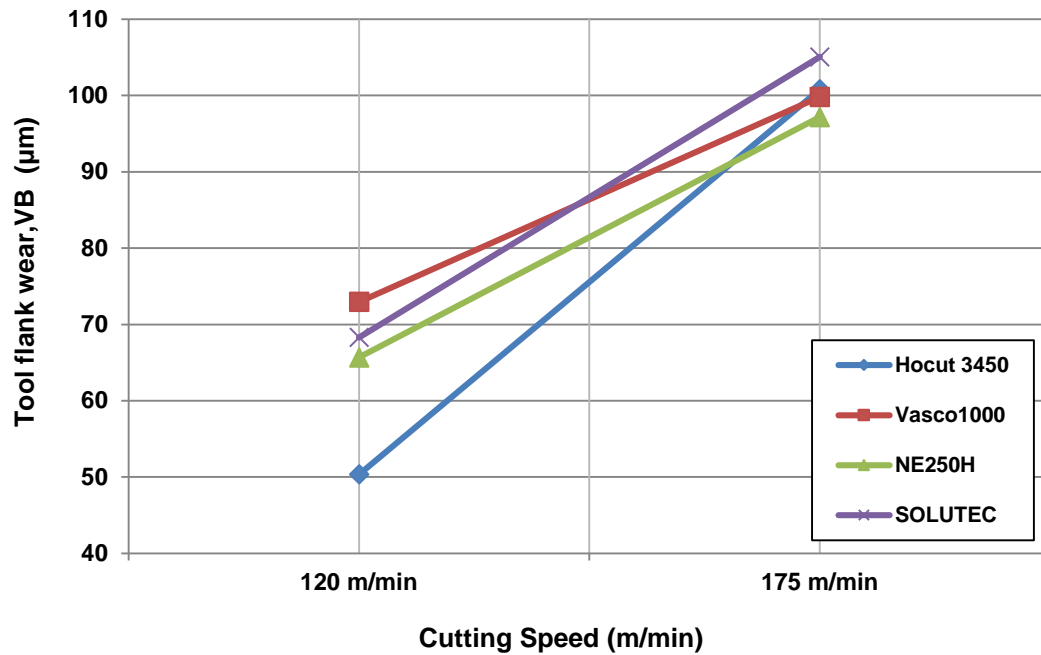


Fig. 5-15 Flank wear results for different cutting fluids using the H13A cutting tool

Table 5-5 ANOVA results for tool flank wear (VB)

Source	DF	SS	MSS	F	P	PCR
Cutting speed (m/min)	2	15169	7584.7	52.4	0.0*	57.75%
Cutting fluid	3	315.6	105.2	0.73	0.549	1.2%
Cutting tool	1	8323.	8323.5	57.58	0.0 *	31.68%
Error	17	2457.	144.6			9.37 %
Total	23	26266				
S= 12.0234 R-Sq = 90.64% R-Sq (adj) =						
DF = Degree of freedom			* Significant at the 5 % level and confidence level of 95%			
SS = Sum of squares			P = Probability			
F= F- test value						

Fig. 5-16 shows images of tool wear scarring on various cutting tools at the higher cutting speed of 175 m/min using the Vasco 1000 cutting fluid. In addition, it was observed that adhesion is the dominant wear mechanism of the CVD-coated cutting tool at the higher cutting speed, particularly when the NE250H cutting fluid was used, as shown in Fig. 5-17. This supports findings in literature [262] suggesting that the majority of coating materials can be removed rapidly by the chemical reaction between the tool and workpiece material (chemical crater wear), which is accelerated at high cutting speeds particularly when machining titanium alloys.

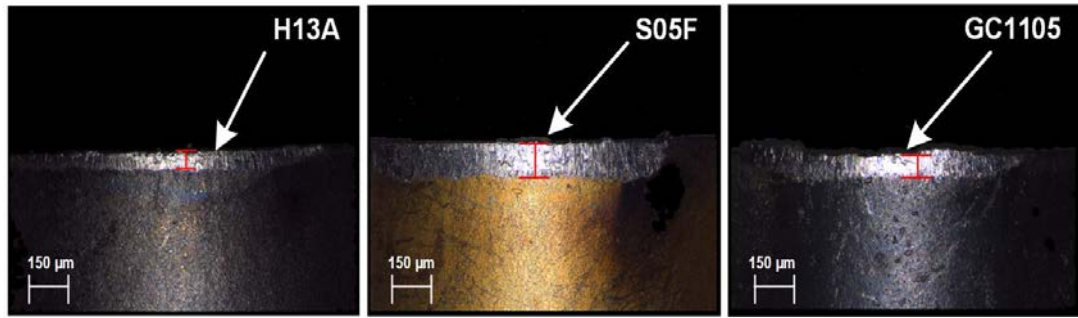


Fig. 5-16 Abrasive tool wear patterns on the flank faces of different cutting tools at a cutting speed of 175 m/min using Vasco 1000 cutting fluid

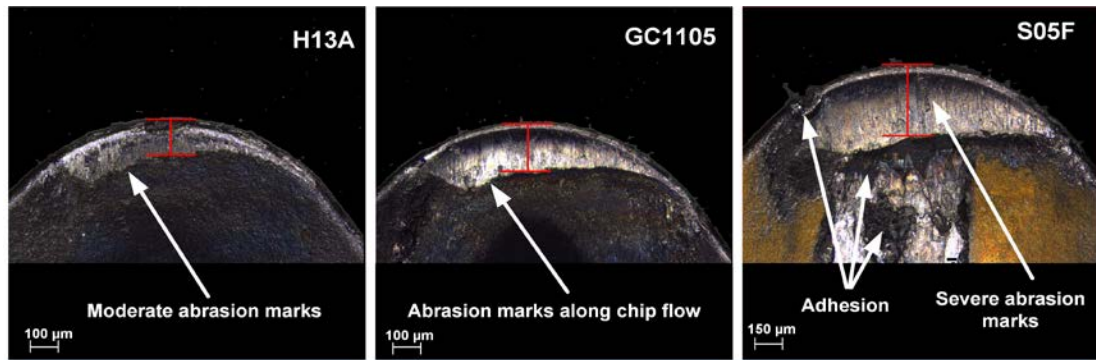


Fig. 5-17 Tool wear scars on the rake faces of different cutting tools at a higher cutting speed of 175 m/min using NE250H cutting fluid

5.3.3 Chip thickness

Fig. 5-18 demonstrates the results for chip thickness (t_c) versus cutting fluid. In general t_c ranged between 0.11 mm and 0.14 mm at cutting speeds between 120 and 175 m/min. It can be seen that, as cutting speed increases, chip thickness decreases. At low cutting speed, due to a large contact area on the rake face and a small shear plane angle (Φ), thick chips are generated. The increase in cutting speed for a given feed rate increases the shear angle and very thin chips are then produced due to the heat involved as well as the reduction in material strength. A marginal variation of up to ~ 0.04 mm was observed among the fluids tested in terms of chip thickness. These results are in agreement with those of Davim et al. [1] who concluded that chip thickness is strongly affected by cutting speed and feed rate, whilst the type of cutting fluid has little effect on chip thickness when cutting titanium alloys.

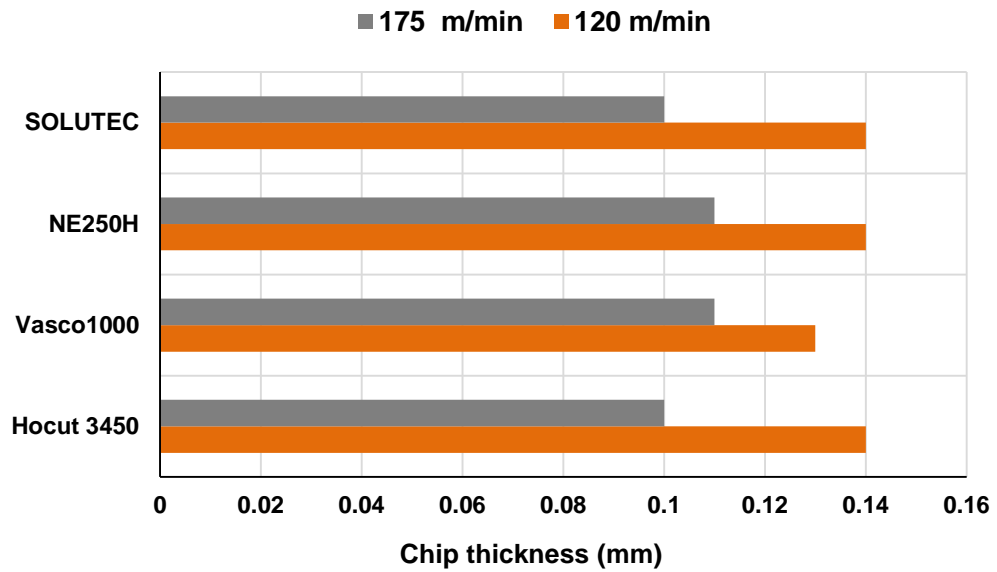


Fig. 5-18 Chip thickness versus cutting fluid at various cutting speeds using H13A tool

Fig. 5-19 illustrates chip thickness ratio (R_c) versus cutting fluids at various cutting speeds. R_c was calculated based on the orthogonal cutting model in turning operations, from the ratio of un-deformed chip thickness t_0 to deformed chip thickness t_c , $R_c = t_0/t_c$. t_0 was considered as equal to feed rate (0.1 mm/rev) and actual thickness was measured using a digital micrometre. Generally, values of R_c varied between 0.7 and 1.0. It was observed that, as the cutting speed increased, R_c also increased when turning Ti-6Al-4V. A marginal variation of up to 0.1 was found among fluids in terms of R_c in all cutting conditions, which implies also that the type of fluid used has little effect on R_c .

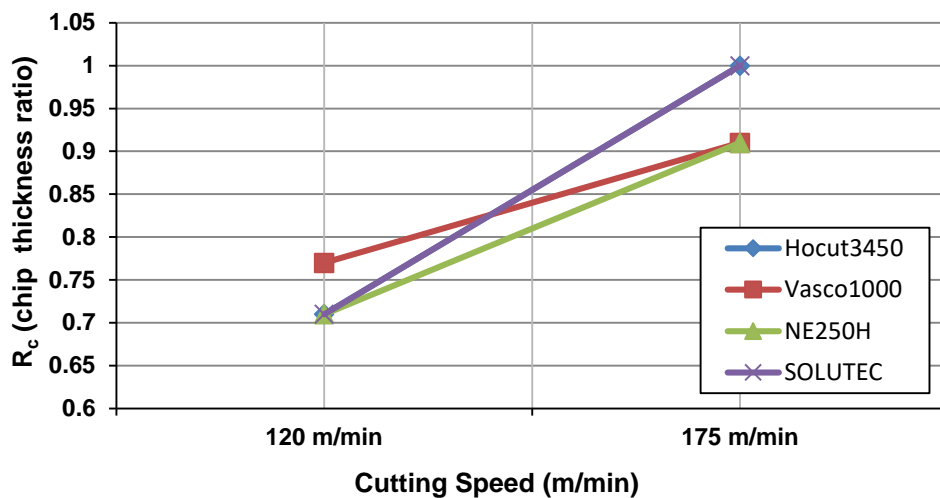


Fig. 5-19 Chip thickness ratio versus cutting fluids using H13A cutting tool

Fig. 5-20 shows the serrated teeth chip style formed at various cutting speeds. It can be seen that both cutting speeds produced desirable discontinuous serrated chips. However, at higher cutting speed, chip thickness and size decreased owing to the increase in shear angle during the cutting process [272].

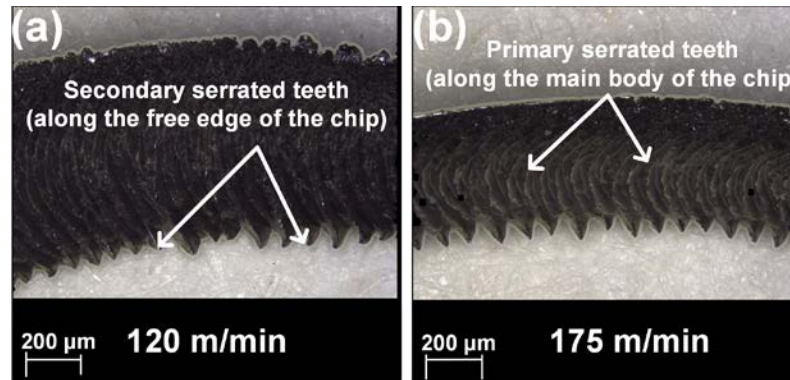


Fig. 5-20 Images of chip style formed at different cutting speeds using Vasco 1000 cutting fluid and H13A cutting tool

5.3.4 Summary

Values of R_a varied between $0.51 \mu\text{m}$ to $0.98 \mu\text{m}$ and the ANOVA analysis showed that all factors evaluated were found to be statistically significant. Cutting tool has the highest PCR of 34.61%, followed by cutting fluid (31.16%) and cutting speed (10.23%). The H13A tool outperformed others in terms of R_a , and these findings somewhat contradict the previous results when the PVD-coated (GC1105) tool achieved the lowest value of R_a . Therefore, H13A will be evaluated further in the next investigation (section 5.4). The Vasco 1000 fluid showed superior machining performance compared to other fluids tested in terms of R_a , while NE250H exhibited inferior potency in minimising R_a . It was concluded that the disparity between the poor results using NE250H and the good results obtained with Vasco1000 in terms of surface roughness could be explained in terms of the relative inefficiency of the former fluid due to its low VO content in the emulsion. In addition, no significant interaction was observed among the factors evaluated except for a low degree of interaction between cutting speed and cutting fluid type at the higher cutting speed. In the same vein, cutting speed is the most influential factor in affecting tool wear, with the highest PCR of 57.75%, followed by cutting tool (PCR of 31.68%), while the type of cutting fluid has little influence on minimising tool wear. H13A

achieved the lowest tool wear values of 50.34 and 97.18 μm at the lower and higher cutting speeds respectively. Conversely, the CVD-coated tool presented inferior cutting performance in terms of tool flank wear, while adhesion is the dominant wear mechanism particularly at the higher cutting speed when the NE250H fluid was used. All cutting fluids showed similar machining performance in terms of tool wear at the higher cutting speed. Chip thickness (t_c) and chip thickness ratio (R_c) ranged between 0.11- 0.14 mm, and 0.7-1.0 respectively. It was found that t_c and R_c are strongly affected by cutting speed and marginal variations of ~ 0.04 mm and 0.1 were observed among the tested fluids in terms of t_c and R_c respectively, suggesting that the type of cutting fluid also has little effect on these measures. The investigation showed that there was a discernible difference in the size of serrated chips formed at various cutting speeds. Hence, a detailed study of chip formation takes place later as described in section 5.5. As the surface quality of the machined parts is the utmost priority with regard to high degrees of safety, particularly in aerospace applications, the Vasco 1000 fluid was chosen as an optimal fluid for the evaluation of the CUT-LIST system owing to its machining performance, especially in terms of R_a . Thus, it will be used in the next experimental study.

5.4 Assessment of cutting fluid concentration ratio

This study aims to identify the preferred concentration ratio of the Vasco1000 cutting fluid for the assessment of CUT-LIST, as described thoroughly in the next section. Investigations of the effect of fluid concentration and cutting conditions of cutting speed and feed rate on the key process measures such as R_a , tool wear and tool life and micro-hardness using different tool materials, are also other intended objectives of this study.

5.4.1 Analysis of average surface roughness results

Fig. 5-21 shows the main effects plot for the average surface roughness (R_a) results. Overall, R_a values varied between 0.47 μm - 1.63 μm . This variety is still lower than the R_a range between 0.8 μm - 2.5 μm achieved recently by Kapoor et al. [273] when turning Ti-6Al-4V under flood cooling conditions at various concentration ratios with PCD cutting tool. Lower R_a values can be obtained using a fluid concentration of 10%, cutting speed of 146 m/min and feed rate at 0.1 mm/rev using the uncoated carbide tool H13A.

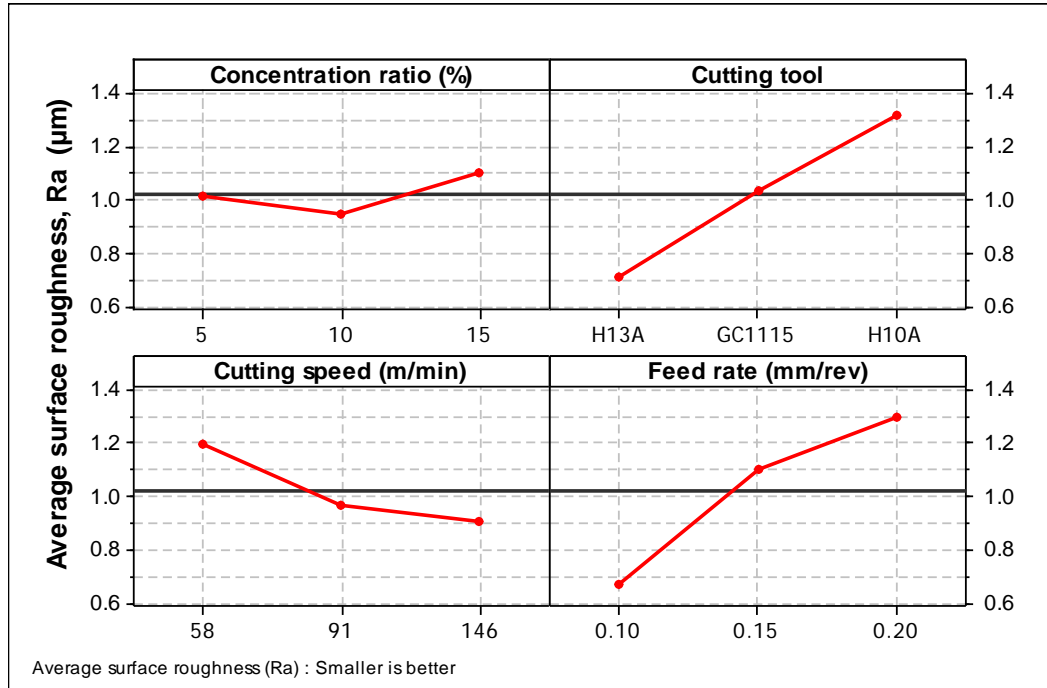


Fig. 5-21 Main effects plot for surface roughness results

5.4.1.1 Fluid concentration effect

It is evident from the main effects plot in Fig. 5-21 that the 10% concentration showed marginally improved performance in terms of average surface roughness, Ra. A similar finding has also been reported by [273] where a concentration of 10% offered superior cutting performance in terms of surface finish and tool life when turning Ti-6Al-4V. This was attributed to its outstanding balance between tribological and thermal properties. Although it was expected that a 15% concentration could achieve a better surface finish due to its higher viscosity (2.2 cP), the machined surfaces at 10% fluid concentration exhibited lower surface roughness of about 0.94 µm, which was anticipated to be as a result of the combined action of two contradictory fluid properties (viscosity and heat capacity). Apparently, at the low concentration of 5%, the lack of a satisfactory lubrication effect (viscosity ~1.8 cP) led to increased friction at the tool-chip interface, leading to higher Ra. On the other hand, at the higher concentration of 15%, the cooling effect is less effective (heat capacity ~ 3.88 J/g°C). This increases cutting temperature and a faster thermal softening of the tool material occurs along with higher friction at the tool-chip-workpiece interaction zones, also resulting in the earlier deterioration of the machined surface.

5.4.1.2 Effect of machining conditions

Understandably, the Ra values of the machined parts increased with increased feed rate and decreased with increased cutting speed (Fig. 5-21), while feed rate is the most influential factor in minimising Ra with a PCR of 45.6% as shown in Table 5-6. Cutting speed was found to have a noticeable statistical contribution in reducing Ra values with a PCR of 10.4 %. Additionally, the H13A tool showed superior performance compared to others in terms of Ra. This supports findings described in the previous section where H13A presented similar outstanding results in reducing Ra. Although the TiAlNi-coated tool (GC11105) and uncoated H10A are fine grain-based tools, GC11105 outperformed H10A in terms of Ra owing to its specific mechanical properties such as low friction and resistance to smearing and plastic deformation. This finding is in line with those in the literature [262] that TiAlNi coating material is more beneficial for fine grain-based tools as it improves tool strength and compensates the instability of the cutting edge due to its relatively low fracture toughness compared to coarse grain-based tools. Cutting tool material was also found to be statistically significant in influencing Ra, with a relatively high PCR of 39.3%. Table 5-6 shows the ANOVA results for Ra where a model error of 2% was found with all P values <0.05, which indicates that all of the factors, including fluid concentration ratio, which had been expected to affect Ra were considered.

Table 5-6 ANOVA results for average surface roughness (Ra)

Source	DF	SS	MSS	F	P	PCR
Concentration ratio (%)	2	0.1112	0.05563	92.72	1.5E-04*	2.7%
Cutting tool	2	1.6650	0.83254	1387.	4.02E-06*	39.3%
Cutting speed (m/min)	2	0.4276	0.21381	354.3	3.2E-05*	10.4%
Feed rate (mm/rev)	2	1.8574	0.92874	1547.	1.05E-06*	45.6%
Error	18	0.0108	0.00060			2%
Total	26	4.0722				
S=0.0244949		R-Sq=99.73%		R-Sq (adj)=99.62%		
DF = Degree of freedom		P = Probability		* Significant at the 5 % level and confidence level of 95%		
SS = Sum of squares,		F= F- test value				

Fig. 5-22 shows the progression of Ra with cutting distance using the H13A tool. In the first stage up to 240 mm, Ra seems to be independent of cutting speed. After that, cutting at a speed of 146 m/min produced significantly higher surface roughness with a prolonged cutting distance of up to 600 mm. This could be attributed to the rapid tool wear observed due to the rise in temperature at the cutting interface. On the other hand, Ra values at the

lower cutting speed of 58 m/min were found to be steady with prolonged cutting distance, which could be due to the low level of tool wear observed. The geometry of the tool cutting edge tended to be maintained for longer periods. These findings are in accordance with those of a recent study of the face-turning of Ti-6Al-4V using a coated W/Co carbide tool [274].

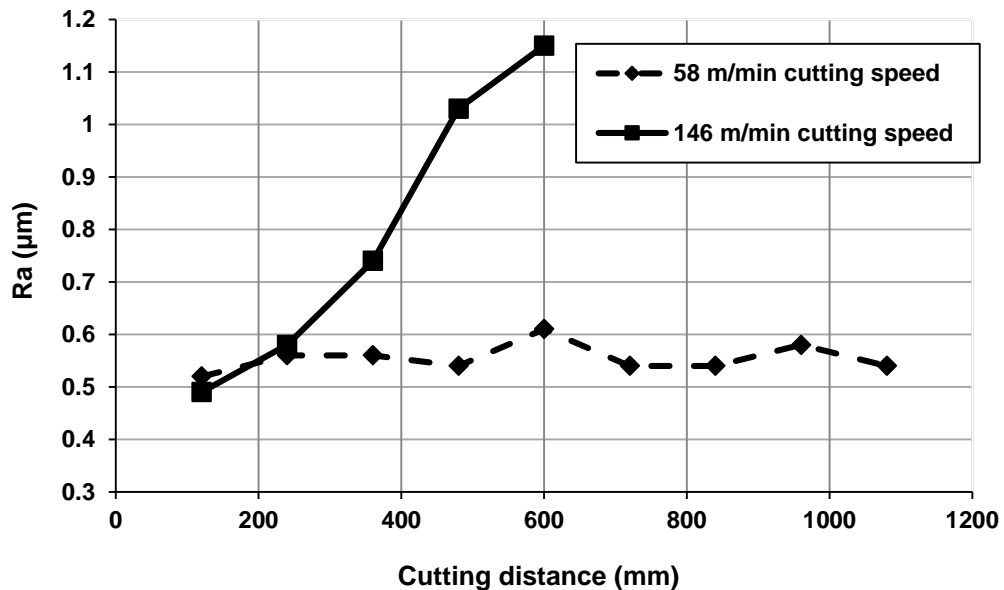


Fig. 5-22 Surface roughness versus cutting distance

5.4.2 Analysis of tool wear and tool life results

Fig. 5-23 presents the main effects plot for the tool flank wear results. Values of VB ranged widely between 28.8-110 μm . The most useful combinations of control factors for minimising tool wear were a fluid concentration of 10%, cutting speed of 58 m/min and feed rate of 0.1 mm/rev using the H13A tool. However, almost no variation in tool wear measures have been observed for different concentration ratios. Understandably, tool flank wear increases with cutting speed owing to the rise in heat generated. The heat at the tool edge would have softened the cutting edge, causing flank wear to increase [192]. Meanwhile the uncoated coarse-grained W/Co H13A tool showed superior performance compared to the other tool materials. This can be attributed to its superb combination of high hot hardness (> 90 HRA), toughness (>13 MPa.m^{1/2}), high thermal conductivity (~ 100 W/m·K) and high TRS (~ 2690 MPa) [262]. Table 5-7 shows ANOVA results for tool wear. Cutting speed, tool material and feed rate were found to have statistically

significant effect on tool wear, and the highest PCR of 83.1% was recorded for cutting speed. However, fluid concentration was found to have no statistical significance for tool wear when machining Ti-6Al-4V.

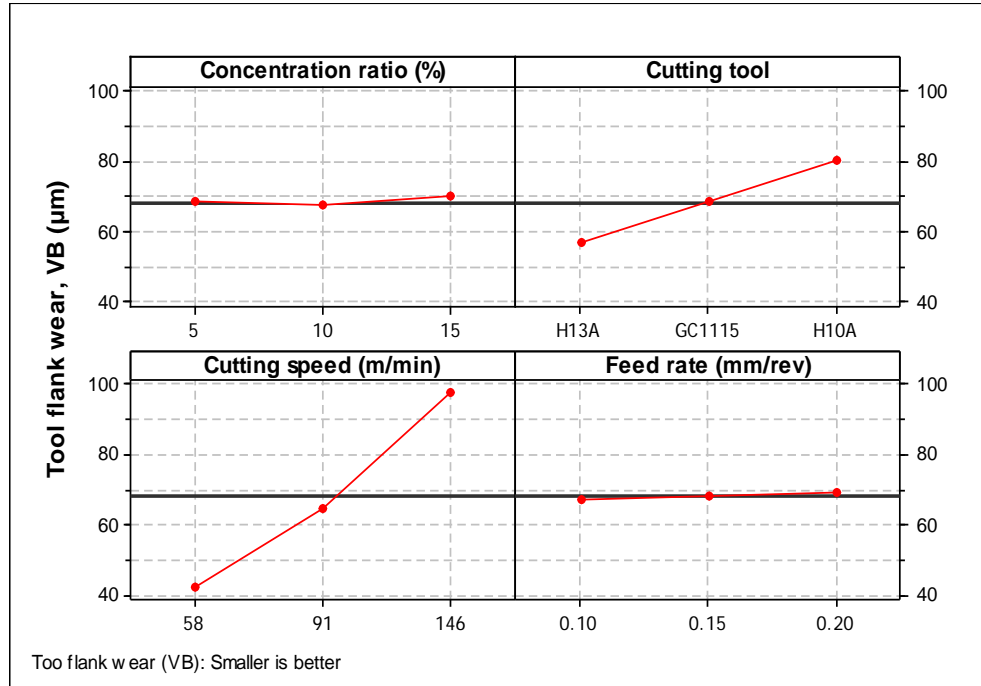


Fig. 5-23 Main effects plot for tool flank wear results

Table 5-7 ANOVA results for tool flank wear

Source	DF	SS	MSS	F	P	PCR
Concentration ratio (%)	2	19.9	9.9	2.59	0.103	0.1%
Cutting tool	2	2488	1244.2	324.57	0.00*	16.1%
Cutting speed (m/min)	2	12910	6455.2	1683.9	0.00*	83.1%
Feed rate (mm/rev)	2	41.0	20.5	5.34	0.01*	0.2%
Error	18	69.0	3.8			0.5%
Total	26	15528				
R-Sq = 99.56%		R-Sq (adj) = 99.36%				
DF = Degree of freedom	P = Probability		* Significant at the 5 % level and confidence level of 95%			
SS = Sum of squares	F= F- test value					

Fig. 5-24 shows tool flank wear results versus cutting distance using the H13A tool. A precautionary wear limit of 300 µm was chosen in estimating tool life (T_L). The results indicated that tool wear at a cutting speed of 146 m/min rapidly increased. This could be attributed to the inadequate time allowed for the tool to cool down, resulting in heat accumulating at the tool tip [275]. On the other hand, flank wear at a cutting speed of 58 m/min increased more steadily with prolonged cutting distance, which could be attributed

to the drop in temperature at the cutting interface. The progression of flank wear with cutting distance at the higher cutting speed using the H13A tool can be seen in Fig. 5-25.

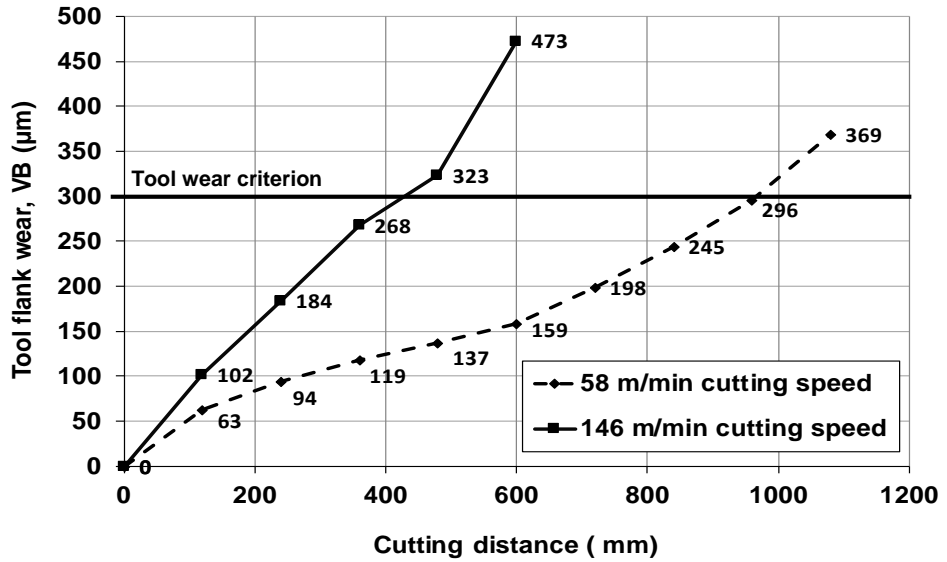


Fig. 5-24 Flank wear versus cutting distance at various cutting speeds using H13A tool

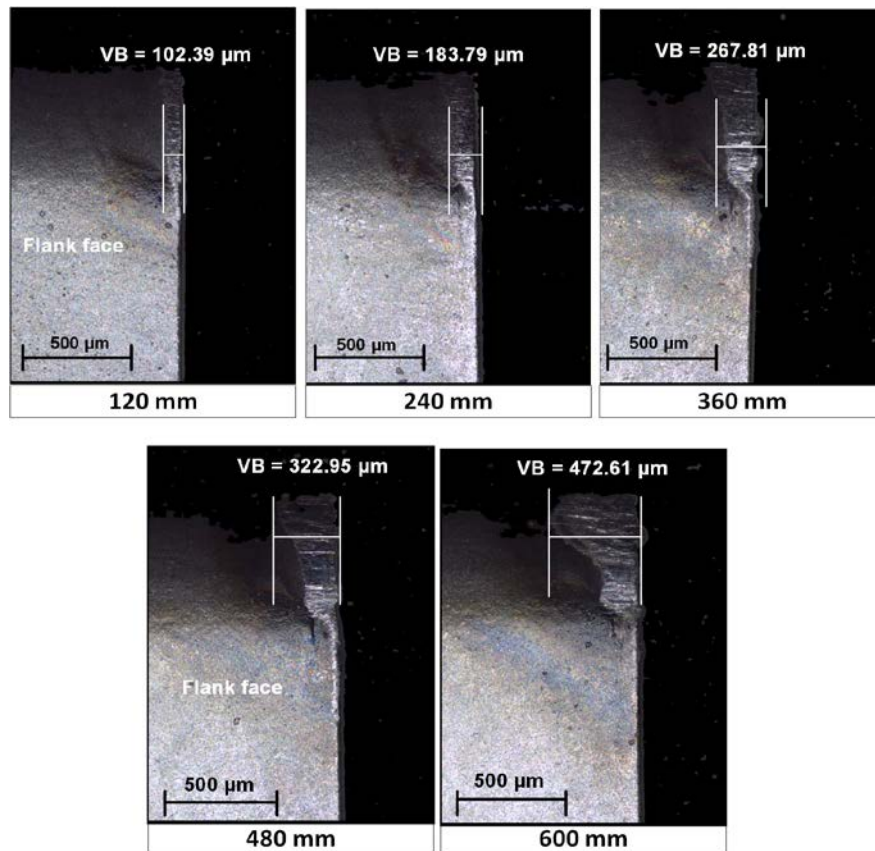


Fig. 5-25 Flank wear on H13A versus cutting distance at a cutting speed of 146 m/min

In relation to tool life (T_L), a cutting insert was rejected and the machining trial was ceased if one or a combination of the following took place: maximum tool flank wear ($VB_{\max} \geq 0.3$ mm), excessive chipping (i.e. flaking) or catastrophic fracture of the cutting edge. Fig. 5-26 illustrates a comparison of tool life at selected cutting speeds tested at a fluid concentration ratio of 10 % using the H13A cutting tool. The graph shows a dramatic drop in tool life at the higher cutting speed of 146 m/min (~ 82.3 %). At high speeds, more stresses are generated on the tool flank face close to the nose region, probably causing the yield strength of the tool to be reduced. This eventually results in higher wear at the nose area, adversely affecting tool life [276]. These trends are in agreement with those observed in recent studies [57, 63] where tool life decreased by 86.38% at the higher cutting speed during milling of Ti-6Al-4V under wet cutting conditions (flood cooling).

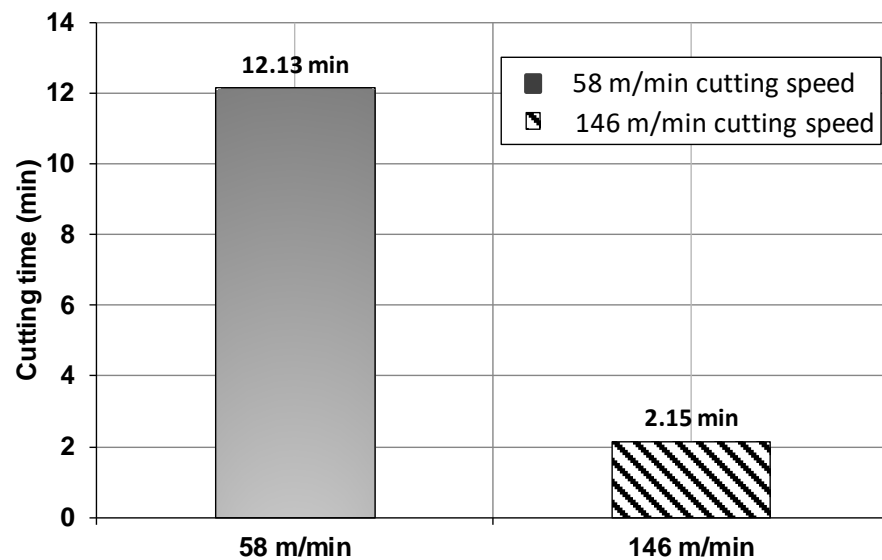


Fig. 5-26 Comparison of tool life recorded at cutting speeds of 58 and 146 m/min

5.4.3 Analysis of micro-hardness

Fig. 5-27 shows results for micro-hardness at a cutting speed of 58 m/min tested starting at 30 μm away from the machined surface. A notable increase in micro-hardness values were found near the surface, (from 330 HV_{100} at the beginning of the test after cutting 120 mm to ~ 366 HV_{100} at a sample taken from the end of the test after cutting 1080 mm). A gradual reduction towards the interior of the specimen until reaching the base material nominal's hardness was then observed. This could be attributed to the plastic deformation

resulting from the cutting action. When cutting temperature increases, there is a greater tendency for plastic deformation of the workpiece to occur in the subsequent layer left by the passage of the cutting tip, and therefore hardness increases [277]. It was suggested also in an investigation by Ezugwu et al. [278] that a hardening effect usually occurs instantaneously in the cutting process, most probably due to the high compressive stresses at the cutting edge. Additionally, the use of a worn tool is suspected to increase the hardening effect as well as causing micro-structural damage owing to the rise in heat accumulation at the tool tip during cutting. However, the material immediate under the surface is softer and this could be attributed to the high temperature generated during cutting resulting from the low thermal conductivity of Ti-6Al-4V [78].

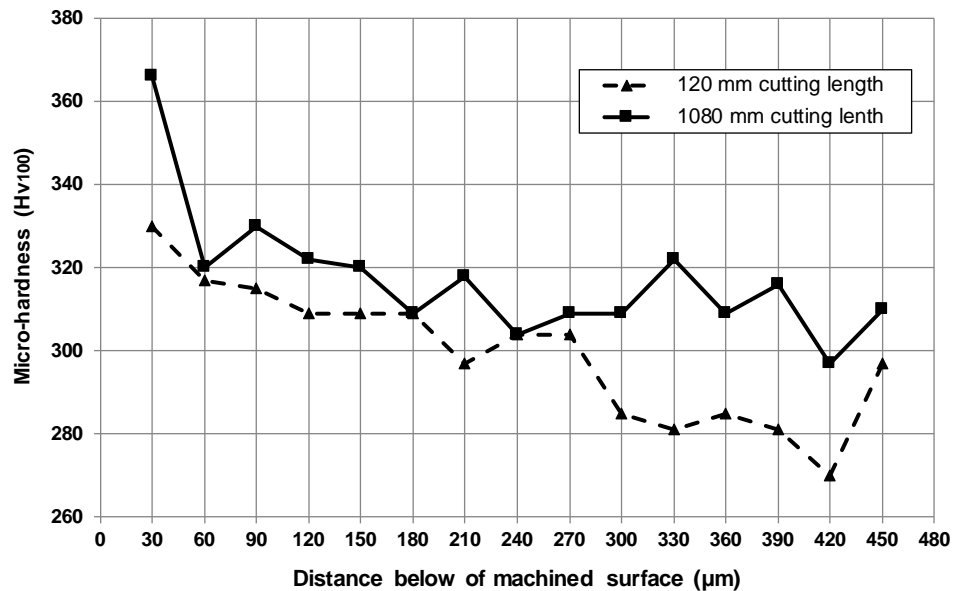


Fig. 5-27 Micro-hardness results beneath the machined surface at a cutting speed of 58m/min using the H13A tool

Fig. 5-28 shows micro-hardness results for different cutting distances in all conditions investigated at two different cutting speeds. It can be noted that these values were within the acceptable hardness range for Ti-6Al-4V aerospace parts of 419.6 HV₁₀₀ max and 284.4 HV₁₀₀ min [78]. Similarly, a rise in micro-hardness values with increases in cutting distance was seen. However, the highest micro-hardness measured was 376 HV₁₀₀ when machining at the higher cutting speed of 146 m/min after the tool had failed, whereas at the lower cutting speed only 366 HV₁₀₀ was recorded. Comparable trends were also

reported in a recent publication [71] on the cutting of Ti-6Al-4V at various cutting speeds using a coated tool. It was revealed that the hardness of the upper layer of the machined surfaces increased significantly with prolonged cutting distance or time when turning Ti-6Al-4V under all conditions investigated. This was attributed to the influence of worn tool that associated with prolonged cutting time or distance which increased the hardening effect owing to the rise in heat accumulation at the insert tip during cutting.

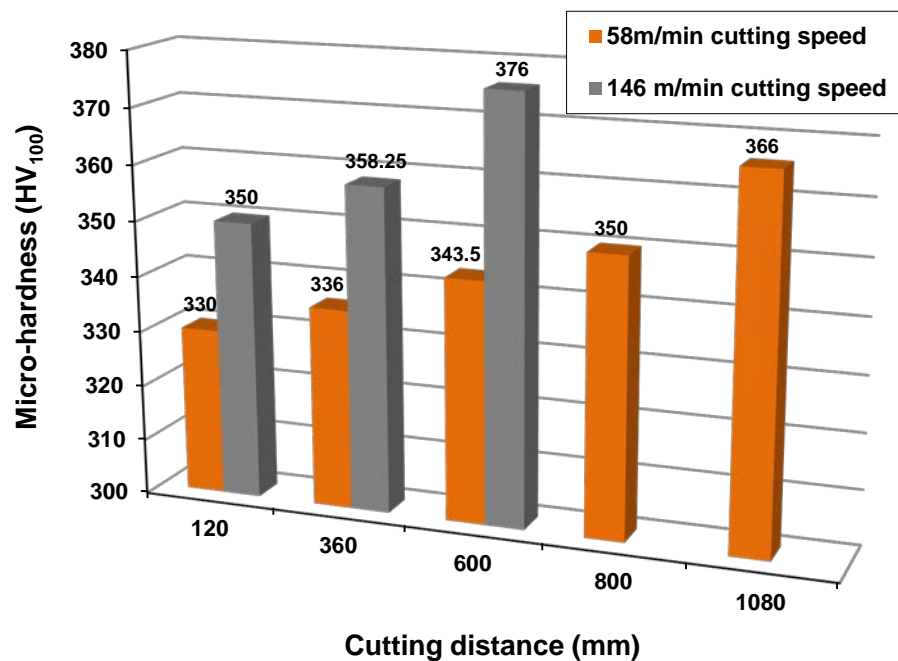


Fig. 5-28 Miro-hardness results versus cutting distance using H13A tool

5.4.4 Summary

Average surface roughness (R_a) varied between 0.47-1.63 μm . Although a small variation in mean R_a values (with a maximum of 0.15 μm) was observed among the concentration ratios tested, a good balance between the cooling and lubrication effects seems to be a reason for selecting the 10% fluid concentration ratio. Thus, a concentration of 10% will be used in the next experimental study in testing the new supply system. Fluid concentration is a significant factor in reducing surface roughness. Machining Ti-6Al-4V at a higher cutting speed produced marginally higher surface roughness with prolonging cutting distance or time. Tool wear was significantly affected by cutting speed, while fluid concentration had little effect on tool wear. Tool wear rapidly increased at higher cutting

speed while steadily progressing with prolonged cutting distance at the lower cutting speed. Additionally, tool life (T_L) was also considerably affected by cutting speed, while a higher tool life (12.13 min) was recorded at the lower cutting speed of 58 m/min. The use of uncoated coarse grain carbide H13A tool produced a better surface finish and lower tool wear in all conditions investigated. All micro-hardness values were below the threshold for critical applications (e.g. 419.6 HV₁₀₀ for aerospace components). The hardness values of the upper layer of the machined surface were typically higher near the machined surfaces and gradually reduced towards the base material. It can be concluded that the turning of Ti-6Al-4V using VO-based cutting fluid always produced significantly higher hardness near the surface with prolonged cutting distance under all tested conditions.

5.5 Evaluation of the CUT-LIST cutting fluid supply system

Since the key input parameters such as the water-miscible type VO-based cutting fluid (Vasco1000), 10% fluid concentration ratio and cutting tool material type (H13A) have been determined in the previous sections, this phase aims to introduce all of the relevant results from the analysis of data in the milling-based machining trials which were performed in order to evaluate the new CUT-LIST supply system. Therefore, in the next section, a detailed comparative study has taken place of the performance of the CUT-LIST and the conventional supply system. Comparison measures and indicators were cutting force, workpiece temperature, tool wear, and chip and burr formation. Aspects of surface integrity such as surface roughness and quality, micro-hardness and surface microstructural damage were also evaluated at different machining conditions.

5.5.1 Performance comparison with a conventional flood supply system

5.5.1.1 Cutting force analysis

The maximum cutting force results are shown in Fig. 5-29. Cutting forces ranged from 1600 to 1903 N when the conventional system was used, while a considerable reduction of up to 16.41% was recorded when CUT-LIST was employed, particularly at a lower feed rate of 0.1 mm/ rev compared to 1.26 % at the feed rate of 0.15 mm/rev and the

cutting speed of 200 m/min. This could be attributed to the high adhesion action of the impinging fluid at the lower feed rate, which gave the fluid droplets enough time to adhere to the workpiece and cutting tool surfaces. Additionally, the relatively higher impinging jet velocity of up to 10.83 m/s (see Table 3-6) was achievable by CUT-LIST and this helped the cutting fluid to penetrate effectively into the machining zone and to form the boundary of the oil film between workpiece and cutter, resulting in minimised contact pressure. A similar phenomenon was reported by Ezugwu et al. [39], where the high-momentum jet produced a hydraulic wedge between the tool and the workpiece interface, offering adequate lubrication with a substantial reduction in friction. In addition, the results also showed analogous trends in increased cutting force with cutting speed regardless of the cooling system used. This is due to the strain rate hardening effect when cutting titanium [85].

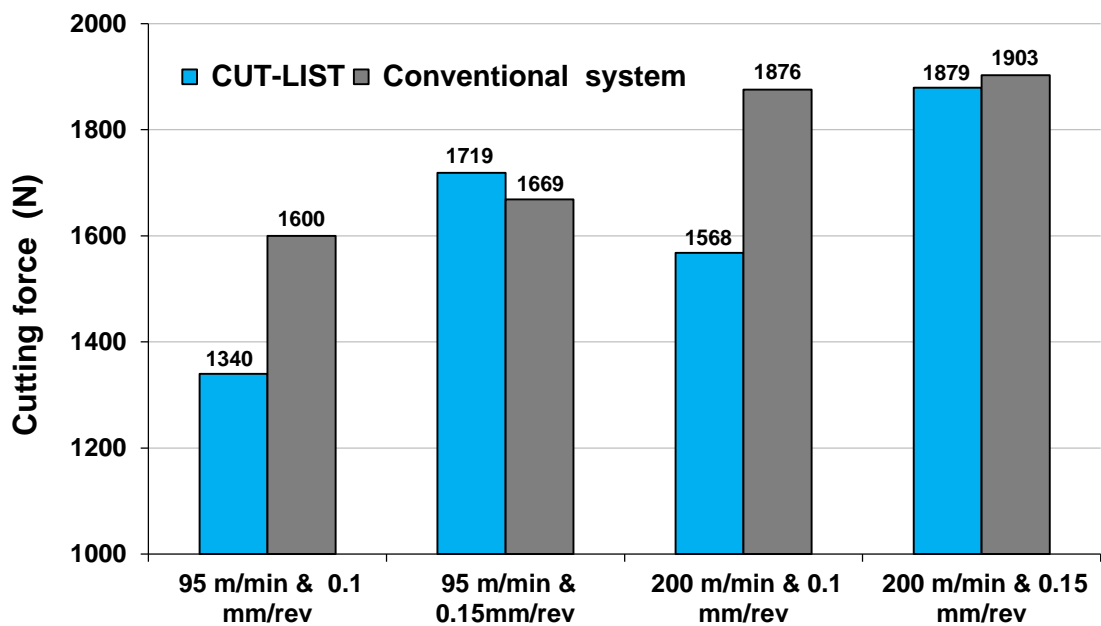


Fig. 5-29 Cutting force results for the two systems in various cutting conditions

5.5.1.2 Workpiece temperature

As shown in Fig. 5-30, average workpiece temperatures ranged between 20.8 and 25.7, and 20.6 and 24.2 °C, for the CUT-LIST and conventional systems respectively. Both systems showed reduced workpiece temperature with a marginal variation (by a maximum of 1.5 °C). This is likely to be because a small proportion (~20%) of the heat

generated when cutting titanium is conducted into the workpiece and chip while 80% of the heat is expected to be transferred to the cutting tool due to the low thermal conductivity of titanium alloy [48]. In addition, the cutting fluid can dissipate more than 30% of the heat generated if it penetrates into the machining zone effectively [279]. Possibly, CUT-LIST helped to form efficient fluid trapping between the tool and workpiece surfaces due to the nozzle positioned in the feed direction, which led to improved fluid access into the machining zone resulting in more heat transferred from the workpiece to the cutting fluid. Additionally, the impingement effect of the high-velocity fluid droplets allowed the fluid to exert its cooling function more efficiently and thus assisted in reducing workpiece temperature. These effects helped the new system to reduce workpiece temperature and compensated for the reduction (~ 42%) in the amount of cutting fluid supplied. In the same vein, both systems exhibited marginal reductions in average workpiece temperature with increased cutting speed and feed rate. This could be due to the increased fluid flow rate associated with increasing cutting energy, which improved the fluid's ability to dissipate heat [280].

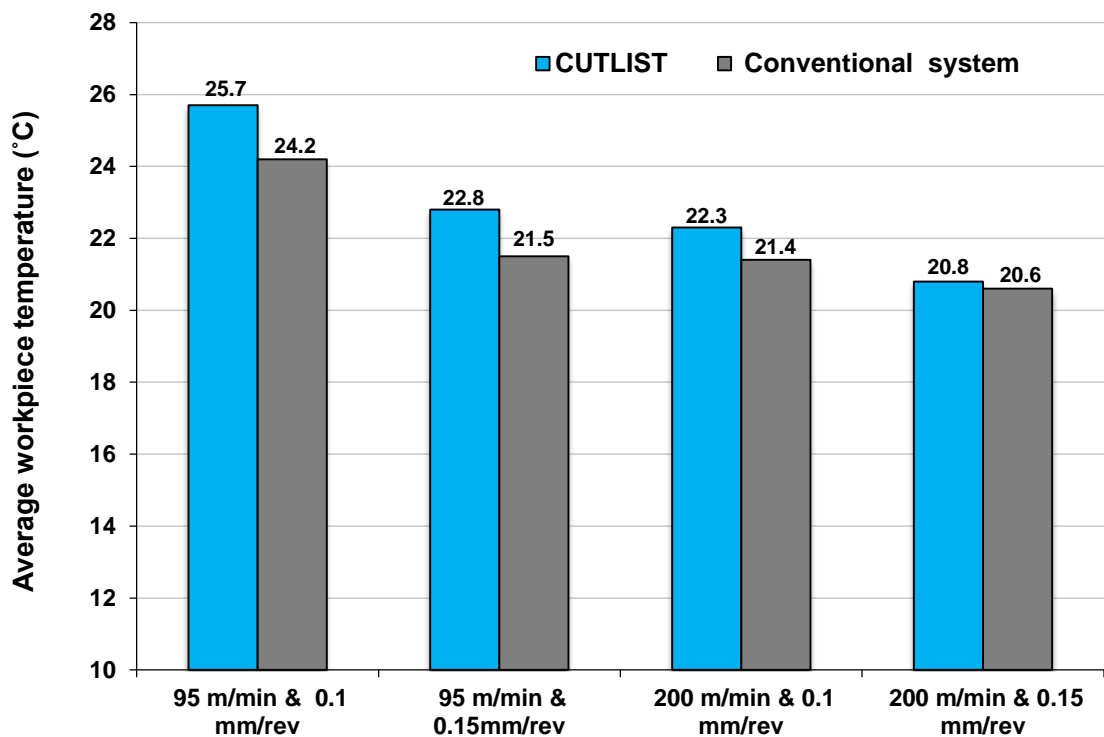


Fig. 5-30 Average workpiece temperature results for the two systems in various cutting conditions

5.5.1.3 Tool wear analysis

Fig. 5-31 presents the tool flank wear data obtained for both systems in various cutting conditions. A considerable reduction in tool wear of up to 46.77% was achieved at the higher cutting speed of 200 m/min and feed rate of 0.15 mm/rev when using CUT-LIST. In general, low flank wear levels of $\sim 30 \mu\text{m}$ were noticed using CUT-LIST, except at a cutting speed of 200 m/min and feed rate of 0.1 mm/rev. This can be attributed to the combined cooling effect on the cutting insert in the in-feed and against-feed directions, where the nozzle position in the feed direction helped the impinging jet to penetrate deeply into the machining zone. The other position against feed direction afforded enough space to assist in chip evacuation and aided in cooling the tool tip at end of the cyclic process. At higher cutting conditions, CUT-LIST affords a larger jet velocity of 10.83 m/s (see Table 3-6), which increased the ability to accelerate heat dissipation from the cutting tip and thereby reducing tool flank wear. On the other hand, the conventional supply system failed to dissipate heat sufficiently from the machining zone at the same cutting conditions, which resulted in accelerated tool flank wear, adhesion, and micro-chipping, as shown in Fig. 5-32.

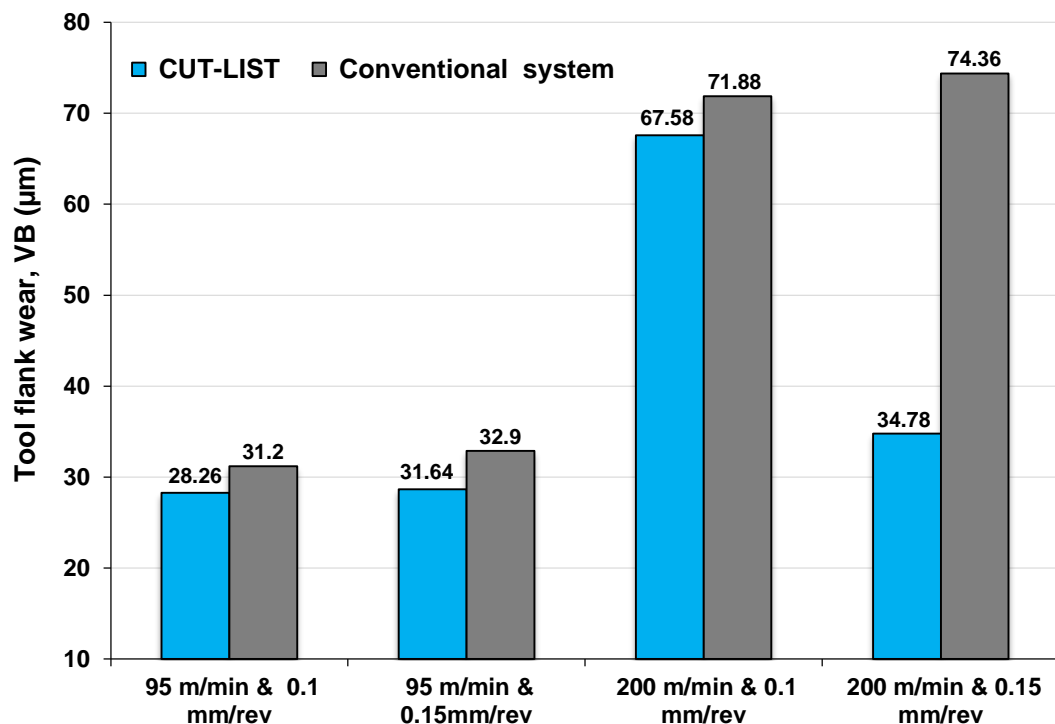


Fig. 5-31 Tool wear results for the two supply systems in various cutting conditions

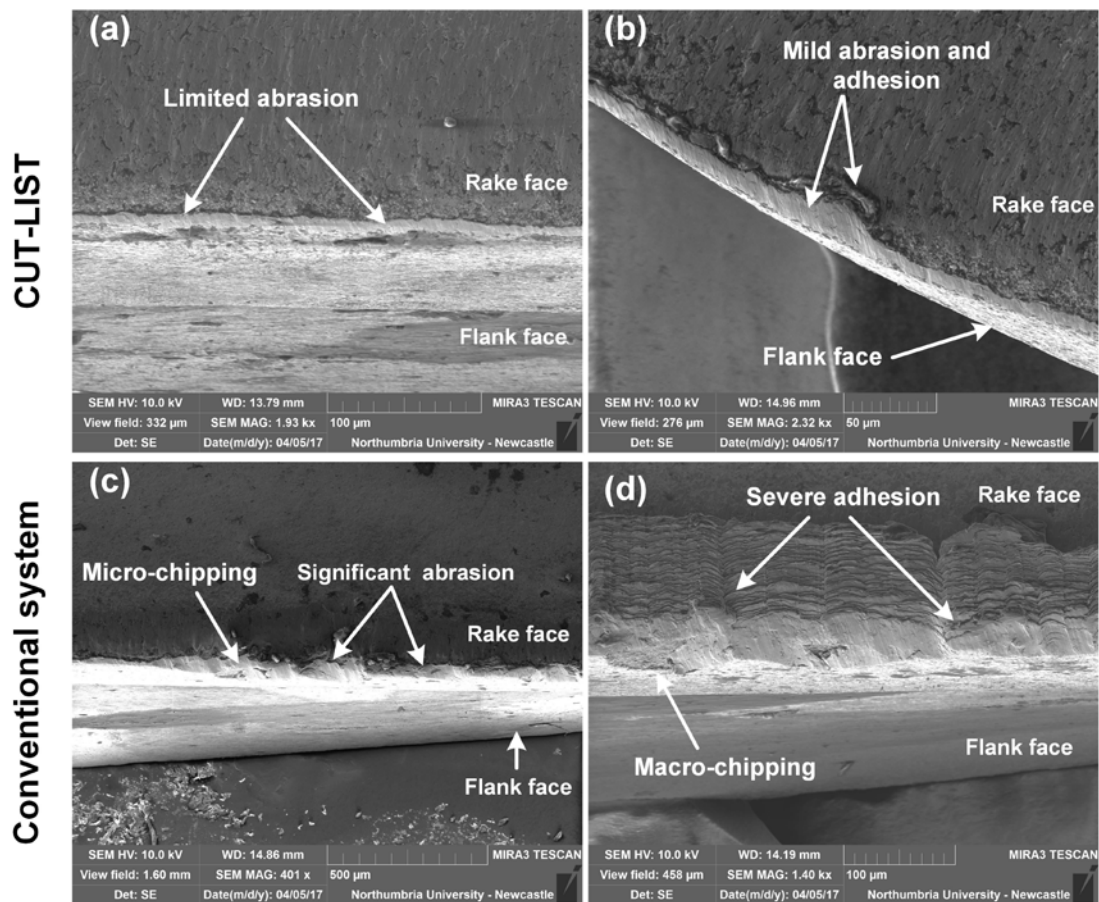


Fig. 5-32 SEM images of the cutting tools used with CUT-LIST at a feed rate of 0.15 mm/rev and cutting speeds of 95 and 200 m/min respectively (a, b) and the conventional supply system at a feed rate of 0.15 mm/rev and cutting speeds of 95 and 200m/min respectively (c, d)

5.5.1.4 Burr formation

Fig. 5-33 details the top burr height results formed by both cutting fluid supply systems. The top burr heights generated by the CUT-LIST were substantially smaller than those produced by the conventional cooling system by up to 60%. Since one of the main reasons for burr formation is tool wear [281], the reduction in burr size is not surprising due to the reduction in tool wear discussed in the previous section. This can also be attributed to the ability of the new system to direct the high momentum impinging jet into the tool-workpiece interface, helping the jet to hit the insert edge effectively and leading to the edge of the cutting tool being maintained in a sharper condition with less of a metal shearing effect. In addition, the results showed a similar trend in decreasing burr height with increased feed rate regardless of the cooling system used.

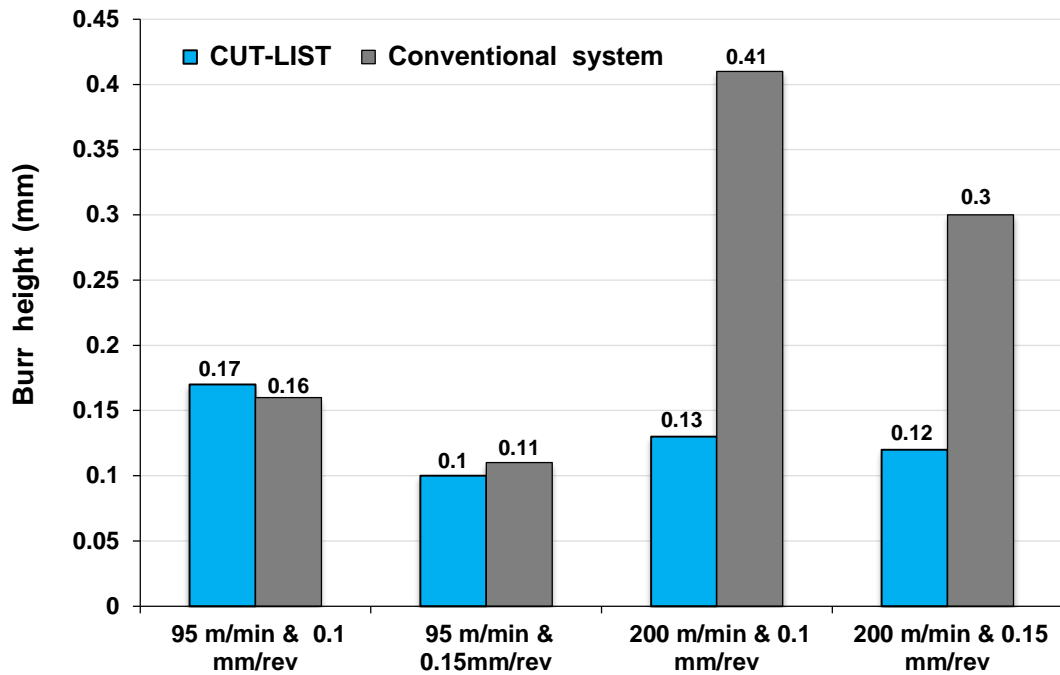


Fig. 5-33 Effect of cutting fluid supply system on burr height at various machining conditions

5.5.1.5 Average surface roughness and surface quality

Fig. 5-34 details the surface roughness (R_a) results achieved by both supply systems. Values of R_a generally ranged between 0.51 and 0.56 μm , and 0.57 and 0.71 μm for CUT-LIST and the conventional systems respectively. Values of R_a are relatively lower with the use of CUT-LIST for all conditions investigated. The new system improved the penetration of the impinging fluid in accessing the machining zone efficiently and forming the boundary of the oil film between workpiece and cutter, thereby reducing friction and improving the quality of the machined surface. Additionally, the new CUT-LIST and the conventional system showed similar trends in decreasing surface roughness with increased cutting speed regardless of feed rate. This is due to the increased cutting fluid flow rate (see Fig. 3-13) associated with increased cutting speed which was found to be in agreement with findings reported by Cai et al. [58]. The SEM analysis showed that surfaces machined using the conventional supply system had chips re-deposited or adhered to the machined surfaces, as detailed in Fig. 5-35. Feed marks were apparent on all machined surfaces regardless of the fluid supply system used. No major damage such as cracks or material tearing was observed, especially when the CUT-LIST system was

used. This is also evident in the relatively low surface roughness values. However, larger smearing was apparent when the conventional system was employed, which is likely to have been the result of the inability of the fluid to reach the machining zone, particularly at higher cutting speeds. The adhered chips observed on the machined surfaces produced when the conventional supply system was used were probably the result of material being trapped between the tool flutes which was subsequently pressure-welded to the machined surfaces due to insufficient cooling. These findings are in agreement with those of Shyha et al. [282] who reported similar observations when drilling titanium/carbon fibre-reinforced plastics (CFRP)/aluminium stacks.

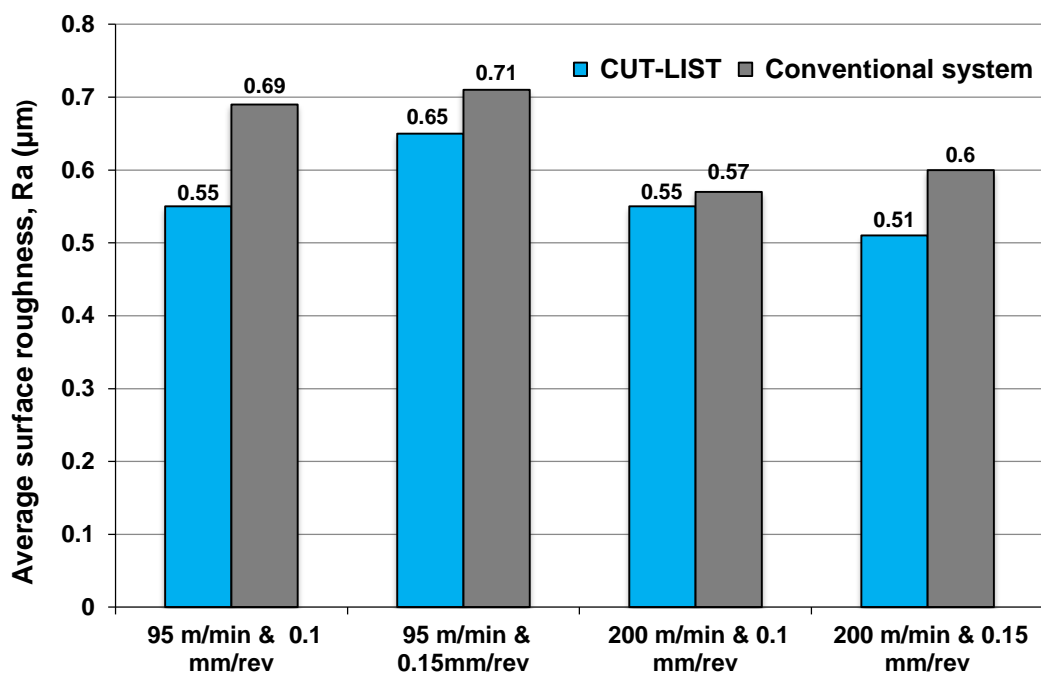


Fig. 5-34 Average surface roughness results versus cutting conditions for the two systems.

In addition, damage in terms of surface cavities and loss of material was seen only when the conventional flood supply system was used at higher cutting speeds, as shown in Fig. 5-36. When the carbide cutting insert becomes worn, particles are occasionally separated from the tool and adhere to the workpiece surface. This phenomenon is known as carbide cracking, and it promotes a sudden increase in shear stress during machining which leads to surface cavities owing to plucking. This process can generate surface cavities on the machined surface as well as the erosion of the workpiece material, creating even more surface quality issues [283, 284].

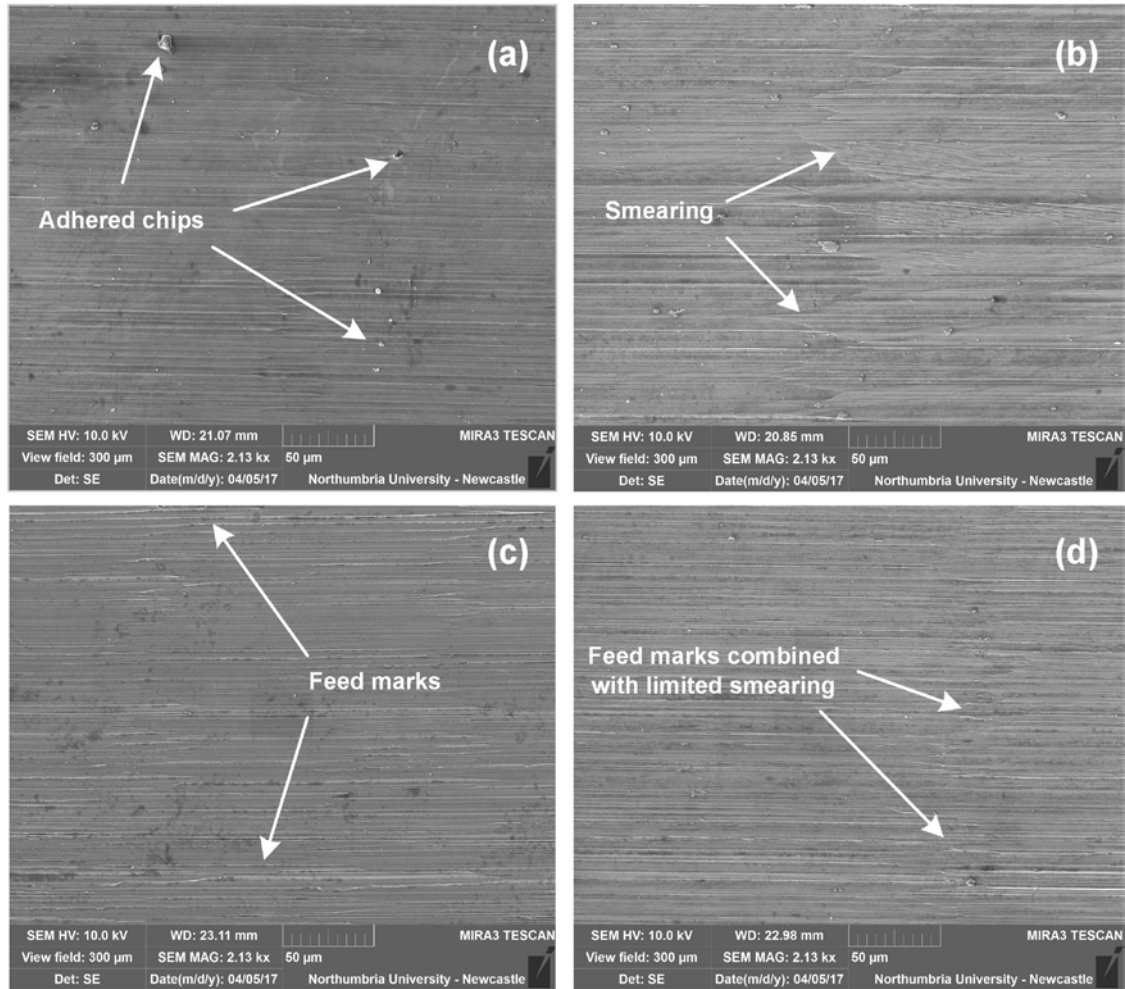


Fig. 5-35 SEM images of surface topography of Ti-6Al-4V machined parts under the conventional supply system at a cutting speed of 200 m/min and feed rates of 0.1 and 0.15 mm/rev respectively (a, b), and CUT-LIST at a cutting speed of 200 m/min and feed rates of 0.1 and 0.15 mm/rev respectively (c, d).

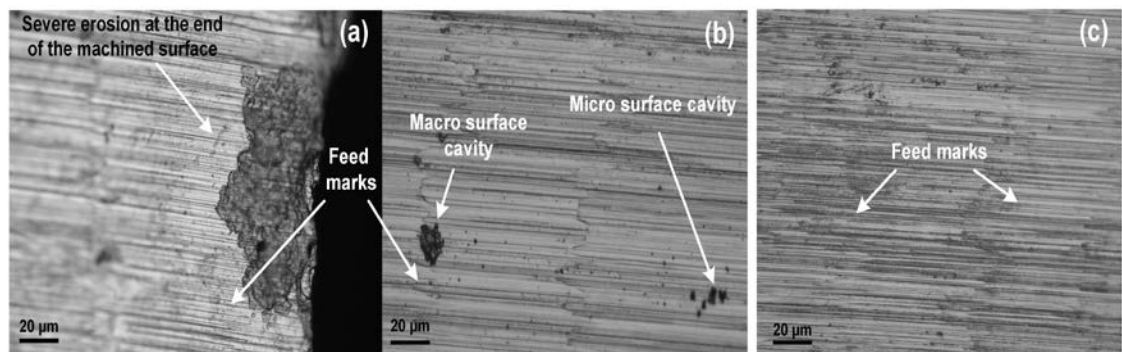


Fig. 5-36 Optical microscope image of the quality of the machined surface: (a, b) damage when using the conventional supply system; and (c) surface provided using CUT-LIST (all at cutting speed of 200 m/min and feed rate of 0.15 mm/rev)

5.5.1.6 Micro-hardness analysis

Fig. 5-37 and Fig. 5-38 show the micro-hardness results for both systems starting from 50 μm away from the machined surface at lower and higher cutting conditions. Both systems showed a notable increase in micro-hardness values at 100 μm below the machined surface and this was gradually reduced towards the interior of the specimen until reaching the base material's nominal hardness at around 349-350 HV_{100} . This could be attributed to the accumulated internal working hardening, induced by interrupted cutting during the milling operation. Additionally, heat generated from the cutting process probably acts as thermal energy softening the outer layer of the machined surface [76]. The thermal energy then moves down to a level of 100 μm beneath the machined surface and accumulates at this level to provide the cyclical heating/cooling which causes internal work hardening. Consequently, a hard sub-surface develops below the machined surface. The thermal energy beyond this region is gradually dissipated and thus at depths more than 100 μm beneath the machined surface the values of micro-hardness gradually decrease towards the base material's nominal hardness.

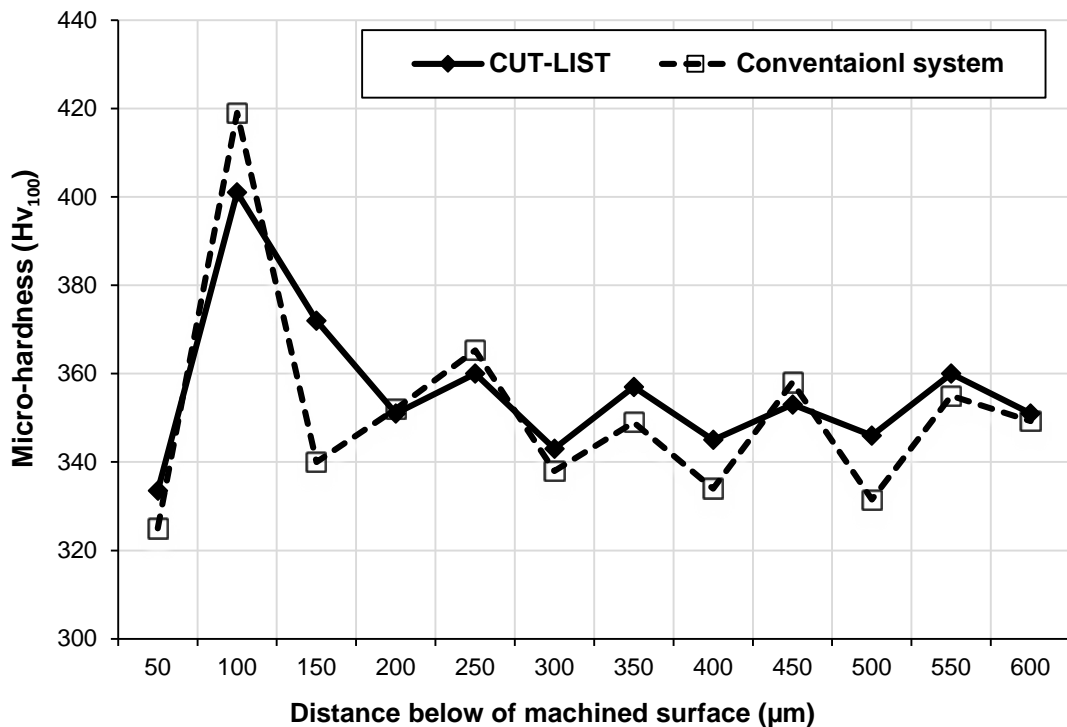


Fig. 5-37 Micro-hardness results below the machined surface at a cutting speed of 95 m/min and feed rate of 0.1 mm/rev for the two systems

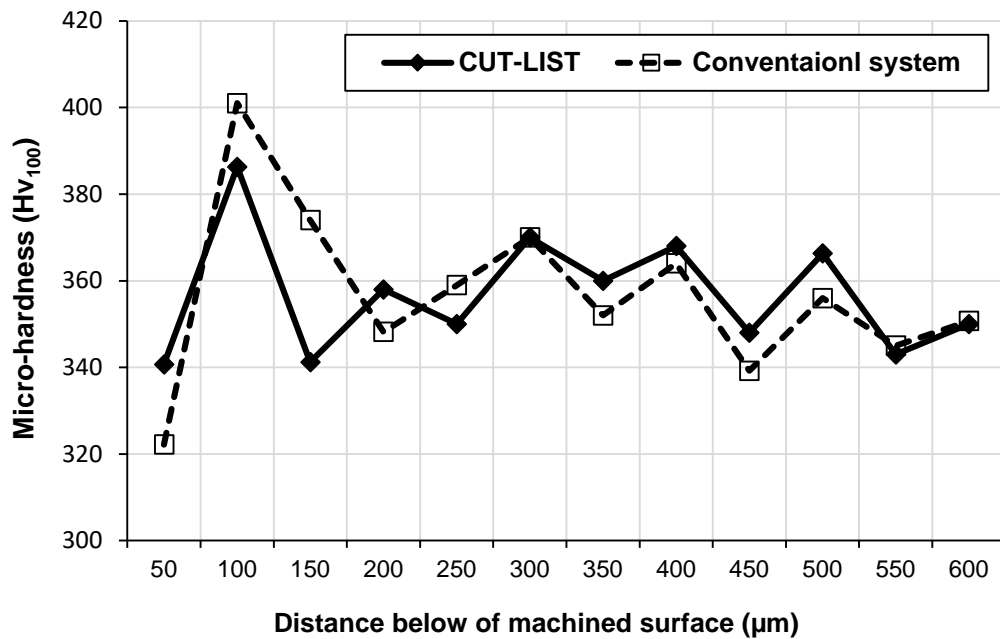


Fig. 5-38 Micro-hardness results beneath the machined surface at a cutting speed of 200 m/min and feed rate of 0.15 mm/rev for the two systems

Fig. 5-39 shows the maximum micro-hardness values recorded for the two systems at 100µm below the machined surfaces under various cutting conditions. Micro-hardness generally ranged between 401-386.3 HV₁₀₀ and 419-401 HV₁₀₀ for the CUT-LIST and conventional systems respectively. It was noticed that the micro-hardness values achieved by both systems were within the acceptable hardness range for titanium aerospace components (i.e. 419.6 HV max and 284.4 HV min) [78]. However, the new system induced lower softening at the outer layers of the machined surfaces by reducing micro-hardness up to ~ 5.5 % compared to the conventional system. This is possibly due to the impingement effect of a high-velocity jet (i.e. up to 10.83 m/s, see Table 3-6), which led to accelerating the effective heat transfer from the machining zone to the cutting fluid. Both systems exhibited a similar drop in micro-hardness values with increased cutting speed and feed rate. This can be attributed to the increase in cutting fluid flow rate associated with increased cutting energy (see Fig. 3-13) resulting in the minimisation of a hardening effect. Similar trends were observed in previous work [78] where increasing fluid pressure minimised the hardening effect during the turning of Ti-6Al-4V, and it was observed that the alteration in micro-hardness was significantly affected by cutting speed rather than feed rate when shoulder-milling Ti-6Al-4V using vegetable oil-based cutting fluid.

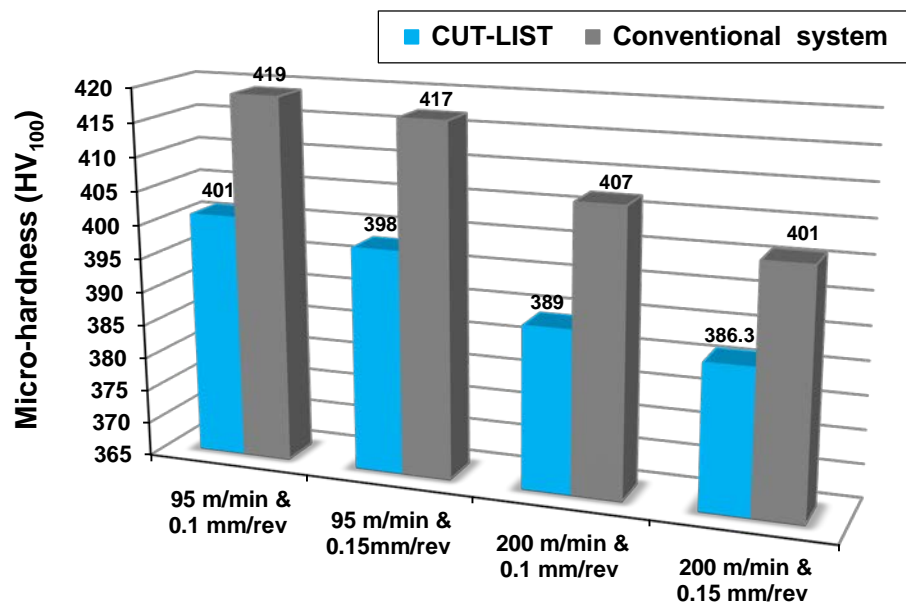


Fig. 5-39 Maximum micro-hardness versus cutting conditions at 100 μm beneath the machined surface for the two supply systems

5.5.1.7 Analysis of microstructure

Fig. 5-40 shows an SEM image of the typical microstructure of as-received Ti-6Al-4V alloy, whilst Fig. 5-41 presents the microstructure of post-machining samples. Grains near the undeformed surface, which will be used as the cutting surface, were similar to the rest of the grains in the material where typical equiaxed grains were observed, samples of which are shown in red dashed lines. Fig. 5-41 depicts a comparison of the microstructures obtained after using the two different fluid supply systems at different cutting speeds and a feed rate of 0.1 mm/rev. Unlike the pre-machined surfaces equiaxed grains, elongated grains were clearly observed near the machined surface at the lower cutting speed when both supply systems were used. At a cutting speed of 200 m/min, the average depths of the deformed layer were 2 μm and 5 μm for CUT-LIST and the conventional system respectively, as shown in Fig. 5-41b,d. Larger deformed layers 10 μm and 14 μm deep in average depth were obtained at a cutting speed of 95 m/min as seen in Fig. 5-41a,c. Heat generated at the lower cutting speed seems to have been more than enough to produce a highly plastic deformation layer, which was relatively deeper with the use of the conventional system. The area below the plastically deformed layer (within the dashed line in Fig. 5-41c) represents grains unaffected by machining. The

thinner deformed layer obtained when CUT-LIST was used is an indication of a reduction in thermal softening owing to better cooling capability, which usually leads to a reduction in compressive stresses and consequently fewer machined subsurface defects [283]. A thin white (recast) layer of $\sim 1\mu\text{m}$ was also observed when the conventional fluid supply system was used at a cutting speed of 95 m/min, while a thinner recast layer was only seen when the higher cutting speed was used on the new system (see Fig. 5-41b). Additionally, the intense plastic deformation induced by the cutting process, particularly when the conventional system was used, led to a thinning and elongation of the β phase of the Ti-6Al-4V machined surface [75], as seen in Fig. 5-42. This implies that plastic deformation was greater at low cutting speeds. This behaviour is ascribed to the increase in the cutting fluid flow rate associated with the increase in cutting speed, which also improved the fluid's capacity to dissipate heat from the machining zone resulting in less microstructural change and subsurface damage. These findings are in agreement with previous observations [72]. Seemingly, when cutting titanium at higher speeds with ample cutting fluid, its strain rate sensitivity dominates the softening effect, resulting in less subsurface damage [24, 280]. Only for a few micrometres below the machined surface does titanium exhibit limited thermal softening, which in turn results in a reduction in micro-hardness below the machined surface. Because there was sufficient coolant and enhanced penetration of the cutting fluid using CUT-LIST, only limited thermal softening occurred below the machined surface. This resulted in a marginal reduction in micro-hardness of up to $\sim 5.5\%$ compared to the conventional cutting fluid supply system, as mentioned earlier.

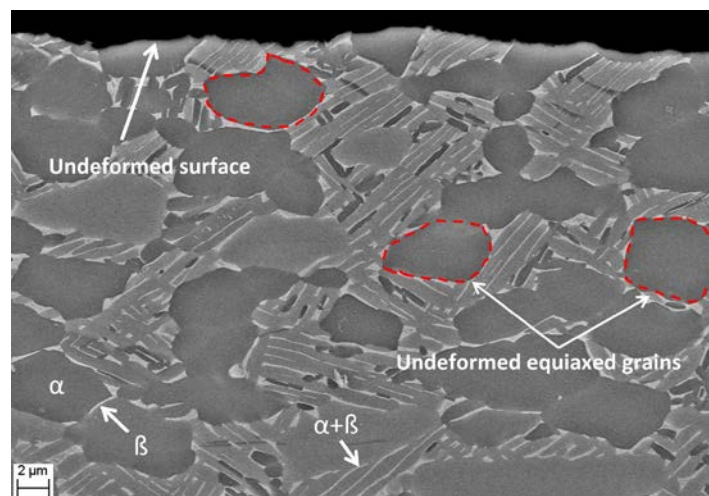


Fig. 5-40 Typical microstructure of Ti-6Al-4V (as-received material)

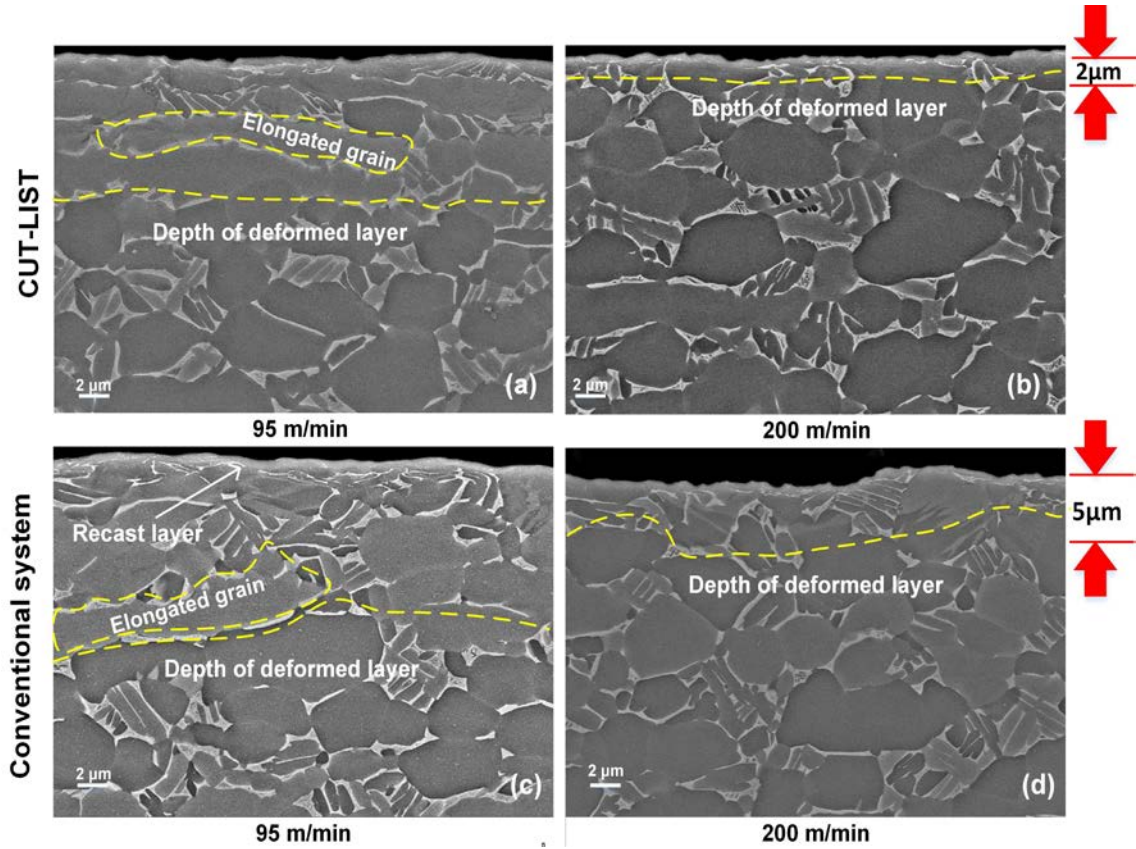


Fig. 5-41 SEM images of surface microstructure of machined parts at 0.1 mm/rev feed rate using CUT-LIST at cutting speeds of (a, b) 95 and 200 m/min respectively and the conventional supply system at cutting speeds of (c, d) 95 and 200 m/min respectively.

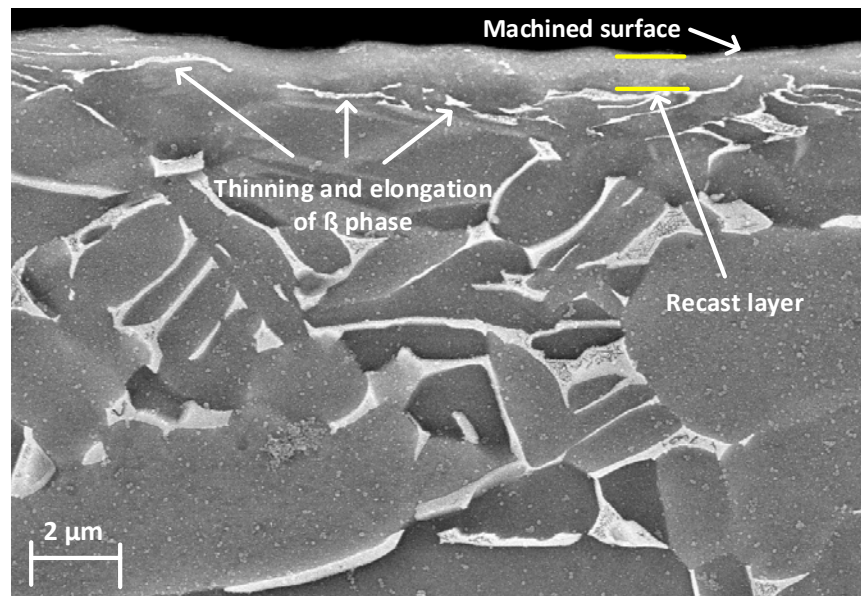


Fig. 5-42 SEM image of thinning and elongation of β phase (conventional system, 95 m/min cutting speed and 0.1 mm/rev feed rate).

5.5.1.8 Chip formation analysis

Chips produced at the beginning of machining trials were coloured silver-rich. They were thick at the beginning of the cut and became thinner at the end, as shown in Fig. 5-43a. This was due to the use of the climb or down-milling process, which is more favourable for titanium milling [81] (see Fig. 5-43b). Fig. 5-44 shows SEM photographs of segmented chips formed by the supply systems. Generally, both systems produced similarly desirable nearly curled/C-shape discontinuous segmented chips, particularly at lower cutting speeds, while a nearly flat discontinuous segmented chip shape was generated at higher speeds. In addition, both systems produced chips with different sizes at lower and higher cutting speeds. At lower cutting temperatures, the chips cannot promote the curl due to their increased hardness and lower ductility [285]. This implies that chip morphology is affected by changes in the volume of cutting fluid delivered into the machining zone as well as changes in cutting speed. Earlier studies also agree [1, 279] that chip morphology relies heavily on changes in cutting parameters and the thermal and physical properties of cutting fluids as well as the quantities supplied. Additionally, with highly deformed waves on the chips' free surface, chip segmentation occurred initially at the lower cutting speed of 95 m/min, which agrees with findings in the literature [286, 287]. However, Liu et al. [288] and Daymi et al. [289] reported that chip segmentation was only observed at cutting speeds ≥ 125 m/min during the machining of Ti-6Al-4V. Relatively irregular (aperiodic) waved-shape segments were seen at 95 m/min whilst partially highly deformed regular (i.e., periodic) waved-shape segments were observed at the higher cutting speed of 200 m/min (see Fig. 5-45). This can be attributed to thermo-plastic instability within the primary shear zone [290].

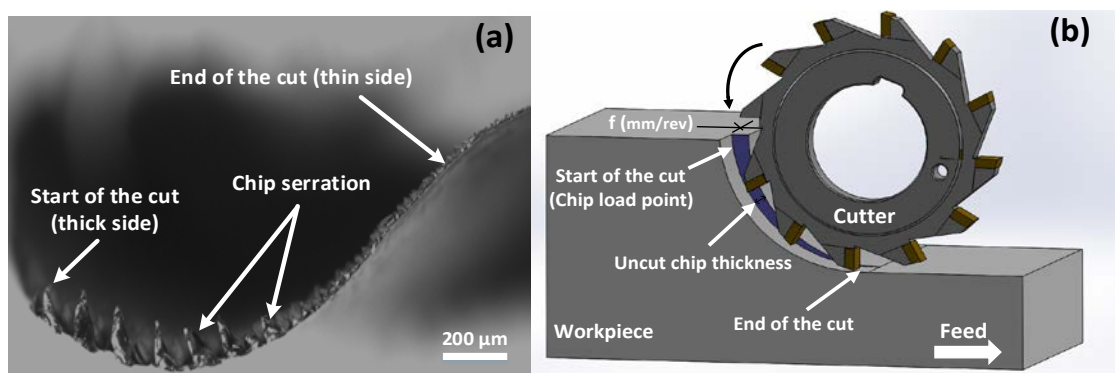


Fig. 5-43 (a) Image of the chip produced; (b) schematic view of the down-milling process

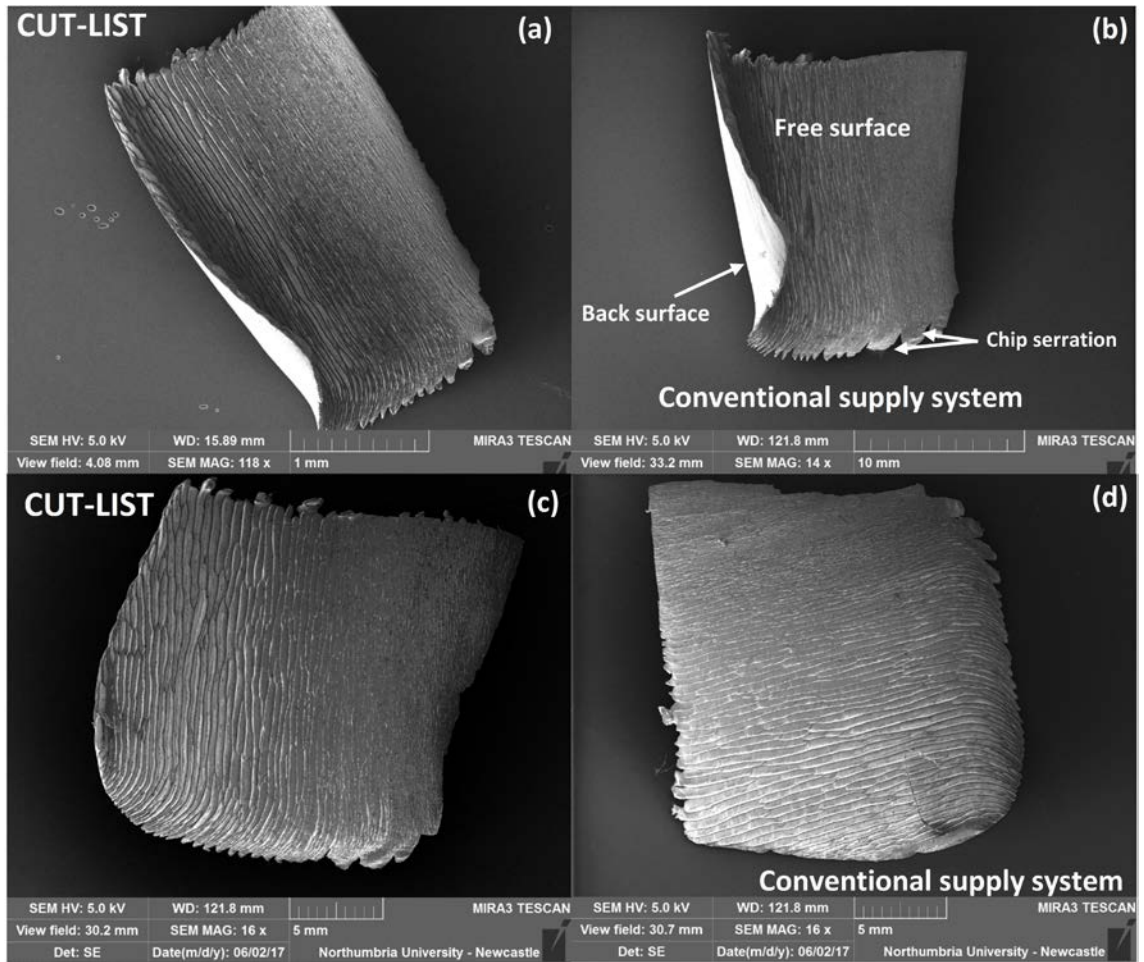


Fig. 5-44 Discontinuous/segmented chips formed at (a, b) 95m/min and (c, d) 200 m/min.

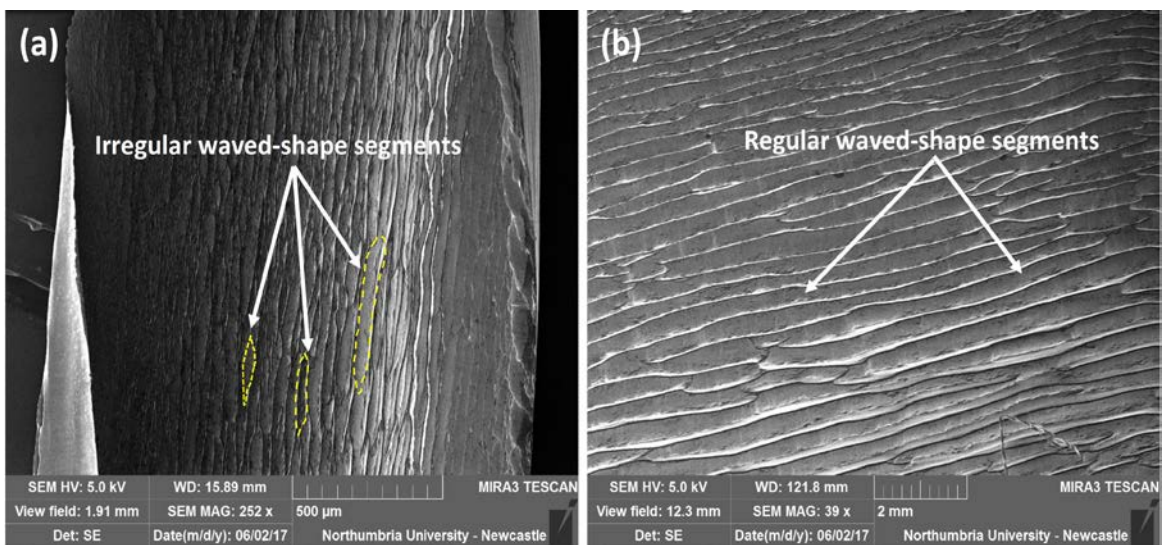


Fig. 5-45 Effect of cutting speed on chip morphology of the free surfaces for CUT-LIST at: (a) 95 m/min and (b) 200 m/min

The use of the conventional supply system also resulted in larger serrations and more crack propagation at the end of the chip-free surface at the lower cutting speed, with a crack depth of up to 200 μm compared with the new system at $\sim 110 \mu\text{m}$ as seen in Fig. 5-46. This is due to the large shearing action caused by the inability of the conventional system to effectively deliver a sufficient amount of cutting fluid into the machining zone. Similar trends have been recorded previously [164], where it was concluded that conventional flood cooling induces much serration at the end of the chip-free surface during the milling process owing to its inferior fluid penetrability compared with an MQL supply mode. Furthermore, these results are in agreement with the theory that crack propagation inside the primary shear zone is the main cause of chip serration at low cutting speeds [81]. At lower cutting speeds, the ductility of chip material is decreased owing to the lower cutting temperature, thus promoting crack initiation in the shear zone [291]. Fig. 5-47 shows the average crack depth for chips produced by both systems and under various cutting conditions. Five different chips were measured and average values were computed each time. Error bars are also shown in Fig. 5-47 with a maximum deviation of $2\mu\text{m}$ (1%). Additionally, chips generated by both systems have a similarly smooth back surface, which is the surface in contact with the cutting tool rake face. Plastic deformation of the back surface is constrained by the rake face, and consequently it encounters high contact pressure and frictional forces as the chip slides over the cutting tool rake face. The combined effects of frictional forces, high contact pressure and high temperature cause the back surface to be smooth and relatively shiny [292].

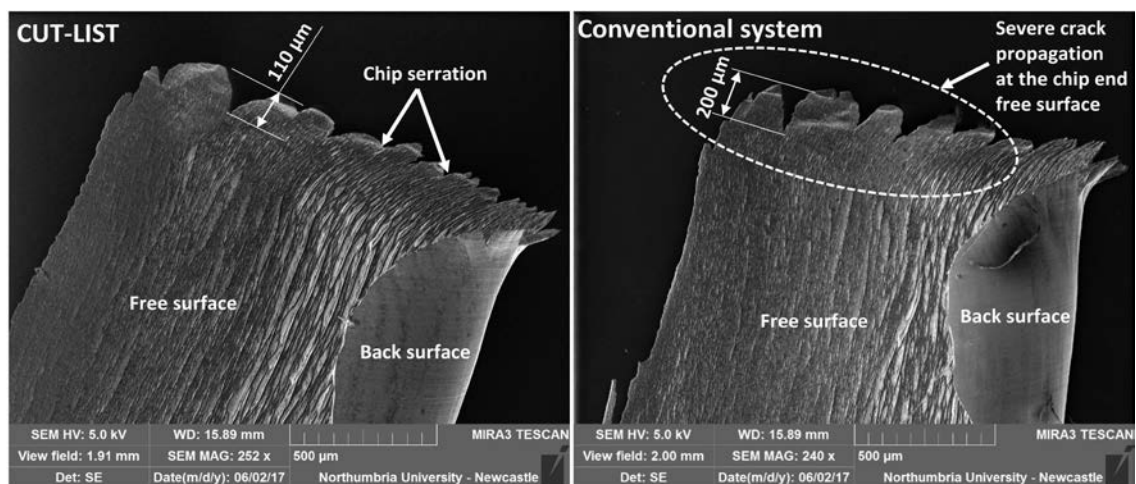


Fig. 5-46 SEM photographs showing the effect of the two supply systems on the morphology of the chip back surface and end free surface at low cutting conditions (95 m/min and 0.1 mm/rev)

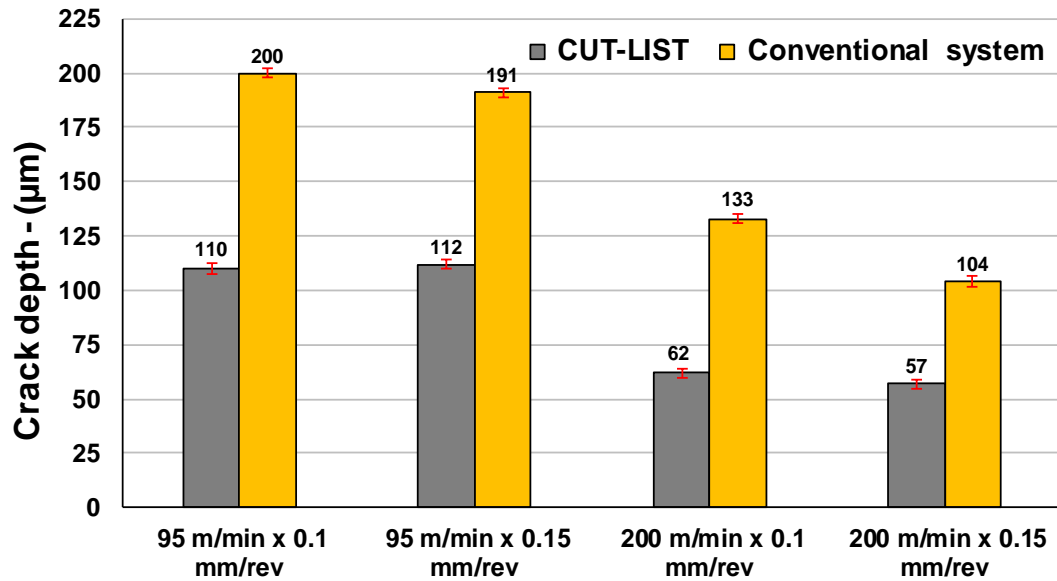


Fig. 5-47 Measured crack depth for different chips at various cutting conditions

Cutting speed has also affected the segmentation characteristics of the chips produced. The average distance between segments is in the range 0.45-0.5 mm and 0.3-0.35 mm for cutting speeds of 95 m/min and 200 m/min respectively, as seen in Fig. 5-48. Similar trends have also been reported during the machining of Ti-6Al-4V, where the segmentation distance decreases with increasing cutting speed [79, 287]. This phenomenon can be explained by the fact that, as the cutting speed increases, the strain needed to overcome the bonding in materials and to promote a crack decreases. Consequently, smaller segmentation distances are formed [293].

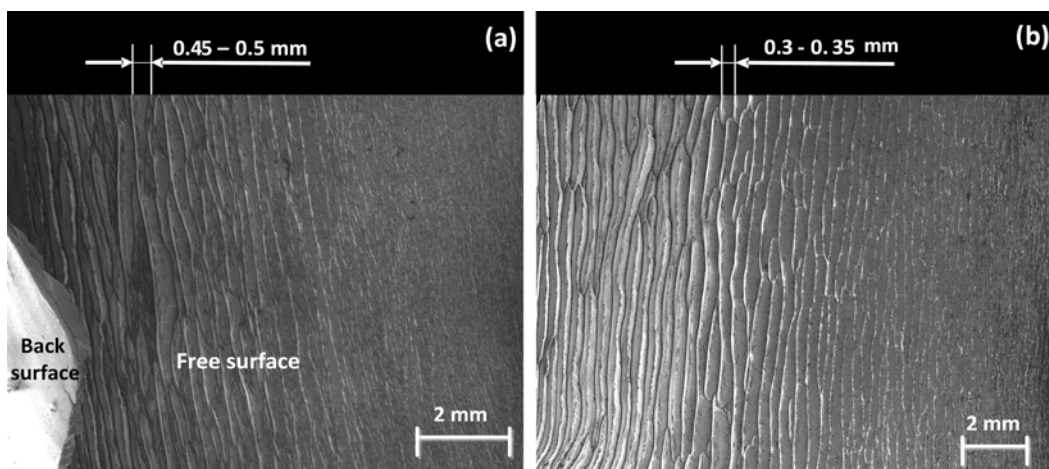


Fig. 5-48 SEM images showing the effect of cutting speed on chip morphology of free surfaces for the new system at cutting speeds of: (a) 50 m/min, and (b) 200 m/min

Fig. 5-49 shows the measured average distance between serrated segments for the two systems at various cutting conditions. A larger variation was obtained for the conventional system (0.0156 mm) compared with 0.014 mm for CUT-LIST as shown in the error bars in Fig. 5-49.

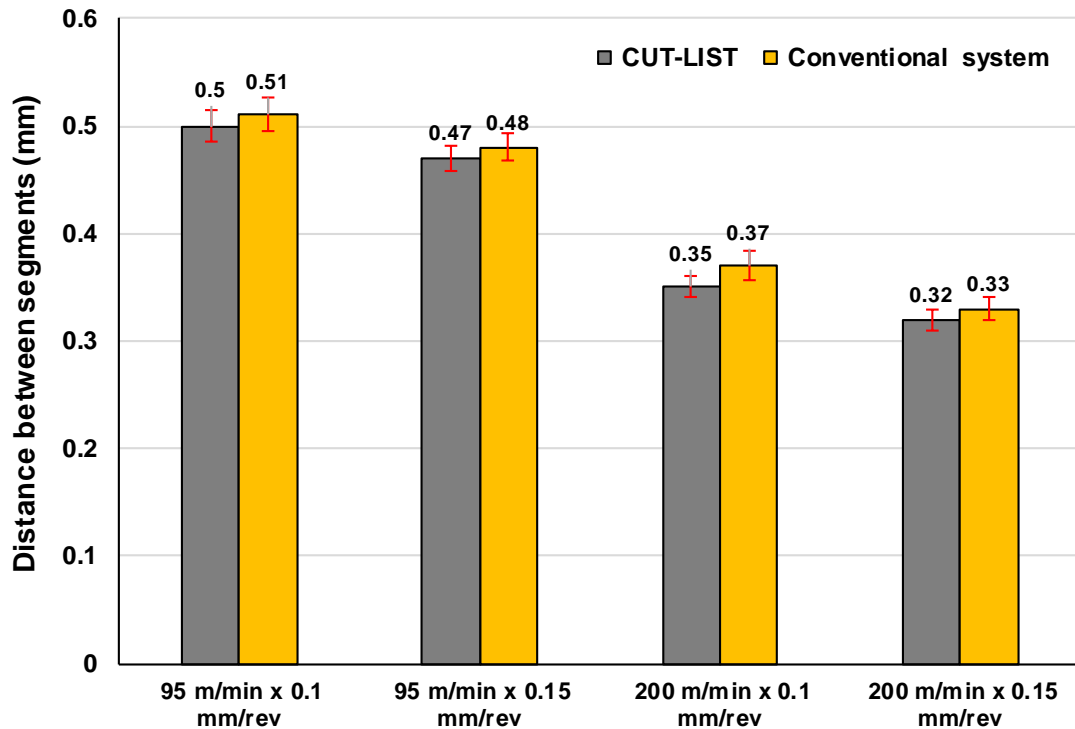


Fig. 5-49 Measured average distance between serrated segments for the two systems at various cutting conditions

Fig. 5-50 shows the saw-tooth geometry of the serrated chips generated by the new system at a cutting speed of 200 m/min and feed rate of 0.1 mm/rev. The maximum saw-tooth height (h_{\max}) of the serrated chips at various cutting conditions was measured using optical images and the results are presented in Fig. 5-51. Similar variations in h_{\max} measurements were seen in Fig. 5-51 (error bars) except at 95 m/min and 0.15 mm/rev when CUT-LIST values varied by only 0.0017 mm compared with 0.0089 mm for the conventional system. It is observed that h_{\max} increases with cutting speed and feed rate for both supply systems, with a minimum of 0.117 mm when CUT-LIST was used. This is also in line with the above conclusion that the use of higher cutting speeds and feed rates can lead to the production of more regular and periodical serration/segmentation

profiles in chips. These findings also accord with the conclusion that the transition from aperiodic to periodic saw-tooth chip formation is more affected by increasing cutting speed and feed rate [81, 290]. Additionally, the saw-tooth height (h_{\max}) for chips produced using the new system was relatively lower compared with those produced by the conventional supply system. This could be attributed to the better fluid accessibility into the cutting interface provided by the new system owing to a higher fluid velocity up to 10.83 m/s (see, Table 3-6), which inevitably leads to the promotion of a short shear area resulting in chips with low saw-tooth height which are also known as thin chips [280, 294]. Thin chips are more favourable in high quality machining as they can break easily and thus clogging in the tool cutting area is minimised [272]. In tandem with these observations, thin chips can also be generated at a larger shear angle (ϕ) due to less contact area between the tool's rake face and the workpiece material. Hence, shear angles caused by both supply systems are discussed in detail in the next section.

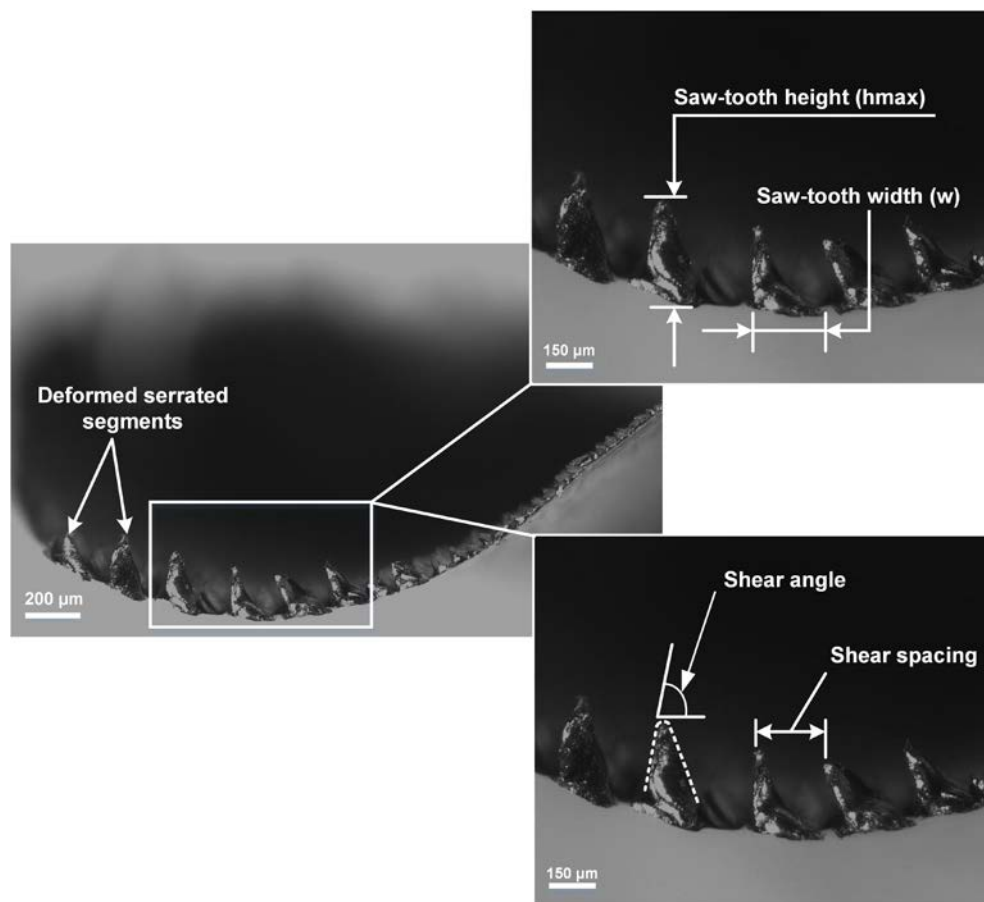


Fig. 5-50 Side view of a deformed chip showing the serration of chips produced using CUT-LIST at 200 m/min and 0.1 mm/rev

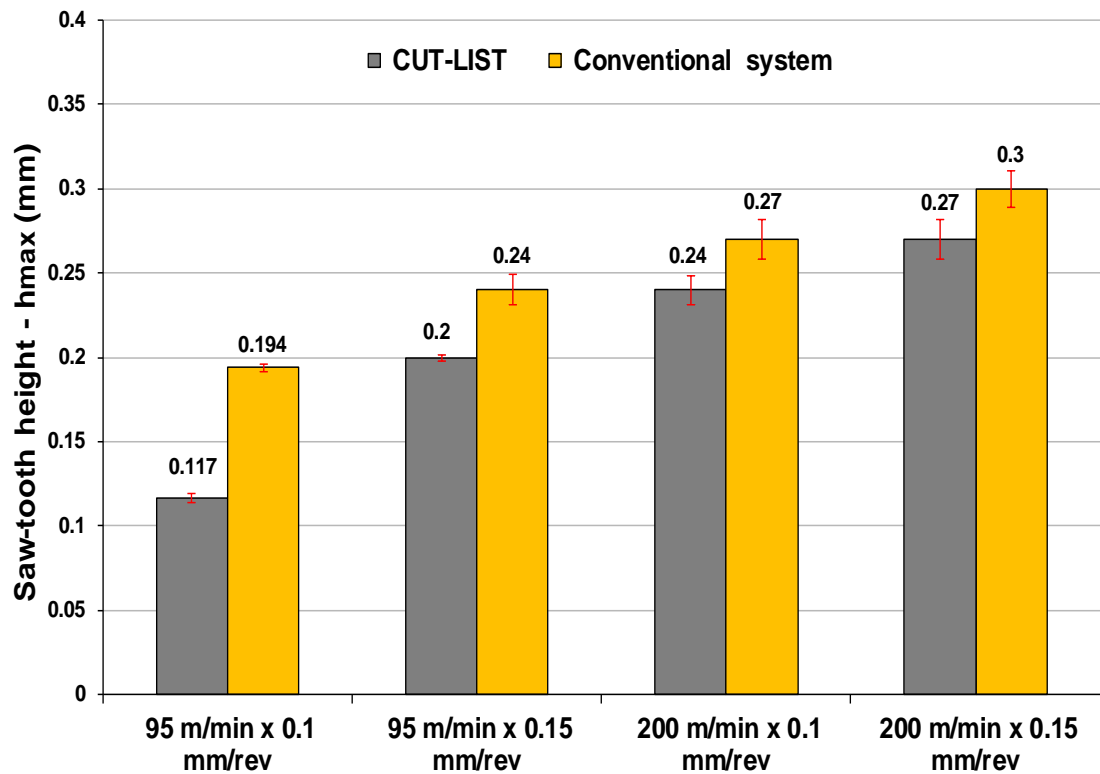


Fig. 5-51 Saw-tooth height at various cutting conditions for the two supply systems

On the other hand, results for the saw-tooth width (w) of segmented chips are presented in Fig. 5-52. Both supply systems showed an increase in saw-tooth width with higher cutting speeds and feed rates. This is likely to be due to the competition between thermal softening owing to increased cutting speed and feed rate and the increase in cutting fluid volumes. This helped to reduce shear formation, thus offering larger shear spacing and an increase in segment width. The width of segmented chips was also found to increase, which helped to promote less shear formation during the ultrasonic-assisted turning of Ti-6Al-4V [295]. However, the use of CUT-LIST resulted in marginally higher segment width, owing to its cooling potency. Error bars showed that high measurement variation was observed at 200 m/min and 0.15 mm/rev, at 0.014 and 0.01mm for CUT-LIST and the conventional systems respectively.

Additionally, chip segmentation frequency is a crucial parameter in quantifying chip segmentation. In machining, it is observed that, due to the formation of shear bands, the forces acting on the cutting tool decline. This promotes a fluctuation in the cutting forces, which in turn introduces vibrations into the tool-workpiece region [28]. In an attempt to

determine variations in chip segmentation frequency with respect to cutting speed, the following equation (5.1) was utilised:

$$f_{chip} = v/w \quad [295] \quad (5.1)$$

where f_{chip} is the frequency of segmentation in Hz, v is cutting speed in m/s and w is the saw-tooth width of the segment in m. Values for f_{chip} are presented in Fig. 5-53, showing that segmentation frequency clearly increases with cutting speed and decreases with increased feed rate. This tendency is in agreement with findings in the literature [84, 296, 297]. In addition, all segment frequencies recorded for both supply systems were within the acceptable range of 4-22 kHz for $\alpha+\beta$ titanium alloy (Ti-6Al-4V) [296]. The use of CUT-LIST resulted in some reduction in values of f_{chip} at all cutting conditions, with a minimum obtained at 95 m/min and 0.15 mm/rev. Larger variations in the data represented in error bars were seen at 200 m/min and 0.15 mm/rev, at 0.842 and 0.721 kHz for CUT-LIST and the conventional supply system respectively.

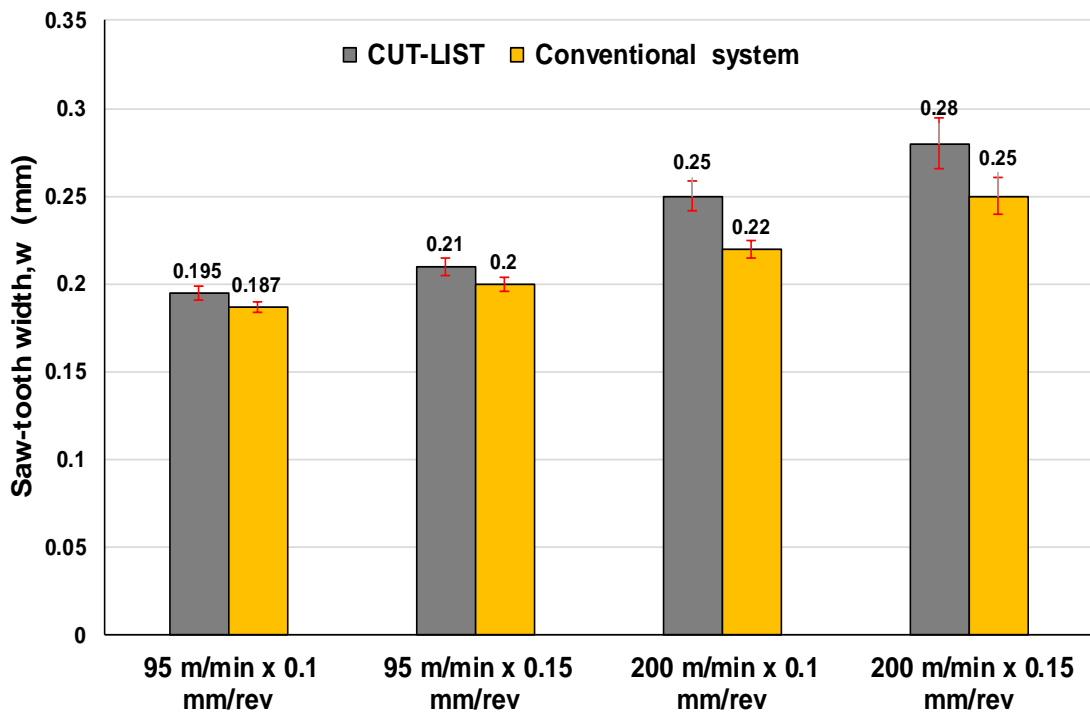


Fig. 5-52 Saw-tooth width at various cutting conditions for the two systems

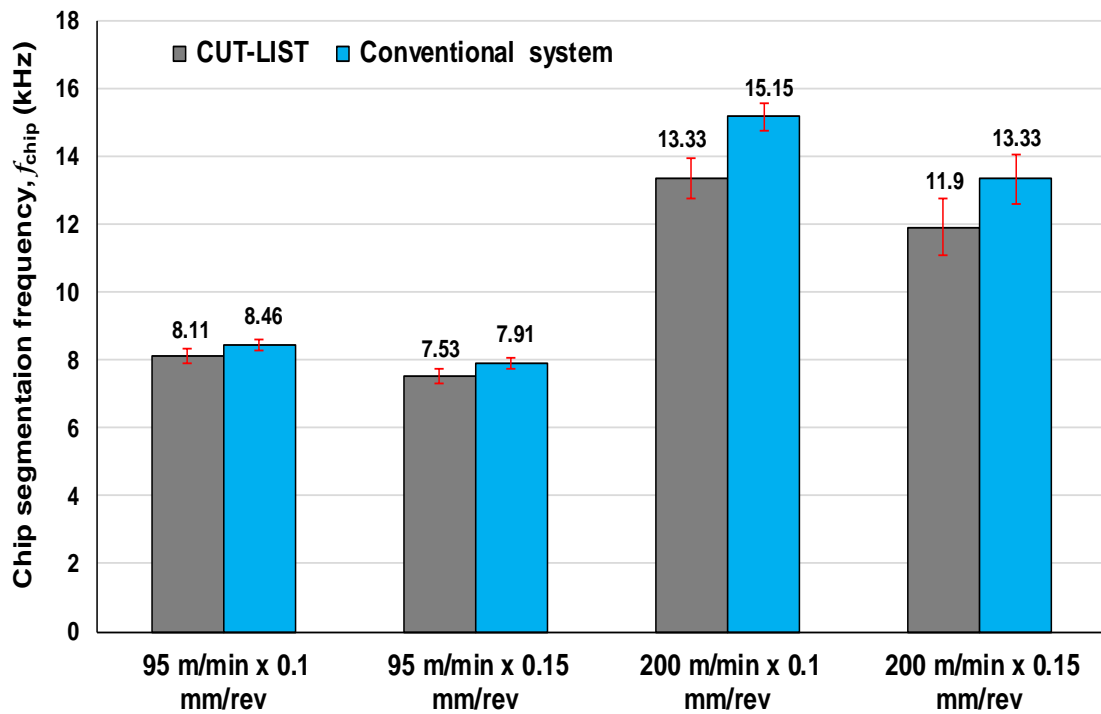


Fig. 5-53 Frequency of segmentation at various cutting conditions for the two systems

Additionally, shearing occurs over a very narrow area of the primary shear zone inclined at the so-called shear angle (ϕ). The shear angle is strongly affected by cutting speed where a higher cutting speed can cause a small contact area on the rake face, resulting in larger angle [298]. Higher shear angles lead to less deformation along the shear plane, thus resulting in lower cutting forces [272]. The effects of different supply systems and cutting conditions on shear angle are shown in Fig. 5-54. Both systems showed increases in shear angle with increasing cutting speed. However, increases of 29.16 % and 32.2 % in shear angle were observed with the use of the new system at lower and higher cutting speeds respectively. Similar trends were reported by Patil et al. [272] where the shear angles caused by high pressure cooling (HPC) were larger than those from dry cutting. The disparity between larger shear angles caused by the new system and lower angles produced by the conventional system can be attributed to the potency of the new supply system, where the cutting fluid penetrates effectively into the machining zone and forms a boundary of oil film in the tool-workpiece interface, resulting in lower contact pressure and frictional force. These results can also be explained in terms of the substantial reduction in cutting force (up to 16.41%) when CUT-LIST was employed compared with the use of conventional system as described earlier in section 5.5.1.1.

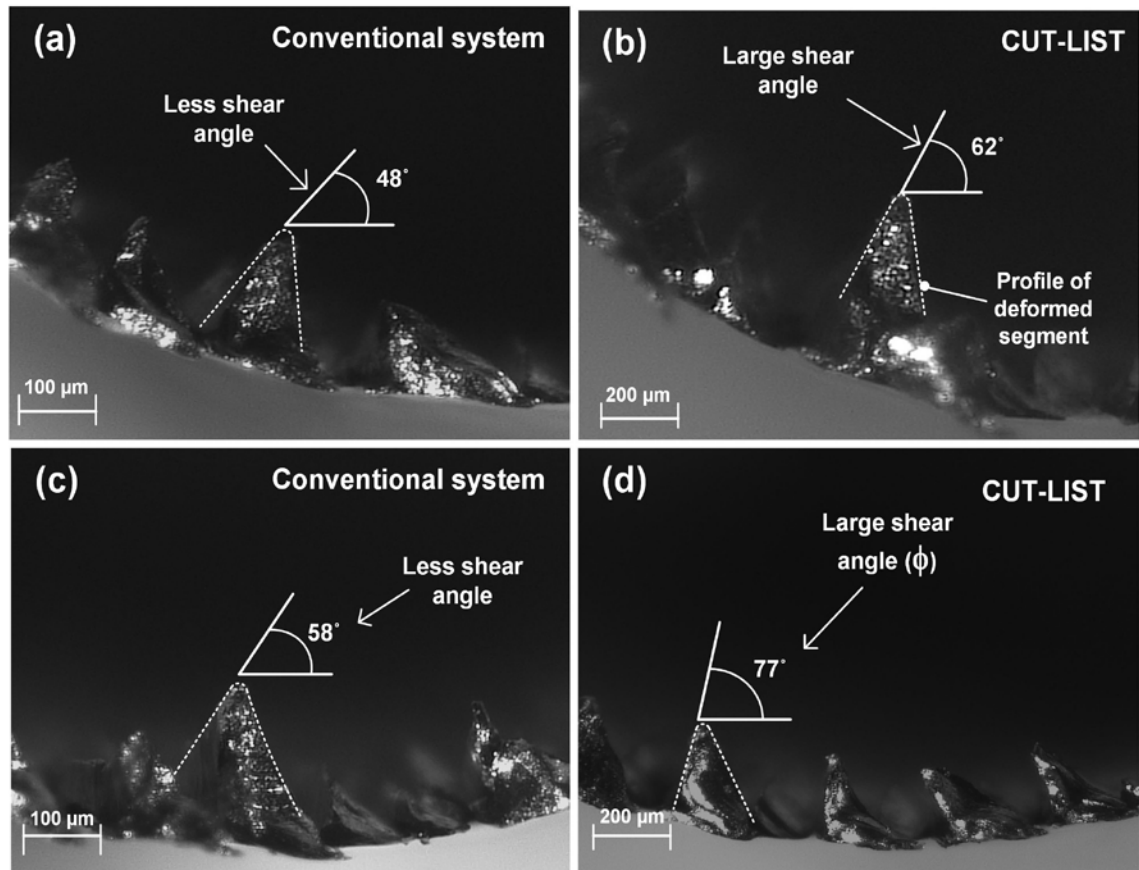


Fig. 5-54 Shear angle (ϕ) observed under both systems at feed rate of 0.15 mm/rev and cutting speeds of 95 m/min (a, b) and 200 m/min (c, d)

5.5.2 Analysis and optimisation of the new system parameters

Following the comparative study performed in the previous section in evaluating the new system against a conventional flood system, which has revealed that the CUT-LIST can possess many advantages. Hence, this section aims to provide a critical analysis of the new system parameters, such as cutting speed, feed rate, nozzle position and angle, and impinging distance, as well as process optimisation. The key process indicators measured were cutting force, workpiece temperature, tool flank wear, burr height and average surface roughness (R_a). Additionally, interaction effect plots of the process parameters on all responses were also presented. A detailed analysis concerning the effect of nozzle position and angle as well as impinging distance on the process followed by the results of repeatability tests are also provided at the end of the study.

5.5.2.1 Cutting force

Fig. 5-55 shows the effect of process variables on cutting force. The best settings to minimise cutting forces when shoulder milling Ti-6Al-4V were found to be 95 m/min cutting speed, 0.1 mm/rev feed rate and nozzle position at 15° in the feed direction, 45° against feed direction, and 75 mm impinging distance. ANOVA results (Table 5-8) showed that the feed rate has the major contribution (47.64%) in minimising the cutting force. This is due to the high correlation between cutting force and cutting area (which uncut chip thickness is part of) and thus with feed rate. It was also noticed that cutting force increased with higher cutting speed. This agrees with the assumption that more energy and hence higher cutting force is required to remove a higher volume of material [36, 299], although this is in disagreement with the finding that higher cutting speeds may cause material softening and thus lower cutting forces when machining steel alloys, as described by Veiga et al. [1]. This could be attributed to the lower strain hardening coefficient of steel (<0.1) compared to titanium (>0.3) [300].

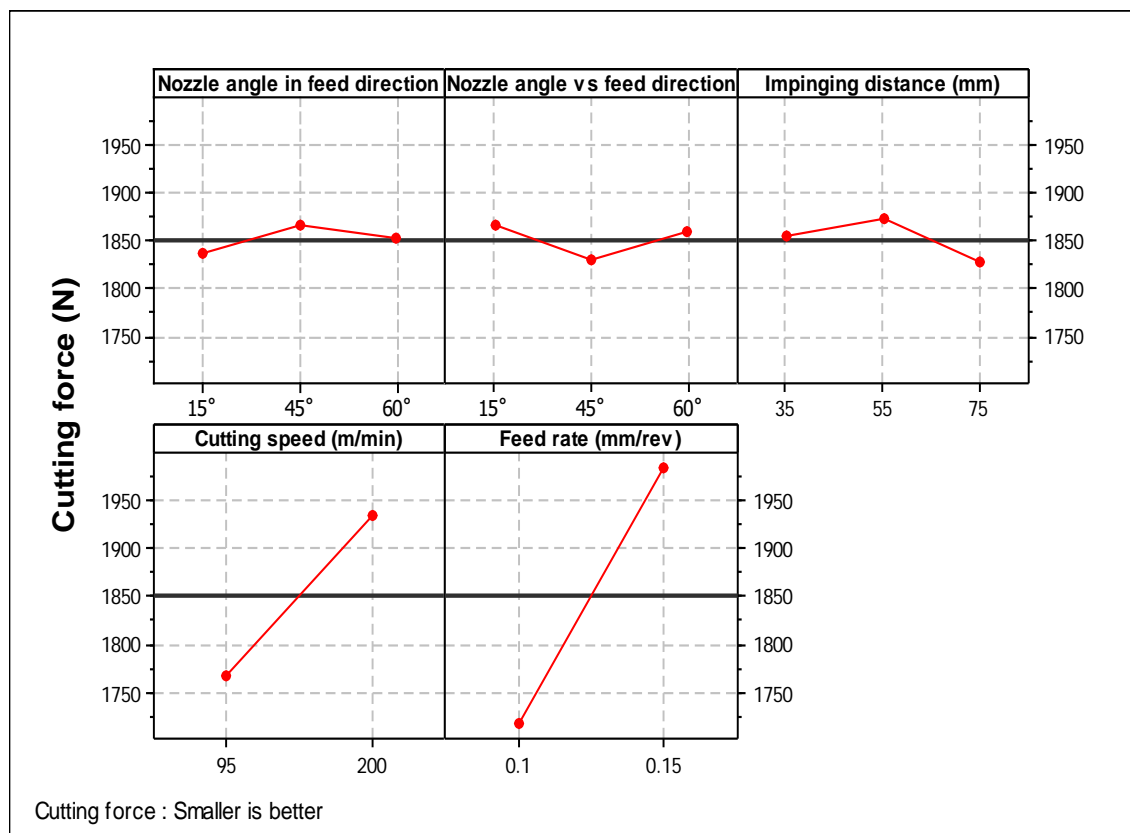


Fig. 5-55 Main effect analysis for cutting force

Additionally, the ANOVA analysis also suggested that nozzle positions and angles and impinging distance are statistically insignificant and had only a limited impact on cutting force. Fig. 5-56 shows the interaction plot for cutting force. It can be seen that there are some mutual interactions among all factors evaluated except between feed rate and cutting speed, which could be the reason for the relatively high error observed in the ANOVA results. In addition, the parallel trends of the lines (shown at the top right of the figure) clearly show a relatively low degree of interaction between feed rate and nozzle positions and between nozzle positions and cutting speed.

Table 5-8 ANOVA results for cutting force

Source	DF	SS	MSS	F	P	PCR
Nozzle angle in feed direction (degree)	2	16525	8263	0.66	0.520	0.41%
Nozzle angle vs feed direction (degree)	2	28991	14495	1.15	0.320	0.72%
Impinging distance(mm)	2	37345	18672	1.49	0.231	0.93%
Cutting speed (m/min)	1	764510	764510	60.86	0.0*	19.14%
Feed rate (mm/rev)	1	1903072	1903072	151.49	0.0*	47.64%
Error	99	1243674	12562			31.13%
Total	107	3994117				

S= 112.082 R-Sq = 68.86% R-Sq (adj) = 66.35%

DF = Degree of freedom * Significant at the 5 % level and confidence level of 95%
 SS = Sum of squares P = Probability
 F= F- test value

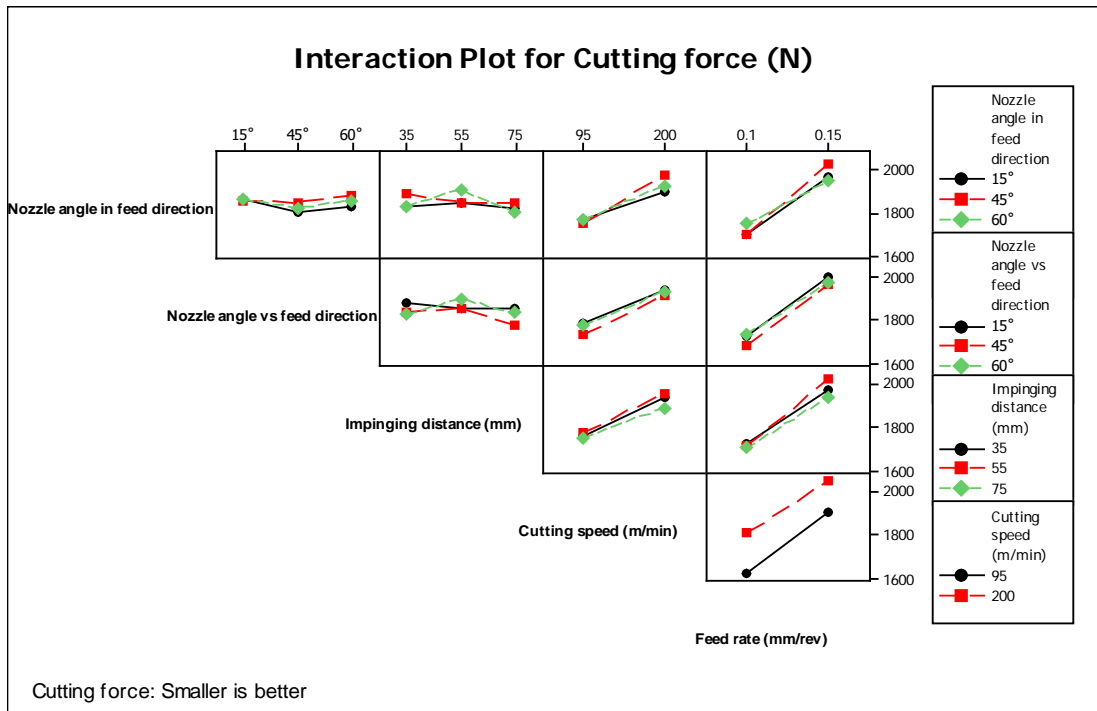


Fig. 5-56 Interaction effects of process parameters on cutting force

5.5.2.2 Workpiece temperature analysis

Fig. 5-57 presents the variation in the effects on average workpiece temperatures of all process variables evaluated in this research. Mean values of average workpiece temperature ranged between 23.5 and 27.5 °C. This is probably because only a small proportion (~20%) of the heat generated when cutting titanium is transferred into the workpiece and chip while 80% of the heat is expected to be transferred to the cutting tool [48]. In addition, the impinging fluid jet on targeted heat-affected zones helped to dissipate more than 30% of the heat generated during the cutting process [279]. Also, the decrease in workpiece temperature with higher cutting speeds can be attributed to the increase in cutting fluid flow rate associated with increasing cutting power (in accordance with increasing cutting conditions, see Fig. 3-13). Increasing the flow rate resulted in improving the cooling capacity of the cutting fluids, which assisted in transferring more heat from the workpiece to the cutting fluid, hence giving a reduction in workpiece temperature. Understandably, the optimal (low) workpiece temperature was recorded at the higher cutting condition, while nozzle position at an angle of 15° in the feed direction and 45°/60° against the feed direction and an impinging distance of 55 mm assisted to minimise workpiece temperature. Possibly these positions helped fluid to access into the machining zone effectively as described in detail in sections 5.5.2.6 and 5.5.2.7.

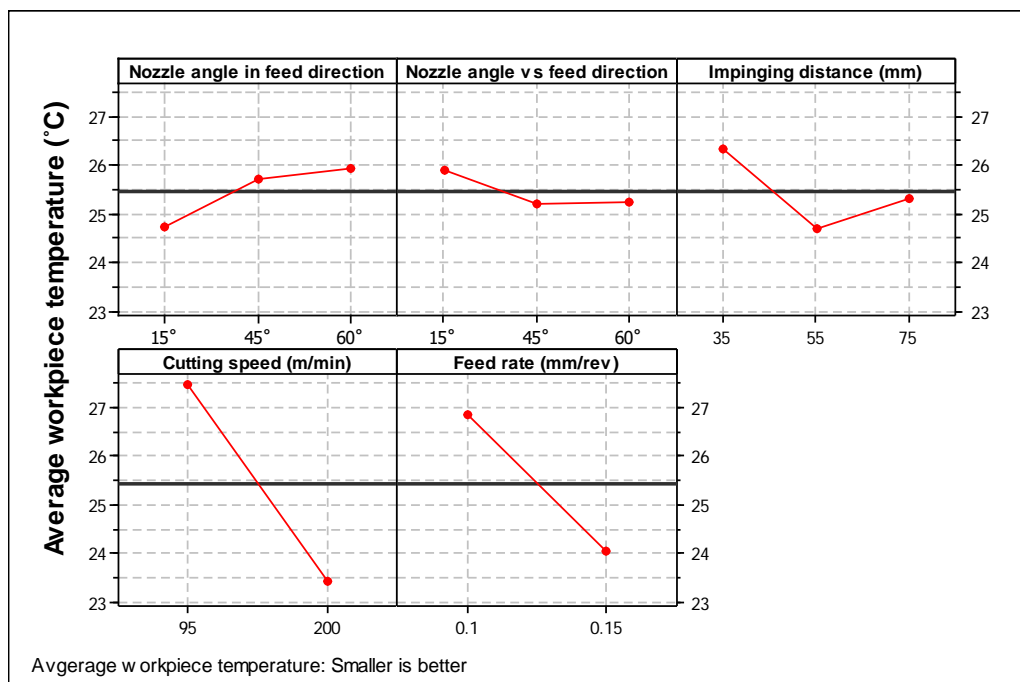


Fig. 5-57 Main effects analysis for workpiece temperature

Additionally, cutting speed is the most influential factor (46.50%) affecting workpiece temperature (see Table 5-9), while feed rate, impinging distance and nozzle angle position in the feed direction showed considerable effects on average workpiece temperature. Fig. 5-58 shows the interaction plot for average workpiece temperature, and obviously no sizeable interactions were observed between the factors studied. However, limited interactions (due to the lower error in ANOVA results) were observed, particularly between nozzle positions (in the feed and against feed directions) and impinging distance.

Table 5-9 ANOVA results for workpiece temperature

Source	DF	SS	MSS	F	P	PCR
Nozzle angle in feed direction (degree)	2	30.805	15.403	7.74	0.001*	3.29 %
Nozzle angle vs feed direction (degree)	2	11.172	5.586	2.811	0.05*	1.19%
Impinging distance(mm)	2	48.751	24.376	12.25	0.0*	5.20%
Cutting speed (m/min)	1	435.206	435.206	218.70	0.0*	46.50%
Feed rate (mm/rev)	1	212.801	212.801	106.94	0.0*	22.74%
Error	99	197.008	1.990			21.05%
Total	107	935.744				

S= 1.410 R-Sq = 78.95% R-Sq (adj) = 77.25%

DF = Degree of freedom * Significant at the 5 % level and confidence level of 95%
 SS = Sum of squares P = Probability
 F= F- test value

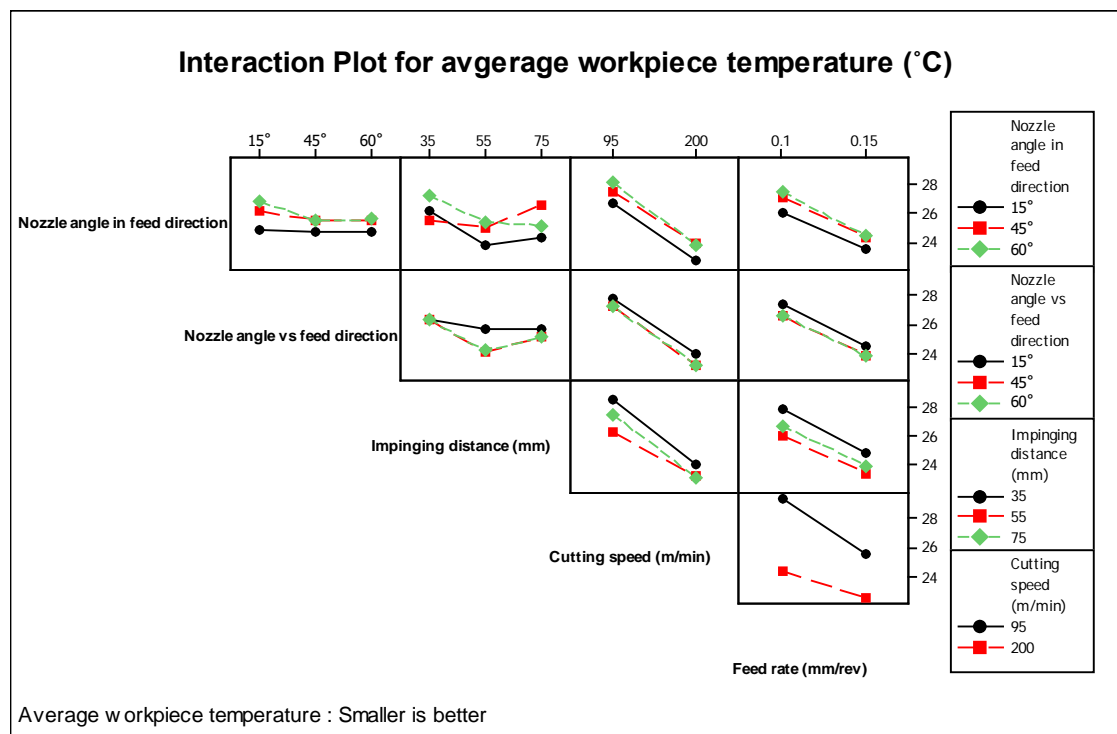


Fig. 5-58 Interaction effects of process parameters on workpiece temperature

5.5.2.3 Tool wear analysis

Fig. 5-59 presents the effects of control factors on the mean values of tool flank wear (VB). Generally, tool wear mean values ranged between 38 μm and 128 μm . A cutting speed of 95 m/min, feed rate of 0.15 mm/rev and nozzle location at 15° in the feed direction and 45° against feed direction and an impinging distance of 75 mm can be selected as the optimal cutting conditions for controlling tool wear. However, the use of the controlled cutting fluid through the developed CUT-LIST system meant that tool flank wear increased rapidly with increased cutting speed owing to the rise in heat generated. The heat generated at the tool edge would have softened the insert edge and reduced tool yield strength, causing tool flank wear to consequently increase [192]. The ANOVA (Table 5-10) results indicate that cutting speed has statistically a substantial impact on minimising VB, with a PCR of 59.23%, while tool wear values seem to be independent of feed rate, nozzle positions, and impinging distance. It can also be concluded that the traditional understanding that cutting speed is the dominant variable affecting tool wear is still applicable to the CUT-LIST cutting fluid supply system.

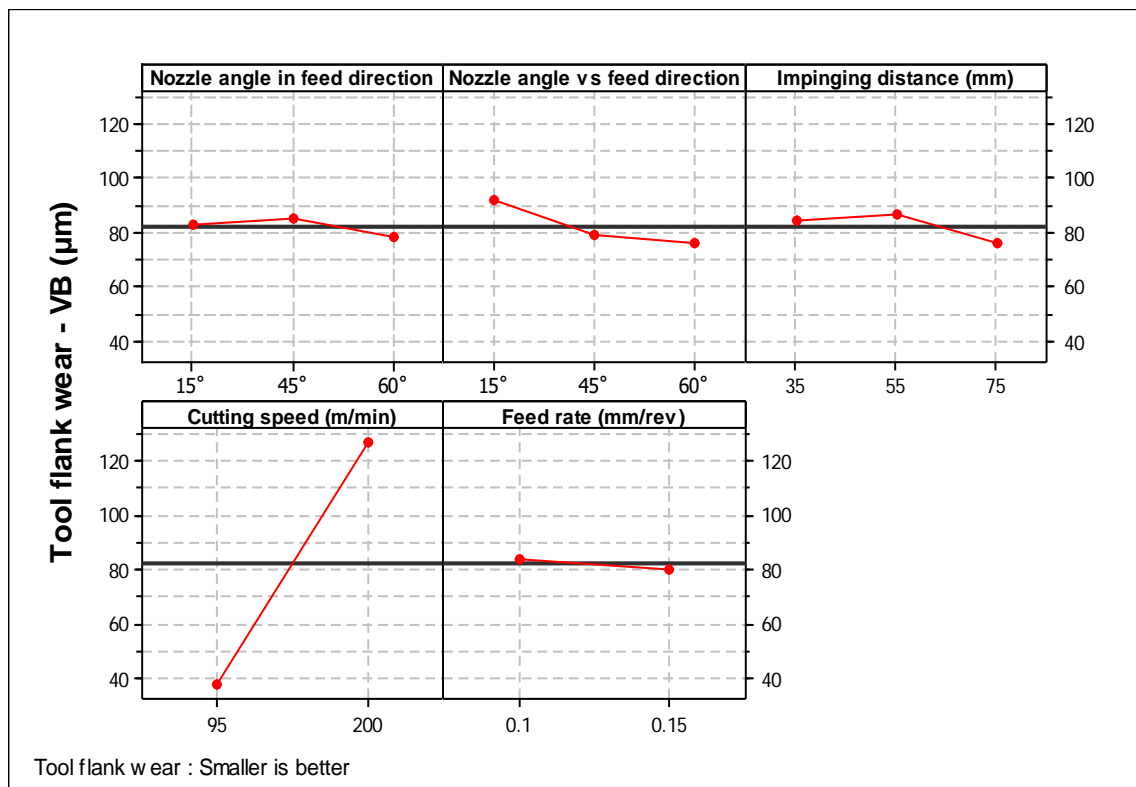


Fig. 5-59 Main effects analysis for tool flank wear

In addition, Fig. 5-60 shows the interaction plot for tool wear. Obviously, there are some noticeable interactions among the factors, except for between feed rate and cutting speed and cutting speed and nozzle positions (against feed direction). On the other hand, the parallel trends (at the lower right of the figure) of the lines clearly show a low degree of or relatively little interaction between feed rate and nozzle position (in the feed direction) and between impinging distance and cutting speed and feed rate and impinging distance.

Table 5-10 ANOVA results for tool flank wear

Source	DF	SS	MSS	F	P	PCR
Nozzle angle in feed direction (degree)	2	807	403	0.29	0.748	0.22%
Nozzle angle vs feed direction (degree)	2	5236	2618	1.89	0.157	1.46%
Impinging distance (mm)	2	2339	1170	0.84	0.434	0.65%
Cutting speed (m/min)	1	212351	212351	152.98	0.0*	59.23%
Feed rate (mm/rev)	1	358	358	0.26	0.613	0.099%
Error	99	137423	1388			38.33%
Total	107	358514				
S= 37.25		R-Sq = 61.67%		R-Sq (adj) = 58.57%		

DF = Degree of freedom
 SS = Sum of squares
 F= F- test value

* Significant at the 5 % level and confidence level of 95%
 P = Probability

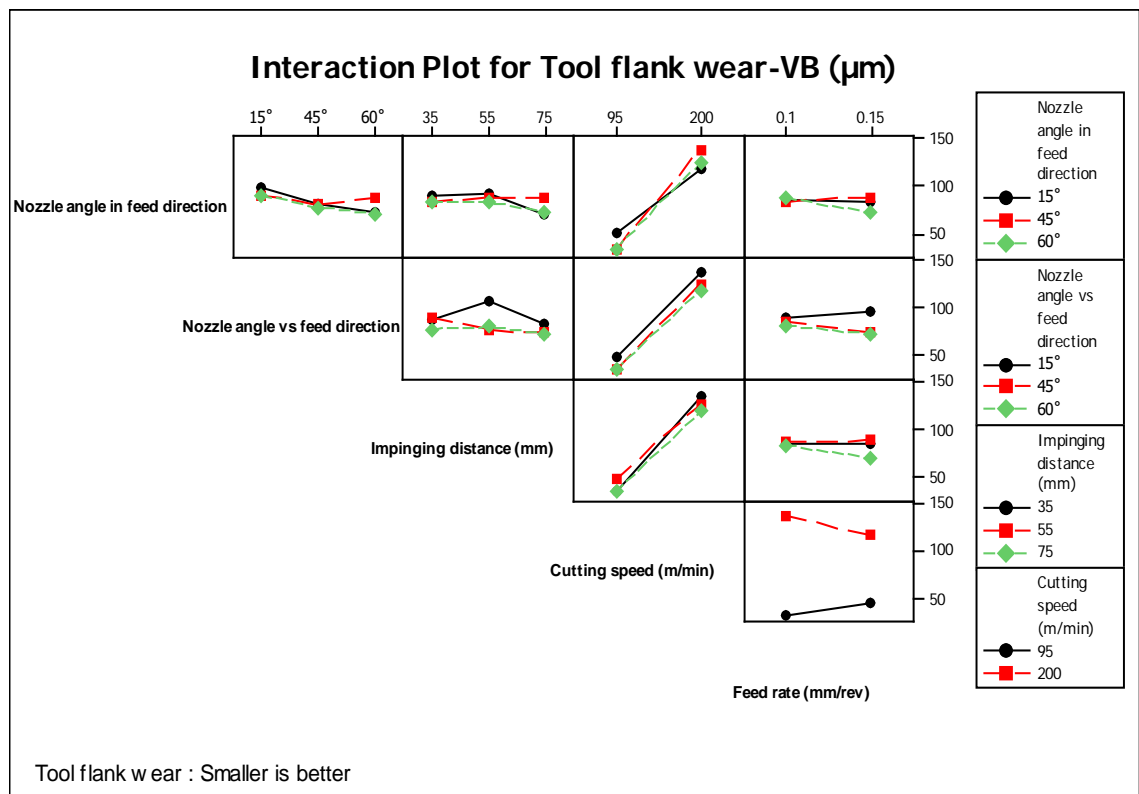


Fig. 5-60 Interaction effects of process parameters on tool flank wear (VB)

Fig. 5-61 shows an SEM analysis of the used uncoated WC cutting tool edges at various cutting conditions. Wear occurred mainly on the flank face of the cutting tool, where uniform abrasive wear was observed at low cutting speed, whereas adhesion has already taken place at higher cutting speed. The adhered substances were examined using EDX and the presence of titanium element in the adhered materials on the rake face of the tool substrate was found, as shown in Fig. 5-62. In addition, a few elements such as tungsten (W) and cobalt (Co) from the tool substrate were found in the adhered workpiece material at higher cutting speed, which proves that diffusion took place. The increase in heat generated with increased cutting energy may offer a good atmosphere for the diffusion of tool material atoms across the tool-workpiece interface, and thus, by impairing bonding strength in the tool materials, diffusion wear has occurred [301].

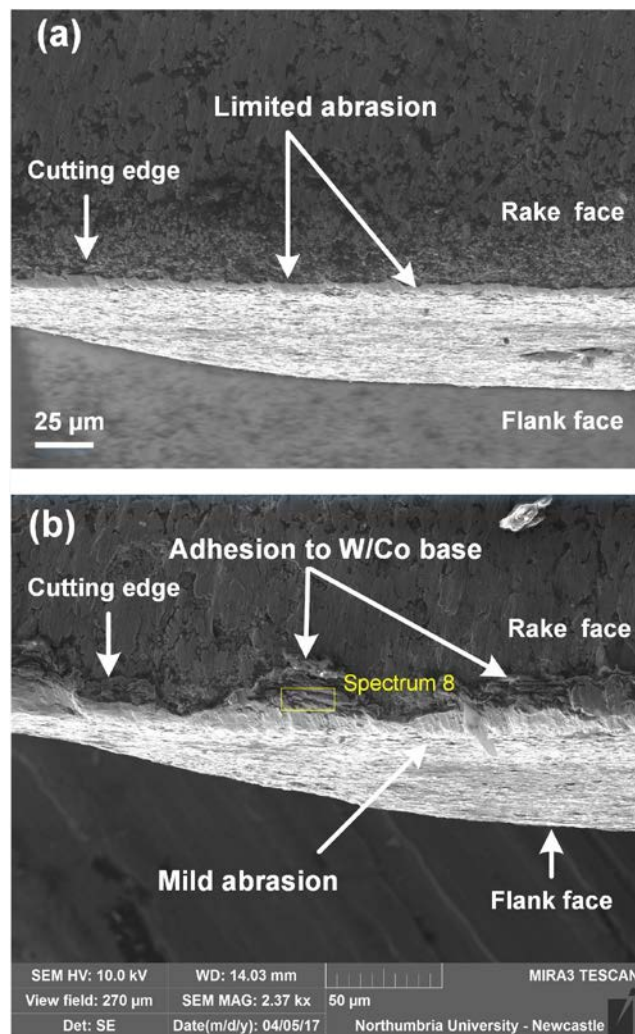


Fig. 5-61 SEM micrographs of worn tools used to machine Ti-6Al-4V at (a) 95 m/min, and (b) 200 m/min with feed rate of 0.1 mm/rev, nozzle positions of 15° and 45° in the feed and against feed direction respectively and an impinging distance of 75 mm

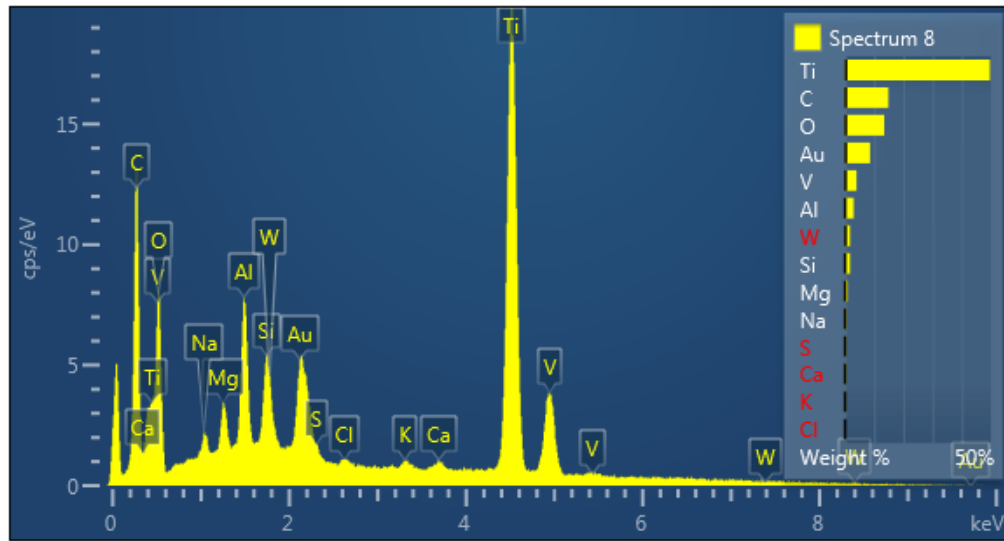


Fig. 5-62 EDX analysis performed on the rake face of the insert at cutting speed of 200 m/min and feed rate of 0.1 mm/rev

5.5.2.4 Burr formation analysis

Fig. 5-63 presents the variation in average burr height measured at the edge of the machined surface as a function of various process variables assessed in this study. The smallest burr height can be achieved at 200 m/min cutting speed, 0.15 mm/rev feed rate, nozzle location at 45° in the feed direction and 45° against feed rate direction, and an impinging distance of 55 mm. It was observed that burr height tends to decrease rapidly with increased cutting speed and feed rate. This could be attributed to the increase in fluid flow rate (see Fig. 3-13) associated with the higher cutting conditions. At lower temperature, the yield stress of the workpiece material increases and smaller burrs are formed [302]. Besides this, it was found that burr formation is relatively sensitive to impinging distance rather than nozzle angle or position. This is deemed to be due to the impinging distance affecting the fluid velocity [58], which leads to the cutting edge being maintained in a sharper condition with less metal tearing. In addition, The ANOVA results in Table 5-11 show that feed rate is the major contributor, with a PCR of 38.69%, in minimising burr formation, while cutting speed and nozzle angle do not have a significant impact on burr height. These trends are in accordance with the findings in a recent report [303] that feed rate and tool nose geometry have a great effect on burr formation while the cutting speed has little influence on top burr height when up-milling Ti-6Al-4V.

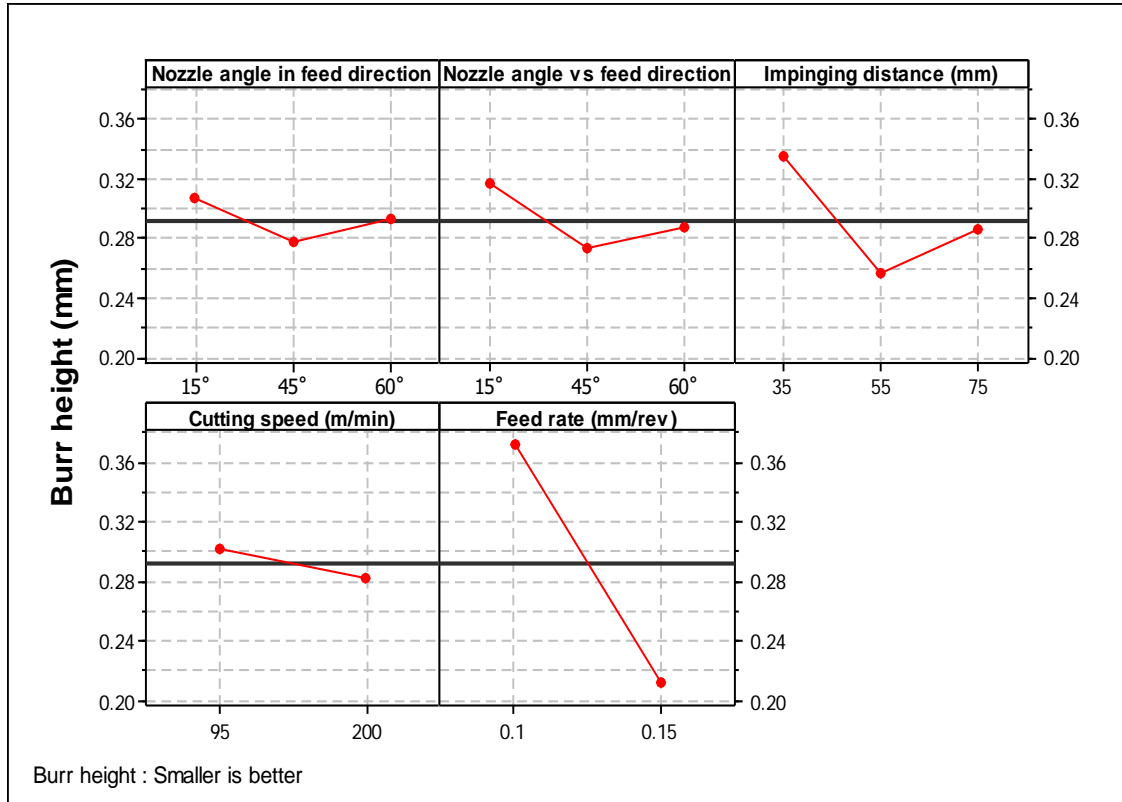


Fig. 5-63 Main effects analysis for average burr height

Table 5-11 ANOVA results for burr formation

Source	DF	SS	MSS	F	P	PCR
Nozzle angle in feed direction (degree)	2	0.01502	0.00751	0.81	0.446	0.85%
Nozzle angle vs feed direction (degree)	2	0.03602	0.01801	1.95	0.147	2.04%
Impinging distance (mm)	2	0.11307	0.05654	6.13	0.003*	6.42%
Cutting speed (m/min)	1	0.01161	0.01161	1.26	0.264	0.62%
Feed rate (mm/rev)	1	0.68163	0.68163	73.95	0.0*	38.69%
Error	99	0.91250	0.00922			51.81%
Total	107	1.76987				
S = 0.096		R-Sq = 48.44%		R-Sq (adj) =		
DF = Degree of freedom			* Significant at the 5 % level and confidence level of 95%			
SS = Sum of squares			P = Probability			
F= F- test value						

Fig. 5-64 shows the interaction effects of process parameters on burr formation. It appears that there are several significant interactions between the parameters tested, which could also be a reason for the high error in the ANOVA results. However, almost no interaction was observed between cutting speed and impinging distance or between feed rate and impinging distance, where all the lines are relatively parallel to each other. Fig. 5-65 shows burrs formed on the milled top surfaces of Ti-6Al-4V at various cutting conditions.

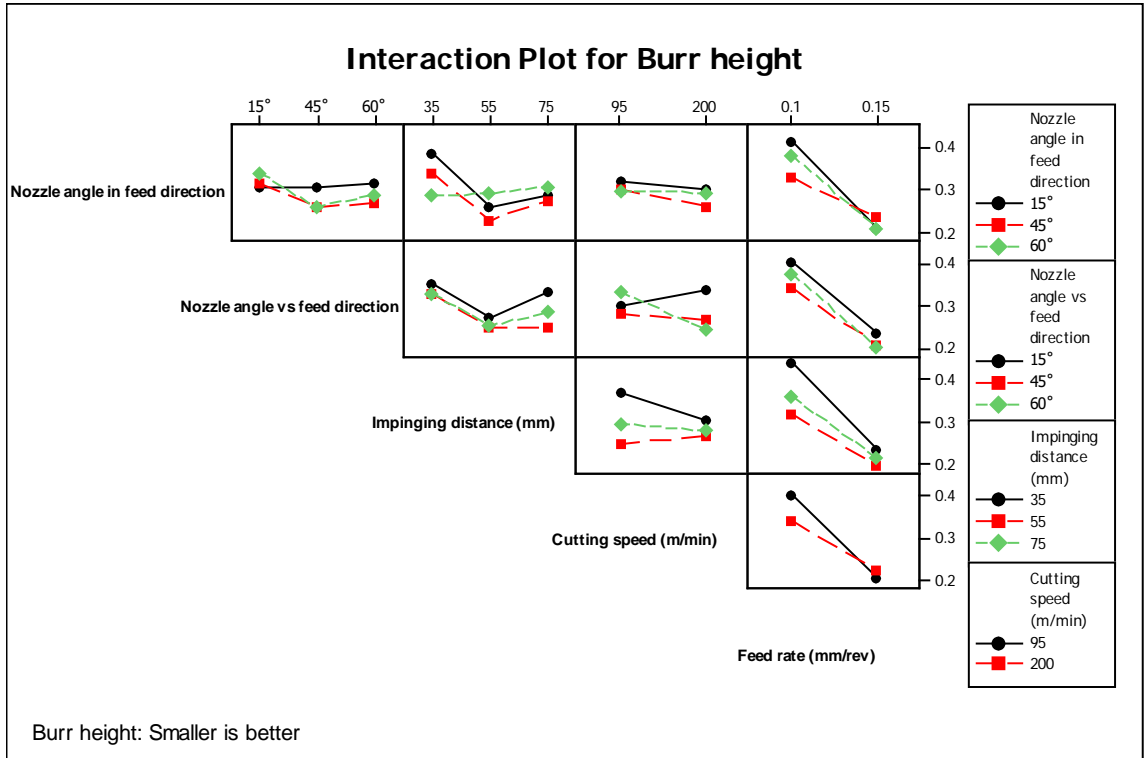


Fig. 5-64 Interaction effects of process parameters on burr formation

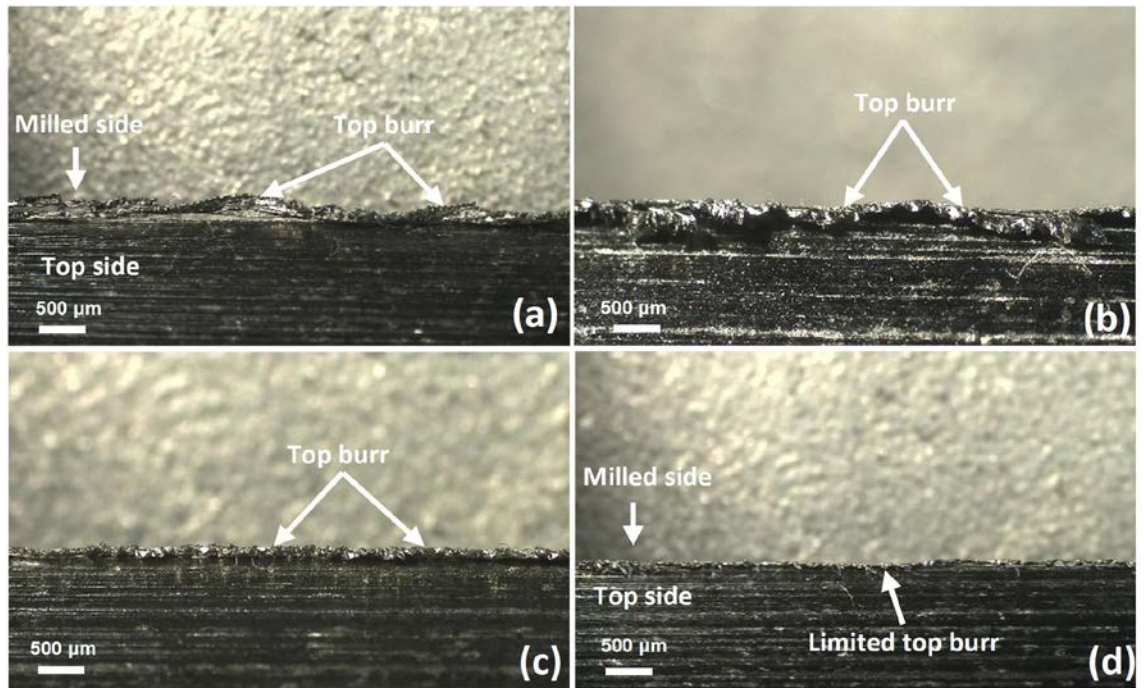


Fig. 5-65 Images of burrs formed on milled top surfaces at different cutting conditions: (a) 95 m/min x 0.1 m/rev, (b) 95 m/min x 0.15 mm/rev, (c) 200 m/min x 0.1 mm/rev and (d) 200 m/min x 0.15 mm/rev

5.5.2.5 Surface roughness analysis

Average surface roughness (Ra) results at various process parameters and system levels are shown in Fig. 5-66. A minimum Ra was achieved at a cutting speed of 200 m/min, feed rate of 0.1 mm/rev, nozzle positions of 45° and 60° in the feed and against the feed directions respectively and an impinging distance of 75 mm. Ra values were found to decrease with rises in cutting speed and decreases in feed rates. This can also be attributed to the increase in cutting fluid flow rate associated with increased cutting speed (see Fig. 3-13). A comparable finding was also reported recently [58] when Cai et al. investigated the end milling of Ti-6Al-4V under MQL at four different fluid supply rates (2, 6, 10 and 14 ml/h). However, the effect of feed rate on Ra seems much higher than that of cutting speed. This is likely to be due to Ra being theoretically directly proportional to the square of the feed per revolution. In the same vein, a decreased feed rate possibly gave the cutting fluid enough time to carry away the heat from the machining zone, leading to a low rate of material removal and the accumulation of chips in the tool-workpiece zone, resulting in an improved surface finish. The ANOVA (Table 5-12) results show that the major effective factor in reducing Ra is the feed rate (PCR 39.10%) followed by cutting speed and impinging distance, while nozzle position had little effect on Ra values.

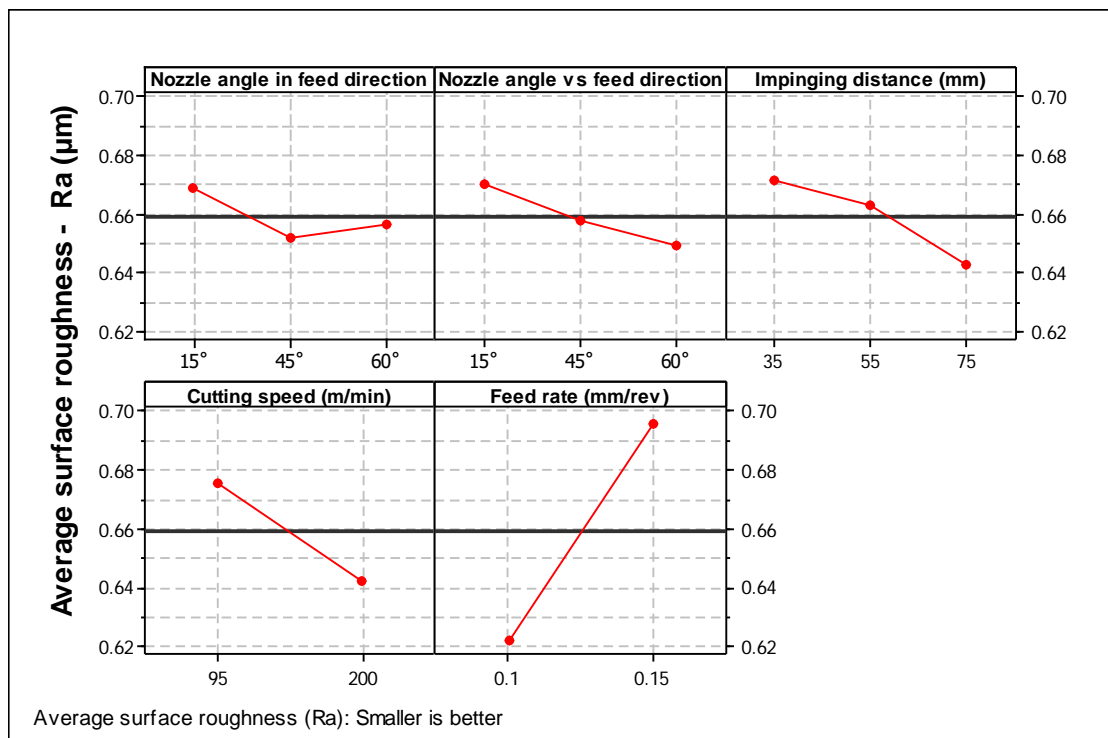


Fig. 5-66 Main effects analysis for surface roughness

Table 5-12 ANOVA results for surface roughness (Ra)

Source	DF	SS	MSS	F	P	PCR
Nozzle angle in feed direction (degree)	2	0.00570	0.00285	1.67	0.1944	1.32%
Nozzle angle vs feed direction (degree)	2	0.00789	0.00394	2.31	0.105	1.86%
Impinging distance (mm)	2	0.01591	0.00795	4.65	0.012*	3.98%
Cutting speed (m/min)	1	0.03033	0.03033	17.73	0.00*	7.97%
Feed rate (mm/rev)	1	0.14740	0.14743	86.18	0.00*	39.10%
Error	99	0.16933	0.0017			44.95%
Total	107	0.37658				
S = 0.01849 R-Sq = 55.03% R-Sq (adj) =						
DF = Degree of freedom			* Significant at the 5 % level and confidence level of 95%			
SS = Sum of squares			P = Probability			
F= F- test value						

In addition, Fig. 5-67 shows the interaction effects of all factors evaluated on Ra. It can be seen that there are noticeable mutual interactions between all of the factors investigated except between cutting speed and feed rate and feed rate and impinging distance. In addition, the parallel trends of the lines also show a low degree of or almost no interaction between cutting speed and nozzle position (against the feed direction) and cutting speed and impinging distance.

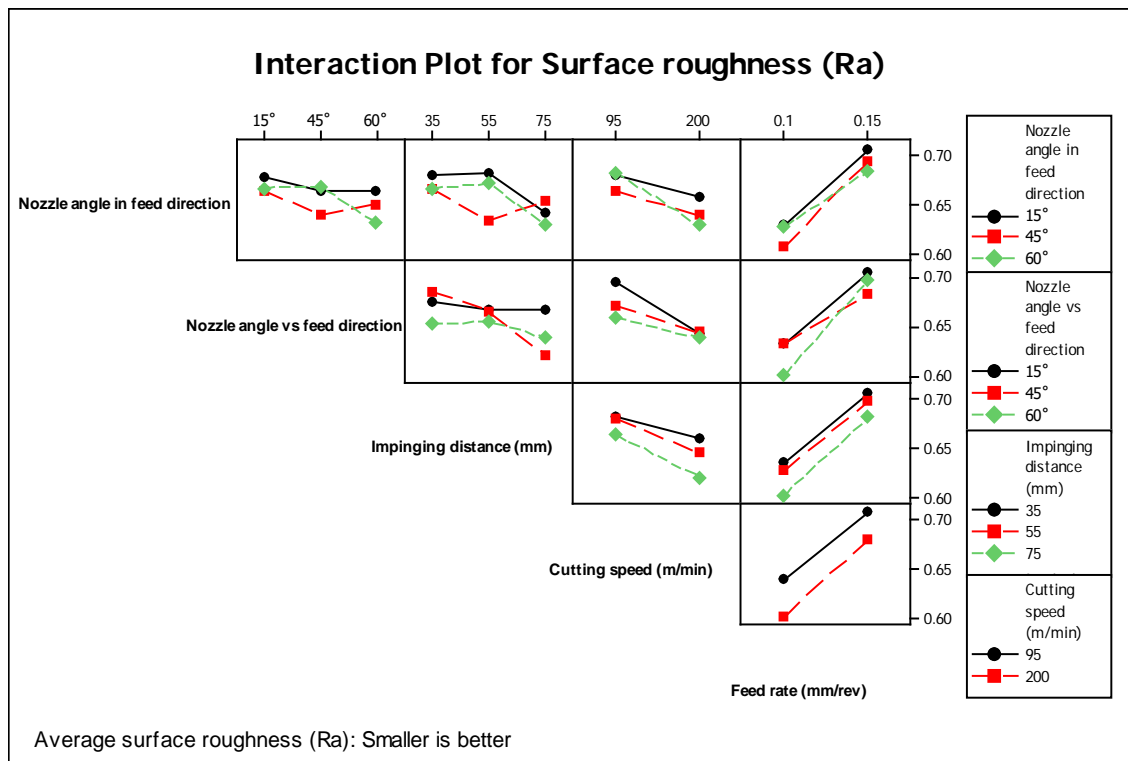


Fig. 5-67 Interaction effects of process parameters on Ra

5.5.2.6 Effect of nozzle position

Average workpiece temperature was found to be influenced by nozzle position/angle, in particular in the feed direction, as can be seen in Fig. 5-68. Locating the nozzle at 15° in the feed direction apparently helped to create an efficient trapping of fluid between the tool and workpiece surfaces which, in turn, led to the improved access of cutting fluid into the machining zone to perform both cooling and lubrication functions adequately. A similar phenomenon has been observed in another study [23] where it was found that shifting the nozzle from a 45° angle to an acute angle of 12.5° in the feed direction when end-milling H13 steel under MQL assisted in increasing the amount of cutting fluid reaching the machining zone. Additionally, the proximity of the nozzle positioned at an angle of 15° from the tool/workpiece contact point contributed in minimising the fluid particle dispersion caused by tool rotation, which allowed the particles to adhere to the tool and workpiece surfaces effectively and to persist in working as a lubricant in the machining zone. Conversely, at nozzle positions of 45° or 60° in the feed direction, more cutting fluid particles are driven away from the tool surface while the cutting tool rotates in a cyclical loop process [212]. In addition, nozzle placement at an angle of 45° or 60° against feed direction tends to offer enough space to assist in chip evacuation and this helped to minimise interference between the impinging jet and the removed chip, leading to better lubrication and cooling ability and consequently improved machined surfaces.

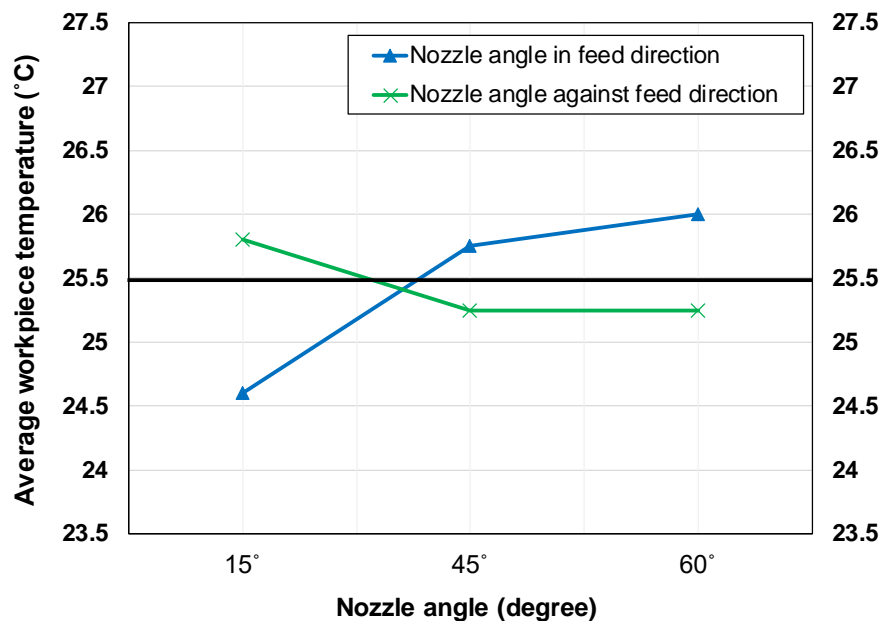


Fig. 5-68 Mean effects analysis of nozzle position/angle for workpiece temperature

5.5.2.7 Impinging distance effect

According to Figs. 5-57, 5-63 and 5-66, impinging distance had a noticeable impact on average workpiece temperature, burr formation and average surface roughness. According to Bernoulli's equation (5.2), the hydraulic head (h) (where in this case, the impinging distance is equal to the hydraulic head) has an effect on jet velocity, and this consequently affects fluid penetration efficiency. The cutting fluid jet velocity (V_j) increases as the impinging distance decreases. However, too short an impinging distance has a negative effect on the cutting fluid droplets owing to their high levels of rebounding from the workpiece and cutter surfaces [212]. Therefore, impinging distance should be controlled at an optimal level, as the impact of shorter impinging distance would be to conspicuously affect workpiece temperature; burr formation and average surface roughness. Since the optimal impinging distances obtained to control the aforementioned responses were 55 or 75 mm, they tend to have a combined action by improving fluid penetration ability with less fluid dispersion and spring-back effects, which in turn assists the cutting fluid droplets in adhering firmly to the workpiece and cutter surfaces. Fig. 5-69 shows the impinging distance and impingement zones in the CUT-LIST configuration.

$$\frac{1}{2} \rho V_j^2 + \rho gh + p = \text{constant} \quad [212] \quad (5.2)$$

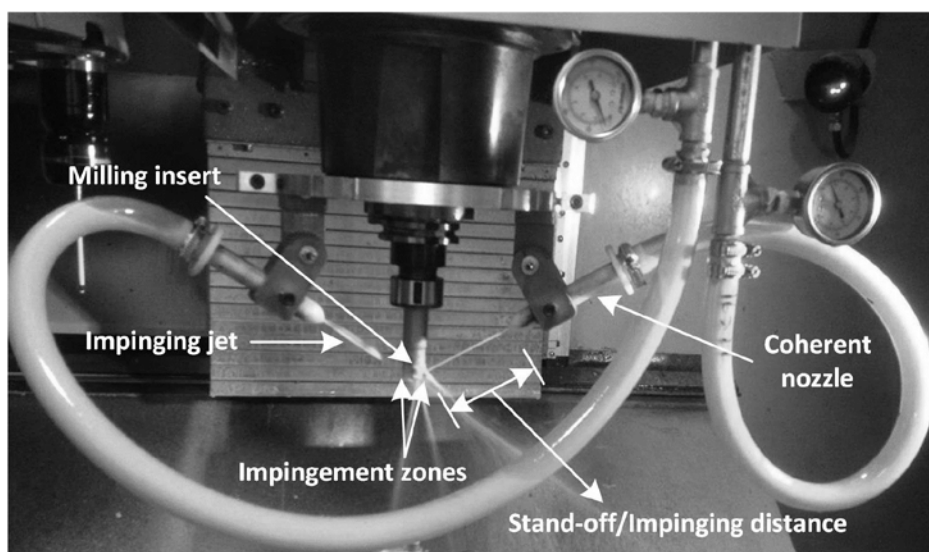


Fig. 5-69 Impinging distance locations in CUT-LIST configuration

5.5.3 Repeatability of trials

Several experimental trials were repeated to improve statistical reliability. In these trials, an output variable can be measured two or more times, usually during or after the same experimental run [304]. In this study, the precision of data collected was checked by preparing 11 tests using the CUT-LIST supply system with a new cutting tool and Ti-6Al-4V material. Key process indicators (responses) such as cutting force, workpiece temperature, tool flank wear, burr height and Ra were also measured. Table 5-13 shows the responses and their measurement conditions in the repeated and original experimental trials.

Table 5-13 Responses and their measurement conditions in the repeated and original trials

	Cutting force	Workpiece temperature	Tool wear	Burr height	Ra
Measurement condition	During experimental run	During experimental run	After experimental run	After experimental run	After experimental run
Number of readings	2 readings for each response including original and a repeated trial				

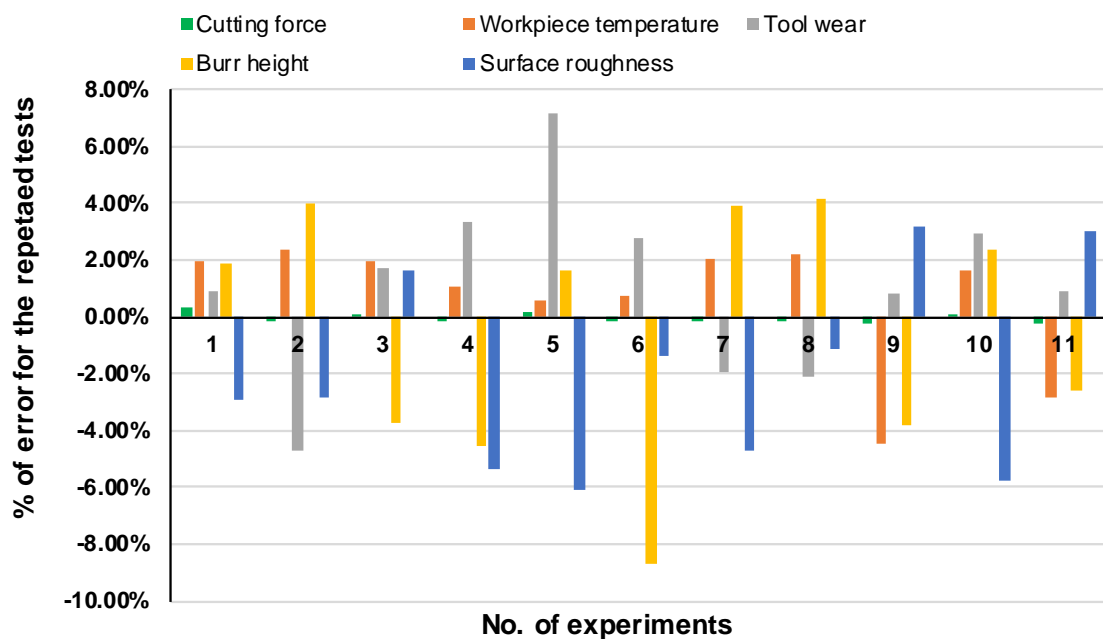
Additionally, every repeated trial was performed under similar working conditions to the original tests in terms of cutting speed, feed rate, nozzle position, impinging distance and cutting fluid flow rates as well as workpiece and cutting tool materials. Measurements followed similar procedures and standards as those used in the original tests. The measurement error for each response was then computed using equation 5.3:

$$\text{Measurement error} = \frac{R_1 - R_2}{\text{Largest value from the readings provided}} \quad [304] \quad (5.3)$$

where R_1 and R_2 are measurement readings obtained from each repeated and the original tests respectively. A summary of the maximum and minimum errors for all responses based on the repeat trials is presented in Table 5-14. Fig. 5-70 shows experimental error variations for all responses during the repeat tests, for which the data sheet and results can be found in Appendix I (I6).

Table 5-14 Experimental maximum and minimum error for all responses

Experimental error (%)	Cutting force	Workpiece temperature	Tool wear	Burr height	Ra
Maximum	0.34%	2.39%	7.16%	4.2%	3.17%
Minimum	0.03%	0.59%	0.8%	1.89%	1.61%

**Fig. 5-70** Experimental error variation for all responses during the repeated tests

Chapter 6 Conclusions and Recommendations for Future Work

6.1 Conclusions

Reducing the use of cutting fluid in the machining process is important to cut down manufacturing costs as well as minimising health and environmental hazards. The delivery of cutting fluid into the machining zone can be applied using several supply methods or systems. Although process improvements are gained from such systems, however, most of them possess inherent economical and technical deficiencies. The knowledge gap addressed in this thesis relates to developing a novel efficient and inexpensive supply system (CUT-LIST), and defining the optimum settings of operating conditions for the best practice in terms of less fluid use when machining titanium alloys. This chapter focuses mainly on the key findings arising from the research. This includes the turning-based experimental trials which were conducted prior to testing the new system, and milling-based experimental trials that have been performed to evaluate CUT-LIST. Thereby, the conclusions are presented in two main sections as follows.

6.1.1 Turning-based experimental trials

- Despite the high content of the base oil (~ 60 %) in the reference MO-based fluid, all cutting fluids tested (i.e. MO- and VO-based fluids) showed relatively marginal variations in Ra values (a maximum of 0.15 μm). This supports the view that VO-based fluids are suitable alternatives to MO-based fluids when cutting titanium alloys.
- Among VO-based fluids, Vasco 1000 fluid showed superior machining performance, particularly in terms of Ra. This was attributed to its superior tribological properties (with VO content of 45 %). Thus, it was selected to evaluate the new supply system.
- The uncoated coarse-grain carbide tool material (H13A) outperformed other tools (i.e. GC1105, S05F, GC1115 and H10A) specifically in terms of Ra and

tool flank wear and tool life. Conversely, CVD-coated tool (S05F) presented inferior cutting performance. H13A tool material was thus chosen for cutting Ti-6Al-4V using the CUT-LIST supply system.

- Small variations in the mean values of surface roughness (with a maximum of 0.15 μm) were observed between the different cutting fluid (Vasco 1000) concentration ratios tested (5%, 10% and 15%). For a good balance between its cooling and lubrication effects, a fluid concentration ratio of 10% seemed to be a feasible choice for the evaluation of the CUT-LIST supply system.
- In this part of the study, machining of titanium was tested at cutting speeds and feed rates ranging between 28 to 175 m/min and 0.1 to 0.2 mm/rev respectively. The results of the trials showed that surface finish was improved by 40% with increasing cutting speed and decreasing feed rate. Thus, machining speed was increased up to 200 m/min when testing the new supply system (in the milling-based trials).
- Turning Ti-6Al-4V using different VO-based cutting fluids produced similar discontinuous serrated chips style. The investigation also showed that there was a discernible difference in chip thickness and size formed using various cutting speeds.
- Tool life was found to increase with decreased cutting speed and to decrease with prolonged cutting distance or time when turning titanium using the VO-based cutting fluid under flood cooling conditions.
- Turning Ti-6Al-4V using a miscible VO-based cutting fluid always produced higher hardness near the machined surface with a prolonged cutting distance or time under all tested conditions.

6.1.2 Milling-based experimental trials using CUT-LIST

Key findings related to evaluating the new supply system include the following:

- Although the fluid supply rates of the CUT-LIST and conventional supply systems were determined based on similar computational criteria (i.e. L/min per kW heat), a dramatic reduction in cutting fluid consumption (up to 42%) was achieved when the new system was used.

- CUT-LIST enabled a significant reduction in cutting force of up to 16.41 % compared to the conventional system. Unlike with steel alloys, cutting force on titanium tends to increase with increased cutting speed owing to the strain rate hardening effect. Feed rate influences mean cutting force, having a high PCR of 47.64%, followed by cutting speed (19.14%). Nozzle angle positions and impinging distances have little effect on reducing cutting force. Noticeable interactions between all factors evaluated were observed except between feed rate and cutting speed.
- Although CUT-LIST led to a significant reduction in cutting fluid consumption (42%), workpiece temperature only increased by 1.5 °C compared with conventional supply system. This can be attributed to the cooling potency of the new system due to its high penetrability and ability to precisely target the cutting fluid into heat-affected zones. Cutting speed was found to be the most influential factor affecting workpiece temperature, with a PCR of 46.50%, followed by feed rate, impinging distance and nozzle angle position (in the feed direction). Nozzles positioned at an angle of 15° in the feed direction, and 45° or 60° against feed direction and an impinging distance of 55 mm are found to be helpful in reducing workpiece temperature. Only limited interaction was observed between factors, particularly between nozzle positions (in the feed and against the feed directions) and impinging distance.
- The use of CUT-LIST reduced tool flank wear by 46.77% compared to the conventional system. A SEM analysis showed accelerated tool flank wear, adhesion, and micro-chipping when the conventional supply system was used owing to its inability to dissipate heat sufficiently from the machining zone. Cutting speed has a substantial effect on tool wear, with a PCR of 59.23%, while tool wear values seem to be independent of feed rate, nozzle position, and impinging distance. The SEM-EDS analysis also confirmed that adhesion is the predominant wear mechanism when milling Ti-6Al-4V, particularly at higher cutting speeds. Considerable interactions were only seen between nozzle position (in all directions) and impinging distance, and cutting speed and nozzle position in the feed direction.
- Burr formation was reduced by 31.70% when employing CUT-LIST. This is attributed to the cooling potency of the new system. At lower temperatures,

the yield stress of the workpiece material increases and smaller burrs are formed. Feed rate was the major contributing factor (PCR of 38.69%) to burr formation, while cutting speed and nozzle angle do not cause significant variations in top burr height. Burr formation is more sensitive to impinging distance rather than nozzle positions. Significant interactions between all process parameters were observed while almost no interaction was noticed between cutting speed and impinging distance.

- Average surface roughness (Ra) values were relatively smaller with the use of the new system. Smearing, chips being re-deposited or adhering to the machined surfaces, and micro surface cavities as well as the erosion of the workpiece material are the main surface damage patterns when the conventional system was used. The major effective factor in reducing Ra is the feed rate (PCR 39.10%) followed by cutting speed and impinging distance, while nozzle position had little effect. It was noted that there were noticeable interactions between all process parameters in affecting Ra, except between cutting speed and feed rate and feed rate and impinging distance.
- Both supply systems achieved acceptable micro-hardness variations (always ranging between 386.3 – 419 HV₁₀₀) while their higher values were recorded at 100 μm below the machined surface with a marginal reduction in micro-hardness up to 5.5% with the use of CUT-LIST. Near the machined surfaces, CUT-LIST always produced lower micro-hardness values under all cutting conditions. The alterations in micro-hardness are affected by cutting speed rather than feed rate when milling Ti-6Al-4V using VO-based cutting fluid.
- Despite noticeable reduction in cutting fluid consumption achieved by CUT-LIST, no significant disparity was found in microstructural damage. A thin plastically deformed layer (always from 2 to 5 μm at higher speed) below the machined surface was observed during the metallurgical investigation of the surfaces produced using both systems. The microstructure was very sensitive to cutting speed, while the increase in cutting fluid flow rate with increasing cutting speeds has assisted in alleviating microstructural damage.
- SEM analysis showed that the formation of discontinuous serrated chips is the main characteristic of the milling of Ti-6Al-4V with both cutting fluid supply

systems, while the increase in cutting fluid flow rate associated with increased cutting speed significantly changed the chip morphology.

- The free surfaces of all chips produced are characterised by highly deformed wave-like-shaped segments, while smooth back surfaces were observed in both systems. A significant difference between the two systems in terms of crack/serration depths (maximum of 90 μm) was observed at the end of the chip free surface.
- CUT-LIST reduced saw-tooth height (h_{max}) by 12.5% and increased the segmented width by 13.63% at higher cutting speed. Meanwhile the transition from regular (periodic) to irregular (aperiodic) serrated chip formation was governed by cutting speed.
- Both fluid supply systems presented a typical frequency range of 7.53-15.15 kHz, while chip segmentation frequency is sensitive to cutting speed.
- CUT-LIST showed increases in shear angle (ϕ) up to 29.16 % and 32.2 % at lower and higher cutting speeds respectively, and shear angle is strongly influenced by cutting speed.
- Impinging distance showed a more profound impact on machining outputs than nozzle angle position. This is because impinging distance is highly correlated to fluid penetrability. However, locating nozzles particularly at acute angles ($\leq 15^\circ$) in the feed direction significantly helps in improving the access of cutting fluid into the machining zone. Whereas a nozzle position against the feed direction at angle ($\geq 45^\circ$) can be considered as a more favourable position for chip evacuation as well as to cool down tool at tool exit point effectively.

In conclusion, the outcomes accomplished by the developed system have proved that CUT-LIST can be deemed as a prospective feasible and inexpensive supply system for less fluid use in machining technology since it possesses several merits over the conventional supply system in terms of the aforementioned machining outputs.

6.2 Recommendations for future work

From the work discussed in this research, potential areas are presented below to improve cutting fluid application in machining using CUT-LIST:

- The coherent nozzle showed a significant contribution in improving the cooling performance of CUT-LIST. Therefore, the effect of coherent nozzle aperture shape and geometry (e.g. rounded or elliptical, etc.) on machining processes can be further investigated.
- Nozzle angle positions and impinging distance exhibited noticeable effects particularly on reducing workpiece temperature, burr formation and surface roughness (R_a). Hence, the impact of nozzle elevation angle (α) on machining performance using CUT-LIST can be involved in further investigation.
- The surface quality of machined titanium parts is crucial along with other aspects of surface integrity such as surface roughness, micro-hardness and microstructure, and thus the impact of CUT-LIST on residual stresses should be considered in another study.
- CUT-LIST should be applied in machining studies with other refractory materials that experience similar machining issues to titanium and its alloys (i.e. nickel-based alloys) to determine the potential breadth of application for this efficient new system. Such a study could also reveal disparities in the cooling potency of CUT-LIST for different work materials.
- CUT-LIST was examined at a maximum cutting speed of 200 m/min. Thus, there is a need to push cutting speed limits further to improve the productivity of the machining process by increasing manufacturing speed.
- Further parameters should be utilised in quantifying chip morphology and segmentation, such as chip compression ratio (CCR) using the weight method and segmentation intensity ratio (SIR) or metric segmentation frequency in additional studies using CUT-LIST.
- In microstructural analysis, the depth of the deformed layer beneath the machined surface could be precisely quantified using a 3D EBSD tomography (electron back-scatter diffraction) technique in conjunction with the SEM

scanning method. Thus, these techniques can also be recommended for future investigations using the new cutting fluid supply system.

- Finally, a comparative study of CUT-LIST and conventional systems in terms of chip formation and particularly adiabatic deformed shear bands, when cutting refractory/or heat resistant materials is also advised.

References

- [1] C. Veiga, P. Davim, and A. Loureiro, "Review on machinability of titanium alloys: the process perspective," *Reviews on Advanced Materials Science*, vol. 34, pp. 148-164, 2013.
- [2] Á. Machado and J. Wallbank, "Machining of titanium and its alloys—a review," *Proceedings of the Institution of Mechanical Engineers, Part B: Journal of Engineering Manufacture*, vol. 204, pp. 53-60, 1990.
- [3] S. Jaffery and P. Mativenga, "Assessment of the machinability of Ti-6Al-4V alloy using the wear map approach," *International journal for Advanced Manufacturing*, vol. 40, pp. 687-696, 9/2/2008 2009.
- [4] V. Sharma, M. Dogra, and N. Suri, "Cooling techniques for improved productivity in turning," *International Journal of Machine Tools and Manufacture*, vol. 49, pp. 435-453, 5// 2009.
- [5] A. Shokrani, V. Dhokia, and S. Newman, "Environmentally conscious machining of difficult-to-machine materials with regard to cutting fluids," *International Journal of Machine Tools and Manufacture*, vol. 57, pp. 83-101, 6// 2012.
- [6] M. El Baradie, "Cutting fluids: Part I. Characterisation," *Journal of Materials Processing Technology*, vol. 56, pp. 786-797, 1// 1996.
- [7] E. Bennett, "Water based cutting fluids and human health," *Tribology international*, vol. 16, pp. 133-136, 1983.
- [8] M. Soković and K. Mijanović, "Ecological aspects of the cutting fluids and its influence on quantifiable parameters of the cutting processes," *Journal of Materials Processing Technology*, vol. 109, pp. 181-189, 2/1/ 2001.
- [9] V. Astakhov. (2001, Accessed on 21/4/2015). *Cutting fluids and their application in deep-hole machining*. Available: <http://viktorastakhov.tripod.com/DH/coolant.pdf>
- [10] S. Lawal, I. Choudhury, and Y. Nukman, "Application of vegetable oil-based metalworking fluids in machining ferrous metals—A review," *International Journal of Machine Tools and Manufacture*, vol. 52, pp. 1-12, 1// 2012.
- [11] S. Alves and J. Oliveira, "Vegetable based cutting fluid-an environmental alternative to grinding process," in *15th CIRP international conference on life cycle engineering, Sydney*, 2008, pp. 664-668.
- [12] S. Lawal, I. Choudhury, I. Sadiq, and A. Oyewole. Vegetable-oil based metalworking fluids research developments for machining processes: survey, applications and challenges [Online].
- [13] S. Lawal, "A Review of application of vegetable oil-based cutting fluids in machining non-ferrous metals," *Indian Journal of Science and Technology*, vol. 6, pp. 3951-3956, 2013.

-
- [14] M. Sharif, S. Pervaiz, and I. Deiab, "Potential of alternative lubrication strategies for metal cutting processes: a review," *The International Journal of Advanced Manufacturing Technology*, vol. 89, pp. 2447-2479, March 01 2017.
- [15] D. Dudzinski, A. Devillez, A. Moufki, D. Larrouquère, V. Zerrouki, and J. Vigneau, "A review of developments towards dry and high speed machining of Inconel 718 alloy," *International Journal of Machine Tools and Manufacture*, vol. 44, pp. 439-456, 3// 2004.
- [16] S. Debnath, M. Reddy, and Q. Yi, "Environmental friendly cutting fluids and cooling techniques in machining: a review," *Journal of Cleaner Production*, vol. 83, pp. 33-47, 11/15/ 2014.
- [17] K. Serope and S. Schmid, *Manufacturing Engineering and Technology*, 4th edition ed. Newjersy, USA: Prentice Hall, 2001.
- [18] R. Revuru, N. Posinasetti, V. Ramana, and M. Amrita, "Application of cutting fluids in machining of titanium alloys—a review," *The International Journal of Advanced Manufacturing Technology*, vol. 91, pp. 2477-2498, 2017.
- [19] D. Koen, "Investigation of a novel cooling methods to enhance aerospace component manufacturing practices," MSc., Industrial Engineering, Stellenbosch, University of Stellen bosch, 2011.
- [20] A. Nandy, M. Gowrishankar, and S. Paul, "Some studies on high-pressure cooling in turning of Ti-6Al-4V," *International Journal of Machine Tools and Manufacture*, vol. 49, pp. 182-198, 2// 2009.
- [21] S. Hong, "Lubrication mechanisms of LN2 in ecological cryogenic machining," *Machining science and technology*, vol. 10, pp. 133-155, 2006.
- [22] A. Hoyne, "A study on the fluid film of an atomization-based cutting fluid (ACF) spray system during titanium machining," MSc MSc, Mechanical Engineering, University of Illinois University of Illinois at Urbana-Champaign, 2013.
- [23] I. Mulyadi, "Improving the performance of minimum quantity lubrication in high speed milling and environmental performance analysis," Ph.D Doctor of Philosophy, School of Mechanical, ASerospace and Civil Engineering, University of Manchester Manchester, UK, 2013.
- [24] M. Calamaz, D. Coupard, and F. Girot, "A new material model for 2D numerical simulation of serrated chip formation when machining titanium alloy Ti-6Al-4V," *International Journal of Machine Tools and Manufacture*, vol. 48, pp. 275-288, 2008/03/01/ 2008.
- [25] A. Paranjpe, "Residual stresses in machined titanium (Ti-6Al-4V) alloys," MSc., Department of Mechanical Engineering, Utah, University of Utah, USA, 2014.
- [26] D. Stephenson and J. Agapiou, "Metal cutting theory and practice," in *Metal cutting theory and practice*, G. Boothyard, Ed., 2nd ed Boca Raton, FL, USA: CRC press, 2006, pp. pp551-574.
- [27] E. Trent and P. Wright, *Metal cutting*: Butterworth-Heinemann, 2000.
-

-
- [28] E. Ezugwu, J. Bonney, and Y. Yamane, "An overview of the machinability of aeroengine alloys," *Journal of Materials Processing Technology*, vol. 134, pp. 233-253, 3/10/ 2003.
- [29] E. Abele and B. Fröhlich, "High speed milling of titanium alloys," *Advances in Production Engineering & Management*, vol. 3, pp. 131-140, 2008.
- [30] F. Khan, "Investigation into advanced coating for bandsaw blades," Ph.D, Mechanical & Construction Engineering Department, Northumbria, Northumbria University, Newcastle, 2011.
- [31] B. Peterson, "Energy dispersive spectroscopy characterization of solute segregation in Ti-6Al-4V," MSc, Materials Science and Engineering, Ohio USA, 2011.
- [32] E. Ezugwu and Z. Wang, "Titanium alloys and their machinability—a review," *Journal of Materials Processing Technology*, vol. 68, pp. 262-274, 8/15/ 1997.
- [33] L. López de lacalle, J. Pérez, J. Llorente, and J. Sánchez, "Advanced cutting conditions for the milling of aeronautical alloys," *Journal of Materials Processing Technology*, vol. 100, pp. 1-11, 4/3/ 2000.
- [34] C. Machai, A. Iqbal, D. Biermann, T. Upmeier, and S. Schumann, "On the effects of cutting speed and cooling methodologies in grooving operation of various tempers of β -titanium alloy," *Journal of Materials Processing Technology*, vol. 213, pp. 1027-1037, 7// 2013.
- [35] M. Rahman, Z. Wang, and Y. Wong, "A review on high-speed machining of titanium alloys," *JSME International Journal Series C*, vol. 49, pp. 11-20, 2006.
- [36] K. Park, G. Yang, M. Lee, H. Jeong, S. Lee, and D. Lee, "Eco-friendly face milling of titanium alloy," *International Journal of Precision Engineering and Manufacturing*, vol. 15, pp. 1159-1164, 2014.
- [37] C. Sandvik. (12 March 2016). *Milling developments for titanium machining*. Available: <http://www.sandvik.coromant.com>
- [38] P. Arrazola, A. Garay, L. Iriarte, M. Armendia, S. Marya, and F. Le Maître, "Machinability of titanium alloys (Ti6Al4V and Ti555.3)," *Journal of Materials Processing Technology*, vol. 209, pp. 2223-2230, 2009/03/01/ 2009.
- [39] E. Ezugwu, "Key improvements in the machining of difficult-to-cut aerospace superalloys," *International Journal of Machine Tools and Manufacture*, vol. 45, pp. 1353-1367, 10// 2005.
- [40] A. Elshwain, N. Redzuan, and N. Yusof, "Machinability of nickel and titanium alloys under of gas-based coolant-lubricants (CLS)—A review," *International Journal of Research in Engineering and Technology*, vol. 2, pp. 690-702, 2013.
- [41] M. Ribeiro, M. Moreira, and J. Ferreira, "Optimization of titanium alloy (6Al-4V) machining," *Journal of Materials Processing Technology*, vol. 143, pp. 458-463, 2003.
-

-
- [42] Á. Machado and J. Wallbank, "Machining of titanium and its alloys. A Review," *Precision Engineering*, vol. 13, pp. 53-60, 1// 1991.
- [43] A. Pramanik, "Problems and solutions in machining of titanium alloys," *The International Journal of Advanced Manufacturing Technology*, vol. 70, pp. 919-928, 2014.
- [44] D. Hammond, "An Investigation of the impact of selected cooling strategies in milling of difficult-to-cut materials with an emphasis on Titanium alloys and Hardened steel," MSc., Industrial Engineering, Stellenbosch, 2013.
- [45] D. Che, P. Han, P. Guo, and K. Ehmann, "Issues in polycrystalline diamond compact cutter–rock interaction from a metal machining point of view—Part I: Temperature, Stresses, and Forces," *Journal of Manufacturing Science and Engineering*, vol. 134, p. 064001, 2012.
- [46] W. Pan, "Machining of titanium alloys with polycrystalline diamond tools," PhD PhD, School of Aerospace, Mechanical and Manufacturing Engineering, RMIT University, Malbourne, Australia, 2014.
- [47] D. Koen, "Investigation of novel cooling methods to enhance aerospace component manufacturing practices," Master of Science in Engineering, Faculty of Engineering Department of Industrial Engineering, Stellenbosch University, Stellenbosch University, 2011.
- [48] E. Ezugwu, R. Da Silva, W. Sales, and A. Machado, "Overview of the machining of titanium alloys," in *Reference Module in Earth Systems and Environmental Sciences*, ed: Elsevier, 2017.
- [49] K. Weinert, I. Inasaki, J. W. Sutherland, and T. Wakabayashi, "Dry machining and minimum quantity lubrication," *CIRP Annals - Manufacturing Technology*, vol. 53, pp. 511-537, // 2004.
- [50] D. Stephenson and J. Agapiou, "Metal cutting theory and practice," Second ed USA: Taylor & Francis, 2006, p. 19.
- [51] G. Byrne, D. Dornfeld, and B. Denkena, "Advancing cutting technology," *CIRP Annals - Manufacturing Technology*, vol. 52, pp. 483-507, 2003/01/01 2003.
- [52] F. Klocke and T. Krieg, "Coated tools for metal cutting – Features and applications," *CIRP Annals - Manufacturing Technology*, vol. 48, pp. 515-525, 1999/01/01 1999.
- [53] C. Sandvik. (2010, Accessed on 22/4/2017). Titanium alloys. 43-74.
- [54] S. Sharif, E. Rahim, and H. Sasahara, "Machinability of titanium alloys in drilling," in *Titanium Alloys-Towards Achieving Enhanced Properties for Diversified Applications*, ed: InTech, 2012.
- [55] Z. Liu, Q. An, J. Xu, M. Chen, and S. Han, "Wear performance of (nc-ALTiN)/(a-Si₃N₄) coating and (nc-AlCrN)/(a-Si₃N₄) coating in high-speed machining of titanium alloys under dry and minimum quantity lubrication (MQL) conditions," *Wear*, vol. 305, pp. 249-259, 7/30/ 2013.
-

-
- [56] Y. Su, N. He, L. Li, and X. L. Li, "An experimental investigation of effects of cooling/lubrication conditions on tool wear in high-speed end milling of Ti-6Al-4V," *Wear*, vol. 261, pp. 760-766, 10/20/ 2006.
- [57] M. Bermingham, W. Sim, D. Kent, S. Gardiner, and M. Dargusch, "Tool life and wear mechanisms in laser assisted milling Ti-6Al-4V," *Wear*, vol. 322-323, pp. 151-163, 1/15/ 2015.
- [58] X. Cai, Z. Liu, M. Chen, and Q. An, "An experimental investigation on effects of minimum quantity lubrication oil supply rate in high-speed end milling of Ti-6Al-4V," *Proceedings of the Institution of Mechanical Engineers, Part B: Journal of Engineering Manufacture*, p. 0954405412458492, 2012.
- [59] S. Pervaiz, I. Deiab, A. Rashid, M. Nicolescu, and H. Kishawy, "Performance evaluation of different cooling strategies when machining Ti-6Al-4V," *Advanced Manufacturing Engineering and Technologies NEWTECH 2013 Stockholm, Sweden 27-30 October 2013*, p. 21, 2013.
- [60] P. Priarone, M. Robiglio, L. Settineri, and V. Tebaldo, "Effectiveness of minimizing cutting fluid use when turning difficult-to-cut alloys," *Procedia CIRP*, vol. 29, pp. 341-346, 2015/01/01/ 2015.
- [61] J. Sun, Y. Wong, M. Rahman, Z. Wang, K. Neo, C. Tan, *et al.*, "Effects of coolant supply methods and cutting conditions on tool life in end milling titanium alloy," *Machining Science and Technology*, vol. 10, pp. 355-370, 2006.
- [62] A. Mohsan, Z. Liu, and G. Padhy, "A review on the progress towards improvement in surface integrity of Inconel 718 under high pressure and flood cooling conditions," *The International Journal of Advanced Manufacturing Technology*, vol. 91, pp. 107-125, July 01 2017.
- [63] A. Patil and I. Sushil, *Machining Challenges in Ti-6Al-4V. A Review* vol. 5, 2015.
- [64] M. Bakar, R. Abdullah, M. Ali, K. Jusoff, H. Sivarao, N. Hussein, *et al.*, "Machining performance of Ti-6Al-4V titanium alloy assisted by high pressure waterjet," *methods*, vol. 4, p. 5, 2013.
- [65] S. Oliaei and Y. Karpat, "Investigating the influence of built-up edge on forces and surface roughness in micro scale orthogonal machining of titanium alloy Ti6Al4V," *Journal of Materials Processing Technology*, vol. 235, pp. 28-40, 2016/09/01/ 2016.
- [66] J. Chen and Q. Zhao, "A model for predicting surface roughness in single-point diamond turning," *Measurement*, vol. 69, pp. 20-30, 2015.
- [67] J. Sun and Y. Guo, "A comprehensive experimental study on surface integrity by end milling Ti-6Al-4V," *Journal of Materials Processing Technology*, vol. 209, pp. 4036-4042, 2009.
- [68] J. Hughes, A. Sharman, and K. Ridgway, "The effect of cutting tool material and edge geometry on tool life and workpiece surface integrity," *Proceedings of the*
-

-
- Institution of Mechanical Engineers, Part B: Journal of Engineering Manufacture*, vol. 220, pp. 93-107, 2006.
- [69] J. Cantero, M. Tardio, J. Canteli, M. Marcos, and M. Miguelez, "Dry drilling of alloy Ti-6Al-4V," *International Journal of Machine Tools and Manufacture*, vol. 45, pp. 1246-1255, 2005.
- [70] G. Revankar, R. Shetty, S. Rao, and V. Gaitonde, "Analysis of surface roughness and hardness in titanium alloy machining with polycrystalline diamond tool under different lubricating modes," *Materials Research*, vol. 17, pp. 1010-1022, 2014.
- [71] A. Antonialli, A. Diniz, and H. Neto, "Tool life and machined surface damage on titanium alloy milling using different cooling-lubrication conditions," 2009.
- [72] K. Edkins, N. Rensburg, and R. Laubscher, "Evaluating the Subsurface Microstructure of Machined Ti-6Al-4V," *Procedia CIRP*, vol. 13, pp. 270-275, 2014/01/01/ 2014.
- [73] C. Che-Haron and A. Jawaid, "The effect of machining on surface integrity of titanium alloy Ti-6% Al-4% V," *Journal of Materials Processing Technology*, vol. 166, pp. 188-192, 8/1/ 2005.
- [74] E. Rahim and S. Sharif, "Investigation on tool life and surface integrity when drilling Ti-6Al-4V and Ti-5Al-4V-Mo/Fe," *JSME International Journal Series C Mechanical Systems, Machine Elements and Manufacturing*, vol. 49, pp. 340-345, 2006.
- [75] J. Velásquez, A. Tidu, B. Bolle, P. Chevrier, and J. Fundenberger, "Sub-surface and surface analysis of high speed machined Ti-6Al-4V alloy," *Materials Science and Engineering: A*, vol. 527, pp. 2572-2578, 2010/04/25/ 2010.
- [76] A. Ginting and M. Nouari, "Surface integrity of dry machined titanium alloys," *International Journal of Machine Tools and Manufacture*, vol. 49, pp. 325-332, 3// 2009.
- [77] K. Moussaoui, M. Mousseigne, J. Senatore, R. Chieragatti, and F. Monies, "Influence of milling on surface integrity of Ti6Al4V—study of the metallurgical characteristics: microstructure and microhardness," *The International Journal of Advanced Manufacturing Technology*, pp. 1-13, 2013.
- [78] E. Ezugwu, J. Bonney, R. Da Silva, and O. Cakir, "Surface integrity of finished turned Ti-6Al-4V alloy with PCD tools using conventional and high pressure coolant supplies," *International Journal of Machine Tools and Manufacture*, vol. 47, pp. 884-891, 2007.
- [79] R. Bejjani, M. Balazinski, H. Attia, P. Plamondon, and G. L'Espérance, "Chip formation and microstructure evolution in the adiabatic shear band when machining titanium metal matrix composites," *International Journal of Machine Tools and Manufacture*, vol. 109, pp. 137-146, 2016/10/01/ 2016.
-

-
- [80] H. Toenshoff and B. Denkena, "Chip formation," in *Basic of Cutting and Abrasive Processed* Berlin Heidelberg: Springer-Verlag Berlin Heidelberg, 2013, pp. 21-36.
- [81] A. Li, J. Zhao, Y. Zhou, X. Chen, and D. Wang, "Experimental investigation on chip morphologies in high-speed dry milling of titanium alloy Ti-6Al-4V," *The International Journal of Advanced Manufacturing Technology*, vol. 62, pp. 933-942, 2012.
- [82] F. Ducobu, E. Rivière-Lorphèvre, and E. Filippi, "Numerical contribution to the comprehension of saw-toothed Ti6Al4V chip formation in orthogonal cutting," *International Journal of Mechanical Sciences*, vol. 81, pp. 77-87, 2014/04/01/ 2014.
- [83] T. Seshacharyulu, S. Medeiros, J. Morgan, J. Malas, W. Frazier, and Y. Prasad, "Hot deformation and microstructural damage mechanisms in extra-low interstitial (ELI) grade Ti-6Al-4V," *Materials Science and Engineering: A*, vol. 279, pp. 289-299, 2000.
- [84] Q. Yang, Y. Wu, D. Liu, L. Chen, D. Lou, Z. Zhai, *et al.*, "Characteristics of serrated chip formation in high-speed machining of metallic materials," *The International Journal of Advanced Manufacturing Technology*, vol. 86, pp. 1201-1206, 2016.
- [85] S. Sun, M. Brandt, and M. Dargusch, "Characteristics of cutting forces and chip formation in machining of titanium alloys," *International Journal of Machine Tools and Manufacture*, vol. 49, pp. 561-568, 2009/06/01/ 2009.
- [86] X. Zhang, R. Shivpuri, and A. Srivastava, "Role of phase transformation in chip segmentation during high speed machining of dual phase titanium alloys," *Journal of Materials Processing Technology*, vol. 214, pp. 3048-3066, 2014.
- [87] J. Vieira, Á. Machado, and E. Ezugwu, "Performance of cutting fluids during face milling of steels," *Journal of Materials Processing Technology*, vol. 116, pp. 244-251, 10/24/ 2001.
- [88] G. Augustin, T. Zigman, S. Davila, T. Udiljak, T. Staroveski, D. Brezak, *et al.*, "Cortical bone drilling and thermal osteonecrosis," *Clinical Biomechanics*, vol. 27, pp. 313-325, 5// 2012.
- [89] E. Kuram, B. Ozcelik, E. Demirbas, and E. Sik, "Effects of the cutting fluid types and cutting parameters on surface roughness and thrust force," in *Proceedings of the World Congress on Engineering*, 2010.
- [90] J. Byers, *Metalworking fluids*, Second Edition ed.: CRC Press, Hoboken, 2006.
- [91] V. P. Astakhov, "Cutting Fluids (Coolants) and Their Application in Deep-Hole Machining," ed, 2007.
- [92] S. El Wakil, *Processes and design for manufacturing*: Prentice-Hall, 1989.
-

-
- [93] J. J. Eppert, K. L. Gunter, and J. W. Sutherland, "Development of Cutting Fluid Classification System Using Cluster Analysis," *Tribology transactions*, vol. 44, pp. 375-382, 2001.
- [94] J. A. Schey, *Introduction to manufacturing processes* vol. 2: McGraw-Hill New York etc., 1987.
- [95] M. P. Groover, *Fundamentals of modern manufacturing: materials processes, and systems*: John Wiley & Sons, 2007.
- [96] H. Kishawy and M. Elbestawi, "Effect of process parameters on chip morphology when machining hardened steel," in *Proc. IMECE, ASME*, 1997, pp. 13-20.
- [97] R. Crafoord, J. Kaminski, S. Lagerberg, O. Ljungkrona, and A. Wretland, "Chip control in tube turning using a high-pressure water jet," *Proceedings of the Institution of Mechanical Engineers, Part B: Journal of Engineering Manufacture*, vol. 213, pp. 761-767, 1999.
- [98] E. Benedicto, D. Carou, and E. M. Rubio, "Technical, economic and environmental review of the lubrication/cooling systems used in machining processes," *Procedia Engineering*, vol. 184, pp. 99-116, // 2017.
- [99] E. Kuram, B. Ozcelik, M. Bayramoglu, E. Demirbas, and B. Simsek, "Optimization of cutting fluids and cutting parameters during end milling by using D-optimal design of experiments," *Journal of Cleaner Production*, vol. 42, pp. 159-166, 3// 2013.
- [100] S. Debnath, M. Reddy, and Q. Yi, "Environmental friendly cutting fluids and cooling techniques in machining: a review," *Journal of Cleaner Production*.
- [101] Y. Shashidhara and S. Jayaram, "Vegetable oils as a potential cutting fluid—an evolution," *Tribology International*, vol. 43, pp. 1073-1081, 2010.
- [102] W. Bartz, "Lubricants and the environment," *Tribology international*, vol. 31, pp. 35-47, 1998.
- [103] J. Zimmerman, A. Clarens, K. Hayes, and S. Skerlos, "Design of hard water stable emulsifier systems for petroleum-and bio-based semi-synthetic metalworking fluids," *Environmental science & technology*, vol. 37, pp. 5278-5288, 2003.
- [104] L. Smith and P. Ball, "Steps towards sustainable manufacturing through modelling material, energy and waste flows," *International Journal of Production Economics*, vol. 140, pp. 227-238, 11// 2012.
- [105] E. O. Bennett, "Water based cutting fluids and human health," *Tribology International*, vol. 16, pp. 133-136, 6// 1983.
- [106] S. Skerlos, "Prevention of metalworking fluid pollution: Environmentaaly conscious manufacturing at the machine tool," in *Environmentaaly Conscious Manufacturing*, ed The university of Michigan at Ann Arbor, USA: The university of Michigan at Ann Arbor, 2006, p. 95.
-

-
- [107] Y. Shokoohi, E. Khosrojerdi, and B. Shiadhi, "Machining and ecological effects of a new developed cutting fluid in combination with different cooling techniques on turning operation," *Journal of Cleaner Production*.
- [108] N. Fox and G. Stachowiak, "Vegetable oil-based lubricants—A review of oxidation," *Tribology international*, vol. 40, pp. 1035-1046, 2007.
- [109] M. Alam, D. Akram, E. Sharmin, F. Zafar, and S. Ahmad, "Vegetable oil based eco-friendly coating materials: A review article," *Arabian Journal of Chemistry*, vol. 7, pp. 469-479, 9// 2014.
- [110] W. Castro, D. Weller, K. Cheenkachorn, and J. Perez, "The effect of chemical structure of basefluids on antiwear effectiveness of additives," *Tribology international*, vol. 38, pp. 321-326, 2005.
- [111] A. Zeman, A. Sprengel, D. Niedermeier, and M. Späth, "Biodegradable lubricants—studies on thermo-oxidation of metal-working and hydraulic fluids by differential scanning calorimetry (DSC)," *Thermochimica Acta*, vol. 268, pp. 9-15, 12/15/ 1995.
- [112] E. Kuram, B. Ozcelik, and E. Demirbas, "Environmentally friendly machining: vegetable based cutting fluids," in *Green Manufacturing Processes and Systems*, ed: Springer, 2013, pp. 23-47.
- [113] H. Wagner, R. Luther, and T. Mang, "Lubricant base fluids based on renewable raw materials: Their catalytic manufacture and modification," *Applied Catalysis A: General*, vol. 221, pp. 429-442, 11/30/ 2001.
- [114] M. Maleque, H. Masjuki, and S. Sapuan, "Vegetable-based biodegradable lubricating oil additives," *Industrial lubrication and Tribology*, vol. 55, pp. 137-143, 2003.
- [115] U. Krahenbuhl and N. Goshen. (2002, 15/3/2017). Vegetable oil-based coolants improve cutting performance. *68(12)*, 34.
- [116] M. Siniawski, N. Saniei, B. Adhikari, and L. Doezema, "Influence of fatty acid composition on the tribological performance of two vegetable-based lubricants," *Journal of Synthetic Lubrication*, vol. 24, pp. 101-110, 2007.
- [117] G. Burton, C. Goo, Y. Zhang, and M. Jun, "Use of vegetable oil in water emulsion achieved through ultrasonic atomization as cutting fluids in micro-milling," *Journal of Manufacturing Processes*, vol. 16, pp. 405-413, 8// 2014.
- [118] L. Quinchia, M. Delgado, T. Reddyhoff, C. Gallegos, and H. Spikes, "Tribological studies of potential vegetable oil-based lubricants containing environmentally friendly viscosity modifiers," *Tribology International*, vol. 69, pp. 110-117, 1// 2014.
- [119] P. Nagendramma and S. Kaul, "Development of ecofriendly/biodegradable lubricants: An overview," *Renewable and Sustainable Energy Reviews*, vol. 16, pp. 764-774, 1// 2012.
-

-
- [120] J. de oliveira, "Vegetable based cuttinf fluid-an envirnomental alternative to grinding process," presented at the 15th CIRP International Conference on Life Cycle Engineering 2008.
- [121] K. Geiser and E. Massawe, "The Dilemma of Promoting Green Products: What We know and Don't Know About Biobased Metalworking Fluids," *Journal of Environmental Health*, vol. 74, 2012.
- [122] J. Coupland and D. McClements, "Physical properties of liquid edible oils," *Journal of the American Oil Chemists' Society*, vol. 74, pp. 1559-1564, 1997.
- [123] S. Lawal, I. Choudhury, and Y. Nukman, "A critical assessment of lubrication techniques in machining processes: a case for minimum quantity lubrication using vegetable oil-based lubricant," *Journal of Cleaner Production*, vol. 41, pp. 210-221, 2// 2013.
- [124] S. Lawal, I. Choudhury, and Y. Nukman, "Developments in the formulation and application of vegetable oil-based metalworking fluids in turning process," *The International Journal of Advanced Manufacturing Technology*, vol. 67, pp. 1765-1776, 2013/07/01 2013.
- [125] A. Diniz and R. Micaroni, "Influence of the direction and flow rate of the cutting fluid on tool life in turning process of AISI 1045 steel," *International Journal of Machine Tools and Manufacture*, vol. 47, pp. 247-254, 2// 2007.
- [126] E. Thorne. (2014, Accessed on 23/3/2017). *Liquid cool*. Available: <https://www.ctemag.com/news-videos/articles/liquid-cool>
- [127] Á. Machado and J. Wallbank, "The effects of a high-pressure coolant jet on machining," *Proceedings of the Institution of Mechanical Engineers, Part B: Journal of Engineering Manufacture*, vol. 208, pp. 29-38, 1994.
- [128] I. Cole, "Mist characterization in drilling 1018 Steel," MSc, North Texas, North Texas University, 2012.
- [129] J. Dasch, C. Ang, M. Mood, and D. Knowles, "Variables affecting mist generation from metal removal fluids," *Tribology & Lubrication Technology*, vol. 58, p. 10, 2002.
- [130] U. Dixit, D. Sarma, and P. Davim, "Machining with minimal cutting fluid," in *Environmentally Friendly Machining*, ed: Springer, 2012, pp. 9-17.
- [131] D. Babic, D. Murray, and A. Torrance, "Mist jet cooling of grinding processes," *International Journal of Machine Tools and Manufacture*, vol. 45, pp. 1171-1177, 8// 2005.
- [132] O. Çakır, M. Kıyak, and E. Altan, "Comparison of gases applications to wet and dry cuttings in turning," *Journal of Materials Processing Technology*, vol. 153-154, pp. 35-41, 11/10/ 2004.
- [133] M. Stanford, P. Lister, C. Morgan, and K. Kibble, "Investigation into the use of gaseous and liquid nitrogen as a cutting fluid when turning BS 970-80A15
-

-
- (En32b) plain carbon steel using WC–Co uncoated tooling," *Journal of Materials Processing Technology*, vol. 209, pp. 961-972, 1/19/ 2009.
- [134] E. Altan, M. Kiyak, and O. Cakir, "The effect of oxygen gas application into cutting zone on machining," in *Proceedings of Sixth Biennial Conference on Engineering system Design and Analysis (ESDA2002), Istanbul, 2002*, pp. 1-5.
- [135] A. Jayal and A. Balaji, "Effects of cutting fluid application on tool wear in machining: Interactions with tool-coatings and tool surface features," *Wear*, vol. 267, pp. 1723-1730, 9/9/ 2009.
- [136] P. Sreejith, "Machining of 6061 aluminium alloy with MQL, dry and flooded lubricant conditions," *Materials Letters*, vol. 62, pp. 276-278, 1/31/ 2008.
- [137] Y. Kamata and T. Obikawa, "High speed MQL finish-turning of Inconel 718 with different coated tools," *Journal of Materials Processing Technology*, vol. 192–193, pp. 281-286, 10/1/ 2007.
- [138] N. Dhar, M. Ahmed, and S. Islam, "An experimental investigation on effect of minimum quantity lubrication in machining AISI 1040 steel," *International Journal of Machine Tools and Manufacture*, vol. 47, pp. 748-753, 4// 2007.
- [139] L. Barczak, A. Batako, and M. Morgan, "A study of plane surface grinding under minimum quantity lubrication (MQL) conditions," *International Journal of Machine Tools and Manufacture*, vol. 50, pp. 977-985, 11// 2010.
- [140] S. Chinchankar and S. Choudhury, "Hard turning using HiPIMS-coated carbide tools: Wear behavior under dry and minimum quantity lubrication (MQL)," *Measurement*, vol. 55, pp. 536-548, 9// 2014.
- [141] Y. Kaynak, "Evaluation of machining performance in cryogenic machining of Inconel 718 and comparison with dry and MQL machining," *The International Journal of Advanced Manufacturing Technology*, vol. 72, pp. 919-933, 2014.
- [142] Y. Yildiz and M. Nalbant, "A review of cryogenic cooling in machining processes," *International Journal of Machine Tools and Manufacture*, vol. 48, pp. 947-964, 7// 2008.
- [143] S. Paul and A. Chattopadhyay, "A study of effects of cryo-cooling in grinding," *International Journal of Machine Tools and Manufacture*, vol. 35, pp. 109-117, 1// 1995.
- [144] G. Chetan, S. Ghosh, and P. Venkateswara Rao, "Application of sustainable techniques in metal cutting for enhanced machinability: a review," *Journal of Cleaner Production*, vol. 100, pp. 17-34, 2015/08/01/ 2015.
- [145] A. Richer. (2017, 01/02/2015) Cryogenic machining systems can extend tool life and reduce cycle times. *Cutting Tool Engineering*.
- [146] S. Raykar, D. D'Addona, and D. Kramar, "Analysis of surface topology in dry machining of EN-8 Steel," *Procedia Materials Science*, vol. 6, pp. 931-938, 2014/01/01/ 2014.
-

-
- [147] Y. Zhang and M. Jun, "Mixed jet of independently atomized water and oil sprays as cutting fluids in micro-milling," *Manufacturing Letters*, vol. 1, pp. 13-16, 10// 2013.
- [148] Y. Shashidhara and S. Jayaram, "Experimental determination of cutting power for turning and material removal rate for drilling of AA 6061-T6 using vegetable oils as cutting fluid," *Advances in Tribology*, vol. 2013, 2013.
- [149] S. Ojolo, M. Amuda, O. Ogunmola, and C. Ononiwu, "Experimental determination of the effect of some straight biological oils on cutting force during cylindrical turning," *Matéria (Rio de Janeiro)*, vol. 13, pp. 650-663, 2008.
- [150] M. Xavier and M. Adithan, "Determining the influence of cutting fluids on tool wear and surface roughness during turning of AISI 304 austenitic stainless steel," *Journal of Materials Processing Technology*, vol. 209, pp. 900-909, 2009.
- [151] P. Vamsi Krishna, R. Srikant, and D. Nageswara Rao, "Experimental investigation on the performance of nanoboric acid suspensions in SAE-40 and coconut oil during turning of AISI 1040 steel," *International Journal of Machine Tools and Manufacture*, vol. 50, pp. 911-916, 10// 2010.
- [152] S. Lawal, I. Choudhury, and Y. Nukman, "Evaluation of vegetable and mineral oil-in-water emulsion cutting fluids in turning AISI 4340 steel with coated carbide tools," *Journal of Cleaner Production*, vol. 66, pp. 610-618, 3/1/ 2014.
- [153] R. Avila and A. Abrao, "The effect of cutting fluids on the machining of hardened AISI 4340 steel," *Journal of Materials Processing Technology*, vol. 119, pp. 21-26, 2001.
- [154] S. Chinchankar, A. Salve, P. Netake, A. More, S. Kendre, and R. Kumar, "Comparative evaluations of surface roughness during hard turning under dry and with water-based and vegetable oil-based cutting fluids," *Procedia Materials Science*, vol. 5, pp. 1966-1975, // 2014.
- [155] G. Perera, H. Herath, I. Perera, and M. Medagoda, "Investigation on white coconut oil to use as a metal working fluid during turning," *Proceedings of the Institution of Mechanical Engineers, Part B: Journal of Engineering Manufacture*, p. 0954405414525610, 2014.
- [156] B. Ozcelik, E. Kuram, M. Huseyin Cetin, and E. Demirbas, "Experimental investigations of vegetable based cutting fluids with extreme pressure during turning of AISI 304L," *Tribology International*, vol. 44, pp. 1864-1871, 11// 2011.
- [157] S. Kolawole and J. Odusote, "Performance evaluation of vegetable oil-based cutting fluids in mild steel machining," *Chemistry and Materials Research*, vol. 3, pp. 35-45, 2013.
- [158] N. Ibrahim, M. Sudin, and M. Nor, "Investigation on the effect of crude palm oil (CPO) on the cutting forces, surface roughness and tool wear in turning SS304," in *National Postgraduate Conference (NPC), 2011*, 2011, pp. 1-6.
-

-
- [159] S. Rohit and P. Kupan, "Experimental investigation of vegetable oil-based cutting fluid during turning of SS316L," *International Journal on Mechanical Engineering and Robotics (IJMER)*, vol. 1, 2013.
- [160] P. Kulkarni and S. Harihar, "An experimental investigation of effect of cutting fluids on chip formation and cycletime in turning of EN-24 and EN-31 material," *International Journal of Engineering Sciences & Research Technology*, vol. 3, pp. 574-582, November 2014.
- [161] W. Belluco and L. De Chiffre, "Surface integrity and part accuracy in reaming and tapping stainless steel with new vegetable based cutting oils," *Tribology International*, vol. 35, pp. 865-870, 12// 2002.
- [162] S. Alves and J. de Oliveira, "Development of new cutting fluid for grinding process adjusting mechanical performance and environmental impact," *Journal of materials processing technology*, vol. 179, pp. 185-189, 2006.
- [163] J. Kelly and M. Cotterell, "Minimal lubrication machining of aluminium alloys," *Journal of Materials Processing Technology*, vol. 120, pp. 327-334, 1/15/ 2002.
- [164] M. Rahman, A. Senthil Kumar, and M. Salam, "Experimental evaluation on the effect of minimal quantities of lubricant in milling," *International Journal of Machine Tools and Manufacture*, vol. 42, pp. 539-547, 4// 2002.
- [165] F. Itoigawa, T. Childs, T. Nakamura, and W. Belluco, "Effects and mechanisms in minimal quantity lubrication machining of an aluminum alloy," *Wear*, vol. 260, pp. 339-344, 2/10/ 2006.
- [166] M. Hadad and M. Hadi, "An investigation on surface grinding of hardened stainless steel S34700 and aluminum alloy AA6061 using minimum quantity of lubrication (MQL) technique," *The International Journal of Advanced Manufacturing Technology*, vol. 68, pp. 2145-2158, 2013.
- [167] M. Khan, M. Mithu, and N. Dhar, "Effects of minimum quantity lubrication on turning AISI 9310 alloy steel using vegetable oil-based cutting fluid," *Journal of Materials Processing Technology*, vol. 209, pp. 5573-5583, 8/1/ 2009.
- [168] T. Obikawa, Y. Kamata, and J. Shinozuka, "High-speed grooving with applying MQL," *International Journal of Machine Tools and Manufacture*, vol. 46, pp. 1854-1861, 11// 2006.
- [169] A. Pathan and M. Kadam, "Experimental study on effect of cutting parameters on chip-tool interface temperature and chip formation in turning EN-31 hardened steel under flooded and MQL conditions," *International Journal of Innovative Science, Engineering & Technology*, vol. Vol. 2, 2015.
- [170] R. Da Silva, J. Vieira, R. Cardoso, H. Carvalho, E. Costa, A. Machado, *et al.*, "Tool wear analysis in milling of medium carbon steel with coated cemented carbide inserts using different machining lubrication/cooling systems," *Wear*, vol. 271, pp. 2459-2465, 7/29/ 2011.
-

-
- [171] G. Mendoza, A. Igartua, I. Arizaga, F. Aspiazu, and G. Santiso, "Metal working fluids based on vegetable oils for grinding operations," *Journal of Mechanical Engineering and Automation*, 2012.
- [172] S. Safian, M. Hisyam, and S. Aman, "Evaluation of vegetable oil as an alternative cutting lubricant when end milling martensitic stainless steel using uncoated carbide tool.," *Manufacturing Technology* vol. 3, pp. 49-56, 2009.
- [173] B. Davoodi and A. Tazehkandi, "Experimental investigation and optimization of cutting parameters in dry and wet machining of aluminum alloy 5083 in order to remove cutting fluid," *Journal of Cleaner Production*, vol. 68, pp. 234-242, 4/1/ 2014.
- [174] S. Ojolo and O. Ohunakin, "Study of rake face action on cutting using palm-kernel oil as lubricant," *Journal of Emerging Trends in Engineering and Applied Sciences (JETEAS)*, vol. 2, pp. 30-35, 2011.
- [175] S. Sharif, N. Mohd Yusof, M. Idris, Z. Ahmad, I. Sudin, A. Ripin, *et al.*, "Feasibility study of using vegetable oil as a cutting lubricant through the use of minimum quantity lubricant during machining," 2009.
- [176] W. Belluco and L. De Chiffre, "Performance evaluation of vegetable-based oils in drilling austenitic stainless steel," *Journal of Materials Processing Technology*, vol. 148, pp. 171-176, 5/15/ 2004.
- [177] K. Li and S. Chou, "Experimental evaluation of minimum quantity lubrication in near micro-milling," *Journal of Materials Processing Technology*, vol. 210, pp. 2163-2170, 11/19/ 2010.
- [178] S. Settu and M. Nandagopal, "Experimental investigation on performance of milling operation using vegetable oil-based nano cutting fluid and its process parameters optimization using Taguchi and ANOVA," 2014.
- [179] A. Yassin and C. Teo, "Effect of pressure and nozzle angle of minimal quantity lubrication on cutting temperature and tool wear in turning," *Applied Mechanics & Materials*, 2014.
- [180] T. Le, M. Tran, D. Nguyen, and V. Nguyen, "An investigation on effect of characteristics of the peanut oil MQL on tool life in hard turning 9CrSi steel," *International Journal of Machining and Machinability of Materials*, vol. 13, pp. 428-438, 2013.
- [181] D. Kramar, P. Krajnik, and J. Kopac, "Capability of high pressure cooling in the turning of surface hardened piston rods," *Journal of Materials Processing Technology*, vol. 210, pp. 212-218, 1/19/ 2010.
- [182] A. Tazehkandi, F. Pilehvarian, and B. Davoodi, "Experimental investigation on removing cutting fluid from turning of Inconel 725 with coated carbide tools," *Journal of Cleaner Production*, vol. 80, pp. 271-281, 10/1/ 2014.
- [183] M. Ramana, G. Rao, and D. Rao, "Effect of process parameters on surface roughness in turning of titanium alloy under different conditions of lubrication,"
-

-
- Recent Advanced in Robotics, Aeronautical and Mechanical Engineering*, pp. 83-91, 2013.
- [184] M. Balažic and J. Kopač, "Machining of titanium alloy Ti-6Al-4V for biomedical applications," *Strojniški vestnik-Journal of Mechanical Engineering*, vol. 56, pp. 202-206, 2010.
- [185] E. Rahim and H. Sasahara, "An analysis of surface integrity when drilling inconel 718 using palm oil and synthetic ester under MQL condition," *Machining Science and Technology*, vol. 15, pp. 76-90, 2011.
- [186] D. Stephenson, S. Skerlos, A. King, and S. Supekar, "Rough turning Inconel 750 with supercritical CO₂-based minimum quantity lubrication," *Journal of Materials Processing Technology*, vol. 214, pp. 673-680, 3// 2014.
- [187] E. Rahim and H. Sasahara, "A study of the effect of palm oil as MQL lubricant on high speed drilling of titanium alloys," *Tribology International*, vol. 44, pp. 309-317, 3// 2011.
- [188] P. Priarone, M. Robiglio, L. Settineri, and V. Tebaldo, "Milling and turning of titanium aluminides by using minimum quantity lubrication," *Procedia CIRP*, vol. 24, pp. 62-67, // 2014.
- [189] X. Qin, L. Gui, H. Li, B. Rong, D. Wang, H. Zhang, *et al.*, "Feasibility study on the minimum quantity lubrication in high-speed helical milling of Ti-6Al-4V," *Journal of Advanced Mechanical Design, Systems, and Manufacturing*, vol. 6, pp. 1222-1233, 2012.
- [190] M. Sadeghi, M. Haddad, T. Tawakoli, and M. Emami, "Minimal quantity lubrication-MQL in grinding of Ti-6Al-4V titanium alloy," *The International Journal of Advanced Manufacturing Technology*, vol. 44, pp. 487-500, 2009.
- [191] E. Vazquez, J. Gomar, J. Ciurana, and C. Rodríguez, "Analyzing effects of cooling and lubrication conditions in micromilling of Ti6Al4V," *Journal of Cleaner Production*, vol. 87, pp. 906-913, 1/15/ 2015.
- [192] S. Thamizhmani and S. Rosli, "A study of minimum quantity lubrication on Inconel 718 steel," *Archives of Materials Science and Engineering*, vol. 39, pp. 38-44, September 2009 2009.
- [193] S. Zhang, J. Li, and Y. Wang, "Tool life and cutting forces in end milling Inconel 718 under dry and minimum quantity cooling lubrication cutting conditions," *Journal of Cleaner Production*, vol. 32, pp. 81-87, 9// 2012.
- [194] C. Wang, M. Chen, Q. An, M. Wang, and Y. Zhu, "Tool wear performance in face milling Inconel 182 using minimum quantity lubrication with different nozzle positions," *International journal of precision engineering and manufacturing*, vol. 15, pp. 557-565, 2014.
- [195] İ. Uçun, K. Aslantaş, and F. Bedir, "The effect of minimum quantity lubrication and cryogenic pre-cooling on cutting performance in the micro milling of Inconel
-

-
- 718," *Proceedings of the Institution of Mechanical Engineers, Part B: Journal of Engineering Manufacture*, p. 0954405414546144, 2014.
- [196] V. Vasu and G. Reddy, "Effect of minimum quantity lubrication with Al₂O₃ nanoparticles on surface roughness, tool wear and temperature dissipation in machining Inconel 600 alloy," *Proceedings of the Institution of Mechanical Engineers, Part N: Journal of Nanoengineering and Nanosystems*, vol. 225, pp. 3-16, 2011.
- [197] M. Okada, A. Hosokawa, N. Asakawa, and T. Ueda, "End milling of stainless steel and titanium alloy in an oil mist environment," *The International Journal of Advanced Manufacturing Technology*, vol. 74, pp. 1255-1266, 2014.
- [198] A. Tazehkandi, M. Shabgard, and F. Pilehvarian, "Application of liquid nitrogen and spray mode of biodegradable vegetable cutting fluid with compressed air in order to reduce cutting fluid consumption in turning Inconel 740," *Journal of Cleaner Production*, vol. 108, pp. 90-103, 2015/12/01/ 2015.
- [199] W. Sales, J. Schoop, and I. Jawahir, "Tribological behavior of PCD tools during superfinishing turning of the Ti6Al4V alloy using cryogenic, hybrid and flood as lubri-coolant environments," *Tribology International*, vol. 114, pp. 109-120, 10// 2017.
- [200] H. Lin, C. Wang, Y. Yuan, Z. Chen, Q. Wang, and W. Xiong, "Tool wear in Ti-6Al-4V alloy turning under oils on water cooling comparing with cryogenic air mixed with minimal quantity lubrication," *The International Journal of Advanced Manufacturing Technology*, vol. 81, pp. 87-101, 2015.
- [201] I. Deiab, S. Raza, and S. Pervaiz, "Analysis of lubrication strategies for sustainable machining during turning of titanium Ti-6Al-4V alloy," *Procedia CIRP*, vol. 17, pp. 766-771, // 2014.
- [202] Y. Kaynak, H. Karaca, R. Noebe, and I. Jawahir, "Tool-wear analysis in cryogenic machining of NiTi shape memory alloys: A comparison of tool-wear performance with dry and MQL machining," *Wear*, vol. 306, pp. 51-63, 8/30/ 2013.
- [203] N. Madanchi, M. Winter, S. Thiede, and C. Herrmann, "Energy Efficient Cutting Fluid Supply: The Impact of Nozzle Design," *Procedia CIRP*, vol. 61, pp. 564-569, 2017.
- [204] M. Morgan, A. Jackson, H. Wu, V. Baines-Jones, A. Batako, and W. Rowe, "Optimisation of fluid application in grinding," *CIRP Annals - Manufacturing Technology*, vol. 57, pp. 363-366, 2008/01/01/ 2008.
- [205] J. Webster, "Improving surface integrity and economics of grinding by optimum coolant application, with consideration of abrasive tool and process regime," *Proceedings of the institution of mechanical engineers, Part B: journal of engineering manufacture*, vol. 221, pp. 1665-1675, 2007.
- [206] Filtermist. (Accessed on 06/02/2018). *Loc-Line Coolant Hose*. Available: <http://www.filtermist.co.uk/products/coolant-control/loc-line-modular-hose.aspx>
-

-
- [207] M. Morgan and V. Baines-Jones, "On the coherent length of fluid nozzles in grinding," *Key Engineering Materials*, vol. 404, pp. 61-67, 2009.
- [208] E. Rouly, R. Bauer, and A. Warkentin, "An investigation into the effect of nozzle shape and jet pressure in profile creepfeed grinding," *Proceedings of the Institution of Mechanical Engineers, Part B: Journal of Engineering Manufacture*, vol. 231, pp. 1116-1130, 2017.
- [209] R. Irani, R. Bauer, and A. Warkentin, "A review of cutting fluid application in the grinding process," *International Journal of Machine Tools and Manufacture*, vol. 45, pp. 1696-1705, 12// 2005.
- [210] J. Webster. (2008, February 2008) Coolant Calculus. *Cutting Tool Engineering* [Scientific]. 8.
- [211] R. Monici, E. Bianchi, R. Catai, and P. de Aguiar, "Analysis of the different forms of application and types of cutting fluid used in plunge cylindrical grinding using conventional and superabrasive CBN grinding wheels," *International Journal of Machine Tools and Manufacture*, vol. 46, pp. 122-131, 2// 2006.
- [212] Z. Liu, X. Cai, M. Chen, and Q. An, "Investigation of cutting force and temperature of end-milling Ti-6Al-4V with different minimum quantity lubrication (MQL) parameters," *Proceedings of the Institution of Mechanical Engineers, Part B: Journal of Engineering Manufacture*, vol. 225, pp. 1273-1279, 2011.
- [213] L. López de Lacalle, C. Angulo, A. Lamikiz, and J. Sánchez, "Experimental and numerical investigation of the effect of spray cutting fluids in high speed milling," *Journal of Materials Processing Technology*, vol. 172, pp. 11-15, 2/20/ 2006.
- [214] O. Pereira, P. Català, A. Rodríguez, T. Ostra, J. Vivancos, A. Rivero, *et al.*, "The use of hybrid CO₂+MQL in machining operations," *Procedia Engineering*, vol. 132, pp. 492-499, 2015/01/01 2015.
- [215] T. Tawakoli, M. Hadad, and M. Sadeghi, "Influence of oil mist parameters on minimum quantity lubrication – MQL grinding process," *International Journal of Machine Tools and Manufacture*, vol. 50, pp. 521-531, 6// 2010.
- [216] M. Da Silva and J. Wallbank, "Cutting temperature: prediction and measurement methods—a review," *Journal of Materials Processing Technology*, vol. 88, pp. 195-202, 4/15/ 1999.
- [217] M. Kikuchi, "The use of cutting temperature to evaluate the machinability of titanium alloys," *Acta Biomaterialia*, vol. 5, pp. 770-775, 2// 2009.
- [218] G. Le Coz, M. Marinescu, A. Devillez, D. Dudzinski, and L. Velnom, "Measuring temperature of rotating cutting tools: Application to MQL drilling and dry milling of aerospace alloys," *Applied Thermal Engineering*, vol. 36, pp. 434-441, 4// 2012.
-

-
- [219] Q. An, Y. Fu, and J. Xu, "Experimental study on turning of TC9 titanium alloy with cold water mist jet cooling," *International Journal of Machine Tools and Manufacture*, vol. 51, pp. 549-555, 2011.
- [220] B. Nedić and M. Erić, "Cutting temperature measurement and material machinability," *Thermal Science*, vol. 18, pp. 259-268, 2014.
- [221] M. Davies, T. Ueda, R. M'Saoubi, B. Mullany, and A. Cooke, "On the measurement of temperature in material removal processes," *CIRP Annals - Manufacturing Technology*, vol. 56, pp. 581-604, // 2007.
- [222] X. Zhang, K. Yamazaki, and Y. Yamaguchi, "A study on a novel tool temperature measurement method in high-speed machining of titanium," in *Proceedings of the 17th Annual Meeting of the American Society for Precision Engineering, St. Louis, MO, 2002*, pp. 425-428.
- [223] A. Goyal, S. Dhiman, S. Kumar, and R. Sharma, "A Study of experimental temperature measuring techniques used in metal cutting," *Jordan Journal of Mechanical & Industrial Engineering*, vol. 8, 2014.
- [224] P. Conradie, G. Oosthuizen, N. Treurnicht, and A. Al Shaalane, "Overview of work piece temperature measurement techniques for machining of Ti6Al4V," *South African Journal of Industrial Engineering*, vol. 23, pp. 116-130, 2012.
- [225] J. McGhee, L. Michalski, and K. Eckersdorf, *Temperature measurements*, First Edition ed. UK: John Wiley, 1991.
- [226] L. Brandão and R. Coelho, "Temperature and heat flow when tapping of the hardened Steel using different cooling systems," *Ingeniare. Revista chilena de ingeniería*, vol. 17, pp. 267-274, 2009.
- [227] M. Rahman, A. Kumar, and M. Choudhury, "Identification of effective zones for high pressure coolant in milling," *CIRP Annals-Manufacturing Technology*, vol. 49, pp. 47-52, 2000.
- [228] L. Brandão, R. Coelho, and A. Rodrigues, "Experimental and theoretical study of workpiece temperature when end milling hardened steels using (TiAl)N-coated and PcBN-tipped tools," *Journal of Materials Processing Technology*, vol. 199, pp. 234-244, 4/1/ 2008.
- [229] T. Yashiro, T. Ogawa, and H. Sasahara, "Temperature measurement of cutting tool and machined surface layer in milling of CFRP," *International Journal of Machine Tools and Manufacture*, vol. 70, pp. 63-69, 7// 2013.
- [230] G. Pittalà and M. Monno, "A new approach to the prediction of temperature of the workpiece of face milling operations of Ti-6Al-4V," *Applied Thermal Engineering*, vol. 31, pp. 173-180, 2// 2011.
- [231] S. Lin, F. Peng, J. Wen, Y. Liu, and R. Yan, "An investigation of workpiece temperature variation in end milling considering flank rubbing effect," *International Journal of Machine Tools and Manufacture*, vol. 73, pp. 71-86, 10// 2013.
-

-
- [232] T. Aoyama, Y. Kakinuma, M. Yamashita, and M. Aoki, "Development of a new lean lubrication system for near dry machining process," *CIRP Annals - Manufacturing Technology*, vol. 57, pp. 125-128, // 2008.
- [233] Y. Park, D. Ko, K. Yi, I. Petrov, and Y. Kim, "Measurement and estimation of temperature rise in TEM sample during ion milling," *Ultramicroscopy*, vol. 107, pp. 663-668, 8// 2007.
- [234] A. Mamedov and I. Lazoglu, "Thermal analysis of micro milling titanium alloy Ti-6Al-4V," *Journal of Materials Processing Technology*, vol. 229, pp. 659-667, 3// 2016.
- [235] E. Ng, D. Lee, A. Sharman, R. Dewes, D. Aspinwall, and J. Vigneau, "High speed ball nose end milling of Inconel 718," *CIRP Annals-Manufacturing Technology*, vol. 49, pp. 41-46, 2000.
- [236] R. Hood, D. Aspinwall, C. Sage, and W. Voice, "High speed ball nose end milling of γ -TiAl alloys," *Intermetallics*, vol. 32, pp. 284-291, 2013.
- [237] G. Sutter, L. Faure, A. Molinari, N. Ranc, and V. Pina, "An experimental technique for the measurement of temperature fields for the orthogonal cutting in high speed machining," *International Journal of Machine Tools and Manufacture*, vol. 43, pp. 671-678, 2003/05/01/ 2003.
- [238] D. O'Sullivan and M. Cotterell, "Temperature measurement in single point turning," *Journal of Materials Processing Technology*, vol. 118, pp. 301-308, 2001/12/03/ 2001.
- [239] B. Sorana and J. Lorentz, "Design of experiments: Useful orthogonal arrays for number of experiments from 4 to 16," *Entropy*, vol. 9, pp. 198-232, 2007.
- [240] M. Ramana, G. Rao, and D. Rao, "Experimental investigation, optimization of process parameters and mathematical modelling in turning of titanium alloy under different lubricat conditions," *Journal of Engineering (IOSRJEN)*, vol. 2, pp. 86-101, 2012 January 2012.
- [241] M. Cavazzuti, "Design of experiments," in *Optimization methods*, ed: Springer, 2013, pp. 13-42.
- [242] I. Mukherjee and P. Ray, "A review of optimization techniques in metal cutting processes," *Computers & Industrial Engineering*, vol. 50, pp. 15-34, 2006/05/01/ 2006.
- [243] E. Dean, "Design of experiments," ed, 2000.
- [244] D. Montgomery, *Design and analysis of experiments*: Wiley New York, 1984.
- [245] G. Taguchi, S. Chowdhury, and y. Wu, *Taguchi's Quality Engineering Handbook*: Wiley online Library, 2005.
- [246] P. Pallmann and L. Hothorn, "Analysis of means: a generalized approach using R," *Journal of Applied Statistics*, vol. 43, pp. 1541-1560, 2016.
-

-
- [247] J. Ghani, I. Choudhury, and H. Hassan, "Application of Taguchi method in the optimization of end milling parameters," *Journal of Materials Processing Technology*, vol. 145, pp. 84-92, 2004/01/01/ 2004.
- [248] H. Terry, *Manufacturing strategy*. London: Macmillan education Ltd., 1987.
- [249] D. Stephenson and J. Agapiou, "Metal cutting theory and practice," in *Metal cutting theory and practice*, ed Boca Raton, FL, USA: CRC press, 2006, p. 19.
- [250] M. Shaw, *Metal cutting principles* vol. 2: Oxford university press New York, 2005.
- [251] G. Boothroyd and W. A., *Fundamental of machining and machine tool*, 3 rd ed. USA: CRC Press Francis & Taylor, 2005.
- [252] C. AB Sandvik, *Modern metal cutting - A practical handbook*, First Edition ed. Sandviken, Sweden: AB Sandvik Coromant, 1994.
- [253] J. Liu, C. Ren, X. Qin, and H. Li, "Prediction of heat transfer process in helical milling," *The International Journal of Advanced Manufacturing Technology*, vol. 72, pp. 693-705, 2014.
- [254] M. Sato, N. Tamura, and H. Tanaka, "Temperature variation in the cutting tool in end milling," *Journal of Manufacturing Science and Engineering*, vol. 133, p. 021005, 2011.
- [255] X. Cui and J. Guo, "Effects of cutting parameters on tool temperatures in intermittent turning with the formation of serrated chip considered," *Applied Thermal Engineering*, vol. 110, pp. 1220-1229, 1/5/ 2017.
- [256] W. Grzesik, "Chapter nine - Heat in metal cutting," in *Advanced Machining Processes of Metallic Materials (Second Edition)*: Elsevier, 2017, pp. 163-182.
- [257] U. Karaguzel, M. Bakkal, and E. Budak, "Modeling and measurement of cutting temperatures in milling," *Procedia CIRP*, vol. 46, pp. 173-176, 2016/01/01 2016.
- [258] J. Metzger, "Superabrasive grinding," in *Superabrasive Grinding*, 1 st ed. London, UK: Butterworths, March 1986, p. 226.
- [259] V. Luchesi and R. Coelho, "Experimental investigations of heat transfer coefficients of cutting fluids in metal cutting processes: analysis of workpiece phenomena in a given case study," *Proceedings of the Institution of Mechanical Engineers, Part B: Journal of Engineering Manufacture*, p. 244, 2012.
- [260] Aerospace-Kennametal. (Accessed on 15 April 2016). *Titanium machining guide*. Available: <https://www.kennametal.com>
- [261] Titaniummetals. (Accessed on 7/01/2015). *Ti-6Al-4V (ASTM B348 Grade 5)*. Available: https://www.titaniummetals.co.uk/contact_titanium_metals.html
- [262] C. Sandvik. (Accessed on 06/12/2017). *Cutting tool materials*. Available: <https://www.sandvik.coromant.com>
-

-
- [263] O. Stina, "Tool wear in titanium machining," MSc., Mechanical Engineering, UPPSALA, Sweden, 2012.
- [264] C. Daniel, K. Rao, W. Olson, and J. Sutherland, "Effect of cutting fluid properties and application variables on heat transfer in turning and boring operations," in *Proceedings of the Japan—USA Symposium on Flexible Automation*, 1996, pp. 1119-1126.
- [265] PerkinElmer. (Accessed on 28/3/2018). *The PerkinElmer DSC-7 Differential Scanning Calorimeter*. Available: <https://www.labx.com/product/perkin-elmer-dsc-7>
- [266] www.bellflowsystems.co.uk. (Accessed on 22/12/2017). *Flow meters, Oval gear flowmeter*.
- [267] www.omega.co.uk. (Accessed on 22/12/2017). *General Purpose Digital Pressure Gauge (DPG8001)*.
- [268] G. Revankar, R. Shetty, S. Rao, and V. Gaitonde, "Analysis of surface roughness and hardness in titanium alloy machining with polycrystalline diamond tool under different lubricating modes," *Material Research*, vol. 17, pp. p.1010-1022, 2014.
- [269] K. Anil, M. Vikas, B. Teja, and K. Rao, "Effect of cutting parameters on surface finish and machinability of graphite reinforced Al-8011 matrix composite," in *IOP Conference Series: Materials Science and Engineering*, 2017, p. 012025.
- [270] P. Palanisamy, I. Rajendran, and S. Shanmugasundaram, "Prediction of tool wear using regression and ANN models in end-milling operation," *The International Journal of Advanced Manufacturing Technology*, vol. 37, pp. 29-41, 2008.
- [271] M. Namb and P. Davim, "Influence of coolant in machinability of titanium alloy (Ti-6Al-4V)," *Journal of Surface Engineered Materials and Advanced Technology*, vol. 1, p. 9, 2011.
- [272] S. Patil, S. Kekade, K. Phapale, S. Jadhav, A. Powar, A. Supare, *et al.*, "Effect of α and β phase volume fraction on machining characteristics of titanium alloy Ti-6Al-4V," *Procedia Manufacturing*, vol. 6, pp. 63-70, 2016/01/01/ 2016.
- [273] C. Nath, S. Kapoor, A. Srivastava, and J. Iverson, "Effect of fluid concentration in titanium machining with an atomization-based cutting fluid (ACF) spray system," *Journal of Manufacturing Processes*, vol. 15, pp. 419-425, 10// 2013.
- [274] S. Patil, S. Jadhav, S. Kekade, A. Supare, A. Powar, and R. Singh, "The influence of cutting heat on the surface integrity during machining of titanium alloy Ti-6Al-4V," *Procedia Manufacturing*, vol. 5, pp. 857-869, 2016/01/01/ 2016.
- [275] P. Zeman and J. Malý, "Cutting tool development for effective milling of Ti-6Al-4V " presented at the 11th International Conference on High Speed Machining 2014.
- [276] C. Che-Haron, "Tool life and surface integrity in turning titanium alloy," *Journal of Materials Processing Technology*, vol. 118, pp. 231-237, 12/3/ 2001.
-

-
- [277] L. de Angelo Sanchez, G. Palma, I. Marinescu, D. Modolo, L. Nalon, and A. Santos, "Effect of different methods of cutting fluid application on turning of a difficult-to-machine steel (SAE EV-8)," *Proceedings of the Institution of Mechanical Engineers, Part B: Journal of Engineering Manufacture*, vol. 227, pp. 220-234, 2013.
- [278] E. Ezugwu and S. Tang, "Conference of the Irish manufacturing committee on advanced manufacturing technology Surface abuse when machining cast iron (G-17) and nickel-base superalloy (Inconel 718) with ceramic tools," *Journal of Materials Processing Technology*, vol. 55, pp. 63-69, 1995/11/15 1995.
- [279] A. Pramanik, "Problems and solutions in machining of titanium alloys," *The International Journal of Advanced Manufacturing Technology*, vol. 70, pp. 919-928, 2014.
- [280] R. Da Silva, Á. Machado, E. Ezugwu, J. Bonney, and W. Sales, "Tool life and wear mechanisms in high speed machining of Ti-6Al-4V alloy with PCD tools under various coolant pressures," *Journal of Materials Processing Technology*, vol. 213, pp. 1459-1464, 8// 2013.
- [281] J. Aurich, D. Dornfeld, P. Arrazola, V. Franke, L. Leitz, and S. Min, "Burrs—Analysis, control and removal," *CIRP Annals - Manufacturing Technology*, vol. 58, pp. 519-542, // 2009.
- [282] I. Shyha, S. Soo, D. Aspinwall, S. Bradley, R. Perry, P. Harden, *et al.*, "Hole quality assessment following drilling of metallic-composite stacks," *International Journal of Machine Tools and Manufacture*, vol. 51, pp. 569-578, 7// 2011.
- [283] D. Ulutan and T. Ozel, "Machining induced surface integrity in titanium and nickel alloys: A review," *International Journal of Machine Tools and Manufacture*, vol. 51, pp. 250-280, 3// 2011.
- [284] B. Zou, M. Chen, and S. Li, "Study on finish-turning of NiCr20TiAl nickel-based alloy using Al₂O₃/TiN-coated carbide tools," *The International Journal of Advanced Manufacturing Technology*, vol. 53, pp. 81-92, 2011.
- [285] S. Ravi and M. Pradeep Kumar, "Experimental investigations on cryogenic cooling by liquid nitrogen in the end milling of hardened steel," *Cryogenics*, vol. 51, pp. 509-515, 2011/09/01/ 2011.
- [286] A. Amin, A. Ismail, and M. Nor Khairusshima, "Effectiveness of uncoated WC-Co and PCD inserts in end milling of titanium alloy—Ti-6Al-4V," *Journal of Materials Processing Technology*, vol. 192-193, pp. 147-158, 10/1/ 2007.
- [287] A. Molinari, C. Musquar, and G. Sutter, "Adiabatic shear banding in high speed machining of Ti-6Al-4V: experiments and modeling," *International journal of Plasticity*, vol. 18, pp. 443-459, 2002.
- [288] H. Liu, J. Zhang, Y. Jiang, Y. He, X. Xu, and W. Zhao, "Investigation on morphological evolution of chips for Ti6Al4V alloys with the increasing milling speed," *Procedia CIRP*, vol. 46, pp. 408-411, 2016.
-

-
- [289] A. Daymi, M. Boujelbene, S. Salem, B. Sassi, and S. Torbaty, "Effect of the cutting speed on the chip morphology and the cutting forces," *Archives of Computational Materials Science and Surface Engineering*, vol. 1, pp. 77-83, 2009.
- [290] J. Barry, G. Byrne, and D. Lennon, "Observations on chip formation and acoustic emission in machining Ti-6Al-4V alloy," *International Journal of Machine Tools and Manufacture*, vol. 41, pp. 1055-1070, 2001.
- [291] A. Sharman, D. Aspinwall, R. Dewes, and P. Bowen, "Workpiece surface integrity considerations when finish turning gamma titanium aluminide," *Wear*, vol. 249, pp. 473-481, 2001/06/01/ 2001.
- [292] Y. Zhao, J. Sun, and J. Li, "Study on chip morphology and milling characteristics of laser cladding layer," *The International Journal of Advanced Manufacturing Technology*, vol. 77, pp. 783-796, 2015.
- [293] T. Mabrouki, S. Belhadi, and J. Rigal, "Fundamental understanding of the segmented chip genesis for smart machining. A contribution in hard material turning," in *Advances in Integrated Design and Manufacturing in Mechanical Engineering II*, ed: Springer, 2007, pp. 443-459.
- [294] E. Ezugwu, J. Bonney, R. Da Silva, A. Machado, and E. Ugwoha, "High productivity rough turning of Ti-6Al-4V alloy, with flood and high-pressure cooling," *Tribology transactions*, vol. 52, pp. 395-400, 2009.
- [295] S. Patil, S. Joshi, A. Tewari, and S. Joshi, "Modelling and simulation of effect of ultrasonic vibrations on machining of Ti6Al4V," *Ultrasonics*, vol. 54, pp. 694-705, 2// 2014.
- [296] S. Joshi, P. Pawar, A. Tewari, and S. Joshi, "Effect of β phase fraction in titanium alloys on chip segmentation in their orthogonal machining," *CIRP journal of manufacturing science and technology*, vol. 7, pp. 191-201, 2014.
- [297] M. Cotterell and G. Byrne, "Dynamics of chip formation during orthogonal cutting of titanium alloy Ti-6Al-4V," *CIRP Annals*, vol. 57, pp. 93-96, 2008/01/01/ 2008.
- [298] S. Thamizhmanii and H. Sulaiman, "Machinability study using chip thickness ratio on difficult to cut metals by CBN cutting tool," in *Key Engineering Materials*, 2012, pp. 1317-1322.
- [299] V. Krishnaraj, S. Samsudeensadham, R. Sindhumathi, and P. Kuppan, "A study on High Speed End Milling of Titanium Alloy," *Procedia Engineering*, vol. 97, pp. 251-257, 2014/01/01 2014.
- [300] R. Gupta, C. Mathew, and P. Ramkumar, "Strain hardening in aerospace alloys," *Frontiers in Aerospace Engineering*, 2015.
- [301] V. Astakhov, "The assessment of cutting tool wear," *International Journal of Machine Tools and Manufacture*, vol. 44, pp. 637-647, 5// 2004.
-

- [302] U. Heisel, M. Schaal, and G. Wolf, "Burr formation in milling with minimum quantity lubrication," *Production Engineering*, vol. 3, pp. 23-30, 2009.
- [303] M. Chen, H. Ni, Z. Wang, and Y. Jiang, "Research on the modeling of burr formation process in micro-ball end milling operation on Ti-6Al-4V," *The International Journal of Advanced Manufacturing Technology*, vol. 62, pp. 901-912, 2012.
- [304] D. Vaux, F. Fidler, and G. Cumming, "Replicates and repeats—what is the difference and is it significant?: A brief discussion of statistics and experimental design," *EMBO reports*, vol. 13, pp. 291-296, 2012.

Appendix A **2D CAD drawings of the CUT-LIST supply system components**

Appendix A contains the following 2D CAD drawings of the new supply system components:

A1: Rear part of the overhead angled nozzle ring

A2: Front part of the overhead angled nozzle ring

A3: Angled mounting wedge

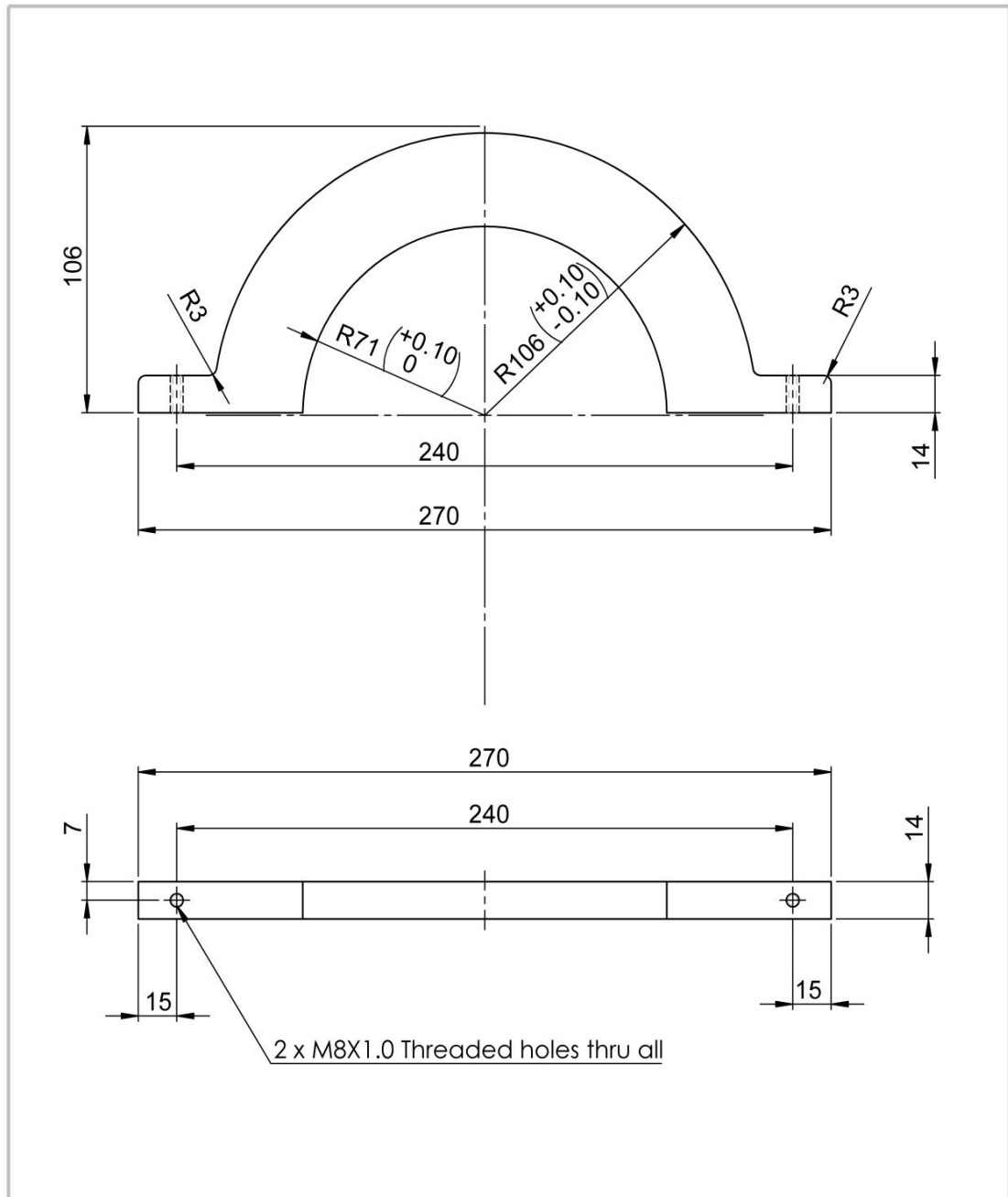
A4: Movable nozzle holder/clamp

A5: Impinging coherent round nozzle

A6: Rear part of the workpiece fixture

A7: Front part of the workpiece fixture

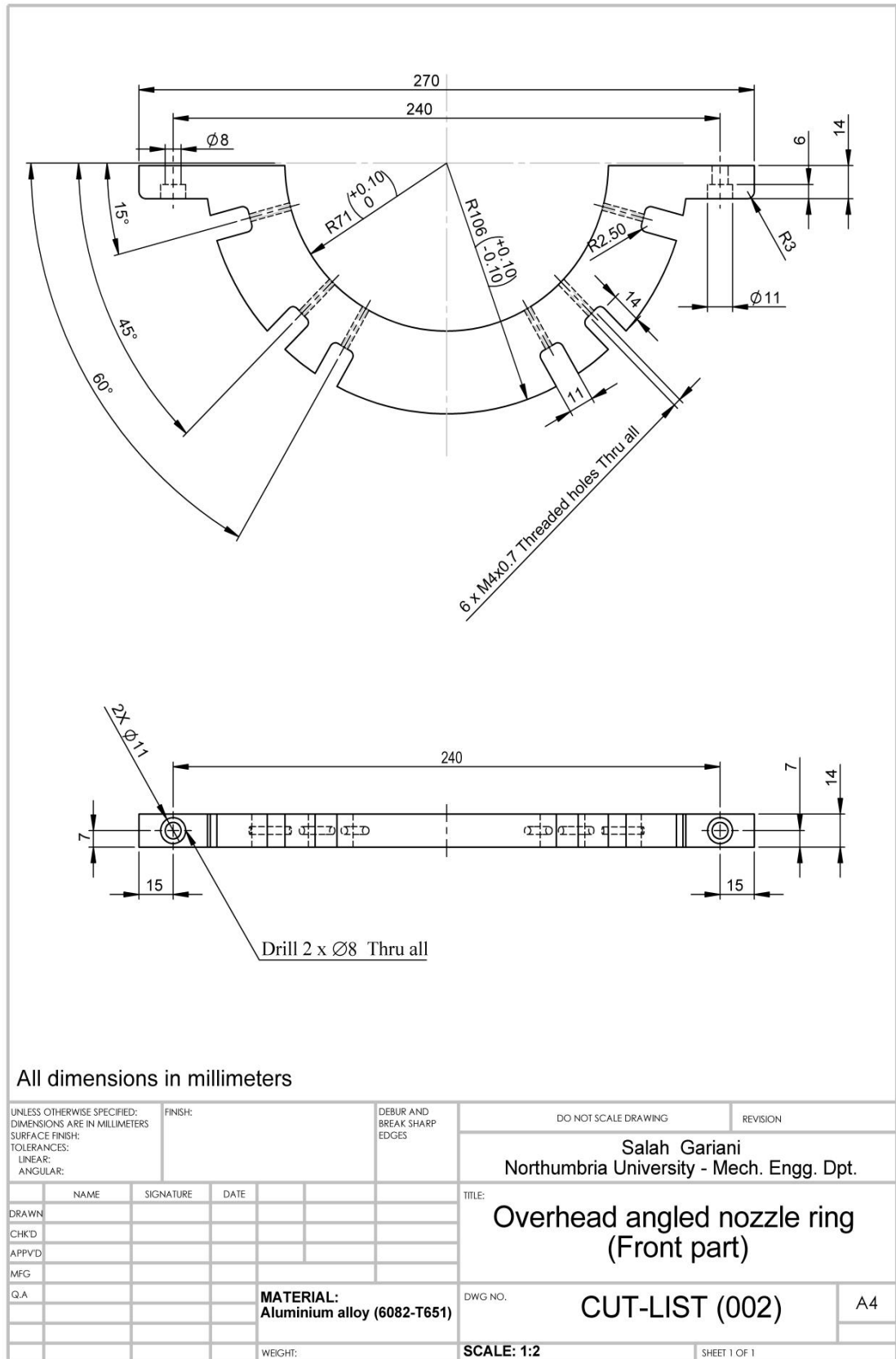
A1 – Rear part of the overhead angled nozzle ring



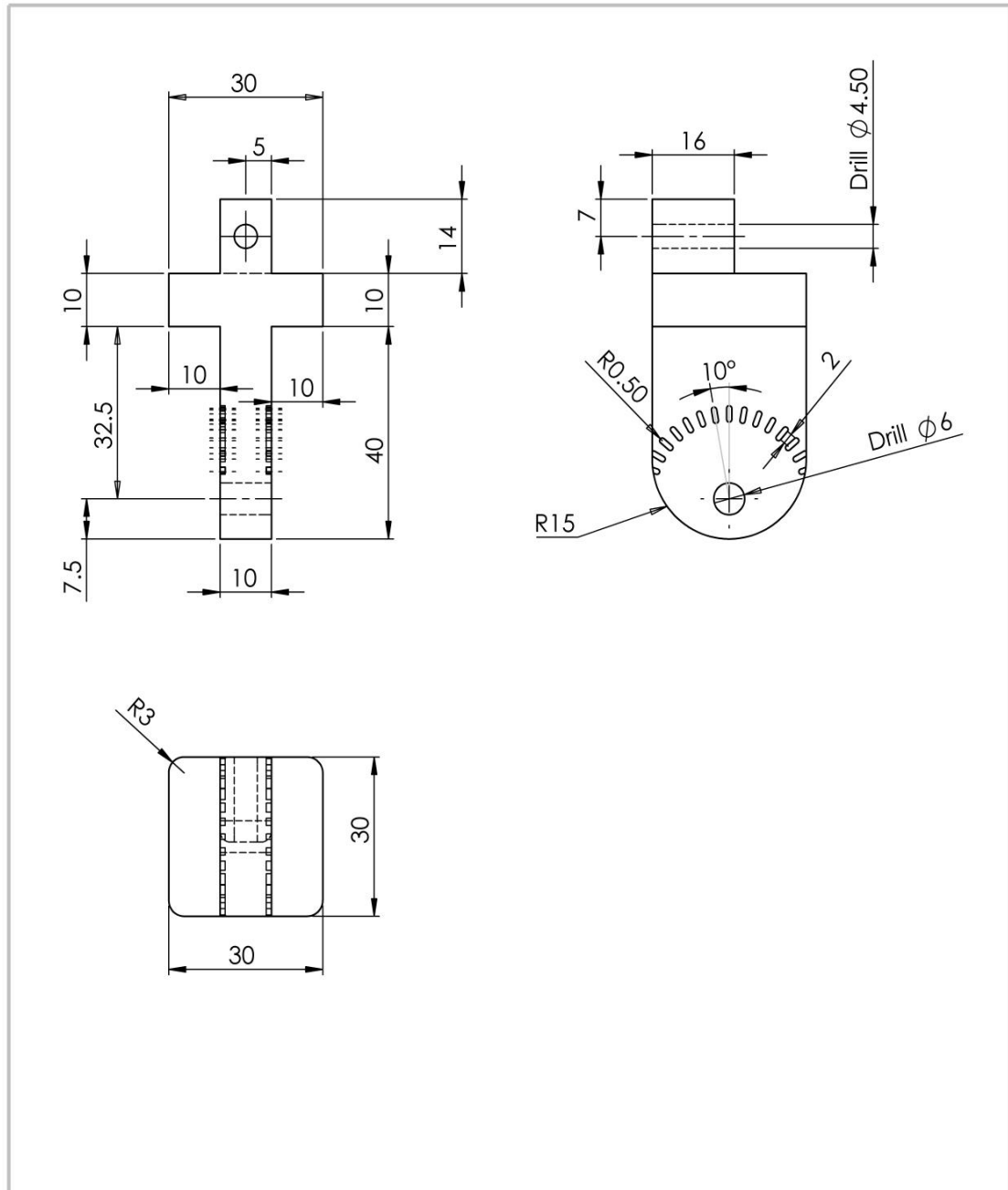
All dimension in millimeters

UNLESS OTHERWISE SPECIFIED: DIMENSIONS ARE IN MILLIMETERS		FINISH:		DEBUR AND BREAK SHARP EDGES		DO NOT SCALE DRAWING		REVISION	
SURFACE FINISH:						Salah Gariani		Northumbria University - Mech. Engg. Dept.	
TOLERANCES: LINEAR:						TITLE:		Overhead angled nozzle ring (Rear part)	
ANGULAR:						DWG NO.		CUT-LIST (001)	
DRAWN	SALAH GARIANI	SIGNATURE	DATE					A4	
CHK'D									
APP'VD									
MFG									
Q.A				MATERIAL: Aluminium alloy (6082-T651)					
				WEIGHT:		SCALE:1:2		SHEET 1 OF 1	

A2 - Front part of the overhead angled nozzle ring



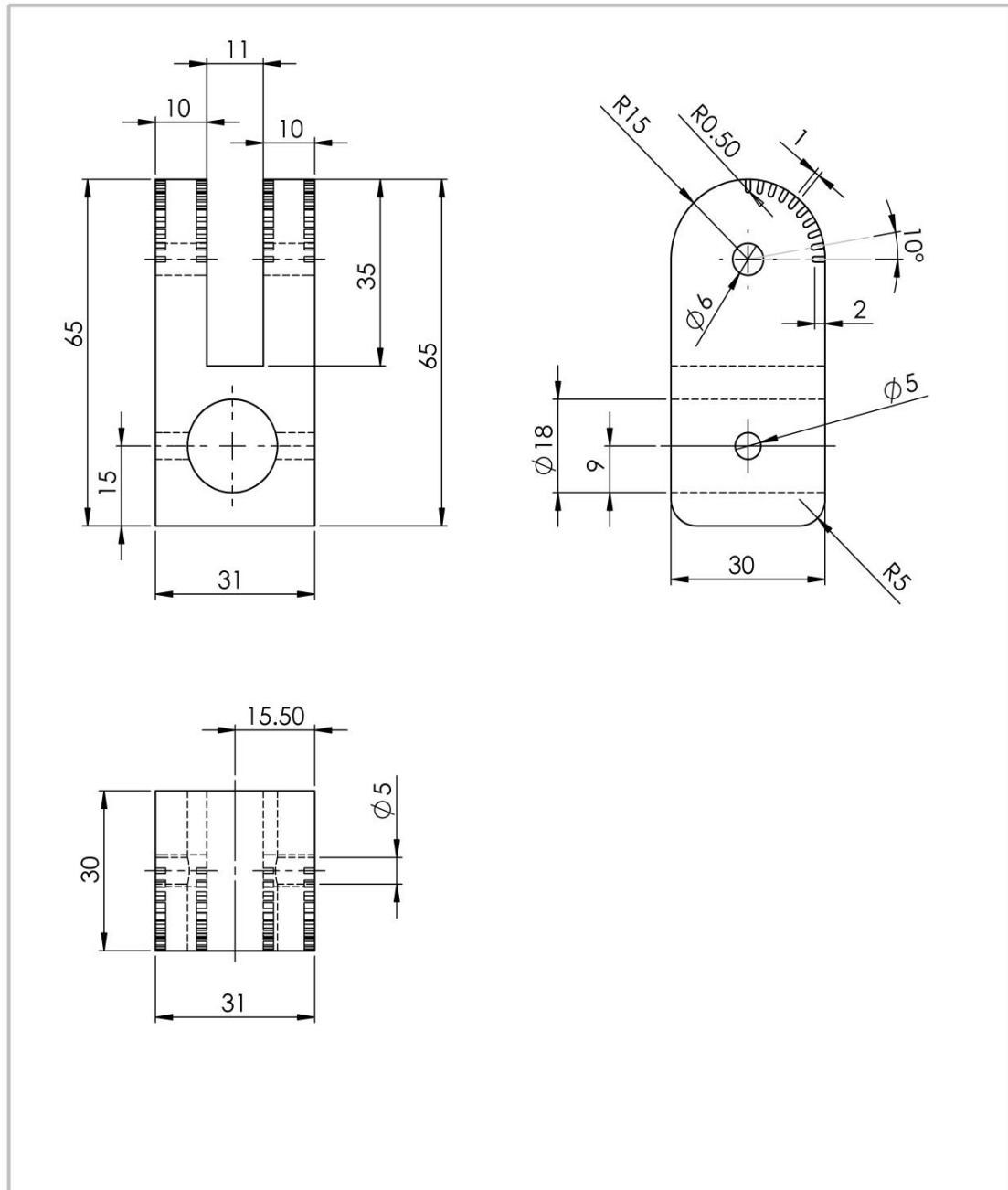
A3 – Angled mounting wedge



All dimension in millimeters

UNLESS OTHERWISE SPECIFIED: DIMENSIONS ARE IN MILLIMETERS		FINISH:		DEBUR AND BREAK SHARP EDGES		DO NOT SCALE DRAWING		REVISION	
SURFACE FINISH:						Salah Gariani Northumbria University-Mech. Engg. Dpt.			
TOLERANCES: LINEAR: ANGULAR:						TITLE: Angled mounting wedge			
DRAWN	NAME	SIGNATURE	DATE			DWG. NO.		A4	
CHK'D	SALAH GARIANI		4/11/15			CUT-LIST (003)			
APP'VD						SCALE: 1:1		SHEET 1 OF 1	
MFG						MATERIAL: Rigid opaque photopolymer			
Q.A						WEIGHT:			

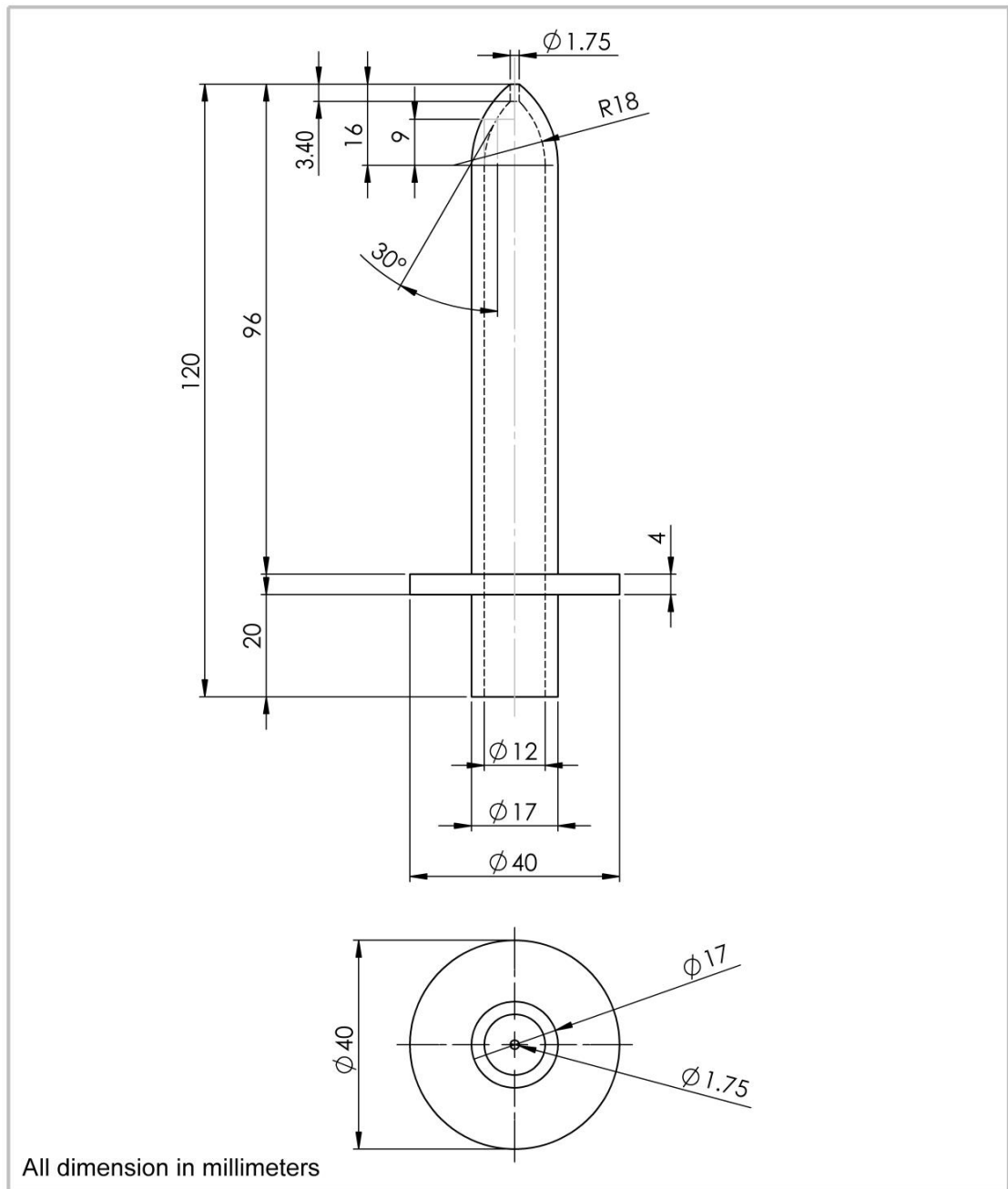
A4 – Movable angled nozzle holder/clamp



All dimension in millimeters

UNLESS OTHERWISE SPECIFIED: DIMENSIONS ARE IN MILLIMETERS SURFACE FINISH: TOLERANCES: LINEAR: ANGULAR:		FINISH:	DEBUR AND BREAK SHARP EDGES	DO NOT SCALE DRAWING	REVISION
				Salah Gariani Northumbria University- Mech. Engg. Dpt.	
NAME	SIGNATURE	DATE		TITLE: Movable angled nozzle holder/clamp	
DRAWN	SALAH GARIANI	4/11/15			
CHK'D					
APP'VD					
MFG					
Q.A			MATERIAL: Rigid opaque photopolymer	DWG NO. CUT-LIST (004)	A4
WEIGHT:			SCALE:1:1	SHEET 1 OF 1	

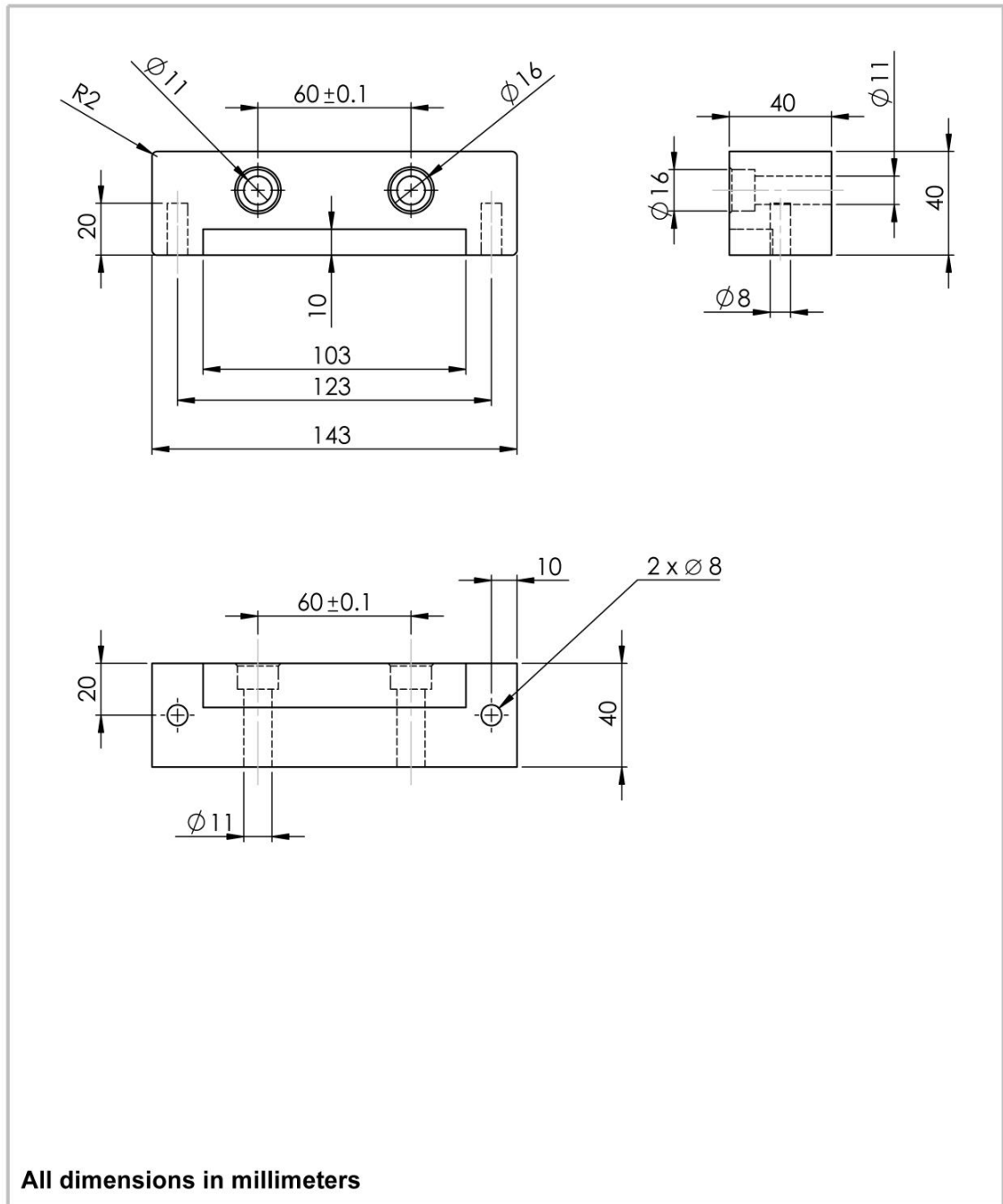
A5 – Impinging coherent round nozzle



All dimension in millimeters

UNLESS OTHERWISE SPECIFIED: DIMENSIONS ARE IN MILLIMETERS		FINISH:		DEBUR AND BREAK SHARP EDGES		DO NOT SCALE DRAWING		REVISION	
SURFACE FINISH:						Salah Gariani Northumbria University-Mech. Engg. Dpt.			
TOLERANCES:						TITLE: Impinging coherent round nozzle			
LINEAR:						DWG NO.		A4	
ANGULAR:						CUT-LIST (005)			
DRAWN		NAME		SIGNATURE		DATE			
CHK'D									
APP'VD									
MFG									
Q.A									
						MATERIAL:			
						Rigid opaque photopolymer			
						WEIGHT:		SCALE:1:1	
								SHEET 1 OF 1	

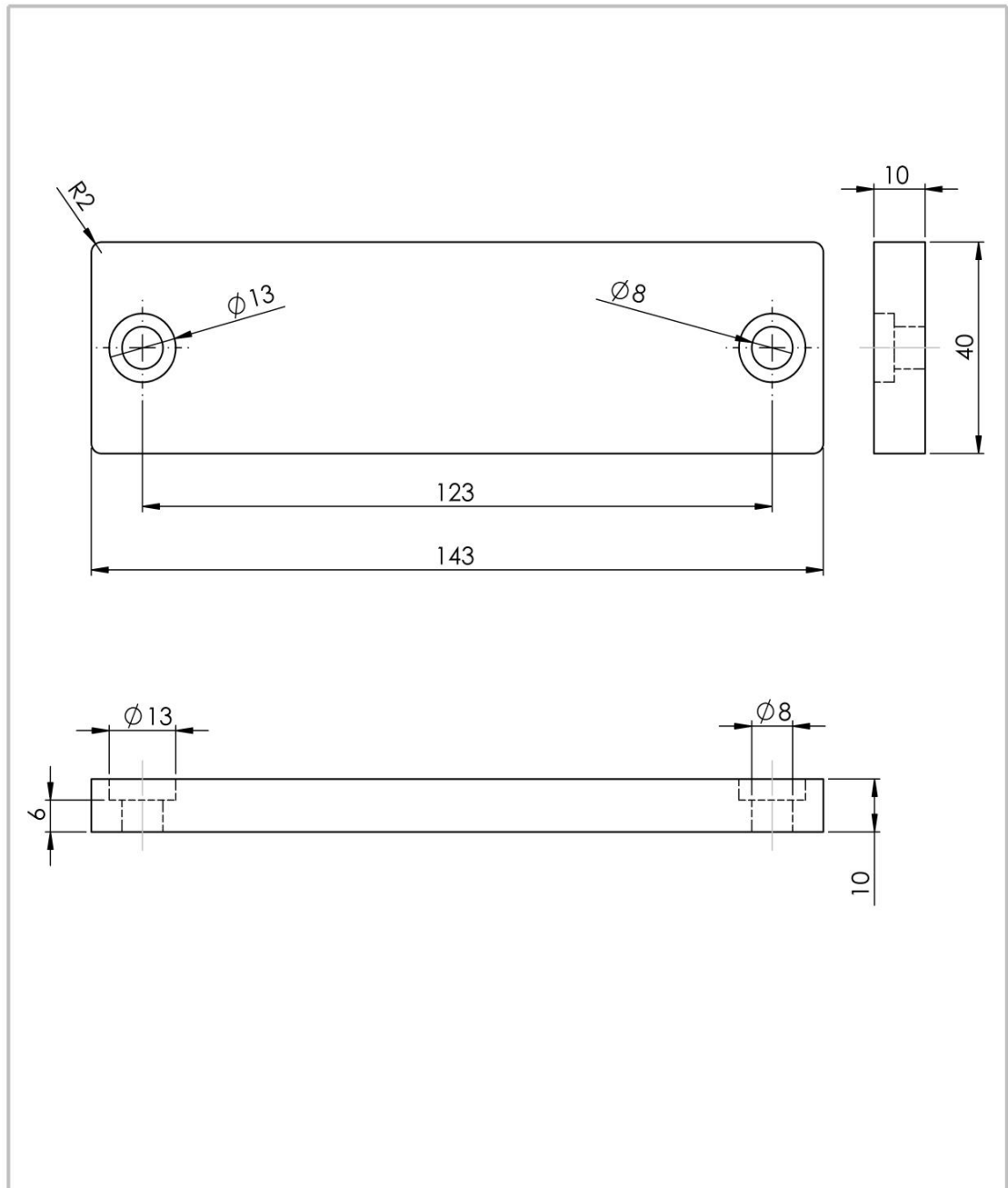
A6 – Rear part of the workpiece fixture



All dimensions in millimeters

UNLESS OTHERWISE SPECIFIED: DIMENSIONS ARE IN MILLIMETERS SURFACE FINISH: TOLERANCES: LINEAR: ANGULAR:		FINISH:	DEBUR AND BREAK SHARP EDGES	DO NOT SCALE DRAWING	REVISION
				Salah Gariani Northumbria University - Mech. Engg. Dpt.	
				TITLE: Workpiece fixture (Rear part)	
				DWG NO.	CUT-LIST (006)
				A4	
				SCALE:1:2	SHEET 1 OF 1
DRAWN:		NAME	SIGNATURE	DATE	
CHKD:					
APPVD:					
MFG:					
Q.A:					
				MATERIAL: Mild steel	
				WEIGHT:	

A7 – Front part of the workpiece fixture



All dimension in millimeters

UNLESS OTHERWISE SPECIFIED: DIMENSIONS ARE IN MILLIMETERS		FINISH:		DEBUR AND BREAK SHARP EDGES		DO NOT SCALE DRAWING		REVISION	
SURFACE FINISH:		TOLERANCES:		LINEAR:		ANGULAR:		Salah Gariani Northumbria University-Mech. Engg. Dpt.	
DRAWN		NAME		SIGNATURE		DATE		TITLE:	
CHK'D								Workpiece fixture (Front part)	
APP'VD								DWG NO.	
MFG								CUT-LIST (007)	
Q.A								A4	
						MATERIAL: Mild steel		SCALE:1:2	
						WEIGHT:		SHEET 1 OF 1	

Appendix B **CNC and MATLAB** **programmes**

Appendix B includes the following documents:

B1: CNC programme for manufacturing the rear part of the overhead nozzle ring

B2: CNC programme for fabrication the front part of the overhead nozzle ring

B3: MATLAB programme for accurate flow rate computations

B4: MATLAB programme for the determination of nozzle aperture diameters and impinging fluid velocity

B1: CNC programme for manufacturing the rear part of the overhead nozzle ring

```

1 %%%% Rear part of the overhead angled nozzle ring %%%%
2 O0001 (SALAH GARIANI - 0001)
3 (DATE=DD-MM-YY - 15-02-16 TIME=HH:MM - 10:34)
4 N100G21
5 N102G0G17G40G49G80G90
6 (TOOL - 1 DIA. OFF. - 1 LEN. - 1 DIA. - 6.)
7 N104T1M6
8 N106G0G90G54X138.Y0.A0.S3500M3
9 N108G43H1Z50.M8
10 N110Z10.N112G1Z-5.F25.
11 N114Y11.F1600.
12 N116G3X132.Y17.R6.
13 N118G1X107.503
14 N120G3X-107.503R109.
15 N122G1X-132.
16 N124G3X-138.Y11.R6.
17 N126G1Y0.
18 N128G3X-135.Y-3.R3.
19 N130G1X-71.
20 N132G3X-68.Y0.R3.
21 N134G2X68.R68.
22 N136G3X71.Y-3.R3.
23 N138G1X135.
24 N140G3X138.Y0.R3.
25 N142G1Z-10.F25.
26 N144Y11.F1600.
27 N146G3X132.Y17.R6.
28 N148G1X107.503
29 N150G3X-107.503R109.
30 N152G1X-132.
31 N154G3X-138.Y11.R6.
32 N156G1Y0.
33 N158G3X-135.Y-3.R3.
34 N160G1X-71.
35 N162G3X-68.Y0.R3.
36 N164G2X68.R68.
37 N166G3X71.Y-3.R3.
38 N168G1X135.
39 N170G3X138.Y0.R3.
40 N172G1Z0.F800.
41 N174G0Z50.
42 N176M5 N178G91G28Z0.M9
43 N180G28X0.Y0.A0.
44 N182M30
45 %end of the program%%%%

```

B2: CNC programme for manufacturing the front part of the overhead angled nozzle ring

```

1 %%% Front part of the overhead angled nozzle ring %%%
2 O0001
3 (SALAH GARIANI - 0002)
4 (DATE=DD-MM-YY - 16-01-16 TIME=HH:MM - 09:46)

```

```
5 N100G21
6 N102G0G17G40G49G80G90
7 (TOOL - 1 DIA. OFF. - 1 LEN. - 1 DIA. - 5.)
8 N104T1M6
9 N106G0G90G54X138.234Y0.A0.S3500M3
10 N108G43H1Z50.M8
11 N110Z10.
12 N112G1Z-5.F25.
13 N114Y11.F1500.
14 N116G3X132.734Y16.5R5.5
15 N118G1X107.972
16 N120G3X105.436Y28.457R108.5
17 N122X102.376Y30.216R2.5
18 N124G1X87.484Y26.226
19 N126X85.931Y32.022
20 N128X100.232Y35.854
21 N130G3X101.916Y39.171R2.5
22 N132X76.7Y77.469R108.5
23 N134X73.182Y77.452R2.5
24 N136G1X62.552Y66.822
25 N138X58.309Y71.064
26 N140X68.458Y81.213
27 N142G3X68.246Y84.938R2.5
28 N144X53.853Y94.608R108.5
29 N146X50.464Y93.678R2.5
30 N148G1X43.101Y80.924
31 N150X37.905Y83.924
32 N152X44.915Y96.067
33 N154G3X43.741Y99.612R2.5
34 N156X-43.472Y99.086R108.5
35 N158X-44.619Y95.553R2.5
36 N160G1X-37.905Y83.924
37 N162X-43.101Y80.924
38 N164X-50.101Y93.049
39 N166G3X-53.516Y93.964R2.5
40 N168X-67.611Y84.268R108.5
41 N170X-67.804Y80.559R2.5
42 N172G1X-58.309Y71.064
43 N174X-62.552Y66.822
44 N176X-72.452Y76.721
45 N178G3X-75.987R2.5
46 N180X-100.589Y38.806R108.5
47 N182X-98.901Y35.497R2.5
48 N184G1X-85.931Y32.022
49 N186X-87.484Y26.226
50 N188X-101.007Y29.85
51 N190G3X-104.069Y28.082R2.5
52 N192X-106.504Y16.5R108.5
53 N194G1X-131.266
54 N196G3X-136.766Y11.R5.5
55 N198G1Y0.
56 N200G3X-134.266Y-2.5R2.5
57 N202G1X-70.266
58 N204G3X-67.766Y0.R2.5
59 N206G2X69.234R68.5
60 N208G3X71.734Y-2.5R2.5
61 N210G1X135.734
62 N212G3X138.234Y0.R2.5
```

```
63 N214G1Z-10.F25.
64 N216Y11.F1500.
65 N218G3X132.734Y16.5R5.5
66 N220G1X107.972
67 N222G3X105.436Y28.457R108.5
68 N224X102.376Y30.216R2.5
69 N226G1X87.484Y26.226
70 N228X85.931Y32.022
71 N230X100.232Y35.854
72 N232G3X101.916Y39.171R2.5
73 N234X76.7Y77.469R108.5
74 N236X73.182Y77.452R2.5
75 N238G1X62.552Y66.822
76 N240X58.309Y71.064
77 N242X68.458Y81.213
78 N244G3X68.246Y84.938R2.5
79 N246X53.853Y94.608R108.5
80 N248X50.464Y93.678R2.5
81 N250G1X43.101Y80.924
82 N252X37.905Y83.924
83 N254X44.915Y96.067
84 N256G3X43.741Y99.612R2.5
85 N258X-43.472Y99.086R108.5
86 N260X-44.619Y95.553R2.5
87 N262G1X-37.905Y83.924
88 N264X-43.101Y80.924
89 N266X-50.101Y93.049
90 N268G3X-53.516Y93.964R2.5
91 N270X-67.611Y84.268R108.5
92 N272X-67.804Y80.559R2.5
93 N274G1X-58.309Y71.064
94 N276X-62.552Y66.822
95 N278X-72.452Y76.721
96 N280G3X-75.987R2.5
97 N282X-100.589Y38.806R108.5
98 N284X-98.901Y35.497R2.5
99 N286G1X-85.931Y32.022
100 N288X-87.484Y26.226
101 N290X-101.007Y29.85
102 N292G3X-104.069Y28.082R2.5
103 N294X-106.504Y16.5R108.5
104 N296G1X-131.266
105 N298G3X-136.766Y11.R5.5
106 N300G1Y0.
107 N302G3X-134.266Y-2.5R2.5
108 N304G1X-70.266
109 N306G3X-67.766Y0.R2.5
110 N308G2X69.234R68.5
111 N310G3X71.734Y-2.5R2.5
112 N312G1X135.734
113 N314G3X138.234Y0.R2.5
114 N316G1Z0.F1000.
115 N318G0Z50.
116 N320M5
117 N322G91G28Z0.M9
118 N324G28X0.Y0.A0.
119 N326M30
120 %%End of the program%%
```

B3: MATLAB programme for accurate flow rate computations

```

clear all;clc;
format short g
D=18.5 % cutter diameter (mm)
Z= 1 % number of teeth/inserts
vc=95; % cutting speed (m/min)
ap= 5 % Axial depth of cut (mm)
ae= 1.3 % Radial depth of cut (mm)
ftt= 0.10 % feed per tooth (mm/rev)
K1=1.96 % feed rate compensation factor
ft=ftt*K1 % Adjusted feed rate to avoid chip thinning (mm/rev)
N=((1000*vc)/(3.14159*D)) % Spindle speed (RPM)
fr=ft*Z*N % Table feed rate/ or speed (mm/min)
MRR=(ae*ap*fr) % Material removal rate mm3/s
U=4 % Specific cutting power of titanium alloy (W.s/mm2)
Pcc1= ((U*MRR)/60)/1000 % Total Cutting power converted into heat (kW)
Pcc2= (U*MRR)/60 % Total cutting power in (Watt)
Pc=Pcc1*0.90 % Generated heat= 90% of cutting energy (kW)
CS=0.948 % specific heat of cutting fluid Vasco1000@ 10% (cal/g*C)
W=0.988 % density of cutting fluid Vasco 1000 @ 10% (g/cm3)
E=0.95 % Coherent nozzle efficiency
T= 2 % Δθ Maximum tolerable temperature increase in cutting fluids
Q=((Pc*60)/(4.184*W*CS*E*T)) % accurate flow rate in L/m
Q1= Q* 0.264 % Gallon per minute [US gpm]
disp('Generated heat in Kw, Qacc in L/m, Qacc in US gpm')
disp([Pc])
disp([Q])
disp([Q1])

```

B4: MATLAB programme for the determination of nozzle aperture diameters and impinging fluid velocity

```

clear all;clc;
format short g
ro= 1; % for water
roCF=0.988; % Density of cutting fluid vasco1000 @ 10% concentration
Cd=0.95; % Coherent nozzle discharge coefficient
results=[];
for P=0.1:0.005:1 % Pressure in bar
    for d=0.0393:0.005:0.59 % Diameter in inch
        Pr=P*14.5; % pressure in psi
        dmm=d .*25.4; % diameter in (mm)
        SG=roCF/ro; % calculate specific gravity
        Vj=sqrt(Pr*535824/SG); % calculate cutting fluid velocity (sfpm)
        V=sqrt(P*200/SG); % calculate cutting fluid velocity (m/s)
        A=pi*d^2/4; % Calculate Nozzle exit area
        QE=A*Cd*Vj/19.25; % Calculate flow rate in (US gpm)
        Q=QE*3.785; % convert flow rate from US gpm to L/min
        results=[results; Vj,V, P,Pr, SG, d, dmm, Q];
    end
end
disp([' velocity ft/min,velocity m/s,Pressure bar, Pressure psi,
specific gravity,Nozzle exit daimetre inch,Nozzle exit daimetre
mm,flow rate L/min'])
disp([results])

```

Appendix C Design specifications of the CUT-LIST supply system

Overall dimension of the overhead nozzle ring:	Ø 270 x 14 mm width
Number of impinging angles:	3 angles (15°, 45° and 60°)
Number of impinging distances:	3 distances (35, 55 and 75 mm)
Range of nozzle elevation angle:	0 to 90 degrees
Supplied flow rate per kW heat/cutting power:	8 L/min, and this can change based on cutting conditions
Total decrease in cutting fluid consumption:	42%
Maximum error between actual and calculated accurate flow rates:	0.16%
Nozzle internal diameter (D):	12 mm, and always equal to the internal diameter of the nozzle feed pipe.
Nozzle head length (L):	16 mm
Nozzle mid-section radius:	18 mm
Nozzle mid-section axial length:	9 mm
Nozzle aperture cross-sectional width (w):	3.4 mm
Actual nozzle aperture diameter (d):	1.75 mm, and always \geq the calculated nozzle exit diameter (d_{\min})
Coherent nozzle contraction ratio (Cr) = D/d:	12/1.75 (6.85:1), and always with a D/d ratio \geq 2:1
Jet coherency length:	Up to 300 mm, and has less fluid dispersion.
Nozzle material:	Rigid plastic (PVC) or similar materials (e.g. rigid opaque photopolymer).

Positions of the fluid system monitoring equipment: All measuring equipment (i.e. digital flow meter and pressure gauge) should be located more than 300 mm away from cutting fluid pump to ensure steady state flow conditions and high monitoring accuracy.

Accuracy of fluid system monitoring equipment: Digital pressure gauge (+/- 0.25%)
Digital flowmeter (+/- 0.5 %)
Filter < 1-50 μm
Refractometer (+/- 0.03)

Other design considerations: This supply system can be used with all water-miscible cutting fluid (emulsion) types as well as any other fluids. However, fluids with low viscosity are preferred to increase fluid penetrability. The cutting fluid pump should be placed close to the cutting fluid tank to reduce pressure drops during the circulation of fluid. The use of 90-degree pipe bends and elbows should also be minimised to prevent fluid back-pressure effects.

Limitations or Restrictions: This supply system requires high-quality fluid filters to prevent any fine particles from entering the measuring equipment and clogging the nozzles. The maximum filter pressure should be ten times pump pressure.

Appendix D Technical data sheets (TDS)

Appendix D contains the technical data sheets (TDS) of the following materials:

D1: Ti-6Al-4V (ASTM B348 Grade 5)

D2: VO-based cutting fluids (Vasco1000, Hocut 3450, NE250H and SOLUTEC)

D3: Mineral oil-based cutting fluid (Castrol-Cooldege BI)

D1: Ti-6Al-4V (ASTM B348 Grade 5)

Ti-6Al-4V (Grade 5)

Technical Datasheet



Titanium Alloy

Service. Quality. Value.

Typical Applications

Aero-engine components, Airframe components, Marine equipment, Offshore oil & gas equipment, Power generation industry, Autosport components, Medical equipment.

Product Description

Ti-6Al-4V (Grade 5), classed as an alpha-beta alloy, is the most widely used of the high strength titanium alloys. The alloy combines its good mechanical strength and low density (4.42 kg/dm³) with excellent corrosion resistance in many media. Grade 5 titanium is fully heat treatable (solution heat treatment plus aging) in sections up to 25mm and can be employed up to around 400°C.

Ti-6Al-4V ELI (Grade 23) has a reduced oxygen content (0.13% max.) compared with Grade 5. This confers improved ductility and fracture toughness with some reduction in mechanical strength. Uses include fracture critical airframe structures and for offshore tubulars.

Availability

Bar, wire, sheet, plate, extrusions, forgings, seamless pipe/tube.

Corrosion Resistance

Grade 5 titanium offers excellent resistance to many marine and offshore oil & gas environments. Titanium and its alloys resist a wide range of acid conditions being highly resistant to oxidising acids, possessing useful resistance to reducing acids and offering good resistance to most organic acids at lower concentrations and temperatures. Titanium should not be used with red fuming nitric acid and is rapidly attacked by hydrofluoric acid. The addition of 0.05% palladium (grade 24), 0.1% ruthenium (grade 29) or 0.05% palladium and 0.5% nickel (grade 25) significantly increases corrosion resistance in reducing acid chloride and sour environments, raising the threshold temperature to well over 200°C.

Material Specifications

- UNS R56400
- BS TA11
- AMS 4928
- ASTM B348 Grade 5
- AMS 4911
- MIL-STD-2154

Fabrication (typical values)

- Weldability - fair
- Specified bend radius for <0.070 in. x thickness - 4.5
- Specified bend radius for >0.070 in. x thickness - 5.0

Chemical Composition (Bar to ASTM B348 Grade 5)

Weight (%)	N	C	H	Fe	O	Al	V
Min						5.5	3.5
Max	0.05	0.08	0.015	0.40	0.20	6.75	4.5

Mechanical Properties (Bar to ASTM B348 Grade 5)

	Minimum	Typical
UTS, MPa	895	1,000
0.2% PS, MPa	828	910
Elongation, % in 4D	10	18
Reduction of area, %	25	-
Elastic modulus, GPa	-	114
Hardness, HRC	-	36
Charpy V-notch impact, J	-	24

Technical Assistance

Our knowledgeable staff backed up by our resident team of qualified metallurgists and engineers, will be pleased to assist further on any technical topic.

www.smithmetal.com

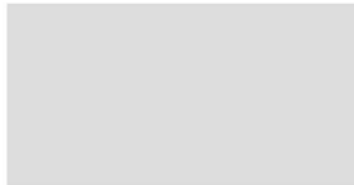
sales@smithmetal.com

Biggleswade 01767 604 604	Birmingham 01889 576 117	Bristol 0117 971 2800	Chelmsford 01245 466 664	Gateshead 0191 469 5428	Horsham 01403 261 981	Leeds 0113 307 5167
London 020 7241 2430	Manchester 0161 794 8650	Nottingham 0115 925 4801	Norwich 01603 789 878	Redruth 01209 315 512	Verwood 01202 824 347	General 0845 527 3331

All information in our data sheet is based on approximate testing and is stated to the best of our knowledge and belief. It is presented apart from contractual obligations and does not constitute any guarantee of properties or of processing or application possibilities in individual cases. Our warranties and liabilities are stated exclusively in our terms of trading. © Smiths Metal Centres 2017



D2: Vegetable oil-based cutting fluids



Art.No 2800-01

Vasco 1000

Description Vasco 1000 is a water miscible, vegetable oil-based, high performance cutting fluid.

Range of application High performance cutting fluid for heavy duty machining of cast iron, steel, aluminium alloys, non-ferrous metals as well as heavily machinable materials. Also applicable for grinding.

Product properties	Benefits
Excellent cutting performance due to properties of vegetable oils →	very long tool life for toughest operations and materials excellent surface finishes
Vegetable oil-base →	renewable raw materials biodegradable
Efficient corrosion protection →	universally applicable on delicate steel, aluminium and non-ferrous metal alloys
Good rinsing behaviour →	clean machines economical through low consumption

Physical-chemical data	Concentrate	Emulsion
Colour	light brown	milky, beige
Mineral oil content	0%	
Vegetable oil content	45%	
Water content	0.1%	
Density at 20°C	0.95 g/cm ³	
Viscosity at 40°C	56 mm ² /s	
Flash point	180°C	
pH-value		8.5–9.2
Refractometer factor		1.0

Note The product does not contain: EP additives containing chlorine, boron compounds, nitrite, nitrite releasing substances, secondary amines, diethanolamine, nitrosamines, silicone, heavy metals, triazine (HHT), PCP, PCB, PCT, TCDD or other dioxin-containing substances.

Concentration of use Variable concentrations from 5% to max. 15%
 – grinding 5%
 – general machining 5–8%
 – heavy duty machining above 7%

Packaging units 25/200 Litres

Information contained in this data sheet is based upon the properties and applications of use as known to us. However, generally no legal liability may be deducted from such information.
 0041 31.01.2006 V.03

ISO 9001/14001 Reg.Nr. 11321

Blaser Swisslube AG
 CH-3415 Hasle-Rüegsau (Switzerland) • Tel. 034 460 01 01 • Fax 034 460 01 00
 www.blaser.com



Hocut 3450

High lubricity mineral oil-free long-life metalworking coolant

DESCRIPTION

Hocut 3450 is a metalworking coolant based on renewable technology derived from vegetable oils. The product has high performance lubricity and antiwear properties designed to give superior component surface finish, with extended tooling and grinding wheel life.

Hocut 3450 is completely mineral oil free and offers an excellent health and safety and environmental profile.

An extended range of compatible Houghton Greenline hydraulic and lubricating oils is also available for users wanting to further reduce dependence on mineral oils in the machine shop.

APPLICATION

The high performance of Hocut 3450 is ideal for machining a wide range of materials including high alloy steels, nickel and titanium alloys. Hocut 3450 is specifically designed with low foaming and low air entrainment properties for high-pressure coolant systems associated with modern machining and grinding operations.

RECOMMENDATION FOR USE

Medium duty machining	4% - 6%
Heavy duty machining	5% - 10%
Heavy duty grinding	5% - 10%

TYPICAL PHYSICAL PROPERTIES

TEST	TYPICAL VALUE	TEST METHOD
<i>Neat concentrate</i>		
Appearance	Hazy amber oil	HI
Specific gravity @ 15.5°C	0.97	ASTM D1298
Refractometer factor	1.00	HI
<i>Emulsion at 5%</i>		
Appearance	Milky white	HI
pH in use	8.6-9.2	HI

All data given in this Product Data Sheet are typical of this material. It does not however constitute a specification. We reserve the right to modify products without prior notice. All products, services and information supplied are provided upon the terms of our standard Conditions of Sale from time to time in force.

ADVANTAGES

- Excellent lubricity and anti-wear properties
- Rich milky emulsion
- Based on renewable lubricant technology
- Free from chlorine, mineral oil, phenolic emulsifiers and boron
- Low foam and air entrainment
- No sticky residues
- Long sump-life
- Resistant to oxidation and lacquer formation
- Very safe to use
- No unpleasant odours

STORAGE

Metal working coolants should be stored indoors in clean, dry conditions. Protect from frost. Recommended storage temperature is between 5°C and 35°C. Tops should be replaced on all containers when not in use. Use stock in delivery rotation. As with all metal working coolants, a shelf life of twelve months can be anticipated.

HEALTH AND SAFETY

Health and Safety Data Sheets are supplied to customers to comply with Section 6 of the Health and Safety at Work Act 1974, and should be closely studied prior to handling or use of the product. Copies are available from your Technical Health and Safety Officer. Various other advisory publications are available from the Health and Safety Executive and Her Majesty's Stationery Office.

13065
11/09

Houghton plc
Beacon Road Trafford Park Manchester M17 1AF
Tel +44(0) 161 874 5000
Fax +44(0) 161 874 5001
E-mail uk.enquiries@houghtoneurope.com



HOUGHTON

TECHNICAL DATA SHEET**Coolant NE250H**

A highly quality, chlorine and mineral oil free, bio-stable water miscible coolant designed to provide the user with a robust, long-sump life product that is compatible with a wide variety of materials. It is highly tolerant of microbial contamination and rejects tramp oil very effectively.

Coolant NE250H has <28% vegetable oil content, which, in conjunction with high lubricant bio-additives, allows a high quality surface finish to be achieved, coupled with prolonged tool life.

It is suitable for use in a wide variety of water qualities, is low foaming and forms an exceptionally stable semi translucent emulsion. Coolant NE250H has been designed to cope with the problems caused in hard water areas by keeping scum formation down to an absolute minimum. This means that Coolant NE250H will maintain system cleanliness far beyond that of more conventional coolants.

Coolant NE250H has been formulated with the operator in mind and as such is free of any Boron compounds or formaldehyde-release or isothiazolinone biocides.

Benefits

- High vegetable oil content (28%)
- Highly stable emulsion
- Extended sum life
- Hazard free formulation
- Low foaming
- Multi-metal compatible
- Enhanced tool-life
- Used with waters >400ppm

Typical physical properties

Appearance	Yellow liquid
Emulsion Type	Semi translucent
Foaming Tendency and pH @5%	Low and 9.4
Vegetable oil content	<28 %
Specific gravity @ 20 °C	0.98

Recommended Dilutions

- General machining of free cutting metals: 4-6 %
 Difficult operation/materials: 8-10%

John Neale Ltd, 25 Fairfield Road, Halesowen, West Midlands, B63 4PT, UK

E-Mail info@johnnealeltd.co.uk Website: www.johnnealeltd.co.uk

Telephone +44(0) 121 585 8793

Coolant NE250H

SOLVTEC

TECHNICAL INFORMATION SHEET

Tel: 01270 214123 FAX 01270 251221

SUPER SYNTH 4

A totally synthetic (mineral oil free), water-soluble cutting fluid, incorporating a vegetable oil based lubricity agent (<35%).

FEATURES

1. Forms a clear solution in most waters.
2. Highly resistant to bacterial and fungal degradation, giving freedom from bad smells and slimy deposits.
3. Good inhibition against corrosion of a wide range of ferrous metals giving protection to both work piece and machined parts. Also good resistance to contact corrosion, so work pieces may be stacked without staining.
4. Non-phenolic, low odour, formaldehyde free, nitrite free and mineral oil free for optimum health, safety and environmental acceptability.
5. This product is readily biodegradable.

TECHNICAL DETAILS

PH VALUE	:	9.2 - 9.4
Specific gravity @ 20 °C	:	0.97
IP 287 Breakpoint	:	50:1
IP 125 Corrosion Test	:	80:1

RECOMMENDED MAXIMUM DILUTIONS

TURNING, MILLING, SAWING	:	50:1
DRILLING, SCREW CUTTING	:	30:1

D3: Mineral oil-based cutting fluid (Castrol-Cooldege BI)



Product Data

Castrol Cooldege BI

General purpose soluble metalworking fluid

Description

Castrol Cooldege™ BI is a general purpose soluble metalworking fluid which is chlorine and boron-free. It contains a unique additive package that provides good lubrication properties and performs well in a wide water range.

Cooldege BI can be used in single sump machines as well large systems.

Application

Cooldege BI is a versatile product recommended for general machining on low-medium alloy steel and aluminium alloys.

	Cast Iron	Low-medium alloyed steel	High alloyed - stainless steel	Aluminium alloys	Magnesium alloys	Yellow metals
Grinding						
Milling, Turning (general machining)	✓	✓✓	✓	✓✓		✓
Drilling	✓	✓✓	✓	✓✓		✓
Reaming, Tapping	✓	✓✓	✓	✓✓		✓
Broaching				✓✓		✓

Advantages

- Boron free for environmental compliance and improved residue characteristics
- Chlorine and nitrite free to fulfill your local legislation, waste treatment and environmental requirements
- Versatile product suitable for wide range of materials and operations
- Low foam in recommended water conditions

Typical Characteristics

	Test Method	Unit	Value
Concentrate			
Appearance	Visual		Amber
Mineral oil content	Calculated	Wt%	> 60
Emulsion			
Appearance	Visual		Milky
pH (5%)	DIN 51361 ASTM E70-97		9.5
Refractometer Factor			1.0

	Boron	Formaldehyde releasing agent	EP-Ester	Amines	Chlorine
Additives	-	✓	-	✓	-

Recommended Concentrations

General Machining	4-7%
Drilling	5-7%
Reaming and tapping	7-10%
Water range	50-400 ppm CaCO ₃

Storage

To avoid product deterioration, keep the container/drum tightly sealed always. Prevent any frost and water ingress.

Store it in a cool and dry place away from direct sunlight. It is preferable to store the product indoors always. For more details, please refer the product safety data sheet.

Castrol, Cooledge, and the Castrol logo are trademarks of the Castrol Limited, used under license

This data sheet and the information it contains is believed to be accurate as of the date of printing. However, no warranty or representation, express or implied, is made as to its accuracy or completeness. Data provided is based on standard tests under laboratory conditions and is given as a guide only. Users are advised to ensure that they refer to the latest version of this data sheet.

It is the responsibility of the user to evaluate and use products safely, to assess suitability for the intended application and to comply with all applicable laws and regulations. Material Safety Data Sheets are available for all our products and should be consulted for appropriate information regarding storage, safe handling, and disposal of the product. No responsibility is taken by either BP plc or its subsidiaries for any damage or injury resulting from abnormal use of the material, from any failure to adhere to recommendations, or from hazards inherent in the nature of the material. All products, services and information supplied are provided under our standard conditions of sale. You should consult our local representative if you require any further information.

Address: Castrol (UK) Limited, Pipers Way, Swindon, Wiltshire SN3 1RE
 Telephone No. Orders/Enquiries 0845 9645111, Technical Enquiries 0845 9000209, Fax 01793 486083
www.castrol.com/industrial

Castrol Cooledge BI
 Page 2 / 2

23 February 2010, Version 1

Appendix E **Bill of Materials (BOM)**

Appendix E presents the bill of materials (BOM) for the following experimental phases:

E1: Turning-based machining trials (sections 4.1 to 4.4)

E2: Milling-based machining tests (section 4.5)

E1: Turning-based machining trials (sections 4.1 to 4.4)

No.	Item	Qty & Unit	Item description/code	Manufacturer/Supplier (UK)
1	Workpiece material	18 pc	Ø 30 mm x 332 mm long Ti-6Al-4V ASTM B348 grade 5 round bar	TML, Titanium Metals Ltd.
2	Tool holder for external turning	1 pc	Tool holder (DCLNR 2525M 12), T-Max P shank tool for single-point turning	Sandvik Coromant
3	H13A and H10A indexable turning insert	10 pc each	Uncoated coarse and fine grained W/Co carbide tools/CNMG 120408-23	
4	H10F turning insert	10 pc	Uncoated fine grain W/Co carbide tool with high cobalt (Co) content/CNMG 120408-23	
5	S05F turning insert	10 pc	CVD coated carbide tool/CNMG 120408-SMR	
6	GC1105 and GC1115 turning inserts	10 pc each	PVD TiAlN coated carbide tools/CNMG 120408-23	
7	Refractometer	1 pc	Oxford portable optical refractometer with 30% brix range	
8	Hocut 3450 cutting fluid	20 L	VO-based fluid with 43% Vegetable oil content	Houghton/J. Clayden Lubricant
9	Vasco 1000 cutting fluid	25 L	VO-based fluid with 45% Vegetable oil content	Swisslube/Jemtech Ltd.
10	NE250H cutting fluid	25 L	VO-based fluid with < 28 Vegetable oil content	John Neale Ltd.
11	Solutec (Synth 4) cutting fluid	15 L	VO-based fluid with < 35% Vegetable oil content	Solutec Ltd.
12	Castrol cooledge BI fluid	20L	MO-based fluid with > 60 % Mineral oil content	Castrol Co.

E2: Milling-based machining trials (section 4.5)

No.	Item	Qty & Unit	Item description/code	Manufacturer/Supplier (UK)
1	Workpiece material	113 pc	103 × 25 × 11 mm rectangular shape blocks (annealed Ti-6Al-4V ASTM B348 grade 5), surface quality: WJ cutting, tolerance (≤ 1mm)	TML, Titanium Metals Ltd.
2	Tool holder for milling	1 pc	CoroMill 390 square shoulder milling cutter (R390-012A16-11L), max speed (68000 rpm)	Sandvik Coromant
3	H13A indexable milling inserts	60 pc	Uncoated coarse grain W/Co carbide tool (R390-11 T3 08M-KL H13A)	
4	Flow meter/regulator	1 pc	Digital flowmeter (BM-LM-OG-I-PVC-LCR)	Bell Flow Systems
5	Cutting fluid filter	1 pc	In-line clear 5 BSPP filter (12 bar)	Magnom Co. Ltd
6	Pressure gauge	1 pc	Digital Pressure gauge (DPGM8001-500)	Omega Engineering Ltd
7	Pressure gauge	2 pc	Dual Scale Liquid-Fillable Utility Pressure Gauge (PGUF-20L-20 bar)	
8	Thermocouple sensors	1 pc	Mineral Insulated TC sensors with threaded M8 pot seal & tails/ 2000 mm length	TEMPCON
9	Thermocouple data logger	1 pc	Onset HOBO -17384 A-UX120 -600M (4 output channel)	
10	Tubes	4 m	Clear Braided PVC Tubing ID 3/8" & 1/2"	RDG Tools

No.	Item	Qty & Unit	Item description/code	Manufacturer/Supplier (UK)	
11	Hand Valve	1 pc	Handle tap 1/2 " BSP	Cromwell Tools	
12	Hose clips	6 pc	JCS HI-GRIP Stainless Hose Clips		
13	Depth gauge	1 pc	Sealey type (Model VS0560) precision digital depth gauge		
14	Hose Tails 3/8"	3 pc	BSP steel Thread Hose tail for 3/8" pipe		
15	Extension fitting	2 pc	1/2" chrome male to female tap / radiator valve extensions		
16	Tee	1 pc	Steel Female Equal Tee 1/2" BSP		
17	Tee	2 pc	Steel Female Equal Tee 3/8" BSP		
18	Nipple	2 pc	Male to Male adaptor 3/8" BSP		
19	Nipple	2 pc	1/2 " Male To Male 1/4 " NPT for pressure gauges		
20	Extension	1 pc	Female to male 3/8" BSP extension		
21	Reducer	2 pc	1" to 1/2 " Male to Male reducer for In-line filter		
22	Ball valve	1 pc	1/2 " BSP Female x 1/2" Male Ball lever long handle valve		
23	Adaptor	1 pc	BSP Female to Female 1/2" equal Bush Adaptor		
24	Nipple	1 pc	Male to Male 1/2" BSP Nipple		
25	Hand wheel	2 pc	4 point hand wheel for nozzle holder		
26	Screws	4 pc	Socket Head Cup Screws M4x0.7 L=24 mm		Context Pneumatic supplies
27	Screws	4 pc	Socket Head Cup Screws M5x0.8 L=12 mm		
28	Screws	4 pc	Socket Head Cup Screws M6x1.0 L=24 mm		
29	Hex Bolts with Nuts	4 pc	M5x0.8 L=50 mm		

Appendix F **ISO designations for the indexable inserts and tool holders**

Appendix F contains the ISO designations for the following items:

F1: Indexable turning inserts

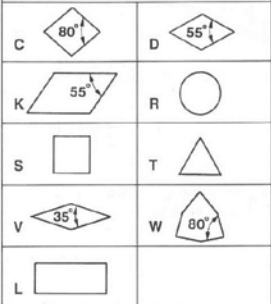
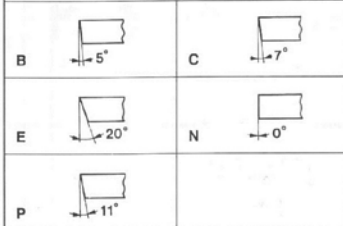
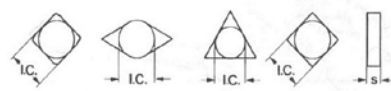
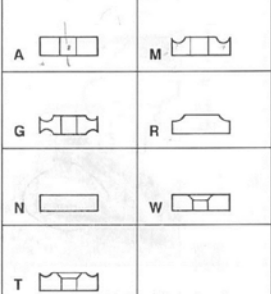
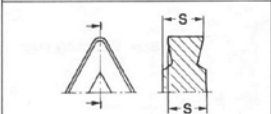
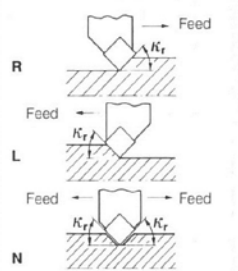
F2: Turning tool holders

F1: Description of ISO designation for indexable turning inserts

INDEXABLE INSERTS - TURNING



Extract from ISO 1832-1985

<p>1 Insert shape and included angle E_r</p> 	<p>2 Clearance angle on major cutting edge</p>  <p>O Specific description</p>	<p>3 Tolerances ± on s and I.C.</p> <table border="1" style="width: 100%; border-collapse: collapse;"> <thead> <tr> <th>Class s</th> <th>I.C.</th> </tr> </thead> <tbody> <tr> <td>G</td> <td>±0,025</td> </tr> <tr> <td>M ±0,13</td> <td>±0,05 - ±0,15¹⁾</td> </tr> <tr> <td>U</td> <td>±0,08 - ±0,25¹⁾</td> </tr> </tbody> </table> <p>¹⁾ Varies depending on the size of I.C. See below.</p>  <table border="1" style="width: 100%; border-collapse: collapse;"> <thead> <tr> <th>Inscribed circle I.C. mm</th> <th colspan="2">Tolerance class</th> </tr> <tr> <th></th> <th>M</th> <th>U</th> </tr> </thead> <tbody> <tr> <td>3,97</td> <td></td> <td></td> </tr> <tr> <td>5,0</td> <td></td> <td></td> </tr> <tr> <td>5,56</td> <td></td> <td></td> </tr> <tr> <td>6,0</td> <td></td> <td></td> </tr> <tr> <td>6,35</td> <td>±0,05</td> <td>±0,08</td> </tr> <tr> <td>8,0</td> <td></td> <td></td> </tr> <tr> <td>9,525</td> <td></td> <td></td> </tr> <tr> <td>10,0</td> <td></td> <td></td> </tr> <tr> <td>12,0</td> <td>±0,08</td> <td>±0,13</td> </tr> <tr> <td>12,7</td> <td></td> <td></td> </tr> <tr> <td>15,875</td> <td></td> <td></td> </tr> <tr> <td>16,0</td> <td>±0,10</td> <td>±0,18</td> </tr> <tr> <td>19,05</td> <td></td> <td></td> </tr> <tr> <td>20,0</td> <td></td> <td></td> </tr> <tr> <td>25,0</td> <td>±0,13</td> <td>±0,25</td> </tr> <tr> <td>25,4</td> <td></td> <td></td> </tr> <tr> <td>31,75</td> <td>±0,15</td> <td>±0,25</td> </tr> <tr> <td>32,0</td> <td></td> <td></td> </tr> </tbody> </table>	Class s	I.C.	G	±0,025	M ±0,13	±0,05 - ±0,15 ¹⁾	U	±0,08 - ±0,25 ¹⁾	Inscribed circle I.C. mm	Tolerance class			M	U	3,97			5,0			5,56			6,0			6,35	±0,05	±0,08	8,0			9,525			10,0			12,0	±0,08	±0,13	12,7			15,875			16,0	±0,10	±0,18	19,05			20,0			25,0	±0,13	±0,25	25,4			31,75	±0,15	±0,25	32,0																																																																																					
Class s	I.C.																																																																																																																																																								
G	±0,025																																																																																																																																																								
M ±0,13	±0,05 - ±0,15 ¹⁾																																																																																																																																																								
U	±0,08 - ±0,25 ¹⁾																																																																																																																																																								
Inscribed circle I.C. mm	Tolerance class																																																																																																																																																								
	M	U																																																																																																																																																							
3,97																																																																																																																																																									
5,0																																																																																																																																																									
5,56																																																																																																																																																									
6,0																																																																																																																																																									
6,35	±0,05	±0,08																																																																																																																																																							
8,0																																																																																																																																																									
9,525																																																																																																																																																									
10,0																																																																																																																																																									
12,0	±0,08	±0,13																																																																																																																																																							
12,7																																																																																																																																																									
15,875																																																																																																																																																									
16,0	±0,10	±0,18																																																																																																																																																							
19,05																																																																																																																																																									
20,0																																																																																																																																																									
25,0	±0,13	±0,25																																																																																																																																																							
25,4																																																																																																																																																									
31,75	±0,15	±0,25																																																																																																																																																							
32,0																																																																																																																																																									
<p>4 Insert type</p>  <p>X Special design</p>	<p>5 Insert size = cutting edge length, l mm</p> <table border="1" style="width: 100%; border-collapse: collapse;"> <thead> <tr> <th></th> <th>C</th> <th>D</th> <th>R</th> <th>S</th> <th>T</th> <th>V</th> <th>W</th> </tr> </thead> <tbody> <tr> <td>I.C. mm</td> <td></td> <td></td> <td></td> <td></td> <td></td> <td></td> <td></td> </tr> <tr> <td>3,97</td> <td></td> <td></td> <td></td> <td></td> <td>06</td> <td></td> <td></td> </tr> <tr> <td>5,0</td> <td></td> <td></td> <td>05</td> <td></td> <td>09</td> <td></td> <td></td> </tr> <tr> <td>5,56</td> <td></td> <td></td> <td></td> <td></td> <td></td> <td></td> <td></td> </tr> <tr> <td>6,0</td> <td></td> <td></td> <td></td> <td></td> <td>11</td> <td></td> <td></td> </tr> <tr> <td>6,35</td> <td>06</td> <td>07</td> <td>08</td> <td></td> <td></td> <td></td> <td></td> </tr> <tr> <td>8,0</td> <td></td> <td></td> <td></td> <td></td> <td></td> <td></td> <td></td> </tr> <tr> <td>9,525</td> <td>09</td> <td>11</td> <td>09</td> <td>09</td> <td>16</td> <td>16</td> <td></td> </tr> <tr> <td>10,0</td> <td></td> <td></td> <td></td> <td></td> <td></td> <td></td> <td></td> </tr> <tr> <td>12,0</td> <td></td> <td></td> <td>12</td> <td></td> <td></td> <td></td> <td></td> </tr> <tr> <td>12,7</td> <td>12</td> <td>15</td> <td>12</td> <td>12</td> <td>22</td> <td></td> <td>08</td> </tr> <tr> <td>15,875</td> <td>16</td> <td></td> <td>15</td> <td>15</td> <td>27</td> <td></td> <td></td> </tr> <tr> <td>16,0</td> <td></td> <td></td> <td></td> <td></td> <td>16</td> <td></td> <td></td> </tr> <tr> <td>19,05</td> <td>19</td> <td></td> <td>19</td> <td>19</td> <td>33</td> <td></td> <td></td> </tr> <tr> <td>20,0</td> <td></td> <td></td> <td></td> <td></td> <td></td> <td></td> <td></td> </tr> <tr> <td>25,0</td> <td></td> <td></td> <td>25</td> <td></td> <td></td> <td></td> <td></td> </tr> <tr> <td>25,4</td> <td></td> <td></td> <td></td> <td></td> <td></td> <td></td> <td></td> </tr> <tr> <td>32</td> <td>25</td> <td></td> <td></td> <td>25</td> <td></td> <td></td> <td></td> </tr> </tbody> </table> <p>For inserts shape K (KNMX, KNUX) only the theoretical cutting edge length is indicated.</p>		C	D	R	S	T	V	W	I.C. mm								3,97					06			5,0			05		09			5,56								6,0					11			6,35	06	07	08					8,0								9,525	09	11	09	09	16	16		10,0								12,0			12					12,7	12	15	12	12	22		08	15,875	16		15	15	27			16,0					16			19,05	19		19	19	33			20,0								25,0			25					25,4								32	25			25			
	C	D	R	S	T	V	W																																																																																																																																																		
I.C. mm																																																																																																																																																									
3,97					06																																																																																																																																																				
5,0			05		09																																																																																																																																																				
5,56																																																																																																																																																									
6,0					11																																																																																																																																																				
6,35	06	07	08																																																																																																																																																						
8,0																																																																																																																																																									
9,525	09	11	09	09	16	16																																																																																																																																																			
10,0																																																																																																																																																									
12,0			12																																																																																																																																																						
12,7	12	15	12	12	22		08																																																																																																																																																		
15,875	16		15	15	27																																																																																																																																																				
16,0					16																																																																																																																																																				
19,05	19		19	19	33																																																																																																																																																				
20,0																																																																																																																																																									
25,0			25																																																																																																																																																						
25,4																																																																																																																																																									
32	25			25																																																																																																																																																					
<p>6 Insert thickness, s mm</p>  <p>01 s = 1,59 T1 s = 1,98 02 s = 2,38 03 s = 3,18 T3 s = 3,97 04 s = 4,76 05 s = 5,56 06 s = 6,35 07 s = 7,94 09 s = 9,52</p>	<p>7 Nose radius, r_n mm</p>  <p>00 r_n = 0 02 r_n = 0,2 04 r_n = 0,4 08 r_n = 0,8 12 r_n = 1,2 16 r_n = 1,6 24 r_n = 2,4 32 r_n = 3,2</p> <p>Round insert: 00 if I.C. is converted from an inch value. M0 if I.C. is a metric value.</p>	<p>8 Cutting edge condition</p> <p>F Sharp cutting edge</p> <p>T Negative land</p>	<p>9 Tool style feed direction</p> 																																																																																																																																																						
<p>10 Manufacturer's option</p>	<p>The ISO code consists of nine symbols including 8 and 9 which are used only when required. In addition the manufacturer may add further two symbols e.g. -QF = finishing operations, -QM = semi-finishing and light roughing operations, -QR = roughing operations.</p>																																																																																																																																																								

F2: Description of ISO designation for turning tool holders

Shank tool, metric

D	C	L	N	R	25	25	M	12	-	2
2	3	4	5	6	7	8	10	11		13

Shank tool, inch

D	C	L	N	R	16	4	D	-	
2	3	4	5	6	7-8	11	10		12

<p>1 Coupling size, mm</p> <p>C = Coromant Capto® D_{5m} = Coupling size</p>  <p>C3 D_{5m} = 32 C4 D_{5m} = 40 C5 D_{5m} = 50 C6 D_{5m} = 63 C8 D_{5m} = 80</p> <p>Coromant Capto®</p>	<p>2 Clamping system</p> <table border="1"> <tr> <td data-bbox="630 593 778 846"> <p>C</p>  <p>Top clamping</p> </td> <td data-bbox="778 593 927 846"> <p>D</p>  <p>Top and hole clamping (RC)</p> </td> <td data-bbox="927 593 1109 846"> <p>M, W</p>  <p>Top and hole clamping</p> </td> <td data-bbox="1109 593 1257 846"> <p>P</p>  <p>Hole clamping</p> </td> <td data-bbox="1257 593 1404 846"> <p>S</p>  <p>Screw clamping</p> </td> </tr> </table>				<p>C</p>  <p>Top clamping</p>	<p>D</p>  <p>Top and hole clamping (RC)</p>	<p>M, W</p>  <p>Top and hole clamping</p>	<p>P</p>  <p>Hole clamping</p>	<p>S</p>  <p>Screw clamping</p>																																
<p>C</p>  <p>Top clamping</p>	<p>D</p>  <p>Top and hole clamping (RC)</p>	<p>M, W</p>  <p>Top and hole clamping</p>	<p>P</p>  <p>Hole clamping</p>	<p>S</p>  <p>Screw clamping</p>																																					
<p>3 Insert shape</p> <table border="1"> <tr> <td>C</td><td>D</td></tr> <tr> <td></td><td></td></tr> <tr> <td>K</td><td>R</td></tr> <tr> <td></td><td></td></tr> <tr> <td>S</td><td>T</td></tr> <tr> <td></td><td></td></tr> <tr> <td>V</td><td>W</td></tr> <tr> <td></td><td></td></tr> </table>	C	D			K	R			S	T			V	W			<p>4 Holder style entering angle (lead angle)</p> <table border="1"> <tr> <td>A 90° (0°)</td> <td>B 75° (15°)</td> <td>D 45° (45°)</td> <td>E 60° (30°)</td> <td>F 91° (-1°)</td> <td>G 91° (-1°)</td> <td>H 107.5° (-17.5°)</td> </tr> <tr> <td>J 93° (-3°)</td> <td>K 75° (15°)</td> <td>L 95° (-5°)</td> <td>M 50° (40°)</td> <td>N 62.5° (27.5°)</td> <td>Q 107.5° (-17.5°)</td> <td>R 75° (15°)</td> </tr> <tr> <td>S 45° (45°)</td> <td>T 60° (30°)</td> <td>U 93° (-3°)</td> <td>V 72.5° (17.5°)</td> <td>Y(X) 85° (5°)</td> <td>Y(Z) 85° (5°)</td> <td>P 62.5° (27.5°)</td> </tr> </table>				A 90° (0°)	B 75° (15°)	D 45° (45°)	E 60° (30°)	F 91° (-1°)	G 91° (-1°)	H 107.5° (-17.5°)	J 93° (-3°)	K 75° (15°)	L 95° (-5°)	M 50° (40°)	N 62.5° (27.5°)	Q 107.5° (-17.5°)	R 75° (15°)	S 45° (45°)	T 60° (30°)	U 93° (-3°)	V 72.5° (17.5°)	Y(X) 85° (5°)	Y(Z) 85° (5°)	P 62.5° (27.5°)
C	D																																								
																																									
K	R																																								
																																									
S	T																																								
																																									
V	W																																								
																																									
A 90° (0°)	B 75° (15°)	D 45° (45°)	E 60° (30°)	F 91° (-1°)	G 91° (-1°)	H 107.5° (-17.5°)																																			
J 93° (-3°)	K 75° (15°)	L 95° (-5°)	M 50° (40°)	N 62.5° (27.5°)	Q 107.5° (-17.5°)	R 75° (15°)																																			
S 45° (45°)	T 60° (30°)	U 93° (-3°)	V 72.5° (17.5°)	Y(X) 85° (5°)	Y(Z) 85° (5°)	P 62.5° (27.5°)																																			
<p>5 Insert clearance angle</p> <table border="1"> <tr> <td>B</td><td>C</td></tr> <tr> <td></td><td></td></tr> <tr> <td>D</td><td>E</td></tr> <tr> <td></td><td></td></tr> <tr> <td>N</td><td>P</td></tr> <tr> <td></td><td></td></tr> <tr> <td colspan="2">O Specific description</td> </tr> </table>	B	C			D	E			N	P			O Specific description		<p>6 Hand of tool</p>   		<p>7 & 8 Shank size (b, width and h, height) inch</p> <table border="1"> <tr> <td>05 = 5/16 X 5/16</td> <td>85 = 1 X 1 1/4</td> </tr> <tr> <td>06 = 3/8 X 3/8</td> <td>86 = 1 X 1 1/2</td> </tr> <tr> <td>08 = 1/2 X 1/2</td> <td>20 = 1 1/4 X 1 1/4</td> </tr> <tr> <td>10 = 5/8 X 5/8</td> <td>24 = 1 1/2 X 1 1/2</td> </tr> <tr> <td>12 = 3/4 X 3/4</td> <td>32 = 2 X 2</td> </tr> <tr> <td>16 = 1 X 1</td> <td></td> </tr> </table> <p>The seventh and eighth position shall be a single significant two digit number which indicates the holder's cross section. For shanks 5/8" square and over, the number will represent the number of sixteenths inch of width and height.</p> <p>For shanks under 5/8" square, the number of sixteenths inch of cross section will be preceded by a zero.</p> <p>For rectangular holders the first digit represents the number of eighths inch width, and the second digit the number of quarters inch of height.</p>		05 = 5/16 X 5/16	85 = 1 X 1 1/4	06 = 3/8 X 3/8	86 = 1 X 1 1/2	08 = 1/2 X 1/2	20 = 1 1/4 X 1 1/4	10 = 5/8 X 5/8	24 = 1 1/2 X 1 1/2	12 = 3/4 X 3/4	32 = 2 X 2	16 = 1 X 1												
B	C																																								
																																									
D	E																																								
																																									
N	P																																								
																																									
O Specific description																																									
05 = 5/16 X 5/16	85 = 1 X 1 1/4																																								
06 = 3/8 X 3/8	86 = 1 X 1 1/2																																								
08 = 1/2 X 1/2	20 = 1 1/4 X 1 1/4																																								
10 = 5/8 X 5/8	24 = 1 1/2 X 1 1/2																																								
12 = 3/4 X 3/4	32 = 2 X 2																																								
16 = 1 X 1																																									

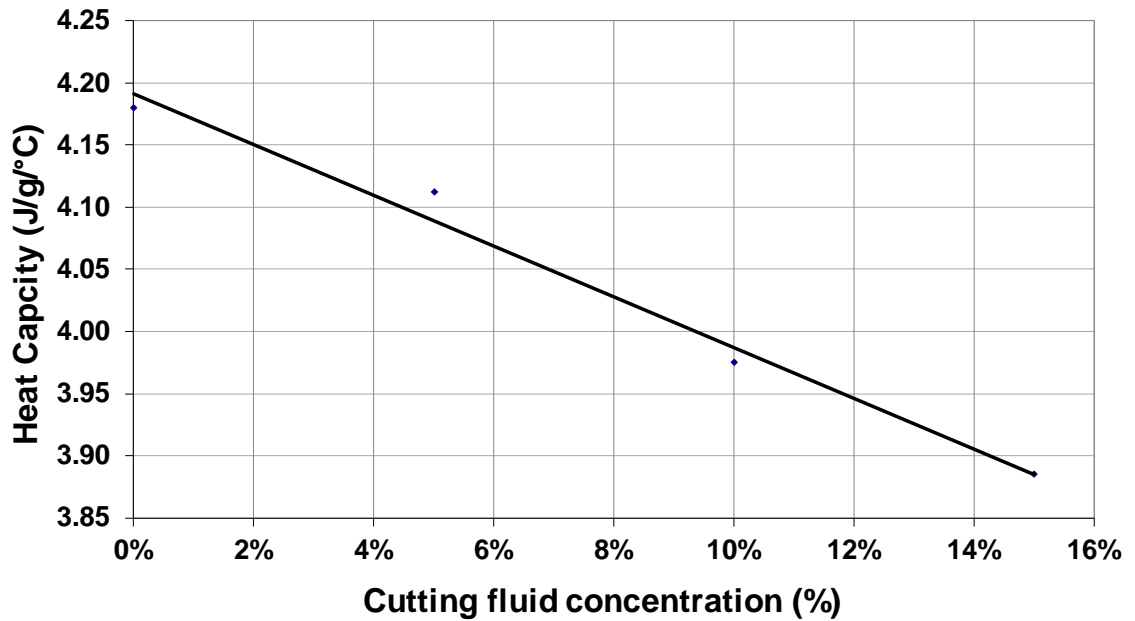
Appendix G Heat capacity measurement results for Vasco 1000 cutting fluid

Vasco 1000 cutting fluid - 5% Solution				
	Specific Heat			
Temperature	Test 1	Test 2	Average	Difference
°C	J/g/°C	J/g/°C	J/g/°C	%
15	4.107	4.120	4.114	0.32
20	4.104	4.120	4.112	0.39
25	4.100	4.120	4.110	0.49
30	4.103	4.121	4.112	0.44
35	4.106	4.122	4.114	0.39
		Average	4.112	

Vasco 1000 cutting fluid - 10% Solution				
	Specific Heat			
Temperature	Test 1	Test 2	Average	Difference
°C	J/g/°C	J/g/°C	J/g/°C	%
15	3.966	3.990	3.978	0.60
20	3.964	3.988	3.976	0.60
25	3.962	3.983	3.973	0.53
30	3.964	3.985	3.975	0.53
35	3.962	3.988	3.975	0.65
		Average	3.975	

Vasco 1000 cutting fluid - 15% Solution				
	Specific Heat			
Temperature	Test 1	Test 2	Average	Difference
°C	J/g/°C	J/g/°C	J/g/°C	%
15	3.885	3.892	3.889	0.18
20	3.879	3.889	3.884	0.26
25	3.879	3.886	3.883	0.18
30	3.882	3.886	3.884	0.10
35	3.885	3.891	3.888	0.15
Average			3.885	

Heat capacity versus cutting fluid concentrations



Appendix H Certificate of conformance for T-type thermocouples

CERTIFICATE OF CONFORMANCE



Certificate No:- C1988
Date Of Issue:- 12th April 2016
Customer:- Northumbria University
Customer Order No:- ND proforma

Tempcon Works Order No:- 72111

ITEM NO	PRODUCT DESCRIPTION	SERIAL NO
A x 3	TMIPPS-10-10-SI-FPPFA-T72-2000-MP Type T MI 1.0mm Ø x 10mm Long Sheath Plain Pot 2mt PFA + MP D1 = 1.0mm Diameter (tolerance +/-0.1mm) L1 = Length up to 10mm (see below) (9mm + hole depth drilling accuracy +/-1 mm). L2 = Plain pot seal L3 = 2 metre lead out Miniature plug termination Sensor and cable to suit working range of +250C Line Code: TMIPPS-10-10-SI-FPPFA-T72-2000-MP	n/a
B	UX120-014M HOBO 4 Channel Thermocouple Data logger with LCD Display	10902140

This is to certify that the whole of the supplies detailed hereon have been inspected and tested using test equipment which has been calibrated by a UKAS accredited laboratory and unless otherwise stated above conforms in all respects with the requirements of the relevant product specification.
 Copies of relevant calibration documents are available upon request.

Signed.....*Ab*.....
Quality Assurance



F112/K

Telephone +44 (0)1243 558270
 Email info@tempcon.co.uk
 Web www.tempcon.co.uk

Ford Lane Business Park, Ford Lane, Ford, West Sussex BN18 0UZ

Registered address: Ford Lane Business Park, Ford Lane, West Sussex BN18 0UZ
 Registered No. 1535366 VAT No. GB322039106

Appendix I **Experimental results**

Appendix I contains the experimental results of the following sections:

I1: Evaluation of different VO- and MO-based fluids and tool materials (section 5.1)

I2: Pre-selection of cutting conditions (section 5.2)

I3: Selection of VO-based fluid and cutting tool material (section 5.3)

I4: Assessment of cutting fluid concentration ratio (section 5.5)

I5: Evaluation of the CUT-LIST cutting fluid supply system (section 5.5)

I6: Repeatability trials

I1: Evaluation of different VO- and MO-based fluids and tool materials (section 5.1)

Exp. No.	Cutting Fluid	Cutting tool	Surface roughness (Ra) - (μm)				Tool wear (μm)
			R _{a-1}	R _{a-2}	R _{a-3}	R _{a,avg}	
1	Hocut 3450	H13A	0.92	0.92	0.86	0.90	53.81
2		GC1105	0.80	0.68	0.56	0.68	39.85
3		H10F	0.84	0.86	0.90	0.87	41.12
4		S05F	0.92	0.86	0.82	0.87	52.65
5	Vasco 1000	H13A	1.08	1.06	1.08	1.07	56.3
6		GC1105	0.80	0.68	0.72	0.73	38.8
7		H10F	0.90	0.88	0.90	0.89	40.2
8		S05F	0.74	0.78	0.82	0.78	54.75
9	NE250 H	H13A	1.16	1.12	1.10	1.13	48.5
10		GC1105	0.74	0.82	0.76	0.77	35.3
11		H10F	0.78	0.80	0.80	0.79	37.2
12		S05F	1.10	1.04	0.94	1.03	46.8
13	SOLUtec	H13A	1.04	1.02	0.98	1.01	51.9
14		GC1105	0.70	0.76	0.58	0.68	37.21
15		H10F	0.92	0.88	0.90	0.90	38.8
16		S05F	0.88	0.86	0.76	0.83	50.7
17	Reference MO-based fluid Cooledge BI	H13A	0.76	0.66	0.72	0.71	59.4
18		GC1105	0.78	0.76	0.70	0.75	42.45
19		H10F	0.82	0.74	0.78	0.78	45.31
20		S05F	0.92	0.90	0.86	0.89	57.2

I1.1: Average values of Ra at various cutting fluids and cutting tools (extracted from H1)

0.9	1.07	1.13	1.01	0.71	0.97	H 13A
0.68	0.73	0.77	0.68	0.75	0.72	GC1105
0.87	0.89	0.79	0.9	0.78	0.85	H10F
0.87	0.78	1.03	0.83	0.89	0.88	S05F
0.83	0.87	0.93	0.86	0.78	Average of Ra (μm)	
Hocut 3450	Vasco 1000	NE250H	Solutec	Cooledge BI		

I1.2: Average values of tool flank wear at various cutting fluids and cutting tools (extracted from H1)

53.81	56.3	48.5	51.9	59.4	40.52	H13A
39.85	38.8	35.3	37.21	42.45	53.98	GC1105
41.12	40.2	37.2	38.8	45.31	38.8	H10F
52.65	54.75	46.8	50.7	57.2	52.42	S05F
46.85	47.51	41.95	44.65	51.17	Average of tool flank wear (μm)	
Hocut 3450	Vasco 1000	NE250	Solutec	Cooledge BI		

I2: Pre-selection of cutting conditions (section 5.2)

Exp. No.	Cutting speed (m/min)	Feed rate (mm/rev)	DoC (mm)	Average surface roughness - (Ra) (μm)				Tool wear (mm)
				R _{a-1}	R _{a-2}	R _{a-3}	R _{a avg}	
1	28	0.1	0.5	0.64	0.76	0.78	0.727	0.031
2		0.1	0.75	0.66	0.70	0.68	0.68	0.033
3		0.1	1	0.62	0.68	0.60	0.633	0.035
4		0.15	0.5	1.0	1.04	1.06	1.033	0.033
5		0.15	0.75	0.86	0.78	0.84	0.827	0.034
6		0.15	1	0.96	1.02	0.96	0.98	0.036
7		0.2	0.5	1.6	1.54	1.58	1.573	0.035
8		0.2	0.75	1.48	1.54	1.54	1.520	0.038
9		0.2	1	1.62	1.64	1.66	1.64	0.039
10	75	0.1	0.5	0.58	0.64	0.68	0.633	0.04
11		0.1	0.75	0.76	0.64	0.70	0.70	0.043
12		0.1	1	0.62	0.54	0.52	0.56 ^a	0.049
13		0.15	0.5	1.02	1.04	1.0	1.02	0.042
14		0.15	0.75	0.86	0.84	0.80	0.833	0.043
15		0.15	1	0.92	0.94	0.98	0.947	0.052
16		0.2	0.5	1.56	1.52	1.48	1.52	0.043
17		0.2	0.75	1.48	1.56	1.42	1.487	0.048
18		0.2	1	1.80	1.82	1.80	1.81 ^b	0.058
19	120	0.1	0.5	0.62	0.60	0.68	0.633	0.051
20		0.1	0.75	0.68	0.64	0.66	0.66	0.069
21		0.1	1	0.60	0.68	0.56	0.613	0.98
22		0.15	0.5	0.84	0.94	0.96	0.913	0.055
23		0.15	0.75	0.84	0.88	0.94	0.887	0.075
24		0.15	1	1.08	1.02	1.00	1.033	0.115
25		0.2	0.5	1.56	1.58	1.60	1.580	0.053
26		0.2	0.75	1.40	1.42	1.40	1.407	0.084
27		0.2	1	1.38	1.36	1.31	1.35	0.132

a and **b** are the lowest and highest values of Ra respectively.

I3: Selection of VO-based fluid and cutting tool material (section 5.3)

Exp. No.	Cutting tool	Cutting fluid	Speed (m/min)	Surface roughness (Ra) - (μm)				Tool wear (μm)	Chip thickness (mm)
				Ra ₁	Ra ₂	Ra ₃	Ra _{avg}		
1	GC 1105	Hocut 3450	120	0.61	0.62	0.61	0.72	70.91	0.13
2			175	0.51	0.52	0.62	0.68	99.92	0.11
3		Vasco 1000	120	0.73	0.70	0.72	0.61	86.67	0.14
4			175	0.70	0.68	0.66	0.55	99.80	0.10
5		NE25 0 H	120	0.71	0.77	0.80	0.76	65.66	0.14
6			175	0.68	0.63	0.78	0.70	114.85	0.12
7		SOLU TEC	120	0.78	0.82	0.76	0.79	78.79	0.13
8			175	0.66	0.72	0.74	0.71	116.73	0.10
9	S05F	Hocut 3450	120	0.7	0.68	0.72	0.70	118.19	0.15
10			175	0.78	0.76	0.9	0.81	157.59	0.10
11		Vasco 1000	120	0.64	0.6	0.62	0.62	120.38	0.14
12			175	0.58	0.52	0.7	0.60	162.84	0.12
13		NE25 0 H	120	0.68	0.74	0.88	0.77	136.58	0.14
14			175	0.68	0.62	0.72	0.67	141.83	0.10
15		SOLU TEC	120	0.62	0.76	1.56	0.98 ^b	119.19	0.14
16			175	0.62	0.66	0.72	0.67	189.11	0.10
17	H13A	Hocut 3450	120	0.5	0.62	0.6	0.57	50.34	0.15
18			175	0.7	0.78	0.76	0.55	120.82	0.11
19		Vasco 1000	120	0.58	0.54	0.52	0.55	72.96	0.12
20			175	0.52	0.52	0.50	0.51 ^a	110.31	0.11
21		NE25 0 H	120	0.72	0.6	0.7	0.67	81.13	0.14
22			175	0.58	0.62	0.56	0.59	97.18	0.12
23		SOLU TEC	120	0.66	0.7	0.64	0.67	68.29	0.14
24			175	0.64	0.52	0.54	0.57	105.06	0.12

a and **b** are the lowest and highest values of Ra respectively.

I4: Assessment of cutting fluid concentration ratio (section 5.4)

Exp. No.	Fluid intensity (%)	Cutting tool	Speed (m/min)	Feed rate (mm/rev)	Surface roughness (Ra) - (μm)				Tool wear (μm)
					Ra ₁	Ra ₂	Ra ₃	Ra _{avg}	
1	5 %	H13A	58	0.1	0.50	0.46	0.46	0.47 ^a	28.88
2		H13A	58	0.1	0.84	0.88	0.90	0.87	49.95
3		H13A	58	0.1	1.36	1.34	1.36	1.35	52.57
4		GC1105	91	0.15	0.76	0.66	0.66	0.69	110.7
5		GC1105	91	0.15	1.06	1.02	0.98	1.02	70.89
6		GC1105	91	0.15	1.56	1.48	1.50	1.51	94.52
7		H10A	146	0.2	0.60	0.58	0.62	0.60	105.0
8		H10A	146	0.2	0.84	0.84	0.86	0.85	91.89
9		H10A	146	0.2	1.48	1.46	1.46	1.47	89.27
10	10 %	H13A	58	0.1	0.58	0.58	0.64	0.60	49.88
11		H13A	58	0.1	0.82	0.80	0.84	0.82	63.01
12		H13A	58	0.1	1.52	1.48	1.44	1.48	78.76
13		GC1105	91	0.15	0.54	0.50	0.52	0.52	76.14
14		GC1105	91	0.15	1.06	1.04	0.98	1.03	91.89
15		GC1105	91	0.15	1.58	1.58	1.56	1.57	70.89
16		H10A	146	0.2	0.52	0.50	0.50	0.51	65.64
17		H10A	146	0.2	0.82	0.84	0.86	0.84	97.14
18		H10A	146	0.2	1.66	1.62	1.62	1.63 ^b	105.0
19	15 %	H13A	58	0.1	0.64	0.56	0.60	0.60	71.67
20		H13A	58	0.1	0.76	0.80	0.78	0.78	55.13
21		H13A	58	0.1	1.56	1.58	1.58	1.57	44.63
22		GC1105	91	0.15	0.72	0.68	0.68	0.69	97.14
23		GC1105	91	0.15	1.02	1.00	1.00	1.01	84..02
24		GC1105	91	0.15	1.70	1.66	1.38	1.58	107.6
25		H10A	146	0.2	0.50	0.50	0.58	0.53	91.89
26		H10A	146	0.2	0.84	0.82	0.88	0.85	85.78
27		H10A	146	0.2	1.54	1.56	1.54	1.55	102.4

a and **b** are the lowest and highest values of Ra respectively

I4.1 Results of tool life test

Cutting conditions:

Feed rate: 0.1 mm/rev

Depth of cut: 0.75 mm

Cutting tool material: uncoated coarse grain carbide (H13A)

Fluid concentration ratio: 10%

Ti-6Al-4V bars diameters and length: \varnothing 22.5 mm x 120 mm

Cutting tool rejection criterion ($VB_{\max} \geq 300 \mu\text{m}$)

Sample No.	T1	T2	T3	T4	T5	T6	T7	T8	T9
Cutting distance (mm)	120	240	360	480	600	720	840	960	1080
VB at cutting speed of 58 m/min	63.014	94.084	118.536	136.906	158.984	198.321	244.661	296.168	368.95
VB at cutting speed of 146 m/min	102.39	183.79	267.81	322.95	472.610				

I4.2 Results of Ra at cutting speed of 58 m/min with various cutting distance

Sample No.	Cutting distance (mm)	Cutting speed (58 m/min)			
		Ra ₁ (μm)	Ra ₂ (μm)	Ra ₃ (μm)	Ra _{avg} (μm)
T1	120	0.58	0.52	0.48	0.52
T2	240	0.60	0.50	0.58	0.56
T3	360	0.56	0.54	0.58	0.56
T4	480	0.62	0.52	0.48	0.54
T5	600	0.76	0.56	0.52	0.61
T6	720	0.60	0.50	0.52	0.54
T7	840	0.54	0.54	0.54	0.54
T8	960	0.66	0.56	0.54	0.58
T9	1080	0.60	0.54	0.48	0.54

I4.3 Results of Ra at cutting speed of 146 m/min with various cutting distance

Sample No.	Cutting distance (mm)	Cutting speed = 146 m/min			
		Ra ₁ (μm)	Ra ₂ (μm)	Ra ₃ (μm)	Ra _{avg} (μm)
T1	120	0.48	0.50	0.50	0.49
T2	240	0.52	0.50	0.74	0.58
T3	360	0.68	0.70	0.84	0.74
T4	480	1.02	1.28	0.80	1.03
T5	600	1.16	1.44	0.86	1.15

I4.4 Results of the micro-hardness test

Sample No. T1 at cutting speed of 146 m/min and 120 mm cutting distance					
Run	Distance below machined surface (μm)	Diagonal values (μm)			HV ₁₀₀
		d _H	d _V	d _{mean}	
1	30	23.5	22.5	23	350
2	60	24	23.5	23.75	329
3	90	29.5	24.5	27	254
4	120	26	25.5	25.75	279.8
5	150	26.5	26	26.25	269
6	180	25.5	25.5	25.5	285.5
7	210	25.5	27	26.25	269
8	240	28.5	29	28.75	214.2
9	270	26	26.5	26.25	269.8
10	300	31	29.5	30.25	202.8
11	330	27.5	27.5	27.5	245
12	360	25	27.5	26.25	269
13	390	26.5	28.5	27.5	245
14	420	27.5	27.5	27.5	245
15	450	29.5	27.5	28.5	228

Sample No. T3 at cutting speed of 146 m/min and 360 mm cutting distance					
Run	Distance below machined surface (μm)	Diagonal values (μm)			HV ₁₀₀
		d _H	d _V	d _{mean}	
1	30	23	22.5	22.75	358.25
2	60	25	24	24.5	309.5
3	90	25.5	24.5	25	297
4	120	26.5	25.5	26	274
5	150	27	25.5	26.25	269
6	180	28	27	27.5	245
7	210	28	27.5	27.75	240.5
8	240	27.5	29	28.25	232
9	270	26.5	26	26.25	269
10	300	27	26	26.5	264
11	330	27	26	26.5	264
12	360	27.5	26	26.75	259
13	390	29	27	28	236
14	420	27	27.5	27.25	249.5
15	450	30	29	29.5	213

Sample No. T5 at cutting speed of 146 m/min and 600 mm cutting distance					
Run	Distance below machined surface (μm)	Diagonal values (μm)			HV ₁₀₀
		d _H	d _V	d _{mean}	
1	30	22	22.5	22.25	374.75
2	60	23	25.5	24.25	315.75
3	90	24	25.5	24.75	303.25
4	120	25.5	25.5	25.5	285.5
5	150	26	25.5	25.75	279.8
6	180	25	26	25.5	285.5
7	210	27	26.5	26.75	259
8	240	24.5	26.5	25.5	285.5
9	270	25.5	27	26.25	269
10	300	24	27.5	25.75	279.8
11	330	25	27.5	26.25	269
12	360	24.5	26.5	25.5	285.5
13	390	25	27	26	274
14	420	25.5	25.5	25.5	285.5
15	450	24.5	25.5	25	297

Sample No. T1 at cutting speed of 58 m/min and 120 mm cutting distance					
Run	Distance below machined surface (μm)	Diagonal values (μm)			HV ₁₀₀
		d _H	d _V	d _{mean}	
1	30	24	23.5	23.75	329
2	60	24	24.5	24.25	315.75
3	90	24	24.5	24.25	315.74
4	120	24	25	24.5	309.5
5	150	24.5	24.5	24.5	309.5
6	180	24.5	24.5	24.5	309.5
7	210	24.5	25.5	25	297
8	240	24	25.5	24.75	303.25
9	270	24	25.5	24.75	303.25
10	300	25	26	25.5	285.5
11	330	26.5	25	25.75	279.8
12	360	25	26	25.5	285.5
13	390	25.5	26	25.75	279.8
14	420	27	25.5	26.25	269
15	450	26.5	26.5	26.5	264

Sample No. T3 at cutting speed of 58 m/min and 360 mm cutting distance					
Run	Distance below machined surface (μm)	Diagonal values (μm)			HV ₁₀₀
		d _H	d _V	d _{mean}	
1	30	23.5	23.5	23.5	336
2	60	27	25.5	26.25	269
3	90	26	24	25	297
4	120	27.5	26	26.75	259
5	150	26	24.5	25.25	291.25
6	180	24	25	24.5	309.5
7	210	25	24.5	24.75	303.25
8	240	24.5	25	24.75	303.25
9	270	26.5	25	25.75	259
10	300	27	25	26	274
11	330	28	25.5	26.75	259
12	360	26.5	25	25.75	259
13	390	25	25	25	297
14	420	26.5	27	26.75	259
15	450	26	24.5	25.25	291.25

Sample No. T5 at cutting speed of 58 m/min and 600 mm cutting distance					
Run	Distance below machined surface (mm)	Diagonal values (μm)			HV ₁₀₀
		d _H	d _V	d _{mean}	
1	30	23	23.5	23.25	343.5
2	60	24	24	24	322
3	90	24	24.5	24.25	303.25
4	120	24.5	23.5	24	322
5	150	23.5	25	24.25	303.25
6	180	26	25.5	25.75	259
7	210	24.5	24.5	24.5	309.5
8	240	25	24.5	24.75	303.25
9	270	25.5	25	25.25	291.25
10	300	26	26	26	274
11	330	24.5	24.5	24.5	309.5
12	360	24	24.5	24.25	303.25
13	390	27.5	27	27.25	249.5
14	420	26	25	25.5	285.5
15	450	26.5	27.5	27	254

Sample No. T7 at cutting speed of 58 m/min and 840 mm cutting distance

Run	Distance below machined surface (mm)	Diagonal values (μm)			HV ₁₀₀
		d _H	d _V	d _{mean}	
1	30	23	23	23	350
2	60	24	26.5	25.25	291.25
3	90	23.5	24.5	24	322
4	120	26	26	26	274
5	150	27.5	23	25.25	291.25
6	180	24.5	23.5	24	322
7	210	25	25.5	25.25	291.25
8	240	26	26.5	26.25	269
9	270	27	26.5	26.75	259
10	300	26.5	25.5	26	274
11	330	26.5	26	26.25	269
12	360	26.5	24	25.25	291.25
13	390	27	25	26	274
14	420	28	27	27.5	245
15	450	26	25.5	25.75	259

Sample No. T9 at cutting speed of 58 m/min and 1080 mm cutting distance

Run	Distance below machined surface (mm)	Diagonal values (μm)			HV ₁₀₀
		d _H	d _V	d _{mean}	
1	30	22.5	22.5	22.5	366.5
2	60	25	26	25.5	285.5
3	90	25	23.5	24.25	315.75
4	120	24	22.5	23.25	343.5
5	150	24.5	25	24.75	303.25
6	180	24.5	26.5	25.5	285.5
7	210	26	27	26.5	264
8	240	24	25	24.5	309.5
9	270	24.5	24.5	24.5	309.5
10	300	25	24	24.5	309.5
11	330	24	26.5	25.25	291
12	360	24.5	26.5	25.5	285.5
13	390	24.5	24	24.25	315.75
14	420	26	27.5	26.75	259
15	450	26.5	26	26.25	269

14.5 Knoop and Vickers micro-hardness conversion chart at load (100gf)

Vickers Load 100gf (0.1kgf)

Diagonal (μm)	Vickers Hardness Number									
	0.0	0.1	0.2	0.3	0.4	0.5	0.6	0.7	0.8	0.9
10	1854	1817	1782	1748	1714	1682	1650	1619	1590	1560
11	1532	1505	1478	1452	1427	1402	1378	1354	1332	1309
12	1288	1266	1246	1225	1206	1187	1168	1149	1132	1114
13	1097	1080	1064	1048	1033	1017	1002	988	974	960
14	946	933	919	907	894	882	870	858	846	835
15	824	813	802	792	782	772	762	752	743	733
16	724	715	706	698	689	681	673	665	657	649
17	642	634	627	619	612	605	599	592	585	579
18	572	566	560	554	548	542	536	530	525	519
19	514	508	503	498	493	488	483	478	473	468
20	464	459	454	450	446	441	437	433	429	424
21	420	416	413	409	405	401	397	394	390	387
22	383	380	376	373	369	366	363	360	357	354
23	350	347	344	342	339	336	333	330	327	325
24	322	319	317	314	311	309	306	304	301	299
25	297	294	292	290	287	285	283	281	279	276
26	274	272	270	268	266	264	262	260	258	256
27	254	252	251	249	247	245	243	242	240	238
28	236	235	233	231	230	228	227	225	224	222
29	220	219	217	216	214	213	212	210	209	207
30	206	205	203	202	201	199	198	197	195	194
31	193	192	190	189	188	187	186	184	183	182
32	181	180	179	178	177	176	174	173	172	171
33	170	169	168	167	166	165	164	163	162	161
34	160	159	159	158	157	156	155	154	153	152
35	151	150	150	149	148	147	146	145	145	144
36	143	142	141	141	140	139	138	138	137	136
37	135	135	134	133	133	132	131	130	130	129
38	128	128	127	126	126	125	124	124	123	123
39	122	121	121	120	119	119	118	118	117	116
40	116	115	115	114	114	113	112	112	111	111
41	110	110	109	109	108	108	107	107	106	106
42	105	105	104	104	103	103	102	102	101	101
43	100	99.8	99.3	98.9	98.4	98.0	97.5	97.1	96.6	96.2
44	95.8	95.3	94.9	94.5	94.0	93.6	93.2	92.8	92.4	92.0
45	91.6	91.1	90.7	90.3	89.9	89.6	89.2	88.8	88.4	88.0
46	87.6	87.2	86.9	86.5	86.1	85.7	85.4	85.0	84.6	84.3
47	83.9	83.6	83.2	82.9	82.5	82.2	81.8	81.5	81.1	80.8
48	80.5	80.1	79.8	79.5	79.1	78.8	78.5	78.2	77.9	77.5
49	77.2	76.9	76.6	76.3	76.0	75.7	75.4	75.1	74.8	74.5
50	74.2	73.9	73.6	73.3	73.0	72.7	72.4	72.1	71.8	71.6
51	71.3	71.0	70.7	70.4	70.2	69.9	69.6	69.4	69.1	68.8
52	68.6	68.3	68.0	67.8	67.5	67.3	67.0	66.8	66.5	66.3
53	66.0	65.8	65.5	65.3	65.0	64.8	64.5	64.3	64.1	63.8
54	63.6	63.3	63.1	62.9	62.6	62.4	62.2	62.0	61.7	61.5
55	61.3	61.1	60.8	60.6	60.4	60.2	60.0	59.8	59.5	59.3
56	59.1	58.9	58.7	58.5	58.3	58.1	57.9	57.7	57.5	57.3
57	57.1	56.9	56.7	56.5	56.3	56.1	55.9	55.7	55.5	55.3
58	55.1	54.9	54.7	54.5	54.4	54.2	54.0	53.8	53.6	53.4
59	53.3	53.1	52.9	52.7	52.5	52.4	52.2	52.0	51.8	51.7
60	51.5	51.3	51.2	51.0	50.8	50.7	50.5	50.3	50.2	50.0
61	49.8	49.7	49.5	49.3	49.2	49.0	48.9	48.7	48.5	48.4
62	48.2	48.1	47.9	47.8	47.6	47.5	47.3	47.2	47.0	46.9
63	46.7	46.6	46.4	46.3	46.1	46.0	45.8	45.7	45.5	45.4

I5: Evaluation of the CUT-LIST cutting fluid supply system (section 5.5)**I5.1 Cutting force**

Exp. No.	Nozzle angle in feed direction (degree)	Nozzle angle against feed direction (degree)	Impinging distance (mm)	Cutting speed (m/min)	Feed rate (mm/min)	Flow rate (L/min)	Maximum cutting force (N)			Resultant cutting force (N)
							F _x	F _y	F _z	
1	15	15	35	95	0.1	1	621.5	1315	375	1502.04
2	15	15	35	95	0.15	1.5	1174	1775	401.4	2165.65
3	15	15	35	200	0.1	2	969	1492	646.7	1892.95
4	15	15	35	200	0.15	3	1006	1479	683	1914.67
5	15	45	35	95	0.1	1	841.5	1406	452.3	1699.86
6	15	45	35	95	0.15	1.5	836	1527	354.7	1776.64
7	15	45	35	200	0.1	2	390.8	1343	708.6	1567.96
8	15	45	35	200	0.15	3	1154	1678	714	2158.05
9	15	60	35	95	0.1	1	354	1419	738	1638.15
10	15	60	35	95	0.15	1.5	799	1482	345	1718.65
11	15	60	35	200	0.1	2	913.7	1536	598.7	1884.83
12	15	60	35	200	0.15	3	1175	1619	387.8	2037.69
13	15	15	55	95	0.1	1	778.8	1429	390.3	1673.59
14	15	15	55	95	0.15	1.5	1034	1732	396.7	2055.81
15	15	15	55	200	0.1	2	973	1457	674.5	1877.37
16	15	15	55	200	0.15	3	935.2	1630	785.2	2036.67
17	15	45	55	95	0.1	1	758	1291	289.6	1524.83
18	15	45	55	95	0.15	1.5	1011	1592	524.3	1957.42
19	15	45	55	200	0.1	2	950.8	1580	560	1927.18

Exp. No.	Nozzle angle in feed direction (degree)	Nozzle angle against feed direction (degree)	Impinging distance (mm)	Cutting speed (m/min)	Feed rate (mm/min)	Flow rate (L/min)	Maximum cutting force (N)			Resultant cutting force (N)
							F _x	F _y	F _z	
20	15	45	55	200	0.15	3	996	1525	462.7	1879.29
21	15	60	55	95	0.1	1	726.5	1324	353.5	1551.04
22	15	60	55	95	0.15	1.5	1109	1678	406.6	2052.04
23	15	60	55	200	0.1	2	706.6	1359	620.3	1652.55
24	15	60	55	200	0.15	3	1247	1582	354.3	2045.30
25	15	15	75	95	0.1	1	807.5	1403	337	1653.49
26	15	15	75	95	0.15	1.5	905	1564	309	1833.19
27	15	15	75	200	0.1	2	904.2	1423	572.3	1780.46
28	15	15	75	200	0.15	3	1202	1614	472	2067.02
29	15	45	75	95	0.1	1	766.4	1243	287.3	1488.27
30	15	45	75	95	0.15	1.5	1130	1585	352.2	1978.17
31	15	45	75	200	0.1	2	799.3	1396	643.7	1732.64
32	15	45	75	200	0.15	3	992	1560*	696.2	1975.44
33	15	60	75	95	0.1	1	910	1461	391.7	1765.23
34	15	60	75	95	0.15	1.5	919	1563	422	1861.62
35	15	60	75	200	0.1	2	890	1407	614	1774.47
36	15	60	75	200	0.15	3	1030	1506	730.4	1965.30
37	45	15	35	95	0.1	1	876.6	1524	353.6	1793.33
38	45	15	35	95	0.15	1.5	921.6	1560*	303.6	1837.15
39	45	15	35	200	0.1	2	1088	1640	597	2056.64
40	45	15	35	200	0.15	3	1187	1678	404.3	2094.78
41	45	45	35	95	0.1	1	643	1262	372	1464.40
42	45	45	35	95	0.15	1.5	1021	1584	370	1920.52
43	45	45	35	200	0.1	2	883.6	1449	473.4	1761.95

Exp. No.	Nozzle angle in feed direction (degree)	Nozzle angle against feed direction (degree)	Impinging distance (mm)	Cutting speed (m/min)	Feed rate (mm/min)	Flow rate (L/min)	Maximum cutting force (N)			Resultant cutting force (N)
							F _x	F _y	F _z	
44	45	45	35	200	0.15	3	1436	1786	747.6	2410.56
45	45	60	35	95	0.1	1	782.8	1453	288.2	1675.42
46	45	60	35	95	0.15	1.5	951.8	1626	379.6	1921.95
47	45	60	35	200	0.1	2	885.2	1379	617.6	1751.19
48	45	60	35	200	0.15	3	993.5	1674	628.7	2045.63
49	45	15	55	95	0.1	1	572	1165	333.3	1339.96
50	45	15	55	95	0.15	1.5	1048	1605	271	1935.92
51	45	15	55	200	0.1	2	868.5	1398	540.5	1732.29
52	45	15	55	200	0.15	3	1157	1746	611.6	2182.02
53	45	45	55	95	0.1	1	781	1378	286.2	1609.58
54	45	45	55	95	0.15	1.5	983.6	1580	295	1884.38
55	45	45	55	200	0.1	2	805.7	1396	630.4	1730.71
56	45	45	55	200	0.15	3	1172	1591	669.8	2086.50
57	45	60	55	95	0.1	1	784	1373	361.6	1621.89
58	45	60	55	95	0.15	1.5	915.7	1596	395	1881.95
59	45	60	55	200	0.1	2	889.6	1583	625.5	1920.55
60	45	60	55	200	0.15	3	1289	1759	696.4	2289.23
61	45	15	75	95	0.1	1	741.7	1328	378	1567.35
62	45	15	75	95	0.15	1.5	1035	1621	417.2	1967.97
63	45	15	75	200	0.1	2	817.4	1325	581.7	1661.97
64	45	15	75	200	0.15	3	1258	1621	675	2160.05
65	45	45	75	95	0.1	1	839.5	1420	302.2	1677.05
66	45	45	75	95	0.15	1.5	856.2	1588	381.2	1843.95
67	45	45	75	200	0.1	2	821	1524	532	1810.98

Exp. No.	Nozzle angle in feed direction (degree)	Nozzle angle against feed direction (degree)	Impinging distance (mm)	Cutting speed (m/min)	Feed rate (mm/min)	Flow rate (L/min)	Maximum cutting force (N)			Resultant cutting force (N)
							F _x	F _y	F _z	
68	45	45	75	200	0.15	3	1093	1558	676	2019.65
69	45	60	75	95	0.1	1	854	1391	304.6	1660.42
70	45	60	75	95	0.15	1.5	925.4	1660	292.7	1922.92
71	45	60	75	200	0.1	2	883.5	1477	545.8	1805.55
72	45	60	75	200	0.15	3	1182	1655	558.8	2109.12
73	60	15	35	95	0.1	1	760	1419	371	1651.91
74	60	15	35	95	0.15	1.5	829.2	1552	409.5	1806.65
75	60	15	35	200	0.1	2	916.7	1451	506	1789.35
76	60	15	35	200	0.15	3	1171	1558	823.2	2115.72
77	60	45	35	95	0.1	1	767.2	1446	332.8	1670.41
78	60	45	35	95	0.15	1.5	1030	1534	291.8	1870.62
79	60	45	35	200	0.1	2	904	1565	533	1884.29
80	60	45	35	200	0.15	3	1016	1534	557.6	1922.58
81	60	60	35	95	0.1	1	744.5	1466	316.7	1674.44
82	60	60	35	95	0.15	1.5	1042	1593	384.8	1942.03
83	60	60	35	200	0.1	2	833	1439	533.3	1746.14
84	60	60	35	200	0.15	3	999.3	1536	657.4	1946.81
85	60	15	55	95	0.1	1	868.8	1423	324.3	1698.50
86	60	15	55	95	0.15	1.5	1092	1619	279	1972.68
87	60	15	55	200	0.1	2	827	1395	610.7	1732.89
88	60	15	55	200	0.15	3	967	1614	711	2011.37
89	60	45	55	95	0.1	1	807.5	1420	300	1660.86
90	60	45	55	95	0.15	1.5	999	1651	352	1961.56
91	60	45	55	200	0.1	2	1015	1572	609.2	1967.88

Exp. No.	Nozzle angle in feed direction (degree)	Nozzle angle against feed direction (degree)	Impinging distance (mm)	Cutting speed (m/min)	Feed rate (mm/min)	Flow rate (L/min)	Maximum cutting force (N)			Resultant cutting force (N)
							F _x	F _y	F _z	
92	60	45	55	200	0.15	3	1176	1607	681	2104.56
93	60	60	55	95	0.1	1	761.3	1399	297	1620.18
94	60	60	55	95	0.15	1.5	1150	1657	299	2039.01
95	60	60	55	200	0.1	2	1031	1623	735.7	2058.72
96	60	60	55	200	0.15	3	1116	1631	762.8	2118.37
97	60	15	75	95	0.1	1	887	1499	338.3	1774.32
98	60	15	75	95	0.15	1.5	1026	1604	433.8	1952.86
99	60	15	75	200	0.1	2	1009	1560	633.4	1962.87
101	60	45	75	95	0.1	1	718	1237	252.7	1452.43
102	60	45	75	95	0.15	1.5	982.4	1459	295.8	1783.62
103	60	45	75	200	0.1	2	867	1402	572	1744.84
104	60	45	75	200	0.15	3	915	1540	626.2	1897.62
105	60	60	75	95	0.1	1	703.7	1496	374.2	1695.06
106	60	60	75	95	0.15	1.5	827.3	1497	330	1741.93
107	60	60	75	200	0.1	2	888.8	1402	562.7	1752.77
108	60	60	75	200	0.15	3	1125	1493	684.4	1990.75
101	60	45	75	95	0.1	1	718	1237	252.7	1452.43
102	60	45	75	95	0.15	1.5	982.4	1459	295.8	1783.62
103	60	45	75	200	0.1	2	867	1402	572	1744.84
104	60	45	75	200	0.15	3	915	1540	626.2	1897.62
105	60	60	75	95	0.1	1	703.7	1496	374.2	1695.06
106	60	60	75	95	0.15	1.5	827.3	1497	330	1741.93
107	60	60	75	200	0.1	2	888.8	1402	562.7	1752.77
108	60	60	75	200	0.15	3	1125	1493	684.4	1990.75

Exp. No.	Nozzle angle in feed direction (degree)	Nozzle angle against feed direction (degree)	Impinging distance (mm)	Cutting speed (m/min)	Feed rate (mm/min)	Flow rate (L/min)	Maximum cutting force (N)			Resultant cutting force (N)
							F _x	F _y	F _z	
109*	-	-	-	95	0.1	1.6	749.4	1383	293.3	1600.10
110*	-	-	-	95	0.15	2.40	899.76	1380	265.88	1668.73
111*	-	-	-	200	0.1	3.38	905.8	1387	880	1875.80
112*	-	-	-	200	0.15	5.2	1168	1357	645.4	1903.21

*Conventional flood supply system

I5.2 Average workpiece temperature

Exp. No.	Nozzle angle in feed direction (degree)	Nozzle angle against feed direction (degree)	Impinging distance (mm)	Cutting speed (m/min)	Feed rate (mm/rev)	Total Q (l/min)	Workpiece temperatures (°C)				Average workpiece temperatures (°C)
							T1	T2	T3	T4	
1	15	15	30	95	0.1	1	33.76	29.45	25.86	28.86	29.5
2	15	15	30	95	0.15	1.5	32.39	28.60	25.26	28.15	28.6
3	15	15	30	200	0.1	2	25.96	23.68	25.2	25.77	25.1
4	15	15	30	200	0.15	3	23.02	21.59	21.91	21.10	21.9
5	15	45	30	95	0.1	1	40.30	33.41	32.24	29.02	33.7
6	15	45	30	95	0.15	1.5	30.83	26.04	23.54	25.64	26.5
7	15	45	30	200	0.1	2	25.90	24.03	22.68	25.05	24.4
8	15	45	30	200	0.15	3	24.41	21.93	20.91	22.16	22.4
9	15	60	30	95	0.1	1	37.73	29.35	27.57	29.88	31.1

Exp. No.	Nozzle angle in feed direction (degree)	Nozzle angle against feed direction (degree)	Impinging distance (mm)	Cutting speed (m/min)	Feed rate (mm/rev)	Total Q (l/min)	Workpiece temperatures (°C)				Average workpiece temperatures (°C)
							T1	T2	T3	T4	
10	15	60	30	95	0.15	1.5	27.66	23.34	21.67	24.04	24.2
11	15	60	30	200	0.1	2	24.94	23.66	24.22	24.11	24.2
12	15	60	30	200	0.15	3	23.03	22.07	22.31	21.76	22.3
13	15	15	50	95	0.1	1	28.07	26.61	26.59	25.10	26.6
14	15	15	50	95	0.15	1.5	26.01	24.67	24.81	23.81	24.8
15	15	15	50	200	0.1	2	24.66	23.24	24.10	23.89	23.9
16	15	15	50	200	0.15	3	22.50	21.88	22.0	21.48	22.0
17	15	45	50	95	0.1	1	27.50	25.26	26.5	26.64	26.5
18	15	45	50	95	0.15	1.5	23.67	22.18	22.8	22.42	22.8
19	15	45	50	200	0.1	2	22.97	22.05	22.5	22.47	22.5
20	15	45	50	200	0.15	3	21.69	20.74	21.0	20.58	21.0
21	15	60	50	95	0.1	1	25.88	25.07	25.7	26.04	25.7
22	15	60	50	95	0.15	1.5	24.59	23.02	23.5	23.00	23.5
23	15	60	50	200	0.1	2	24.10	22.44	23.1	22.81	23.1
24	15	60	50	200	0.15	3	22.21	21.59	21.7	21.25	21.7
25	15	15	70	95	0.1	1	28.80	26.21	27.3	26.93	27.3
26	15	15	70	95	0.15	1.5	24.62	23.42	23.9	23.77	23.9
27	15	15	70	200	0.1	2	22.60	21.94	22.3	22.40	22.3
28	15	15	70	200	0.15	3	22.11	21.32	21.7	21.69	21.7
29	15	45	70	95	0.1	1	26.76	27.86	26.7	25.61	26.7
30	15	45	70	95	0.15	1.5	26.55	24.41	24.8	23.42	24.8
31	15	45	70	200	0.1	2	23.05	22.27	22.7	22.68	22.7

Exp. No.	Nozzle angle in feed direction (degree)	Nozzle angle against feed direction (degree)	Impinging distance (mm)	Cutting speed (m/min)	Feed rate (mm/rev)	Total Q (l/min)	Workpiece temperatures (°C)				Average workpiece temperatures (°C)
							T1	T2	T3	T4	
32	15	45	70	200	0.15	3	21.87	21.83	21.7	21.36	21.7
33	15	60	70	95	0.1	1	30.38	28.64	28.5	26.36	28.5
34	15	60	70	95	0.15	1.5	26.48	24.75	25.3	24.71	25.3
35	15	60	70	200	0.1	2	24.38	23.72	24.0	23.99	24.0
36	15	60	70	200	0.15	3	22.73	22.32	22.3	21.85	22.3
37	45	15	30	95	0.1	1	28.55	26.46	27.2	26.49	27.2
38	45	15	30	95	0.15	1.5	26.04	24.94	25.3	24.92	25.3
39	45	15	30	200	0.1	2	25.37	24.69	25.2	25.67	25.2
40	45	15	30	200	0.15	3	25.10	23.55	24.1	23.73	24.1
41	45	45	30	95	0.1	1	31.73	28.24	29.2	27.48	29.2
42	45	45	30	95	0.15	1.5	26.07	23.60	24.4	23.57	24.4
43	45	45	30	200	0.1	2	24.70	23.34	23.8	23.45	23.8
44	45	45	30	200	0.15	3	23.38	22.41	23.1	23.41	23.1
45	45	60	30	95	0.1	1	32.45	29.19	30.3	29.19	30.3
46	45	60	30	95	0.15	1.5	28.83	26.31	26.8	25.40	26.8
47	45	60	30	200	0.1	2	24.99	23.47	24.1	23.74	24.1
48	45	60	30	200	0.15	3	23.12	22.15	22.8	23.13	22.8
49	45	15	50	95	0.1	1	30.98	28.54	29.2	28.07	29.2
50	45	15	50	95	0.15	1.5	27.74	25.92	26.3	25.28	26.3
51	45	15	50	200	0.1	2	27.54	25.95	26.7	26.61	26.7
52	45	15	50	200	0.15	3	23.37	22.10	22.5	22.08	22.5
53	45	45	50	95	0.1	1	30.06	28.16	28.6	27.64	28.6

Exp. No.	Nozzle angle in feed direction (degree)	Nozzle angle against feed direction (degree)	Impinging distance (mm)	Cutting speed (m/min)	Feed rate (mm/rev)	Total Q (l/min)	Workpiece temperatures (°C)				Average workpiece temperatures (°C)
							T1	T2	T3	T4	
54	45	45	50	95	0.15	1.5	26.67	25.49	25.52	24.26	25.5
55	45	45	50	200	0.1	2	23.56	22.96	23.36	22.94	23.2
56	45	45	50	200	0.15	3	21.77	21.38	21.41	21.14	21.4
57	45	60	50	95	0.1	1	28.79	27.04	27.60	26.84	27.6
58	45	60	50	95	0.15	1.5	24.29	23.70	23.58	22.91	23.6
59	45	60	50	200	0.1	2	23.40	22.39	23.12	23.36	23.1
60	45	60	50	200	0.15	3	22.49	21.86	22.3	22.47	22.3
61	45	15	70	95	0.1	1	31.43	29.31	30.1	29.50	30.1
62	45	15	70	95	0.15	1.5	29.15	25.92	27.19	26.55	27.2
63	45	15	70	200	0.1	2	27.60	25.13	26.42	26.33	26.4
64	45	15	70	200	0.15	3	23.28	22.48	23.1	23.15	23.0
65	45	45	70	95	0.1	1	33.39	28.88	30.98	30.35	30.9
66	45	45	70	95	0.15	1.5	28.34	26.49	26.5	24.70	26.5
67	45	45	70	200	0.1	2	27.64	25.37	26.5	26.36	26.5
68	45	45	70	200	0.15	3	23.40	22.62	23.1	23.11	23.05
69	45	60	70	95	0.1	1	32.04	28.81	30.7	31.22	30.7
70	45	60	70	95	0.15	1.5	30.88	26.2	22.51	25.17	26.2
71	45	60	70	200	0.1	2	25.99	24.5	22.40	25.04	24.5
72	45	60	70	200	0.15	3	24.75	23.42	23.76	23.00	23.7
73	60	15	30	95	0.1	1	33.36	31.49	27.35	33.90	31.5
74	60	15	30	95	0.15	1.5	29.05	26.63	23.32	27.34	26.6
75	60	15	30	200	0.1	2	27.37	26.21	23.22	28.13	26.2

Exp. No.	Nozzle angle in feed direction (degree)	Nozzle angle against feed direction (degree)	Impinging distance (mm)	Cutting speed (m/min)	Feed rate (mm/rev)	Total Q (l/min)	Workpiece temperatures (°C)				Average workpiece temperatures (°C)
							T1	T2	T3	T4	
76	60	15	30	200	0.15	3	25.90	23.88	21.90	25.12	24.2
77	60	45	30	95	0.1	1	35.16	30.43	24.12	32.06	30.4
78	60	45	30	95	0.15	1.5	28.85	27.82	26.85	27.60	27.8
79	60	45	30	200	0.1	2	27.81	26.15	24.09	26.51	26.1
80	60	45	30	200	0.15	3	25.07	23.46	24.21	23.78	24.1
81	60	60	30	95	0.1	1	39.05	33.55	35.05	28.14	33.9
82	60	60	30	95	0.15	1.5	28.92	27.01	26.56	27.5	27.5
83	60	60	30	200	0.1	2	27.76	25.4	26.74	21.69	25.4
84	60	60	30	200	0.15	3	24.82	23.71	24.58	21.76	23.7
85	60	15	50	95	0.1	1	35.85	32.36	31.51	24.89	31.2
86	60	15	50	95	0.15	1.5	30.58	26.76	26.81	22.42	26.6
87	60	15	50	200	0.1	2	27.77	26.43	27.55	24.02	26.4
88	60	15	50	200	0.15	3	24.11	22.71	23.43	20.19	22.6
89	60	45	50	95	0.1	1	30.67	29.16	26.97	21.35	27.0
90	60	45	50	95	0.15	1.5	27.31	24.55	24.31	20.21	24.1
91	60	45	50	200	0.1	2	25.82	24.5	24.97	22.73	24.5
92	60	45	50	200	0.15	3	24.25	22.98	23.52	20.19	22.7
93	60	60	50	95	0.1	1	33.79	31.58	27	21.98	28.6
94	60	60	50	95	0.15	1.5	26.18	23.99	24.70	20.13	23.8
95	60	60	50	200	0.1	2	24.34	24.02	24.70	21.08	23.5
96	60	60	50	200	0.15	3	24.51	22.87	23.87	23.8	23.8
97	60	15	70	95	0.1	1	40.39	32.04	27.66	31.61	32.9

Exp. No.	Nozzle angle in feed direction (degree)	Nozzle angle against feed direction (degree)	Impinging distance (mm)	Cutting speed (m/min)	Feed rate (mm/rev)	Total Q (l/min)	Workpiece temperatures (°C)				Average workpiece temperatures (°C)
							T1	T2	T3	T4	
98	60	15	70	95	0.15	1.5	30.07	26.15	23.73	25.75	26.4
99	60	15	70	200	0.1	2	26.24	23.28	22.60	25.36	24.4
100	60	15	70	200	0.15	3	24.25	22.24	21.45	21.90	22.5
101	60	45	70	95	0.1	1	31.61	28.72	27.63	30.02	29.5
102	60	45	70	95	0.15	1.5	29.45	25.07	23.51	26.44	26.1
103	60	45	70	200	0.1	2	24.16	22.11	20.89	22.43	22.4
104	60	45	70	200	0.15	3	22.53	19.95	20.8	20.01	20.8
105	60	60	70	95	0.1	1	30.38	27.78	28.4	26.97	28.4
106	60	60	70	95	0.15	1.5	26.73	22.73	24.4	23.65	24.4
107	60	60	70	200	0.1	2	24.28	21.78	20.99	22.15	22.3
108	60	60	70	200	0.15	3	22.35	21.09	20.46	21.15	21.3
109*	-	-	-	95	0.1	1.6	27.14	23.32	21.80	24.40	24.2
110*	-	-	-	95	0.15	2.4	23.19	21.24	19.81	21.71	21.5
111*	-	-	-	200	0.1	3.38	21.91	20.66	21.4	21.56	21.4
112*	-	-	-	200	0.15	5.2	21.80	19.52	20.62	20.39	20.6

*Conventional flood supply system

I5.3 Tool flank wear and burr height

Exp. No.	Nozzle angle in feed direction (degree)	Nozzle angle against feed direction (degree)	Impinging distance (mm)	Cutting speed (m/min)	Feed rate (mm/rev)	Flow rate (l/min)	Tool flank wear (μm)	Burr height (mm)
1	15	15	30	95	0.1	1	32.91	0.52
2	15	15	30	95	0.15	1.5	35.82	0.24
3	15	15	30	200	0.1	2	169.71	0.53
4	15	15	30	200	0.15	3	89.37	0.22
5	15	45	30	95	0.1	1	34.24	0.61
6	15	45	30	95	0.15	1.5	32.28	0.23
7	15	45	30	200	0.1	2	138.18	0.49
8	15	45	30	200	0.15	3	223.20	0.23
9	15	60	30	95	0.1	1	35.75	0.52
10	15	60	30	95	0.15	1.5	35.83	0.42
11	15	60	30	200	0.1	2	151.84	0.39
12	15	60	30	200	0.15	3	74.53	0.17
13	15	15	50	95	0.1	1	32.52	0.25
14	15	15	50	95	0.15	1.5	288.36	0.10
15	15	15	50	200	0.1	2	163.60	0.45
16	15	15	50	200	0.15	3	113.66	0.14
17	15	45	50	95	0.1	1	30.16	0.30
18	15	45	50	95	0.15	1.5	40.37	0.17
19	15	45	50	200	0.1	2	114.83	0.40
20	15	45	50	200	0.15	3	63.29	0.19
21	15	60	50	95	0.1	1	30.12	0.53
22	15	60	50	95	0.15	1.5	37.26	0.16

Exp. No.	Nozzle angle in feed direction (degree)	Nozzle angle against feed direction (degree)	Impinging distance (mm)	Cutting speed (m/min)	Feed rate (mm/rev)	Flow rate (l/min)	Tool flank wear (μm)	Burr height (mm)
23	15	60	50	200	0.1	2	126.18	0.15
24	15	60	50	200	0.15	3	61.79	0.23
25	15	15	70	95	0.1	1	28.61	0.42
26	15	15	70	95	0.15	1.5	35.81	0.19
27	15	15	70	200	0.1	2	106.02	0.33
28	15	15	70	200	0.15	3	71	0.26
29	15	45	70	95	0.1	1	32.97	0.27
30	15	45	70	95	0.15	1.5	34.54	0.14
31	15	45	70	200	0.1	2	128.32	0.35
32	15	45	70	200	0.15	3	98.11	0.26
33	15	60	70	95	0.1	1	35.53	0.51
34	15	60	70	95	0.15	1.5	37.13	0.10
35	15	60	70	200	0.1	2	106.13	0.38
36	15	60	70	200	0.15	3	117.50	0.19
37	45	15	30	95	0.1	1	30.01	0.43
38	45	15	30	95	0.15	1.5	32.97	0.22
39	45	15	30	200	0.1	2	149.42	0.46
40	45	15	30	200	0.15	3	135.96	0.38
41	45	45	30	95	0.1	1	31.43	0.48
42	45	45	30	95	0.15	1.5	33.80	0.20
43	45	45	30	200	0.1	2	123.85	0.31
44	45	45	30	200	0.15	3	124.94	0.27
45	45	60	30	95	0.1	1	31.55	0.67
46	45	60	30	95	0.15	1.5	31.64	0.24

Exp. No.	Nozzle angle in feed direction (degree)	Nozzle angle against feed direction (degree)	Impinging distance (mm)	Cutting speed (m/min)	Feed rate (mm/rev)	Flow rate (l/min)	Tool flank wear (μm)	Burr height (mm)
47	45	60	30	200	0.1	2	67.58	0.20
48	45	60	30	200	0.15	3	196.58	0.18
49	45	15	50	95	0.1	1	30.06	0.17
50	45	15	50	95	0.15	1.5	31.85	0.27
51	45	15	50	200	0.1	2	127.80	0.29
52	45	15	50	200	0.15	3	135.96	0.25
53	45	45	50	95	0.1	1	31.61	0.18
54	45	45	50	95	0.15	1.5	35.34	0.18
55	45	45	50	200	0.1	2	124.45	0.21
56	45	45	50	200	0.15	3	94.26	0.27
57	45	60	50	95	0.1	1	31.43	0.36
58	45	60	50	95	0.15	1.5	33.62	0.15
59	45	60	50	200	0.1	2	179.45	0.22
60	45	60	50	200	0.15	3	180.16	0.15
61	45	15	70	95	0.1	1	30.28	0.22
62	45	15	70	95	0.15	1.5	37.49	0.30
63	45	15	70	200	0.1	2	130.20	0.43
64	45	15	70	200	0.15	3	195.46	0.30
65	45	45	70	95	0.1	1	33.17	0.41
66	45	45	70	95	0.15	1.5	34.40	0.21
67	45	45	70	200	0.1	2	161	0.13
68	45	45	70	200	0.15	3	127.22	0.24
69	45	60	70	95	0.1	1	30.28	0.52
70	45	60	70	95	0.15	1.5	33.17	0.16

Exp. No.	Nozzle angle in feed direction (degree)	Nozzle angle against feed direction (degree)	Impinging distance (mm)	Cutting speed (m/min)	Feed rate (mm/rev)	Flow rate (l/min)	Tool flank wear (μm)	Burr height (mm)
71	45	60	70	200	0.1	2	142.91	0.15
72	45	60	70	200	0.15	3	78.81	0.19
73	60	15	30	95	0.1	1	28.26	0.49
74	60	15	30	95	0.15	1.5	32.90	0.18
75	60	15	30	200	0.1	2	176.12	0.39
76	60	15	30	200	0.15	3	126.27	0.13
77	60	45	30	95	0.1	1	31.37	0.41
78	60	45	30	95	0.15	1.5	34.38	0.18
79	60	45	30	200	0.1	2	108.32	0.26
80	60	45	30	200	0.15	3	149.03	0.24
81	60	60	30	95	0.1	1	32.95	0.39
82	60	60	30	95	0.15	1.5	37.32	0.17
83	60	60	30	200	0.1	2	126.50	0.35
84	60	60	30	200	0.15	3	96.84	0.24
85	60	15	50	95	0.1	1	30.11	0.32
86	60	15	50	95	0.15	1.5	37.15	0.20
87	60	15	50	200	0.1	2	109.45	0.52
88	60	15	50	200	0.15	3	169.44	0.29
89	60	45	50	95	0.1	1	30.08	0.30
90	60	45	50	95	0.15	1.5	34.42	0.20
91	60	45	50	200	0.1	2	199.73	0.35
92	60	45	50	200	0.15	3	104.30	0.20
93	60	60	50	95	0.1	1	30.01	0.46
94	60	60	50	95	0.15	1.5	35.76	0.15

Exp. No.	Nozzle angle in feed direction (degree)	Nozzle angle against feed direction (degree)	Impinging distance (mm)	Cutting speed (m/min)	Feed rate (mm/rev)	Flow rate (l/min)	Tool flank wear (μm)	Burr height (mm)
95	60	60	50	200	0.1	2	120.62	0.24
96	60	60	50	200	0.15	3	82.18	0.21
97	60	15	70	95	0.1	1	30.64	0.53
98	60	15	70	95	0.15	1.5	37.32	0.31
99	60	15	70	200	0.1	2	175.45	0.45
100	60	15	70	200	0.15	3	117.68	0.22
101	60	45	70	95	0.1	1	35.86	0.38
102	60	45	70	95	0.15	1.5	32.65	0.18
103	60	45	70	200	0.1	2	124.09	0.27
104	60	45	70	200	0.15	3	34.78	0.12
105	60	60	70	95	0.1	1	30.12	0.21
106	60	60	70	95	0.15	1.5	32.89	0.23
107	60	60	70	200	0.1	2	130.66	0.51
108	60	60	70	200	0.15	3	85.91	0.24
109*	-	-	-	95	0.1	1.6	31.20	0.16
110*	-	-	-	95	0.15	2.40	32.90	0.10
111*	-	-	-	200	0.1	3.38	71.88	0.41
112*	-	-	-	200	0.15	5.2	74.36	0.30

*Conventional flood supply system

I5.4 Surface roughness (Ra)

Exp. No.	Nozzle angle in feed direction (degree)	Nozzle angle against feed direction (degree)	Impinging distance (mm)	Cutting speed (m/min)	Feed rate (mm/rev)	Flow rate (l/min)	Average surface roughness – Ra (μm)			
							Ra ₁	Ra ₂	Ra ₃	Ra _{avg}
1	15	15	30	95	0.1	1	0.7	0.64	0.72	0.69
2	15	15	30	95	0.15	1.5	0.7	0.78	0.66	0.71
3	15	15	30	200	0.1	2	0.6	0.6	0.62	0.61
4	15	15	30	200	0.15	3	0.78	0.74	0.74	0.75
5	15	45	30	95	0.1	1	0.66	0.68	0.64	0.66
6	15	45	30	95	0.15	1.5	0.7	0.76	0.68	0.71
7	15	45	30	200	0.1	2	0.62	0.68	0.62	0.64
8	15	45	30	200	0.15	3	0.64	0.78	0.68	0.70
9	15	60	30	95	0.1	1	0.54	0.66	0.62	0.61
10	15	60	30	95	0.15	1.5	0.72	0.74	0.6	0.69
11	15	60	30	200	0.1	2	0.68	0.64	0.64	0.65
12	15	60	30	200	0.15	3	0.76	0.78	0.7	0.75
13	15	15	50	95	0.1	1	0.7	0.62	0.7	0.67
14	15	15	50	95	0.15	1.5	0.72	0.74	0.76	0.74
15	15	15	50	200	0.1	2	0.5	0.76	0.66	0.64
16	15	15	50	200	0.15	3	0.74	0.76	0.58	0.69
17	15	45	50	95	0.1	1	0.7	0.62	0.66	0.66
18	15	45	50	95	0.15	1.5	0.78	0.76	0.7	0.75
19	15	45	50	200	0.1	2	0.6	0.6	0.66	0.62
20	15	45	50	200	0.15	3	0.74	0.7	0.7	0.71

Exp. No.	Nozzle angle in feed direction (degree)	Nozzle angle against feed direction (degree)	Impinging distance (mm)	Cutting speed (m/min)	Feed rate (mm/rev)	Flow rate (l/min)	Average surface roughness – Ra (μm)			
							Ra ₁	Ra ₂	Ra ₃	Ra _{avg}
21	15	60	50	95	0.1	1	0.66	0.6	0.6	0.62
22	15	60	50	95	0.15	1.5	0.76	0.76	0.78	0.77
23	15	60	50	200	0.1	2	0.56	0.66	0.62	0.61
24	15	60	50	200	0.15	3	0.66	0.7	0.76	0.71
25	15	15	70	95	0.1	1	0.64	0.74	0.72	0.70
26	15	15	70	95	0.15	1.5	0.68	0.7	0.78	0.72
27	15	15	70	200	0.1	2	0.62	0.54	0.6	0.59
28	15	15	70	200	0.15	3	0.76	0.62	0.52	0.63
29	15	45	70	95	0.1	1	0.62	0.52	0.5	0.55
30	15	45	70	95	0.15	1.5	0.64	0.7	0.68	0.67
31	15	45	70	200	0.1	2	0.62	0.66	0.58	0.62
32	15	45	70	200	0.15	3	0.68	0.72	0.64	0.68
33	15	60	70	95	0.1	1	0.66	0.56	0.6	0.61
34	15	60	70	95	0.15	1.5	0.74	0.68	0.72	0.71
35	15	60	70	200	0.1	2	0.64	0.56	0.58	0.59
36	15	60	70	200	0.15	3	0.68	0.52	0.74	0.65
37	45	15	30	95	0.1	1	0.72	0.68	0.7	0.70
38	45	15	30	95	0.15	1.5	0.72	0.74	0.74	0.73
39	45	15	30	200	0.1	2	0.54	0.7	0.6	0.61
40	45	15	30	200	0.15	3	0.7	0.76	0.62	0.69
41	45	45	30	95	0.1	1	0.56	0.6	0.64	0.60
42	45	45	30	95	0.15	1.5	0.66	0.62	0.66	0.65

Exp. No.	Nozzle angle in feed direction (degree)	Nozzle angle against feed direction (degree)	Impinging distance (mm)	Cutting speed (m/min)	Feed rate (mm/rev)	Flow rate (l/min)	Average surface roughness – Ra (μm)			
							Ra ₁	Ra ₂	Ra ₃	Ra _{avg}
43	45	45	30	200	0.1	2	0.7	0.74	0.7	0.71
44	45	45	30	200	0.15	3	0.64	0.72	0.8	0.72
45	45	60	30	95	0.1	1	0.6	0.64	0.52	0.59
46	45	60	30	95	0.15	1.5	0.7	0.74	0.78	0.74
47	45	60	30	200	0.1	2	0.74	0.56	0.5	0.60
48	45	60	30	200	0.15	3	0.72	0.68	0.58	0.66
49	45	15	50	95	0.1	1	0.6	0.62	0.54	0.59
50	45	15	50	95	0.15	1.5	0.68	0.72	0.64	0.68
51	45	15	50	200	0.1	2	0.56	0.52	0.6	0.56
52	45	15	50	200	0.15	3	0.76	0.68	0.7	0.71
53	45	45	50	95	0.1	1	0.56	0.58	0.68	0.61
54	45	45	50	95	0.15	1.5	0.64	0.66	0.74	0.68
55	45	45	50	200	0.1	2	0.52	0.52	0.66	0.57
56	45	45	50	200	0.15	3	0.66	0.64	0.56	0.62
57	45	60	50	95	0.1	1	0.62	0.72	0.58	0.64
58	45	60	50	95	0.15	1.5	0.64	0.78	0.66	0.69
59	45	60	50	200	0.1	2	0.58	0.5	0.64	0.57
60	45	60	50	200	0.15	3	0.7	0.66	0.7	0.69
61	45	15	70	95	0.1	1	0.68	0.66	0.6	0.65
62	45	15	70	95	0.15	1.5	0.74	0.78	0.66	0.73
63	45	15	70	200	0.1	2	0.52	0.68	0.5	0.57
64	45	15	70	200	0.15	3	0.88	0.74	0.62	0.75

Exp. No.	Nozzle angle in feed direction (degree)	Nozzle angle against feed direction (degree)	Impinging distance (mm)	Cutting speed (m/min)	Feed rate (mm/rev)	Flow rate (l/min)	Average surface roughness – Ra (μm)			
							Ra ₁	Ra ₂	Ra ₃	Ra _{avg}
65	45	45	70	95	0.1	1	0.68	0.6	0.62	0.63
66	45	45	70	95	0.15	1.5	0.7	0.7	0.74	0.71
67	45	45	70	200	0.1	2	0.52	0.5	0.64	0.55
68	45	45	70	200	0.15	3	0.68	0.6	0.62	0.63
69	45	60	70	95	0.1	1	0.56	0.64	0.56	0.59
70	45	60	70	95	0.15	1.5	0.78	0.7	0.74	0.74
71	45	60	70	200	0.1	2	0.56	0.54	0.72	0.61
72	45	60	70	200	0.15	3	0.7	0.66	0.7	0.69
73	60	15	30	95	0.1	1	0.66	0.72	0.7	0.69
74	60	15	30	95	0.15	1.5	0.84	0.68	0.62	0.71
75	60	15	30	200	0.1	2	0.66	0.5	0.52	0.56
76	60	15	30	200	0.15	3	0.7	0.72	0.52	0.65
77	60	45	30	95	0.1	1	0.66	0.74	0.68	0.69
78	60	45	30	95	0.15	1.5	0.74	0.78	0.8	0.77
79	60	45	30	200	0.1	2	0.56	0.68	0.72	0.65
80	60	45	30	200	0.15	3	0.7	0.72	0.76	0.73
81	60	60	30	95	0.1	1	0.66	0.52	0.68	0.62
82	60	60	30	95	0.15	1.5	0.72	0.74	0.72	0.73
83	60	60	30	200	0.1	2	0.5	0.54	0.64	0.56
84	60	60	30	200	0.15	3	0.6	0.68	0.64	0.64
85	60	15	50	95	0.1	1	0.7	0.84	0.66	0.73
86	60	15	50	95	0.15	1.5	0.76	0.66	0.68	0.70

Exp. No.	Nozzle angle in feed direction (degree)	Nozzle angle against feed direction (degree)	Impinging distance (mm)	Cutting speed (m/min)	Feed rate (mm/rev)	Flow rate (l/min)	Average surface roughness – Ra (μm)			
							Ra ₁	Ra ₂	Ra ₃	Ra _{avg}
87	60	15	50	200	0.1	2	0.52	0.6	0.68	0.60
88	60	15	50	200	0.15	3	0.68	0.76	0.66	0.70
89	60	45	50	95	0.1	1	0.76	0.8	0.74	0.77
90	60	45	50	95	0.15	1.5	0.66	0.76	0.64	0.69
91	60	45	50	200	0.1	2	0.66	0.6	0.68	0.65
92	60	45	50	200	0.15	3	0.68	0.58	0.76	0.67
93	60	60	50	95	0.1	1	0.64	0.56	0.6	0.60
94	60	60	50	95	0.15	1.5	0.7	0.64	0.64	0.66
95	60	60	50	200	0.1	2	0.54	0.6	0.64	0.59
96	60	60	50	200	0.15	3	0.72	0.78	0.64	0.71
97	60	15	70	95	0.1	1	0.68	0.7	0.6	0.66
98	60	15	70	95	0.15	1.5	0.68	0.74	0.78	0.73
99	60	15	70	200	0.1	2	0.56	0.52	0.66	0.58
100	60	15	70	200	0.15	3	0.76	0.68	0.66	0.70
101	60	45	70	95	0.1	1	0.58	0.58	0.58	0.58
102	60	45	70	95	0.15	1.5	0.6	0.74	0.76	0.70
103	60	45	70	200	0.1	2	0.56	0.64	0.66	0.62
104	60	45	70	200	0.15	3	0.5	0.5	0.52	0.51
105	60	60	70	95	0.1	1	0.62	0.58	0.6	0.60
106	60	60	70	95	0.15	1.5	0.7	0.62	0.7	0.67
107	60	60	70	200	0.1	2	0.62	0.5	0.52	0.55
108	60	60	70	200	0.15	3	0.68	0.68	0.62	0.66

Exp. No.	Nozzle angle in feed direction (degree)	Nozzle angle against feed direction (degree)	Impinging distance (mm)	Cutting speed (m/min)	Feed rate (mm/rev)	Flow rate (l/min)	Average surface roughness – Ra (μm)			
							Ra ₁	Ra ₂	Ra ₃	Ra _{avg}
109*	-	-	-	95	0.1	1.6	0.76	0.74	0.74	0.69
110*	-	-	-	95	0.15	2.40	0.68	0.72	0.68	0.71
111*	-	-	-	200	0.1	3.38	0.64	0.52	0.7	0.57
112*	-	-	-	200	0.15	5.2	0.56	0.58	0.7	0.60

*Conventional flood supply system

15.5 Summary of results for 27 test at cutting speed of 95 m/min and feed rate of 0.1 mm/rev (CUT-LIST and conventional supply system)

Exp. No.	Nozzle angle in feed direction (deg)	Nozzle angle against feed direction (deg)	Impinging distance (mm)	Cutting speed (m/min)	Feed rate (mm/rev)	Cutting time (sec)	Flow rate (L/min)	Cutting force (N)	Workpiece temperature (°C)	Tool wear (μm)	Burr height (mm)	Ra (μm)
1	15	15	35	95	0.1	20	1	1502.04	29.5	32.91	0.52	0.69
5	15	45	35	95	0.1	20	1	1699.86	33.7	34.24	0.615	0.66
9	15	60	35	95	0.1	20	1	1638.15	31.1	35.75	0.52	0.61
13	15	15	55	95	0.1	20	1	1673.59	26.6	32.52	0.25	0.67
17	15	45	55	95	0.1	20	1	1524.83	26.5	30.16	0.31	0.66
21	15	60	55	95	0.1	20	1	1551.04	25.7	30.12	0.53	0.62
25	15	15	75	95	0.1	20	1	1653.49	27.3	28.61	0.427	0.7
29	15	45	75	95	0.1	20	1	1488.27	26.7	32.97	0.27	0.55
33	15	60	75	95	0.1	20	1	1765.23	28.5	35.53	0.51	0.61
37	45	15	35	95	0.1	20	1	1793.33	27.2	30.01	0.43	0.7
41	45	45	35	95	0.1	20	1	1464.4	29.2	31.43	0.48	0.6
45	45	60	35	95	0.1	20	1	1675.42	30.3	31.55	0.67	0.59
49	45	15	55	95	0.1	20	1	1339.96	29.2	30.06	0.17	0.59
53	45	45	55	95	0.1	20	1	1609.58	28.6	31.61	0.18	0.61
57	45	60	55	95	0.1	20	1	1621.89	27.6	31.43	0.36	0.64
61	45	15	75	95	0.1	20	1	1567.35	30.1	30.28	0.22	0.65
65	45	45	75	95	0.1	20	1	1677.05	30.9	33.17	0.41	0.63
69	45	60	75	95	0.1	20	1	1660.42	30.7	30.28	0.52	0.59
73	60	15	35	95	0.1	20	1	1651.91	31.5	28.26	0.49	0.69
77	60	45	35	95	0.1	20	1	1670.41	30.4	31.37	0.41	0.69
81	60	60	35	95	0.1	20	1	1674.44	33.9	32.95	0.39	0.62
85	60	15	55	95	0.1	20	1	1698.5	31.2	30.11	0.32	0.73
89	60	45	55	95	0.1	20	1	1660.86	27	30.08	0.3	0.77
93	60	60	55	95	0.1	20	1	1620.18	28.6	30.01	0.46	0.66
97	60	15	75	95	0.1	20	1	1774.32	32.9	30.64	0.53	0.66
101	60	45	75	95	0.1	20	1	1452.43	29.5	35.86	0.38	0.58
105	60	60	75	95	0.1	20	1	1695.06	28.4	30.12	0.21	0.6
109*	-	-	-	95	0.1	20	1.6	1600.1	24.2	31.2	0.16	0.69

* Conventional flood supply system

15.6 Summary of results for 27 trial at cutting speed of 95 m/min & feed rate of 0.15 mm/rev (CUT-LIST and conventional supply system)

Exp. No.	Nozzle angle in feed direction (deg)	Nozzle angle against feed direction (deg)	Impinging distance (mm)	Cutting speed (m/min)	Feed rate (mm/rev)	Cutting time (sec)	Flow rate (L/min)	Cutting force (N)	Workpiece temperature (°C)	Tool wear (µm)	Burr height (mm)	Ra (µm)
2	15	15	35	95	0.15	13	1.5	2165.65	28.6	35.82	0.24	0.71
6	15	45	35	95	0.15	13	1.5	1776.64	26.5	32.28	0.23	0.71
10	15	60	35	95	0.15	13	1.5	1718.65	24.2	35.83	0.42	0.69
14	15	15	55	95	0.15	13	1.5	2055.81	24.8	38.36	0.11	0.74
18	15	45	55	95	0.15	13	1.5	1957.42	22.8	40.37	0.17	0.75
22	15	60	55	95	0.15	13	1.5	2052.04	23.5	37.26	0.16	0.77
26	15	15	75	95	0.15	13	1.5	1833.19	23.9	35.81	0.19	0.72
30	15	45	75	95	0.15	13	1.5	1978.17	24.8	34.54	0.14	0.67
34	15	60	75	95	0.15	13	1.5	1861.62	25.3	37.13	0.1	0.71
38	45	15	35	95	0.15	13	1.5	1837.15	25.3	32.97	0.22	0.73
42	45	45	35	95	0.15	13	1.5	1920.52	24.4	33.8	0.2	0.65
46	45	60	35	95	0.15	13	1.5	1921.95	26.8	31.64	0.24	0.74
50	45	15	55	95	0.15	13	1.5	1935.92	26.3	31.85	0.27	0.68
54	45	45	55	95	0.15	13	1.5	1884.38	25.5	35.34	0.18	0.68
58	45	60	55	95	0.15	13	1.5	1881.95	23.6	33.62	0.15	0.69
62	45	15	75	95	0.15	13	1.5	1967.97	27.2	37.49	0.3	0.73
66	45	45	75	95	0.15	13	1.5	1843.95	26.5	34.4	0.21	0.71
70	45	60	75	95	0.15	13	1.5	1922.92	26.2	33.17	0.16	0.74
74	60	15	35	95	0.15	13	1.5	1806.65	26.6	32.9	0.18	0.71
78	60	45	35	95	0.15	13	1.5	1870.62	27.8	34.38	0.18	0.77
82	60	60	35	95	0.15	13	1.5	1942.03	27.5	37.32	0.17	0.73
86	60	15	55	95	0.15	13	1.5	1972.68	26.6	37.15	0.2	0.7
90	60	45	55	95	0.15	13	1.5	1961.56	24.1	34.42	0.2	0.69
94	60	60	55	95	0.15	13	1.5	2039.01	23.8	35.76	0.15	0.66
98	60	15	75	95	0.15	13	1.5	1952.86	26.4	37.32	0.31	0.73
102	60	45	75	95	0.15	13	1.5	1783.62	26.1	32.65	0.18	0.7
106	60	60	75	95	0.15	13	1.5	1741.93	24.4	32.89	0.23	0.67
110*	-	-	-	95	0.15	13	2.4	1668.73	21.5	32.9	0.11	0.71

* Conventional flood supply system

IS.7 Summary of results for 27 test at cutting speed of 200 m/min and feed rate of 0.1 mm/rev (CUT-LIST and conventional supply system)

Exp. No.	Nozzle angle in feed direction (deg)	Nozzle angle against feed direction (deg)	Impinging distance (mm)	Cutting speed (m/min)	Feed rate (mm/rev)	Cutting time (sec)	Flow rate (L/min)	Cutting force (N)	Workpiece temperature (°C)	Tool wear (µm)	Burr height (mm)	Ra (µm)
3	15	15	35	200	0.1	10	2	1892.95	25.1	169.71	0.53	0.61
7	15	45	35	200	0.1	10	2	1567.96	24.4	138.18	0.49	0.64
11	15	60	35	200	0.1	10	2	1884.83	24.2	151.84	0.39	0.65
15	15	15	55	200	0.1	10	2	1877.37	23.9	163.6	0.45	0.64
19	15	45	55	200	0.1	10	2	1927.18	22.5	114.83	0.4	0.62
23	15	60	55	200	0.1	10	2	1652.55	23.1	126.18	0.15	0.61
27	15	15	75	200	0.1	10	2	1780.46	22.3	106.02	0.33	0.59
31	15	45	75	200	0.1	10	2	1732.64	22.7	128.32	0.34	0.62
35	15	60	75	200	0.1	10	2	1774.47	24	106.13	0.38	0.59
39	45	15	35	200	0.1	10	2	2056.64	25.2	149.42	0.46	0.61
43	45	45	35	200	0.1	10	2	1761.95	23.8	123.85	0.31	0.71
47	45	60	35	200	0.1	10	2	1751.19	24.1	67.58	0.2	0.6
51	45	15	55	200	0.1	10	2	1732.29	26.7	127.8	0.29	0.56
55	45	45	55	200	0.1	10	2	1730.71	23.2	124.45	0.21	0.57
59	45	60	55	200	0.1	10	2	1920.55	23.1	179.45	0.22	0.57
63	45	15	75	200	0.1	10	2	1661.97	26.4	130.2	0.43	0.57
67	45	45	75	200	0.1	10	2	1810.98	26.5	161	0.13	0.55
71	45	60	75	200	0.1	10	2	1805.55	24.5	142.91	0.15	0.61
75	60	15	35	200	0.1	10	2	1789.35	26.2	176.12	0.39	0.56
79	60	45	35	200	0.1	10	2	1884.29	26.1	108.32	0.26	0.65
83	60	60	35	200	0.1	10	2	1746.14	25.4	126.5	0.35	0.56
87	60	15	55	200	0.1	10	2	1732.89	26.4	109.45	0.52	0.6
91	60	45	55	200	0.1	10	2	1967.88	24.5	199.73	0.35	0.65
95	60	60	55	200	0.1	10	2	2058.72	23.5	120.62	0.24	0.59
99	60	15	75	200	0.1	10	2	1962.87	24.4	175.45	0.45	0.58
103	60	45	75	200	0.1	10	2	1744.84	22.4	124.09	0.27	0.62
107	60	60	75	200	0.1	10	2	1752.77	22.3	130.66	0.51	0.55
111*	-	-	-	200	0.1	10	3.38	1875.8	21.4	71.88	0.41	0.57

* Conventional flood supply system

15.8 Summary of results for 27 trial at cutting speed of 200 m/min & feed rate of 0.15 mm/rev (CUT-LIST and conventional supply system)

Exp. No.	Nozzle angle in feed direction (deg)	Nozzle angle against feed direction (deg)	Impinging distance (mm)	Cutting speed (m/min)	Feed rate (mm/rev)	Cutting time (sec)	Flow rate (L/min)	Cutting force (N)	Wokpiece temperature (°C)	Tool wear (µm)	Burr height (mm)	Ra (µm)
4	15	15	35	200	0.15	7	3	1914.67	21.9	89.37	0.22	0.75
8	15	45	35	200	0.15	7	3	2158.05	22.4	123.2	0.23	0.7
12	15	60	35	200	0.15	7	3	2037.69	22.3	74.53	0.17	0.75
16	15	15	55	200	0.15	7	3	2036.67	22	113.66	0.14	0.69
20	15	45	55	200	0.15	7	3	1879.29	21	63.29	0.19	0.71
24	15	60	55	200	0.15	7	3	2045.3	21.7	61.79	0.23	0.71
28	15	15	75	200	0.15	7	3	2067.02	21.7	71	0.26	0.63
32	15	45	75	200	0.15	7	3	1975.44	21.7	98.11	0.26	0.68
36	15	60	75	200	0.15	7	3	1965.3	22.3	117.5	0.19	0.65
40	45	15	35	200	0.15	7	3	2094.78	24.1	135.96	0.38	0.69
44	45	45	35	200	0.15	7	3	2410.56	23.1	124.94	0.27	0.72
48	45	60	35	200	0.15	7	3	2045.63	22.8	196.58	0.18	0.66
52	45	15	55	200	0.15	7	3	2182.02	22.5	135.96	0.25	0.71
56	45	45	55	200	0.15	7	3	2086.5	21.4	94.26	0.27	0.62
60	45	60	55	200	0.15	7	3	2289.23	22.3	180.16	0.15	0.69
64	45	15	75	200	0.15	7	3	2160.05	23	195.46	0.3	0.75
68	45	45	75	200	0.15	7	3	2019.65	23	127.22	0.24	0.63
72	45	60	75	200	0.15	7	3	2109.12	23.7	78.81	0.19	0.69
76	60	15	35	200	0.15	7	3	2115.72	24.2	126.27	0.13	0.65
80	60	45	35	200	0.15	7	3	1922.58	24.1	149.03	0.24	0.73
84	60	60	35	200	0.15	7	3	1946.81	23.7	96.84	0.24	0.64
88	60	15	55	200	0.15	7	3	2011.37	22.6	169.44	0.29	0.7
92	60	45	55	200	0.15	7	3	2104.56	22.7	104.3	0.2	0.67
96	60	60	55	200	0.15	7	3	2118.37	23.8	82.18	0.21	0.71
100	60	15	75	200	0.15	7	3	1930.77	22.5	117.68	0.22	0.7
104	60	45	75	200	0.15	7	3	1897.62	20.8	34.78	0.12	0.51
108	60	60	75	200	0.15	7	3	1990.75	21.3	85.91	0.24	0.66
112*	-	-	-	200	0.15	7	5.2	1903.21	20.6	74.36	0.3	0.6

* Conventional flood supply system

I5.9 Micro-hardness results

Sample No. T7		Cutting speed: 200 m/min and Feed rate: 0.1 mm/rev							System: CUT-LIST					
Run	Distance below machined surface (mm)	Diagonal values (μm) at position A			HV ₁₀₀	Diagonal values (μm) at position B			HV ₁₀₀	Diagonal values (μm) at position C			HV ₁₀₀	HV _{100aveg}
		d _H	d _V	d _{mean}		d _H	d _V	d _{mean}		d _H	d _V	d _{mean}		
1	50	22.5	24.5	23.5	336	22	22	22	383	22	22.5	22.25	374.5	364.5
2	100	21.5	22.5	22	383	21.5	22	21.75	392	21.5	22	21.75	392	389.0
3	150	22	25	23.5	336	22	22.5	22.25	374.5	22	23.5	22.75	358.5	356.3
4	200	22.5	22.5	22.5	366	22.5	24.5	23.5	336	22	22.5	22.25	374.5	370.0
5	250	22	24	23	350	22	24	23	350	22.5	22.5	22.5	366	355.3
6	300	22	23	22.5	366	22	22.5	22.25	374.5	22	22	22	383	374.5
7	350	21.5	23	22.25	374.5	22	25	23.5	336	22.5	24.5	23.5	336	348.8
8	400	22	25	23.5	336	21.5	24	22.75	358.5	22	23.5	22.75	358.5	354.0
9	450	21.5	24	22.75	358.5	22.5	22.5	22.5	366	21.5	24	22.75	358.5	361.0
10	500	22	25	23.5	336	22.5	24.5	23.5	336	22	23	22.75	366	346.0
11	550	22	23	22.5	366	22	22	22	383	22	22	22	383	377.3
12	600	22.5	24.5	23.5	336	22.5	22.5	22.5	366	22.5	22.5	22.5	366	356.0

Sample No. T10		Cutting speed: 95 m/min and Feed rate: 0.15 mm/rev							System: CUT-LIST					
Run	Distance below machined surface (mm)	Diagonal values (μm) at position A			HV ₁₀₀	Diagonal values (μm) at position B			HV ₁₀₀	Diagonal values (μm) at position C			HV ₁₀₀	HV _{100aveg}
		d _H	d _V	d _{mean}		d _H	d _V	d _{mean}		d _H	d _V	d _{mean}		
1	50	26	26	26	274	23	24	23.5	336	25	25	25	297	302.3
2	100	21	21	21	420	21	21	21	420	21	22.5	21.75	392	410.7
3	150	23.5	23.5	23.5	336	22.5	22.5	22.5	366	22	24	23	350	350.7
4	200	23.5	22	22.75	358.5	23	23	23	350	22	23.5	22.75	358.5	355.7
5	250	23	22.5	22.75	358.5	22	22.5	22.25	374.5	23	24.5	23.75	358.5	363.8
6	300	23	23	23	350	22	23	22.5	366	22.5	23	22.75	358.5	358.2
7	350	23	22.5	22.75	358.5	23	24.5	23.75	328.5	22	22.5	22.25	374.5	353.8
8	400	24	22	23	350	22	22	22	383	21	23	22	383	372.0
9	450	23	22	22.5	366	22.5	23	22.75	358.5	23	24	23.5	336	353.5
10	500	25	25	25	297	22.5	24	23.25	328.5	22	25	23.5	336	320.5
11	550	22.5	22.5	22.5	366	22	25	23.5	336	22.5	24.5	23.5	336	346.0
12	600	23.5	22.5	23	350	22	24	23	350	22	24.5	23.25	328.5	342.8

Sample No. T18		Cutting speed: 95 m/min and Feed rate: 0.15 mm/rev							System: CUT-LIST					
Run	Distance below machined surface (mm)	Diagonal values (μm) at position A			HV ₁₀₀	Diagonal values (μm) at position B			HV ₁₀₀	Diagonal values (μm) at position C			HV ₁₀₀	HV _{100aveg}
		d _H	d _V	d _{mean}		d _H	d _V	d _{mean}		d _H	d _V	d _{mean}		
1	50	22.5	24	23.25	343	22	24	23	350	22	23.5	22.75	358.5	350.5
2	100	20.5	22	21.25	410	20.5	22.5	21.5	401	20	22	21	420	410.3
3	150	22	22	22	383	22.5	22.5	22.5	366	22.5	23	22.75	358.5	369.2
4	200	23	23	23	350	22.5	24	23.25	343	23	24	23.5	336	343.0
5	250	22	23	22.5	366	23	24.5	23.75	328.5	22	24.5	23.25	343	345.8
6	300	21	24	22.5	366	22	24	23	350	21	24	22.5	366	360.7
7	350	26	27	26.5	264	23.5	23.5	23.5	336	22	24	23	350	316.7
8	400	22	23.5	22.75	358.5	21.5	25	23.25	343	21.5	22	21.75	392	364.5
9	450	24	24	24	322	22	22.5	22.25	374.5	24.5	24	24.25	315.5	337.3
10	500	22.5	24.5	23.5	336	21	23.5	22.25	374.5	22	24	23	350	353.5
11	550	22.5	22.5	22.5	366	21.5	24	22.75	358.5	21	23	22	383	369.2
12	600	22	24	23	350	21.5	23.5	22.5	366	24	24	24	322	346.0

Sample No. T20		Cutting speed: 200 m/min and Feed rate: 0.15 mm/rev							System: CUT-LIST					
Run	Distance below machined surface (mm)	Diagonal values (μm) at position A			HV ₁₀₀	Diagonal values (μm) at position B			HV ₁₀₀	Diagonal values (μm) at position C			HV ₁₀₀	HV _{100aveg}
		d _H	d _V	d _{mean}		d _H	d _V	d _{mean}		d _H	d _V	d _{mean}		
1	50	22.5	26	24.5	315.5	22	26	24	322	22	25	23.5	336	324.5
2	100	21	22.5	21.75	392	21	22	21.5	401	21.5	23.5	22.5	366	386.3
3	150	22	25	23.5	336	22	23	22.5	366	22	24.5	23.25	343	348.3
4	200	22	24.5	23.25	343	23	23.5	23.25	343	22	26	24	322	336.0
5	250	22	23	22.5	366	23	24.5	23.75	328.5	22.5	24	23.25	343	345.8
6	300	22	24	23	350	22	24.5	23.25	343	22	24	23	350	347.7
7	350	22	22.5	22.25	374.5	22	24	23	350	22.5	24.5	23.5	343	355.8
8	400	22	23.5	22.75	358.5	22	23.5	22.75	358.5	22	24	23	350	355.7
9	450	21.5	23.5	22.5	366	22	24	23	350	22	26	24	322	346.0
10	500	22	24	23	350	22	23.5	22.75	358.5	22	24	23	350	352.8
11	550	22	23.5	22.75	358.5	23	23	23	350	22.5	24.5	23.5	336	348.2
12	600	22	26	24	322	22	23	22.5	366	22.5	25	23.75	328.5	338.8

Sample No. T21		Cutting speed: 95 m/min and Feed rate: 0.1 mm/rev							System: CUT-LIST					
Run	Distance below machined surface (mm)	Diagonal values (μm) at position A			HV ₁₀₀	Diagonal values (μm) at position B			HV ₁₀₀	Diagonal values (μm) at position C			HV ₁₀₀	HV _{100aveg}
		d _H	d _V	d _{mean}		d _H	d _V	d _{mean}		d _H	d _V	d _{mean}		
1	50	23	25	24	322	22	23.5	22.75	358.5	22	24	23	350	343.5
2	100	22.2	21	21.6	397	21.5	21.5	21.5	401	20	22.8	21.4	405	401.0
3	150	22	22.5	22.25	374.5	22	24	23	350	22	24	23	350	358.2
4	200	22.5	24.5	23.5	336	22	23	22.5	366	22	23	22.5	366	356.0
5	250	22	24	23	350	22	25	23.5	336	22	22	22	383	356.3
6	300	23	23	23	350	22	22	22	383	22.5	22.5	22.5	366	366.3
7	350	22.5	24.5	23.5	336	22	23	22.5	366	23	23	23	350	350.7
8	400	22	24	23	350	22	22.5	22.25	374.5	22.5	23	22.75	358.5	361.0
9	450	22	24.5	23.25	343	22.5	24.5	23.5	336	22	24	23	350	343.0
10	500	22.5	23.5	23	350	22	23.5	22.75	358.5	23	23.5	23.25	343	350.5
11	550	21.5	23.5	22.5	366	21.5	23.5	22.5	366	22.5	23	22.75	358.5	363.5
12	600	22	23	22.5	366	22	24	23	350	22	23.5	22.75	358.5	358.2

Sample No. T24		Cutting speed: 200m/min and Feed rate: 0.15 mm/rev							System: CUT-LIST					
Run	Distance below machined surface (mm)	Diagonal values (μm) at position A			HV ₁₀₀	Diagonal values (μm) at position B			HV ₁₀₀	Diagonal values (μm) at position C			HV ₁₀₀	HV _{100aveg}
		d _H	d _V	d _{mean}		d _H	d _V	d _{mean}		d _H	d _V	d _{mean}		
1	50	22.5	25	23.75	328.5	23	24.5	23.75	328.5	22	23.5	22.75	358.5	338.5
2	100	21.5	22	21.75	392	21.5	22	21.75	392	21.5	22.5	22	383	389.0
3	150	22	25.5	23.75	328.5	22	23.5	22.75	358.5	22.5	23.5	23	350	345.7
4	200	22	23	22.5	366	22	23	22.5	366	23	23	23	350	360.7
5	250	22.5	24	23.25	343	22	24	23	350	22	22	22	383	358.7
6	300	22	23.5	22.75	358.5	21.5	23.5	22.5	366	22	23	22.5	366	363.5
7	350	22.5	24.5	23.5	336	22	24	23	350	23	23.5	23.25	343	343.0
8	400	22	24	23	350	22	23.5	22.75	358.5	22	22	22	383	363.8
9	450	22.5	23	22.75	358.5	22.5	24	23.5	343	22.5	24.5	23.5	336	345.8
10	500	23	25	24	322	21.5	23.5	22.5	366	22	22	22	383	357.0
11	550	22.5	24	23.5	343	22	22	22	383	22.5	22	22.25	374.5	366.8
12	600	21.5	24.5	23	350	22	23	22.5	366	22.5	22.5	22.5	366	360.7

Sample No. T29		Cutting speed:95 m/min and Feed rate: 0.1 mm/rev							System: CUT-LIST					
Run	Distance below machined surface (mm)	Diagonal values (μm) at position A			HV ₁₀₀	Diagonal values (μm) at position B			HV ₁₀₀	Diagonal values (μm) at position C			HV ₁₀₀	HV _{100aveg}
		d _H	d _V	d _{mean}		d _H	d _V	d _{mean}		d _H	d _V	d _{mean}		
1	50	23	24	25	322	23	23	23	350	22	25.5	23.75	328.5	333.5
2	100	20	22.8	21.4	405	21.5	21.5	21.5	401	22.2	21	21.6	397	401.0
3	150	22	22.5	22.25	374.5	22	22	22	383	22	22.5	22.25	374.5	377.3
4	200	22.5	24.5	23.5	336	21.5	24	22.75	358.5	22	23.5	22.75	358.5	351.0
5	250	23	23	23	350	22	25	23.5	336	22	24.5	23.25	343	343.0
6	300	22.5	24	23.25	343	22	24.5	23.25	343	22	24	23	350	345.3
7	350	24	23.5	23.75	328.5	22	26	24	322	23	24.5	23.75	328.5	326.3
8	400	22	23.5	22.75	358.5	21	24	22.5	366	21.5	22	21.75	392	372.2
9	450	22	23	22.5	366	21	25.5	23.25	343	21.5	24.5	23	350	353.0
10	500	22	24	23	350	21.5	24.5	23	350	22	23.5	22.75	358.5	352.8
11	550	22	22	22	383	22.5	24.5	23.5	336	21.5	24.5	23	350	356.3
12	600	22	23	22.5	366	22	23.5	22.75	358.5	23	24.5	23.75	328.5	351.0

Sample No. T49		Cutting speed: 95 m/min and Feed rate: 0.1 mm/rev							System: CUT-LIST					
Run	Distance below machined surface (mm)	Diagonal values (μm) at position A			HV ₁₀₀	Diagonal values (μm) at position B			HV ₁₀₀	Diagonal values (μm) at position C			HV ₁₀₀	HV _{100aveg}
		d _H	d _V	d _{mean}		d _H	d _V	d _{mean}		d _H	d _V	d _{mean}		
1	50	22	25	23.5	336	22.5	24	23.25	343	23	23	23	350	343.0
2	100	21.4	21.4	21.4	405	19.5	23	21.25	411	21.4	21.4	21.4	405	407.0
3	150	23	23.5	23.25	343	22.5	23	22.75	358.5	23.5	23.5	23.5	336	345.8
4	200	23.5	23.5	23.5	336	23	23	23	350	21.5	23	22.25	374.5	353.5
5	250	22	22	22	383	22	22	22	383	22.5	23.5	23	350	372.0
6	300	22.5	22.5	22.5	366	22.5	23.5	23	350	21.5	23	22.25	374.5	363.5
7	350	21	22.5	21.75	392	21.5	24.5	23	350	22.5	23.5	23	350	364.0
8	400	24	23	23.5	336	22.5	24	23.25	343	21.5	23	22.25	374.5	351.2
9	450	23.5	23.5	23.5	336	22	24.5	23.25	343	24	24	24	350	343.0
10	500	22	23	22.5	366	22	24	23	350	22	23.5	22.25	322	346.0
11	550	24	25	24.5	309	23	24	23.5	336	21.5	23	22.25	374.5	339.8
12	600	22	24	23	350	22	23.5	22.75	358.5	21.5	23	22.25	374.5	361.0

Sample No. T56		Cutting speed: 200 m/min and Feed rate: 0.15 mm/rev							System: CUT-LIST					
Run	Distance below machined surface (mm)	Diagonal values (μm) at position A			HV ₁₀₀	Diagonal values (μm) at position B			HV ₁₀₀	Diagonal values (μm) at position C			HV ₁₀₀	HV _{100aveg}
		d _H	d _V	d _{mean}		d _H	d _V	d _{mean}		d _H	d _V	d _{mean}		
1	50	22	23	22.5	366	22	24	23	350	22	23.5	22.75	358.5	358.2
2	100	21.5	21.5	21.5	401	21.5	21.5	21.5	401	21.5	21.5	21.5	401	401.0
3	150	22.5	23.5	23	350	22	22.5	22.25	374.5	22	22	22	383	369.2
4	200	22	25	23.5	336	22	24	23	350	22	25	23.5	336	340.7
5	250	23	23	23	350	22	24.5	23.25	343	22	23	22.5	366	353.0
6	300	22	23.5	22.75	358.5	21	25	23	350	22	22.5	22.25	374.5	361.0
7	350	22.5	23.5	23	350	22	23	22.5	366	22	22	22	383	366.3
8	400	22	24.5	23.25	343	22	22.5	22.25	374.5	22	23	22.5	366	361.2
9	450	22	24	23	350	22.5	23.5	23	350	22	22	22	383	361.0
10	500	22	24.5	23.5	343	22	23.5	22.75	358.5	22	23.5	22.75	358.5	353.3
11	550	22	23	22.5	366	22	22	22	383	22	23.5	22.75	366	371.7
12	600	22	24.5	23.25	343	22.5	23.5	23	350	23	23	23	350	347.7

Sample No. T71		Cutting speed: 200 m/min and Feed rate:0.1 mm/rev							System: CUT-LIST					
Run	Distance below machined surface (mm)	Diagonal values (μm) at position A			HV ₁₀₀	Diagonal values (μm) at position B			HV ₁₀₀	Diagonal values (μm) at position C			HV ₁₀₀	HV _{100aveg}
		d _H	d _V	d _{mean}		d _H	d _V	d _{mean}		d _H	d _V	d _{mean}		
1	50	22.5	24.5	23.5	336	22	23	22.5	366	23	24	23.5	358.5	361.0
2	100	21.5	22	21.75	392	21.5	22	21.75	392	21.5	21.5	21.5	401	395.0
3	150	23.5	23.5	23.5	336	22	23	22.5	366	22	22.5	22.25	350	350.7
4	200	23	23	23	350	22	23.5	22.75	358.5	22.5	22.5	22.5	366	361.2
5	250	22.5	22.5	22.5	366	22.5	22.5	22.5	366	22	22.5	22.25	383	377.3
6	300	22	22	22	383	22	22	22	383	23	23	23	343	353.5
7	350	22.5	23.5	23	350	23.5	23	23.5	343	22.5	22.5	22.5	350	347.6
8	400	22	23	22.5	366	23	23	23	350	22	24	23	366	354.2
9	450	22	22.5	22.25	374.5	22	22	22	383	22	23	22.5	366	361.0
10	500	22.5	22.5	22.5	366	22	22.5	22.25	374.5	22	23.5	22.75	350	352.8
11	550	22	22.5	22.25	374.5	22.5	23.5	23	350	22.5	22.5	22.5	358.5	358.2
12	600	22.5	22.5	22.5	366	23	23	23	350	22	22	22	358.5	350.5

Sample No. T104		Cutting speed: 200 m/min and Feed rate: 0.15 mm/rev							System: CUT-LIST					
Run	Distance below machined surface (mm)	Diagonal values (μm) at position A			HV ₁₀₀	Diagonal values (μm) at position B			HV ₁₀₀	Diagonal values (μm) at position C			HV ₁₀₀	HV _{100aveg}
		d _H	d _V	d _{mean}		d _H	d _V	d _{mean}		d _H	d _V	d _{mean}		
1	50	22	24	23	350	22	25	23.5	336	22	25	23.5	336	340.7
2	100	21.5	21.5	21.5	401	21	21.5	21.5	401	21.5	22	21.75	392	398.0
3	150	22	24.5	23.25	343	24	24	24	322	22	23.5	22.75	358.5	341.2
4	200	23	23	23	350	23	23	23	350	23	23	23	350	350.0
5	250	21	24	22.5	366	22	22	22	383	22	22	22	383	377.3
6	300	21	23	22	383	21.5	22	21.75	392	21	22	21.5	401	392.0
7	350	21.5	22	21.75	392	23	23	23	350	22	23	22.5	366	369.3
8	400	21	24	23	350	22	22	22	383	21.5	23	22.25	358.5	363.8
9	450	22	22	22	383	21.5	23	22.25	358.5	22	22	22	383	374.8
10	500	22.5	22.5	22.5	366	22	24	23	350	21	23	22	383	366.3
11	550	22	22	22	383	21	23	22	383	22	22	22	383	383.0
12	600	23	23	23	350	22	24	23	350	22.5	23.5	23	350	350.0

Sample No. T106		Cutting speed: 95 m/min and Feed rate: 0.15 mm/rev							System: CUT-LIST					
Run	Distance below machined surface (mm)	Diagonal values (μm) at position A			HV ₁₀₀	Diagonal values (μm) at position B			HV ₁₀₀	Diagonal values (μm) at position C			HV ₁₀₀	HV _{100aveg}
		d _H	d _V	d _{mean}		d _H	d _V	d _{mean}		d _H	d _V	d _{mean}		
1	50	21.5	24	22.75	358.5	21	24	22.5	366	22	23.5	22.75	358.5	361.0
2	100	21.5	21.5	21.5	401	21	22.5	21.75	392	21.5	21.5	21.5	401	398.0
3	150	22	23	22.5	366	23	24	23.5	336	23	23	23	350	350.7
4	200	23	23.5	23.25	343	22	22.5	22.25	374.5	22	23	22.5	366	361.2
5	250	21	23	22	383	22	23	22.5	366	21.5	22.5	22	383	377.3
6	300	22.5	24	23.25	343	21.5	23	22.25	374.5	22	24.5	23.25	343	353.5
7	350	24	25	24.5	309	23.5	24	23.75	328.5	22	24	23	350	329.2
8	400	23.5	24.5	24	322	21	23.5	22.25	374.5	22	23	22.5	366	354.2
9	450	22.5	23	22.75	358.5	21.5	24	22.75	358.5	21.5	23.5	22.5	366	361.0
10	500	22	24	23	350	22	23.5	22.75	358.5	22	24	23	350	352.8
11	550	21	24	22.5	366	22	24	23	350	22	23.5	22.75	358.5	358.2
12	600	22	24.5	23.25	343	21.5	24.5	23	350	21.5	24	22.75	358.5	350.5

Sample No. T107		Cutting speed: 200 m/min and Feed rate: 0.1 mm/rev							System: CUT-LIST					
Run	Distance below machined surface (mm)	Diagonal values (μm) at position A			HV ₁₀₀	Diagonal values (μm) at position B			HV ₁₀₀	Diagonal values (μm) at position C			HV ₁₀₀	HV _{100aveg}
		d _H	d _V	d _{mean}		d _H	d _V	d _{mean}		d _H	d _V	d _{mean}		
1	50	22.5	25.5	24	322	23	23	23	350	23	23	23	350	340.7
2	100	21.5	22.5	22	383	21.5	22	21.75	392	21.5	21.5	21.5	401	392.0
3	150	24.5	23	23.75	328.5	22	24	23	350	22.5	22.5	22.5	366	348.2
4	200	22	23	22.5	366	22	23.5	22.75	358.5	22	22	22	383	369.2
5	250	23	22.5	22.75	358.5	22	23	22.5	366	22.5	22.5	22.5	366	363.5
6	300	22.5	24	23.25	343	22.5	22	22.25	374.5	22	22	22	383	366.8
7	350	22	23.5	22.75	358.5	22	23	22.5	366	23	23	23	350	358.2
8	400	22	23	22.5	366	22	22.5	22.25	374.5	22	22	22	383	374.5
9	450	22.5	22.5	22.5	366	22	22	22	383	23	24	23.5	336	361.7
10	500	22	23.5	22.75	358.5	22	22.5	22.25	374.5	22	22	22	383	372.0
11	550	22	22.5	22.25	374.5	22.5	22.5	22.5	366	22.5	22.5	22.5	366	368.8
12	600	22	22	22	383	22.5	23	22.75	358.5	22.5	23.5	23	350	363.8

Sample No. T109		Cutting speed: 95 m/min and feed rate: 0.1 mm/rev							System: Conventional flood supply system					
Run	Distance below machined surface (mm)	Diagonal values (μm) at position A			HV ₁₀₀	Diagonal values (μm) at position B			HV ₁₀₀	Diagonal values (μm) at position C			HV ₁₀₀	HV _{100aveg}
		d _H	d _V	d _{mean}		d _H	d _V	d _{mean}		d _H	d _V	d _{mean}		
1	50	22.5	25.5	24	322	21	25	23	350	22.5	22.5	22.50	366	346.0
2	100	21.5	22	21.75	392	19	21	20	464	21.5	21.5	21.5	401	419.0
3	150	22.5	24.5	23.5	336	22	23	22.50	366	22.5	24	23.25	343	348.3
4	200	22	22	22	383	22	22.5	22.25	374.5	22	22	22	383	380.2
5	250	22	23	22.5	366	23	23.5	23.25	343	23	23	23	350	353.0
6	300	23	23	23	350	22	24	23	350	22	22	22	383	361.0
7	350	21.5	22.5	22	383	22	24.5	23.25	343	25	26	25.5	285	337.0
8	400	22	22	22	383	22.5	23.5	23	350	22	24	23	350	361.0
9	450	22	23.5	22.75	358.5	22	23	22.5	366	22.5	23	22.75	358.5	361.0
10	500	22	22.5	22.25	374.5	22	23.5	22.25	374.5	23	23	23	350	366.3
11	550	22	24.5	23.25	343	22.5	22.5	22.5	366	21	23.5	22.25	374.5	361.2
12	600	22	23	22.50	366	22	24.5	23.25	343	22.5	23	22.75	358.5	355.8

Sample No. T110		Cutting speed: 95 m/min and Feed rate: 0.15 mm/rev							System: Conventional flood supply system					
Run	Distance below machined surface (mm)	Diagonal values (μm) at position A			HV ₁₀₀	Diagonal values (μm) at position B			HV ₁₀₀	Diagonal values (μm) at position C			HV ₁₀₀	HV _{100aveg}
		d _H	d _V	d _{mean}		d _H	d _V	d _{mean}		d _H	d _V	d _{mean}		
1	50	22	24	23	350	22	23	22.5	366	22	22	22	383	366.3
2	100	21	21	21	420	20.25	22.25	21.25	411	21	21	21	420	417.0
3	150	22.5	22.5	22.5	366	22.5	22.5	22.5	366	23	23	23	350	360.7
4	200	23.5	23.5	23.5	336	22.5	21	21.75	392	22.5	22.5	22.5	366	364.7
5	250	23	23	23	350	21	22	21.5	401	22	22	22	383	378.0
6	300	21	24	22.5	366	21	25.5	23.25	343	22	21.5	21.75	392	367.0
7	350	23.5	25.5	24.5	309	22	24.5	23.25	343	21.5	21.5	21.5	401	351.0
8	400	25	25	25	297	22.5	21.5	22	383	23	23	23	350	343.3
9	450	22.5	22.5	22.5	366	23	23	23	350	21	23	22	383	366.3
10	500	21.5	23	22.25	366	22	22	22	383	21	22.5	21.75	392	380.3
11	550	21	23.5	22.25	366	22	22	22	383	22	22	22	383	377.3
12	600	22.5	22.5	22.5	366	23	23	23	350	22.5	22.5	22.5	366	360.7

Sample No. T111		Cutting speed: 200 m/min and feed rate: 0.1mm/rev							System: Conventional flood supply system					
Run	Distance below machined surface (mm)	Diagonal values (μm) at position A			HV ₁₀₀	Diagonal values (μm) at position B			HV ₁₀₀	Diagonal values (μm) at position C			HV ₁₀₀	HV _{100aveg}
		d _H	d _V	d _{mean}		d _H	d _V	d _{mean}		d _H	d _V	d _{mean}		
1	50	20	26	23	350	20	25.5	22.75	358.5	20	26.5	23.25	343	350.5
2	100	21.4	21.4	21.4	405	21.4	21.4	21.4	405	19.5	23	21.25	411	407
3	150	18	26	22	358.5	20	25	22.50	366	19.5	28	23.75	328.5	351.0
4	200	21	24	22.5	383	20	26.5	23.25	343	20	26	23	350	358.7
5	250	20.5	24.5	22.5	366	20	25.5	22.75	358.5	19	26	22.5	366	363.5
6	300	21	23.5	22.25	366	19	26	22.50	366	19.5	26	22.75	358.5	363.5
7	350	19	25.5	22.25	374.5	20.5	27	23.75	328.5	19.5	25	22.25	374.5	359.2
8	400	20.5	26	23.25	374.5	19	27	23	350	20.5	25.5	23	350	358.2
9	450	21	27	24	343	20	25	22.50	366	20.5	25	22.75	358.5	355.8
10	500	21.5	23.5	22.5	322	20	27	23.5	336	22.5	23.5	23	350	336.0
11	550	20.5	25.5	23	366	19.5	25.5	22.25	366	20.5	26.5	23.5	336	356.0
12	600	20.5	25.5	23	350	23	25	24	322	20	25.5	22.75	358.5	343.5

Sample No. T112		Speed: 200 m/min and feed rate: 0.15 mm/rev							System: Conventional flood supply system					
Run	Distance below machined surface (μm)	Diagonal values (μm) at position A			HV ₁₀₀	Diagonal values (μm) at position B			HV ₁₀₀	Diagonal values (μm) at position C			HV ₁₀₀	HV _{100aveg}
		d _H	d _V	d _{mean}		d _H	d _V	d _{mean}		d _H	d _V	d _{mean}		
1	50	26.5	28	27.5	250.5	21	24	22.5	366	22.5	23.5	23	350	322.2
2	100	21	22	21.5	401	21.5	21.5	21.5	401	20	23	21.5	401	401
3	150	21.5	23.5	22.5	366	22	23	22.5	366	22.5	22.5	22.5	366	366.0
4	200	23	22.5	22.75	358.5	22	24	23	350	22.5	24.5	23.5	336	348.2
5	250	22	24.5	23.25	343	23.5	23.5	23.5	336	21.5	23	22.25	374.5	351.2
6	300	22	24	23	350	22	24	23	350	22.5	23.5	23	350	350.0
7	350	22.5	23	22.75	358.5	22.5	23	22.75	358.5	22.5	24.5	23.5	336	351.0
8	400	23	24	23.5	336	22.5	24.5	23.50	336	22	23	22.5	366	346.0
9	450	24	25	24.5	309	22.5	23.5	23	350	21	24.5	22.75	358.5	339.2
10	500	21	24.5	22.75	358.5	25	24	24.5	309	21	23.5	22.25	374.5	347.3
11	550	21.5	23	22.25	374.5	21	22.5	21.75	392	21.5	24.5	23	350	372.2
12	600	21	24	22.50	366	21	25	23	350	22	23	22.5	366	360.7

I5.10 Summary of the micro-hardness results (CUT-LIST and the conventional supply system)

	Micro-hardness HV ₁₀₀												
	95 m/min x 0.1 mm/rev			95 m/min x 0.15 mm/rev			200 m/min x 0.1 mm/rev			200 m/min x 0.15 mm/rev			
Sample No.	T21	T29	T49	T10	T18	T106	T7	T71	T107	T20	T24	T56	T104
CUT-LIST	401*	401*	407	410.7	410.3	398*	389*	395	392	386.3*	389	401	398
Sample No.	T109			T110			T111			T112			
Conventional system	419			417			407			401			

*Minimum values of micro-hardness using CUT-LIST

I6: Results of the repeatability trials

Run	Cutting force (N)			Workpiece temperature (°C)			Tool wear (VB) (µm)			Burr height (mm)			Ra (µm)		
	R1	R2	error	R1	R2	error	R1	R2	error	R1	R2	error	R1	R2	error
1	1507.12	1502.04	0.34%	30.1	29.5	1.99%	33.21	32.91	0.90%	0.53	0.52	1.89%	0.67	0.69	-2.90%
2	2162.04	2165.65	-0.17%	29.3	28.6	2.39%	34.13	35.82	-4.72%	0.25	0.24	4.20%	0.7	0.71	-2.82%
3	1893.44	1892.95	0.03%	25.6	25.1	1.95%	172.66	169.71	1.71%	0.51	0.49	3.92%	0.66	0.64	1.61%
4	1912.05	1914.67	-0.14%	22.14	21.9	1.08%	92.43	89.37	3.31%	0.21	0.22	-4.55%	0.73	0.75	-5.33%
5	1703.18	1699.86	0.19%	33.9	33.7	0.59%	36.88	34.24	7.16%	0.62	0.61	1.61%	0.68	0.66	-6.06%
6	1774.32	1776.64	-0.13%	26.7	26.5	0.75%	33.19	32.28	2.74%	0.21	0.23	-8.70%	0.72	0.71	-1.41%
7	1565.33	1567.96	-0.17%	24.9	24.4	2.01%	135.54	138.18	-1.91%	0.51	0.49	3.92%	0.65	0.64	-4.69%
8	2154.66	2158.05	-0.16%	22.9	22.4	2.18%	218.42	223.2	-2.14%	0.24	0.23	4.17%	0.69	0.7	-1.43%
9	1633.87	1638.15	-0.26%	29.7	31.1	-4.50%	36.04	35.75	0.80%	0.5	0.52	-3.85%	0.6	0.61	3.17%
10	1720.1	1718.65	0.08%	24.6	24.2	1.63%	36.9	35.83	2.90%	0.43	0.42	2.33%	0.68	0.69	-5.80%
11	1879.83	1884.83	-0.27%	23.71	24.4	-2.83%	153.22	151.84	0.90%	0.38	0.39	-2.56%	0.62	0.65	2.99%

R1 and **R2** are measurement readings obtained from each repeated and the original tests respectively.

Max error	0.34%	2.39%	7.16%	4.2%	3.17%
Min error	0.03%	0.59%	0.8%	1.89%	1.61%